LOSS OF MAINS DETECTION AND AMELIORATION ON ELECTRICAL DISTRIBUTION NETWORKS

A thesis submitted to The University of Manchester for the degree of
PhD
in the Faculty of Engineering and Physical Sciences

2010

CHUI FEN TEN

SCHOOL OF ELECTRICAL AND ELECTRONIC ENGINEERING

LIST OF CONTENTS

Word Count = 42808

LIST OF TABLES

ABSTRACT

Title: Loss of Mains Detection and Amelioration on Electrical Distribution Networks
Candidate: Chui Fen Ten Institution: The University of Manchester
Degree: Doctor of Philosophy (PhD) Date: 27 October 2010

Power system islanding is gaining increasing interest as a way to maintain power supply continuity. However, before this operation become viable, the technical challenges associated with its operation must first be addressed. A possible solution to one of these challenges, out-of synchronism reclosure, is by running the islanded system in synchronism with the mains whilst not being electrically connected. This concept, known as "synchronous islanded operation" avoids the danger of out-of-synchronism reclosure of the islanded system onto the mains.

The research in this thesis was based on the concepts presented in [1-3] and specifically applied to multiple-DG island scenarios. The additional control challenges associated with this scenario are identified and an appropriate control scheme, more suited for the operation of multiple-DG synchronous islands, is proposed. The results suggest that multiple-DG synchronous islanded operation is feasible, but a supervisory controller is necessary to facilitate the information exchange within the islanded system and enable stable operation.

For maximum flexibility, the synchronous island must be capable of operating with a diversity of generation. The difficulties become further complicated when some or all of the generation consists of intermittent sources. The performance of the proposed control scheme in the presence of a significant contribution of renewable sources within the island is investigated. Two types of wind technologies were developed in PSCAD/EMTDC for this purpose, they are a fixed speed induction generator (FSIG) based wind farm and a doubly-fed induction generator (DFIG) based wind farm. The results show that although synchronous islanded operation is still achievable, the intermittent output has an adverse effect on the control performance, and in particular limits the magnitude of disturbances that can happen in the island without going beyond the relaxed synchronisation limits of $\pm 60^{o}$.

Energy storage is proposed as a way to reduce the wind farm power variation and improve phase controller response. A supplementary control is also proposed such that DFIG contributes to the inertial response. The potential of the proposed scheme (energy storage + supplementary control) is evaluated using case studies. The results show massive improvement to the load acceptance limits, even beyond the case where no wind farm is connected. The benefit of the proposed scheme is even more apparent as the share of wind generated energy in the island grows.

DECLARATION

No portion of the work referred to in the thesis has been submitted in support of an application for another degree or qualification of this or any other university or other institute of learning

COPYRIGHT STATEMENT

The author of this thesis (including any appendices and/or schedules to this thesis) owns certain copyright or related rights in it (the "Copyright") and s/he has given The University of Manchester certain rights to use such Copyright, including for administrative purposes.

Copies of this thesis, either in full or in extracts and whether in hard or electronic copy, may be made only in accordance with the Copyright, Designs and Patents Act 1988 (as amended) and regulations issued under it or, where appropriate, in accordance with licensing agreements which the University has from time to time. This page must form part of any such copies made.

The ownership of certain Copyright, patents, designs, trade marks and other intellectual property (the "Intellectual Property") and any reproductions of copyright works in the thesis, for example graphs and tables ("Reproductions"), which may be described in this thesis, may not be owned by the author and may be owned by third parties. Such Intellectual Property and Reproductions cannot and must not be made available for use without the prior written permission of the owner(s) of the relevant Intellectual Property and/or Reproductions.

Further information on the conditions under which disclosure, publication and commercialisation of this thesis, the Copyright and any Intellectual Property and/or Reproductions described in it may take place is available in the University IP Policy (see http://documents.manchester.ac.uk/DocuInfo.aspx? DocID=487), in any relevant Thesis restriction declarations deposited in the University Library, The University Library's regulations (see http://www.manchester.ac.uk/library/aboutus/regulations) and in The University's policy on Presentation of Theses.

ACKNOWLEDGEMENT

I would like to express my gratitude to my supervisor Prof. Peter Crossley for his help, guidance and support throughout the period of this research. His ideas were truly inspirational, and the exceptional effort he spent on reviewing this thesis has led to the successful completion of this thesis.

Special acknowledgement to Dr. Robert Best for his guidance and helps throughout the course of this research.

Last but not the least, I would like to thank my family, especially my parents for their continuous support.

DEDICATION

To my father, mother, family and Jhan Yhee

CHAPTER 1

INTRODUCTION

1.1 Introduction

One of the trends in the electricity industry is the shift towards smaller scale generation, more commonly known as distributed generations (DG). They are seen as an alternative, or rather an enhancement to the conventional centralised power system. One of the major drivers leading to this change is the deregulation of the electricity market. The move to liberalise the energy market has opened up more opportunities and invited participants from various levels into the power industry.

Government policies and commitments in combating climate change are the other major drivers fuelling the change in the power system's structure. According to the Low Carbon Transition Plan 2009, by year 2020, 15% of UK energy is to be produced from renewable generation and by year 2050, carbon dioxide (CO_2) emissions are to be reduced by at least 80% [4] In order to meet these targets, financial incentives and obligatory schemes were introduced, which indirectly promoted the growth of DG.

There are of course other factors that encourage the growing popularity of DG. These include development advances in DG technologies and reduction in manufacturing costs, increasing demand to improve power system efficiency and reduce network losses as well as enhancement of supply reliabilities.

Proliferation of DG into the electricity networks has indeed brought numerous advantages, but at the same time also poses several new challenges to the current

network. The introduction of DG into the system inevitably affects the operational characteristic of the electricity network and increases the complexity of the power system. Existing operational procedures are not sufficient to accommodate these changes. Consequently new operational strategies are vital in coping with the rising numbers of DG.

1.2 Power System Islanding

Power system islanding is one of the challenges that result from the introduction of DG into the power system. It refers to the situation in which part of the distribution network remains energized by DG whilst electrically isolated from the main utility supply.

Due to safety concerns and the risks associated with islanding operation, current legislation requires immediate disconnection of the DG units once islanding of the distribution network occurs.

Such requirements undoubtedly limit the potential offered by DG. Tripping of DG is the simplest approach to prevent island operation. This move was acceptable in the past, when DG accounted for a relatively insignificant capacity in the system, however, as the share of DG increases, their capability to sustain an island also increased. Disconnecting them may no longer be appropriate especially when they can continue to supply the islanded demand, or critical loads, within the statutory limits.

If DG units are allowed to operate during an islanding event, they have the potential to maintain the continuity of supply of the islanded network; the alternative is a blackout. This will undoubtedly reduce the number and duration of network interruption, subsequently improving the security of supply, which is obviously an advantage for all consumers. DG owners will also benefit from the income generated during the extra connection time, as compared to the alternative of being forced to disconnect unnecessarily. Utilities too gain from this change, benefitting from the ancillary support offered by DG, such as the black start capability. It is hence

considered desirable for DG to stay connected and contribute to the network during an upstream interruption.

The idea of operating DG in island mode seems to resonate with other researchers, even utilities from around the world. Impact of islanding operation were investigated thoroughly and presented in [5-10] Numerous control strategies to cope with the transition from grid-connected to islanded mode were also proposed to regulate and maintain the electricity supplies of the islanded network within statutory limits [10-12]. Strategies to split the system into operable and optimised islands were also researched.[13, 14]

One of the critical issues associated with the operation of islanded network is the risk of out of synchronism reclosure. In order for safe reconnection of the islanded network to the main utility network, adequate synchronising equipment must be in place. For maximum flexibility, as long as a sustained island is formed, geographical location or size of island should not be a constraint. This indicates that sync-checkers have to be retrofitted in every circuit breaker in order to support flexible islanding. Obviously, this is not economically justifiable and may not be realised. The other alternative may be to pre-determine the island topology and clearly this approach tends to limit the potential of island topology reconfiguration.

A novel concept which addresses the above concern was suggested in [1-3]. This concept, which is termed "synchronous islanded operation", proposes a control technique which holds the islanded network in synchronism with the main utility system, allowing the former to be reconnected to the latter at any times with minimal transients. This technique not only negates the needs for synchronising equipments, at the same time offers maximum flexibility for island topology reconfiguration.

Islanding operation offers the opportunity for greater utilisation of DG. If the challenges associated with islanding operation can be overcame, it is envisioned to become an integral part of the future power system.

1.3 Scope of Thesis

The main aim of this research is to further explore and develop the concept of synchronous islanded operation. This was achieved by first gaining a comprehensive understanding and background concerning islanding operation. Existing codes and practice towards islanding were researched. A thorough review of existing islanding protections, i.e. loss-of-mains (LOM) detection schemes was carried out in order to identify the advantages as well as weaknesses of these techniques.

Most commonly employed LOM detection technique, i.e. rate of change of frequency (ROCOF) was then modelled and its operating performance was investigated through simulation based case studies. The rise in the number of DG integrated within the network has increased the possibility of multiple DG being connected to the same feeder. The impact of this scenario was investigated; in particular, the possible interference among LOM detection relays, connected to the same feeder was analysed.

Next, the challenges associated with the operation of a synchronous island with multiple DG units were assessed and identified. Possible control adaptations to the existing scheme were then suggested. The feasibility of a proposed scheme was next investigated using simulation studies.

It is envisaged that not all generating units trapped in the formed island, will be equipped with the proposed control capability. Hence, the performance of the proposed control scheme when operating in an island with a different mix of generation sources was examined. In order to reflect a more realistic scenario, intermittent power sources, i.e. wind energy were also included in the studies. The impact on the proposed control scheme of the non-controllability and varying nature of the sources were then analysed and identified. The feasibility of the scheme when operating with varying power sources is also discussed.

Possible adaptations to a wind farm or wind generator to support the implementation of synchronous island were then proposed. Integration of energy storage and novel supplementary control were suggested and developed using a simulation tool. The

benefits and effectiveness of the proposed methods were then assessed using predetermined case studies.

1.4 Chapter Outline

Chapter 2 provides an overview about power system islanding, explaining how it is formed and the challenges associated with its formation. This chapter also presents an intensive literature review of the loss-of-mains detection techniques available for distributed generators. It also provides an insight on how peoples' perspectives have changed towards islanding and highlighted a particular concept called synchronous islanded operation, which can be employed to overcome the problem of out-of-synchronism reclosure between an islanded system and the main grid.

Chapter 3 reviews the working principle of the most commonly implemented LOM detection technique, ROCOF relay and addresses the existing problems associated with it. Factors that affect the detection capability of a ROCOF relay are also discussed. The operating performances of this relay during islanding and system disturbance are also demonstrated through simulation studies. The relays were next tested in a multiple DG environment in order to investigate the possibility of interference between them. Simulation results are analyzed and discussed.

Chapter 4 considers the implementation of synchronous islanded operation in a multiple synchronous generators based island. The challenges involved in the implementations are also discussed. An appropriate control system for a multiple-set islanded system is proposed, which incorporates a load sharing ability. An islanding operating algorithm is detailed to give a clear insight of the concept of synchronous islanded operation. Simulation results are presented to illustrate the effectiveness of the proposed method.

Chapter 5 examines the impact of variable power sources to the effectiveness of the proposed phase control. A wind farm was chosen to represent the varying power sources in this thesis; two different types of wind farms were modelled, namely one with fixed speed induction generator (FSIG) and one with doubly fed induction

generator (DFIG) type wind farms. Actual measurements of wind output were used in the simulation to truly reflect the impact of changing the variables. Comparative analyses of the performance of the proposed phase control under the influence of both types of wind farms were also carried out. These results are also referenced to the no wind farm connected scenarios.

Chapter 6 proposes the integration of energy storage into the DFIG based wind farm. This is to improve the performance of the phase control and consequently support the implementation of synchronous islanded operation. The operation of the DFIG with energy storage is discussed thoroughly, including the limitation of storage in reflecting a true operating scenario. Supplementary control is also proposed for the DFIG and the energy storage system; this further complements and supports synchronous islanded operation. Through simulation results, the effectiveness of the proposed system and control scheme is demonstrated.

Chapter 7 concludes this thesis by summarising all the findings accomplished from the work undertaken. It ends with recommendations for possible future work.

CHAPTER 2

LITERATURE REVIEW

2.1 Introduction

This chapter gives a brief introduction of islanding and the risk associated with operating an unintentional islanded system, highlighting the importance of loss of mains detection schemes. It is then followed by an intensive review of the major techniques available for islanding detection.

2.2 Introduction to Islanding

Islanding, also known as loss of mains or loss of grid, occurs when a section of the distribution network becomes electrically isolated from the main utility supply, yet continues to be energized by one or more distributed generators (DG). Island can be formed at various locations, involving one or more distribution feeders, substations and voltage levels. Figure 2-1 illustrates the possible locations of island formation, in which each island is associated with one or more disconnection points.

2.2.1 Formation of Island

The common reason for the formation of an island is the opening of a recloser or circuit breaker in response to its downstream fault. Ideally, the DG protection should be able to detect the fault and trip the DG before an island is formed. However, this might not always be the case. If the protection fails to sense the fault or the circuit breaker opens due to manual switching, islanding can happen [15]. Islands can be

sustained as long as the voltage and frequency remain within the statutory limits. Considering the rapid growth of DG penetration in recent years, the possibility of sustained islanding has significantly increased and this phenomenon has subsequently raised concern over the impacts of islanding.

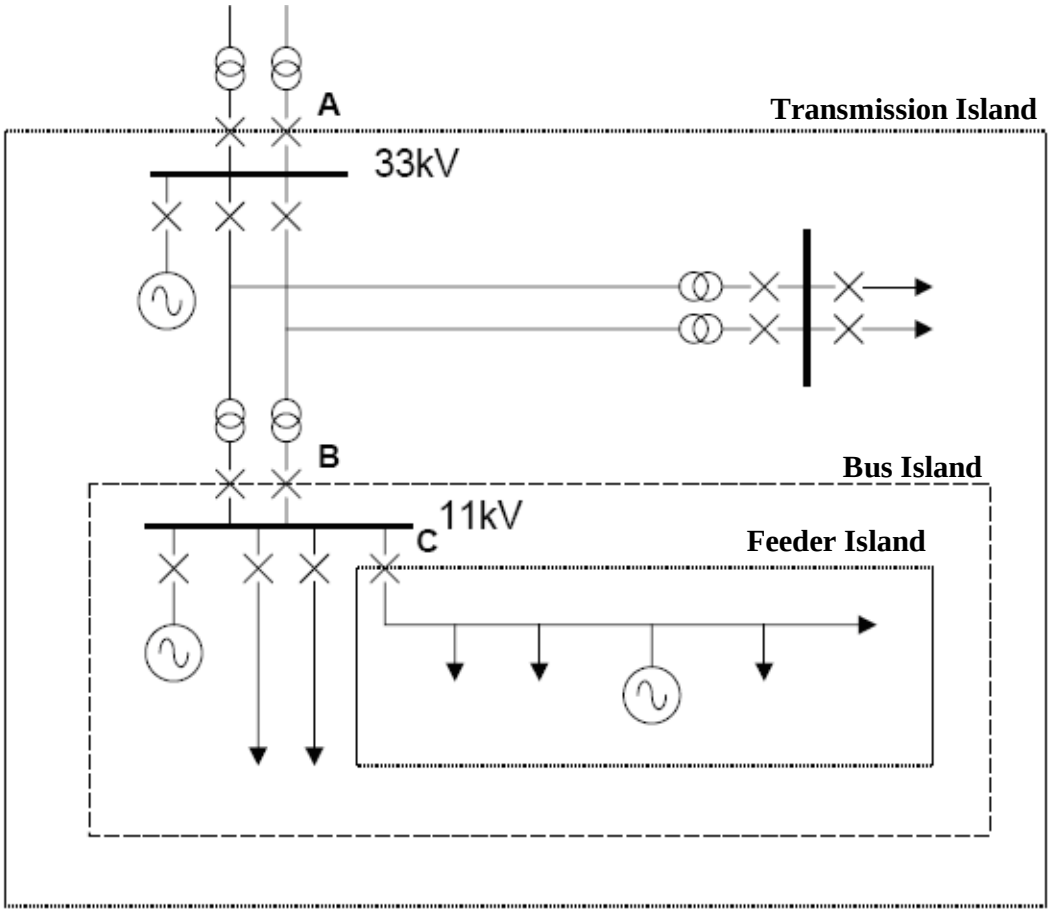

Figure 2-1 Possible Formation of Island

2.3 Hazards and Risk of Islanding

Energizing an island without support from the main utility presents a number of problems, as outlined below:

2.3.1 **Power Quality**

The power quality seen by the utility customer in the formed island is the main concern of the distribution network operator (DNO). They hold responsibility to

provide regulation and high quality of supply to their customer. However, in an islanded system, the voltage and frequency provided to the customers can vary significantly, and may be out of the statutory limits. This situation presents high risk to the customers' equipment yet the utility has no control over them. As a result, customers' equipments are jeopardized and the DNO are liable for the consequences.

2.3.2 **Personnel Safety**

The power system was designed to work as a passive network with "top-down" unidirectional power flow. Yet, with the penetration of DG, the power flow becomes bi-directional. After the main supply has been disconnected, owing to fault or abnormal situation, a section of network which is assumed to be dead can remain energized by DG units. Utility personnel sent out for maintenance work may get in contact with the live part of equipment. This circumstance poses safety hazard to utility maintenance workers and general public and is viewed as the most severe safety hazard caused by islanding [15]

2.3.3 **Earthing and Protection**

In the UK, the standard practice for a Medium Voltage (MV) system is to use single point earthing in which the earth connection is supplied by the utility. The downside of this practice is that whenever the connection to the earth point is lost, the system earthing is also lost. Islanding, for example, may leave a particular section of the utility system unearthed, causing the system to be potentially unsafe and presenting serious health and safety hazards. Moreover, operating without a secure earth connection is illegal according to UK regulation [16]

2.3.4 **Out of Synchronism Reclosure**

An auto recloser is commonly used in a distribution network to restore service after fault events and has been reported to effectively reduce the customer minutes lost. This is because 85%-90% of overhead line faults are temporary [17]. Nevertheless, there is still a minimum time for reconnection of a radial feeder to allow fault arcs to extinguish such that fault does not continue after reclosing. The immediate reclosing

attempt can be as fast as 2 seconds, which is done to minimize the effect on power quality. Usually, due to the possibility of a temporary fault persisting during the initial attempt, several reclosing attempts are made. The successive second and third attempts could be delayed by 15 and 30 seconds respectively from the first reclosure.

Operation of islanding however, has given rise to a challenging issue for the standard operation of an auto recloser. Continual operation of DG during auto recloser opening time may prevent fault arc extinction and lead to unsuccessful reclosing attempts. This not only results in deterioration of networks reliability, network components are also subjected to increased stress as they are repeatedly closed against a fault. As a result, a longer first attempt reclosing time is needed. In UK, the first reclosing time is set between 3-30 seconds. This is essential to provide sufficient time for loss of mains protection to operate, which varies from 0.5 seconds up to 2 seconds, according to G59/1 and IEEE Standard 1547-2003 respectively. [18, 19]

Even more serious and undesirable is the risk of out of synchronism reclosure, where the reclosing occurs at a time when either the frequency, voltage magnitude or voltage phases of the separated network are different from the grid. Out of synchronism reclosure may cause overvoltages, overcurrents and severe torque transients, which subsequently put rotating machines and other equipments that are connected to the network at risk [20, 21]. It also may result in mal-operation of protection system, leading to nuisance tripping [15].

2.4 Current Practices to Prevent Islanding

Owing to the risk of islanding outlined in the previous section, it is not favourable to operate an islanded part of network isolated from the main utility supply. In UK, the Electricity Association's Engineering Recommendation G59/1 has set out regulations that require the immediate disconnection of all DG units connected to the islanded section of the utility network and remain disconnected until the normal grid supply is restored [19]. In order to meet this requirement, dedicated protection to correctly detect islanding and automatically disconnect the associate DG is needed. Typical

protection configuration for DG embedded in distribution network is illustrated in Figure 2-2. [23].

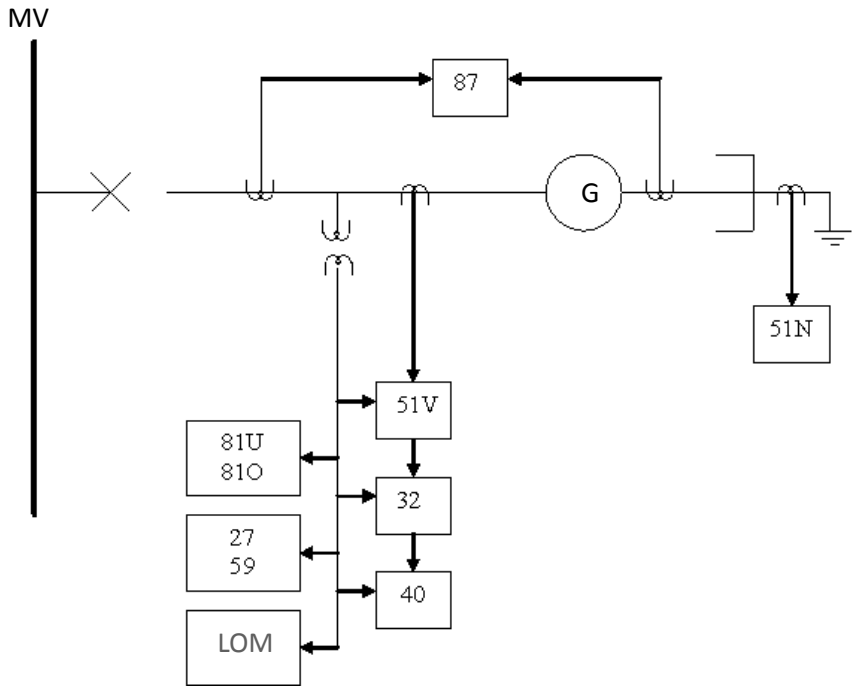

32 : Reverse Power
40 : Loss of Excitation
87 : Differential Protection
81U/810 : Under/Over Frequency
27/59 : Under/Over Voltage
LOM : Loss of Mains Protection
51V :Voltage-controlled Time-delayed Overcurrent
51N : Earth Fault Time-delayed Overcurrent

Figure 2-2 Protection Scheme for a Distributed Generator

The loss of mains protection seen in Figure 2-2 is responsible for the islanding detection. The basic requirements for this detection scheme are:

a) Dependable

The scheme must be able to detect all islanding events, taking into account that the behaviour of each island can be very different from the others.

b) Secure

The scheme must not respond to events or disturbances in the system other than islanding. Failure to comply with this requirement may cause the disconnection of DG unnecessarily.

c) Fast

The scheme has to detect the islanding occurrence within a required time frame. The main concerns here are to prevent out of synchronism reclosing and to reduce the period of islanding operation, consequently, minimizing the risk to utility maintenance personnel. An auto-recloser typically recloses after a time delay of about 3 to 30 second. Hence, the anti-islanding scheme must be able to trip the associate DG units before the reclosing happens. The typical islanding detection time recommended by G59/1 is 0.5 seconds [19]

2.5 Review of Islanding Detection Techniques

Before adopting a loss of mains protection, it is important to consider the characteristics of the DG unit. Generally, there are two types of DG – rotating machine based DG and inverter based DG. Rotating machine based DG can be either synchronous generator or induction generator whereas inverter based DG comprises PV panels, fuel cells, micro turbine, etc [16].

Among these, loss of mains protection for synchronous distributed generator is seen as the most challenging task faced today. This is due to the limited options available to control the usually large power rating generators to facilitate islanding detection [16].On top of that, synchronous generators are highly capable of sustaining an island, which only serve to worsen the situation [16].

Considering the importance of loss of mains protection for synchronous distributed generator, the remainder of this chapter will focus on the main anti-islanding techniques.

As shown in Figure 2-3, anti-islanding scheme can be broadly classified into two categories according to their working principle: communication based methods and local detection methods. Local detection methods can then be further divided into passive and active methods. The operation and performance of these techniques are described and assessed in the following section.

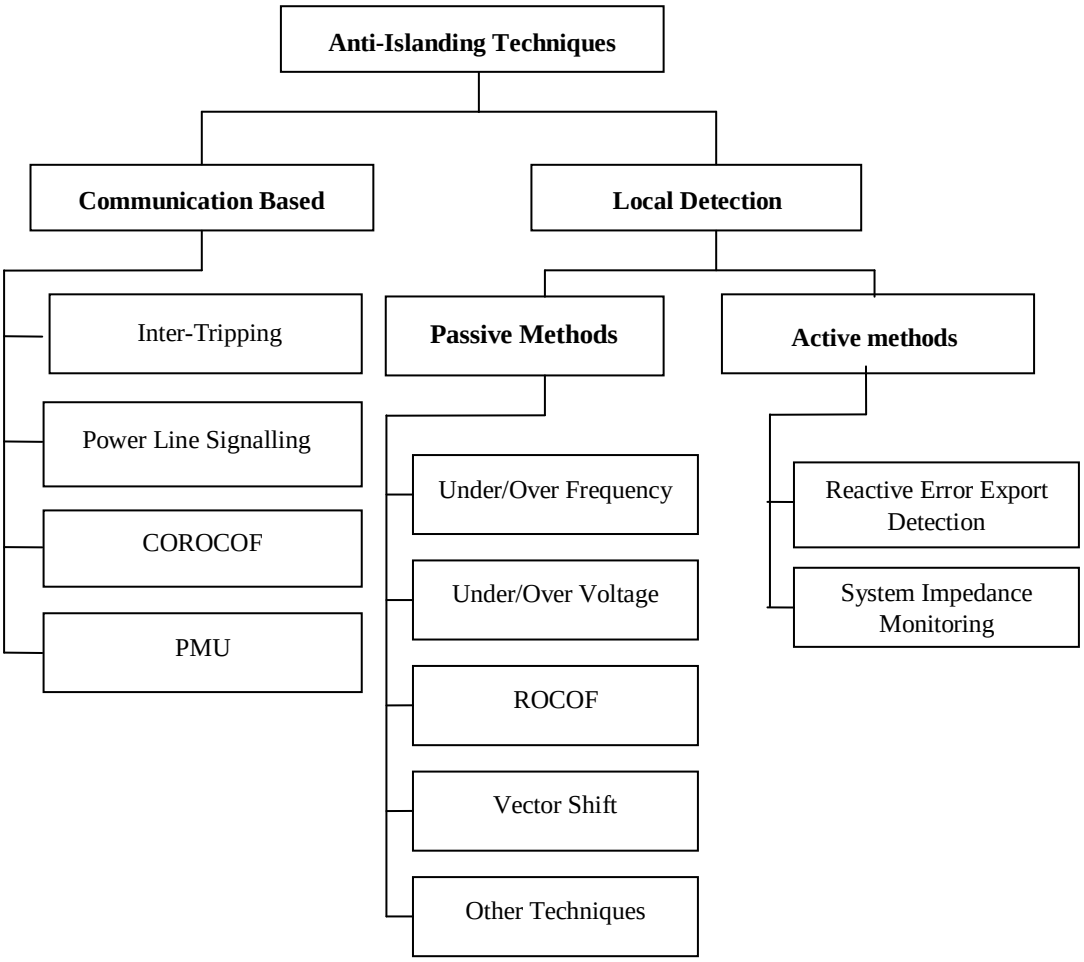

Figure 2-3 Classification of Anti-Islanding Techniques

2.5.1 **Communication based Techniques**

Communication based techniques rely on telecommunication to alert and trip DG units when islands are detected. Their performances are independent of the type of DG involved. They do not have issues on non-detection zone and are therefore very

reliable for islanding detection. However, these techniques tend to be very costly to implement, particularly on small DG units, rendering them less attractive compared to local detection techniques.

Considering the current pace of development in the field of communication, it is foreseeable that more affordable means of communication will be available in the near future. This is extremely beneficial to the development of anti-islanding schemes. Nevertheless, if the communication system fails, so does the loss of mains protection. Hence, reliability is another important issue that needs to be taken into consideration.

2.5.1.1. **Inter-Tripping Scheme**

This scheme utilizes communication links between two or more nodes in the system to ensure that DG units are correctly disconnected in response to loss of mains detection [15]

An inter-tripping scheme, also known as transfer trip [22], works on the basis of monitoring the status of all the reclosers and circuit breakers that could result in islanding of DG in a distribution system [15, 16]. When a switching operation produces disconnection to the utility network, a trip signal will be sent to the respective DG units in the islanded areas. This signal is usually direct acting, without any local checking or qualification. For example, in Figure 2-4, if a fault occurred at point A, protective device trips CB_A and a trip signal is sent to initiate the opening of circuit breaker of DG. This prevents the occurrence of islanding zone 1.

The concept of this scheme is very simple and direct. Nevertheless, it relies very much on a dependable medium to transfer the trip signal over long distances (up to 50km – the normal limit of 11kV and 33kV circuits) [15]. The possible mediums suitable for these tripping signals are leased telephone line, radio or microwave and hard wire. Among these, leased telephone lines and radio communication are the most commonly employed mediums [16].

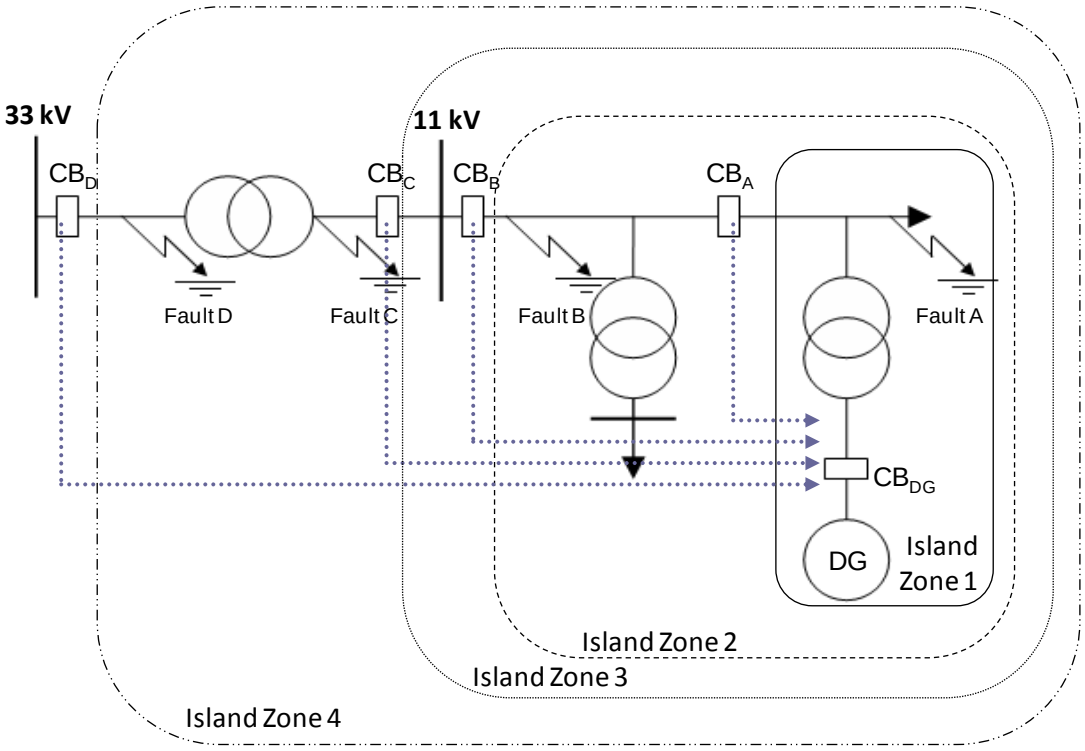

Figure 2-4 Inter-tripping Scheme

a) Leased Telephone Line Based Inter-Tripping Scheme

Figure 2-5(a) shows an inter-tripping scheme using a leased telephone line as medium. A leased communication channel is essentially a private analogue channel on a public telephone network with a bandwidth range of 3-4 kHz. Two different (variable frequency) tones are used to indicate a change in the status of a circuit breaker or recloser. This helps to provide greater security and resistance from noise. Information contained in the tone changes are then encoded and decoded by the interface units located at each end. Due to the high speed operations of these interface units; a short tripping time of approximately 20 milliseconds is possible. The system constantly monitors the communication link and will generate a Supervisory Control and Data Acquisition (SCADA) alert if it is out of service. However, it needs to be noted that this medium may not be reliable in rural areas [15].

b) Radio or Microwave Based Inter-Tripping Scheme

The radio or microwave based inter-tripping scheme, as illustrated in Figure 2-5(b), works on a similar principle as a leased telephone line scheme. The only difference is

the medium involves electro-magnetic radiation and the data is usually in digital format. Radio signals are sent to DG units constantly and absences of signals are considered as the opening of the associated circuit breakers [15]. The transmission coverage of this scheme is restricted by atmospheric attenuation and line of sight. [15]

c) Optical Fibre or Copper Based Inter-Tripping Scheme

Figure 2-5(c) shows the inter-tripping scheme using hard wire such as copper or optical fibre. Copper wires may exist in the form of pilot cables, either strung underneath power lines or buried with power cables [22]. They can be used as inter-trip medium. The main concerns are the induced voltage and the necessity for proper termination and insulation design [22].

Optical fibres may be retrofitted to power lines, providing immunity for the communication system against induced voltage. The bandwidth available using optical fibres are much greater than that required for inter-tripping scheme. Hence, it is normal to use the standard voice frequency (vf) signalling equipment, multiplexed on the fibre optics with other signal (voice, data and control) [22].

In general, due to the high cost, optical fibre or copper based inter-tripping scheme is not likely to be a primary resort for anti-islanding purpose. It will only be cost-effective when other communication requirements are present and other techniques are not feasible.

As an inter-tripping scheme monitors the circuit breaker status directly and does not operate based on electrical parameter measurements, it does not suffer from non-detection zone. It can be very straightforward and effective for anti-islanding purposes in distribution feeder with fixed topology. Moreover, this scheme enables the utility to have additional control on DG units, which helps to improve the coordination between them.

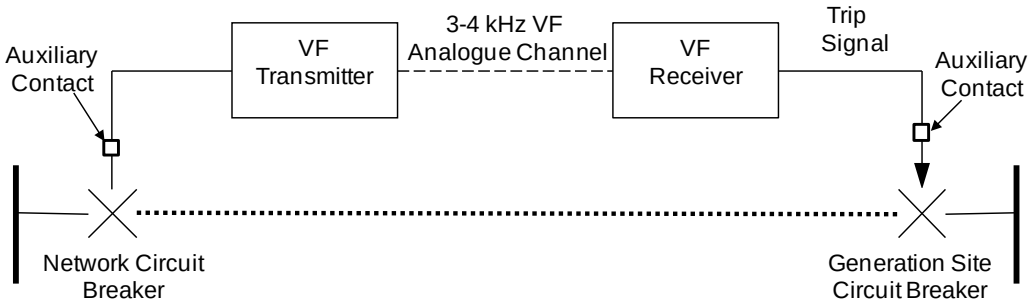

(a)

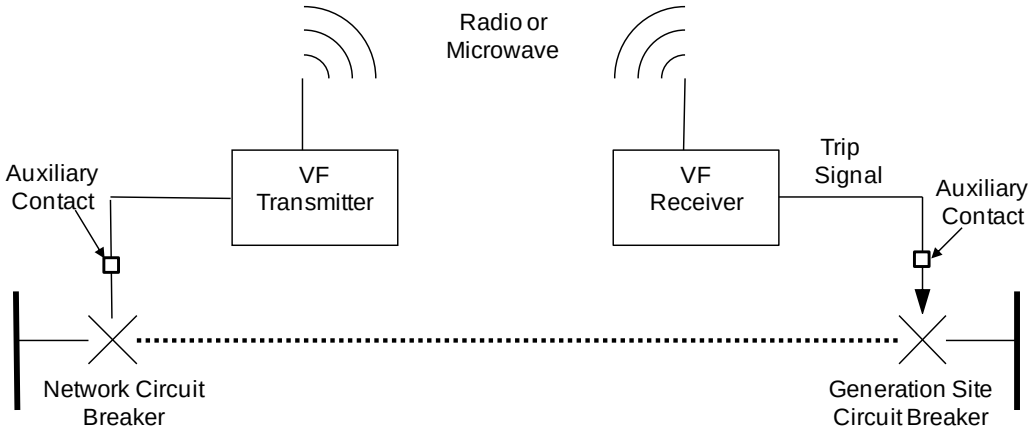

(b)

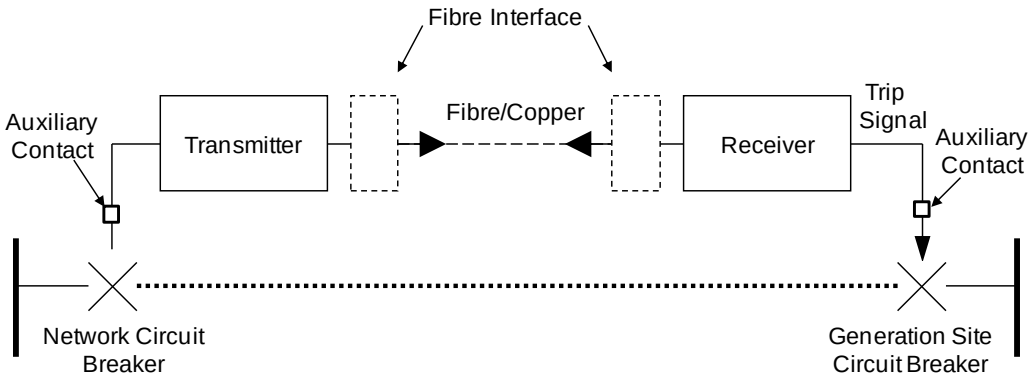

(c)

Figure 2-5 Mediums of Inter-tripping Scheme: (a) Leased Line (b) Radio/Microwave (c) Fibre/Copper Cable

However, the implementation of inter-tripping scheme can be quite complicated if the feeder topology changes. Figure 2-6 illustrates a common situation where topology changes due to feeder reconfiguration. Initially, DG2 is connected to

substation 1 and all the reclosers associated with this substation needs to be monitored. If due to certain operating scenarios, the normally open point is reconfigured from switch B to A, DG2 will be transferred to substation 2. When this happen, the potential island zone is changed and hence, inter-tripping must be similarly reconfigured and reclosers associated to substation 2 should now be monitored to correctly determine the islanding status of DG2.

The potential complexity of this scheme if the network topology varies is clearly observed. A centralised monitoring system may be required to determine the location of islands and the DG units involved to reliably implement this scheme [15].

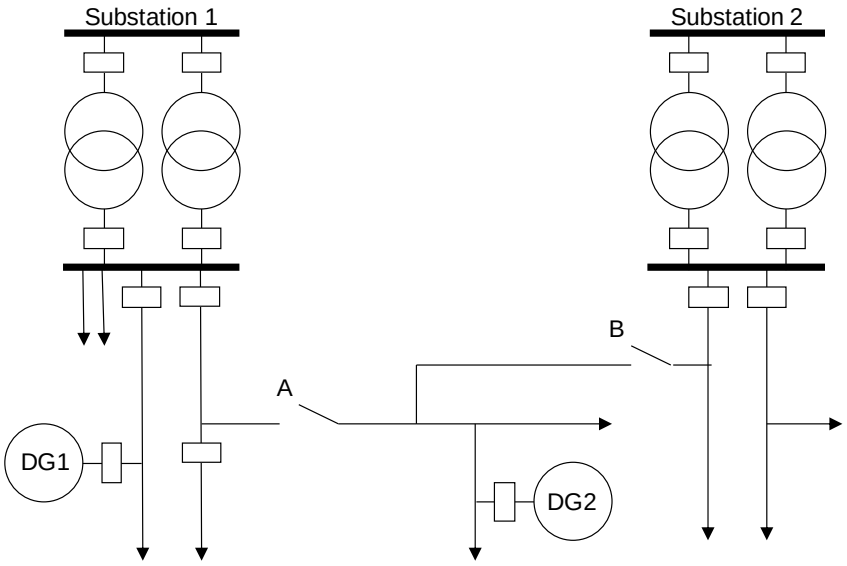

Figure 2-6 Network with changeable feeder topology

In addition, communication coverage must be available for all DG locations as signal transmitters are needed for all possible island disconnecting points to reliably detect islanding occurrence. Hence, if the radio coverage or telephone line or fibre cables are not readily available in the distribution network, implementing inter-tripping scheme may be considered very costly. [15]

Inter-tripping schemes can be very effective for networks with fixed topology. However, the high cost involved and the potential complexity with changeable topologies make this scheme less attractive.

Power line signalling is an alternative that utilizes power line as a signal carrier to overcome the aforementioned changeable topology problem.

2.5.1.2. **CETC Power Line Signalling Scheme**

This scheme is very similar to above-mentioned inter-tripping scheme except that it utilizes the power line as the medium, as shown in Figure 2-7. It is hence, sometimes regarded as part of the inter-tripping scheme [22]. However, unlike those techniques, in which signal transmitters are needed for every possible disconnection points in the network, this scheme only requires one signal transmitter. The transmitter, a signal generator, is connected to the secondary side of the utility's substation bus. It continuously broadcasts a low energy signal to the signal receiver at each DG, through the power line connecting them. Failure to sense the signal will be regarded as islanding condition and result in immediate tripping of the DG units. [16]

Since the signal is transmitted along the power line, there is no need to worry about the feeder topology change (Figure 2-8). Besides, signal generator is available at each utility's station, thus this scheme will still be feasible if DG switches to a different substation [15].

Moreover, the signal generator is equipped with several auxiliary inputs. Any one of these inputs can stop the signal broadcast, resulting in tripping of respective DG units. This feature enables the control of DG units operation by the utility companies [16].

This scheme can be a very reliable method for prevention of islanding. However, the high cost associated with the signal generator and its installation may make this scheme unattractive, especially when there are only a few DG units sharing this service. Also, issue on the possible interference of the signal with other power line

communication applications such as automatic meter reading needs to be considered [16].

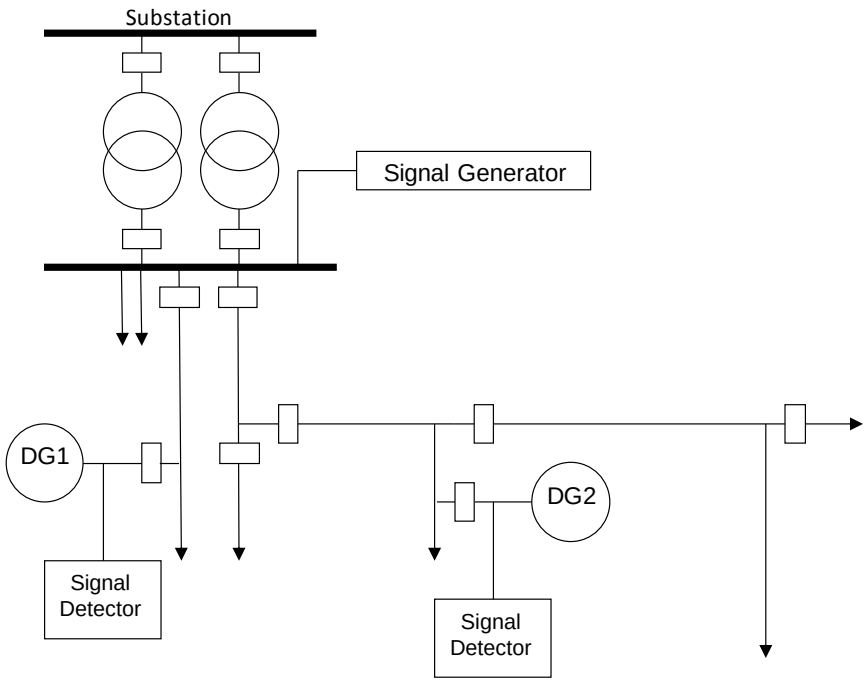

Figure 2-7 Power Line Signalling Scheme

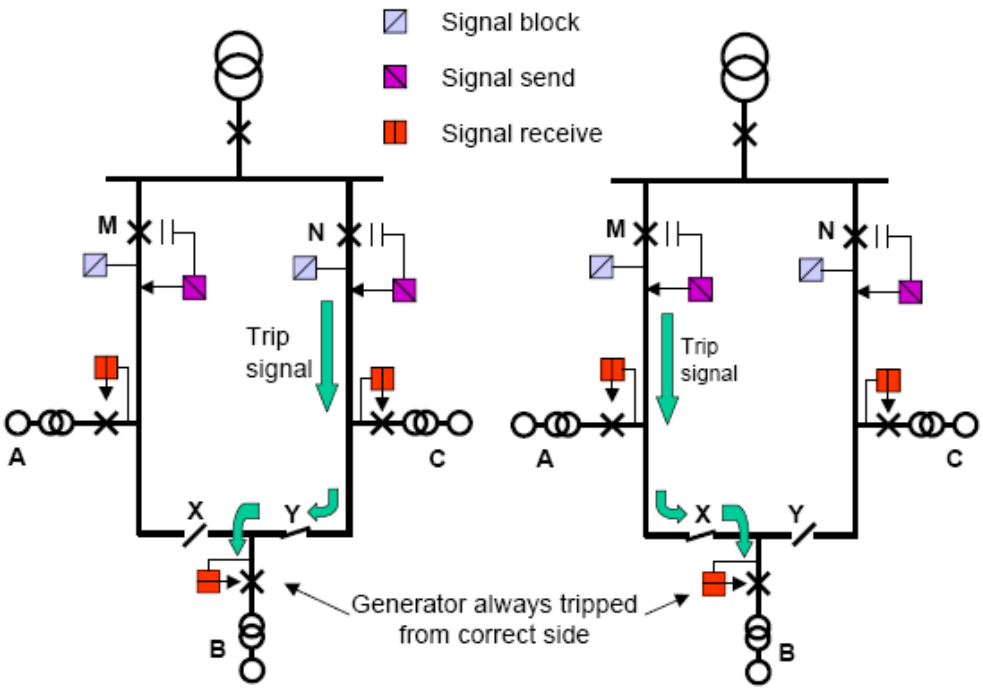

Figure 2-8 Operation of Power Line Signalling [22]

2.5.1.3. **COROCOF**

This method compares the frequency changes at two locations in the network. At the substation, the rate of change of frequency is measured and a block signal is sent to the DG if the value has exceeded the predetermined value. At the DG site, the rate of change of frequency is also measured. When a frequency change exceeding the threshold is measured while no signal is received from the substation, the DG will be tripped. This method provides immunity to the wide-area frequency change resulting from bulk generation failure or faults [23, 25, 26].

2.5.1.4. **Phasor Measurement Units (PMU)**

This scheme comprises two phasor measurement units (PMU), one installed at the utility substation and the other at the DG site, as shown in Figure 2-9.

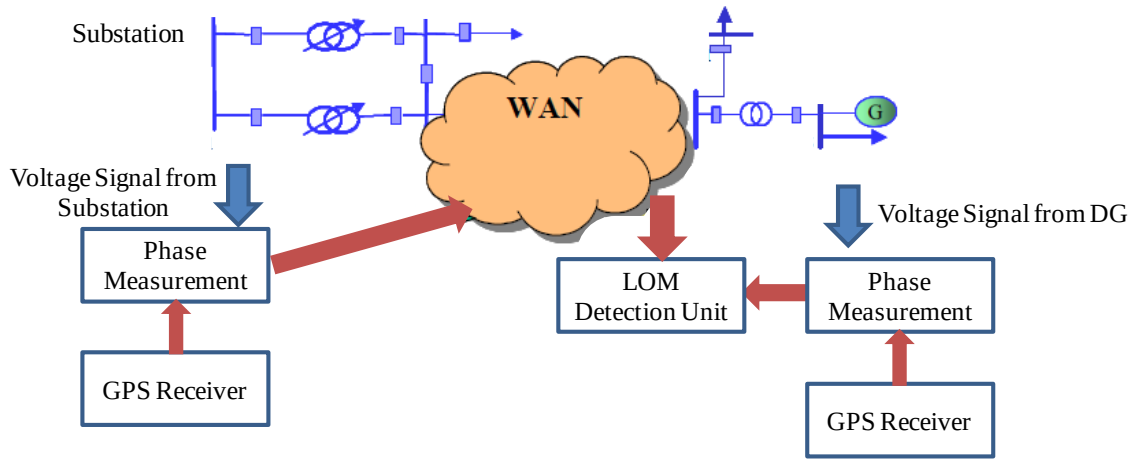

Figure 2-9 Phasor Measurement Units Detection Method

PMU located at the utility substation measures the utility's voltage phase angle with respect to Global Positioning System (GPS) time stamp. This information is then sent to the receiver at the DG site via certain communication medium. By using this information and the measurements available from the DG's site PMU, the LOM detection unit then calculates the voltage phase angle difference between the DG and utility substation. The calculated result is then compared with the initial phase angle

difference. If the resulting value exceeds the preset threshold setting, a trip signal is initiated (equation (2-1)). [27,28]

$$\Delta\theta = \left|\theta_{SG} - \theta_{SG_0}\right| > \theta_{threshold} \quad (2\text{-}1)$$

where θ_{SG} = difference between the DG terminal voltage and the utility substation voltage

θ_{SGo} = the initial phase angle difference

$\theta_{threshold}$ = threshold setting for islanding detection

In order to eliminate the phase error caused by change of network topology, the initial phase angle difference is periodically updated during steady state [27, 28]. As this scheme compares the relative angular difference between the current state and the initial state, it is immune to the phase shift due to transformers connected between the two measuring points.

To further enhance the stability of this scheme during network faults, [27] incorporated under-voltage interlock feature into the scheme. If the terminal voltage of the DG or substation drops below a predetermined value, the tripping signal from the LOM detection unit is blocked.

PMU is employed in this scheme for its capability in providing time-stamped voltage phasor from all three phases. Positive sequence phasor can then be calculated from these measurements. [27] and [28] suggested the use of positive sequence phasor for this scheme due to the less influence from faults on positive sequence phase angle compare to single voltage phase angle. An added advantage from using positive sequence phasor is the reduced data transfer requirement [57].

The synchrophasor standard, IEEE Std C37.118-2005 [116] defines a standard information structure for data transmission to facilitate the real time comparison of measurements from two different PMUs. However, when comparing measurements between PMU of different vendor, it is essential to know how the measurements were taken by each PMU [57]. This is because they may be using different sampling

window or measuring algorithm that will lead to slightly different results. Besides, the time stamp could be made at any point in the sampling window, which can lead to a steady state error between the measurements of PMU using different schemes [57]. To avoid this, IEEE Std C37.118-2005 outlines certain requirements on how to precisely measure the phase angle with respect to the coordinated universal time (UTC). However, it does not specify what measuring algorithm to use. Yet, the standard does specify the Total Vector Error (TVE) allowed in evaluating the phasor to allow interoperability between PMUs of different vendor [116-117].

In this scheme, the geographical distance between the reference PMU (installed at utility substation) and the DG's PMU could be more than several 100 km. Therefore significant communications delay is anticipated when transmitting time-stamped phasor measurements in real time. The extent of this delay depends upon the communication medium employed, which can be either dedicated or shared.

2.5.2 **Passive Methods**

Passive methods detect loss of mains by monitoring the changes in locally available system parameters [20]. Its operating principle is based on the assumption that a loss of mains will result in a measurable deviation in the system parameters, i.e. voltage or frequency [21]. Hence, the abnormal operation of DG can be detected by monitoring the variation of one or more of these parameters [15]. The main advantage of these methods is they do not directly interact with the system operation, and thus do not give rise to the power quality issues. Besides, communication is not required to build up the detection system, making them cost-attractive options. However, the downside of these techniques is they suffer from a non-detection zone.

2.5.2.1. **Under/Over Frequency**

During normal operation, DG runs in parallel with the utility grid and the frequency is relatively constant. When islanding happens, load and generation in the formed island are rarely exactly matched, resulting in changes in frequency. Hence,

frequency out of limits can be used to indicate islanding. The threshold setting must be out of the range of statutory limits. In UK, the recommended settings for under frequency and over frequency are 47Hz and 50.5Hz respectively [22].

In UK, G59/1 outlined that once the measured frequency falls outside the defined limits, a DG has to be tripped off within 0.5 seconds [19]. However, since the frequency changes relatively slowly and not instantaneously, this scheme may be rather slow in islanding detection. Furthermore, this method relies on a large power mismatch to drive the frequency out of the predetermined limits. Lack of sufficient sensitivity, a big non-detection zone can exist which could increase the likelihood of island formation [15]. Due to these drawbacks, under/over frequency relays are normally only used as backup protection for islanding detection.

2.5.2.2. **Under/Over Voltage**

Voltage is another parameter commonly employed to detect islanding event [15]. Similar to the former relays, under/over voltage relays work based on the assumption that there is always reactive power mismatch in the formed island. This unbalance leads to a change in the voltage level – surplus of reactive power will drive up the voltage and vice versa. Hence, it can be an indicator of islanding. The voltage changes relatively faster than frequency since there is no mechanical 'inertia' associated with it [15].

The threshold setting for under/over voltage relays must be outside the statutory voltage limits. The standard settings used in the UK are ±10% of the nominal voltage [23]. Once the voltage goes beyond these limits, the DG has to be tripped off in 0.5 second.

However, this method is affected by many other network disturbances, which can result in unwanted tripping. An example is the mass tripping of DG by under voltage relays in Western Denmark due to faults in the high voltage transmission grid [15]. Besides, it can be hard to determine islanding under the circumstance where

generation and load are closely matched. Island may sustain until the load or generation variation drives the voltage out of limits.

2.5.2.3. **Rate of Change of Frequency (ROCOF)**

This is the most commonly utilized method to detect the unintentional islanding. It relies on the assumption that there is always an imbalance between the generation and load in the formed island [15, 23]. Immediately after islanding, the resulting power imbalance will cause a rapid change of frequency which, neglecting the governor action, can be approximated by the following equation: [15, 29]

$$\frac{df}{dt} = -\left(\frac{P_L - P_G}{2H \times S_{GN}} \times f_r \right) \tag{2-2}$$

Where P_G = Output of the distributed generator

P_L = Load in the island

S_{GN} = Rated capacity of the distributed generator

H = Inertia constant of generating plant

f_r = Rated frequency

It is worth to note that this approach only considers the frequency change due to islanding and does not take into account the effect of fault. [15]

As illustrated in Figure 2-10, the relay is initiated if the corresponding frequency slope (df/dt) exceeds the threshold setting, and vice versa. Typical pickup values for ROCOF relays operating in a 50Hz power system range from 0.1Hz/s to 1.0Hz/s [29]. This setting depends on the strength of the system, the weaker the system, the higher the setting [15]. In the UK, the recommended ROCOF relays settings are 0.125Hz/s, whilst in Northern Ireland, the settings are 0.45-0.5Hz/s [30]. The ROCOF relays operating time vary from 0.2 to 0.5 seconds, depending on the measuring periods the relays adopted. The minimum and maximum number of measuring periods is normally two (40ms at 50Hz) and 100 (2s at 50Hz) respectively [29].

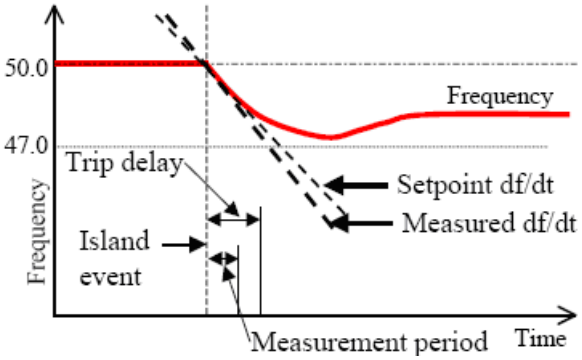

Figure 2-10 ROCOF Detection Method [22]

ROCOF is generally being considered as a sensitive and dependable method for detecting loss of mains on a distribution network. However, this relay will fail to detect islanding when the power mismatch in the formed island is small.

In addition, there are several reports on mal-operation of ROCOF relays. ROCOF fails to discriminate between actual islanding and other network transient events [16, 31], resulting in nuisance tripping and directly jeopardizing the system's integrity. In the UK, major loss of bulk generation and uncontrolled tripping of transmission lines could result in a df/dt of around 0.16 Hz/s and these events can happen quite often [15, 30]. An extremely rare case can cause a df/dt up to 1Hz/s [15]. Under those cases, DG units might be incorrectly disconnected by ROCOF using the current recommended threshold setting [15, 29].

Besides, it is reported in [32] that commercially available ROCOF relays from different manufacturers respond rather differently to the same event, even when they are configured with the same settings. This phenomenon is most likely due to the different techniques employed by those relays.

In general, ROCOF is considered as a viable option for islanding detection. However, this relay suffers from non-detection zone and cannot provide effective protection when the load-generation mismatch in the formed island is small. Besides, it can cause excessive nuisance tripping due to network transients, i.e. load switching, frequency excursion due to loss of bulk generation and network faults.

2.5.2.4. **Vector Shift**

Vector shift is also referred to as phase displacement or phase jump method [31]. It detects islanding by monitoring the phase angle changes of the voltage waveform.

During normal operation, DG runs in parallel with the grid and supplies part of the load. This is illustrated in Figure 2-11 where DG and grid are both represented as equivalent circuits, feeding the load. The synchronous electromotive force (E_f) will lead the terminal voltage, V_t of the DG by a rotor displacement angle φ, which is defined by the voltage difference between E_f and V_t, i.e. $\Delta V = I_G \times jX_d$ as shown in Figure 2-13(a). If the grid is suddenly disconnected by the opening of switch A (Figure 2-12) the generator will need to supply the entire load. This sudden change of load in turn causes a shift in the rotor displacement angle. The terminal voltage jumps to a new value, V_t' and the rotor displacement angle changes to a new value φ' as shown in Figure 2-12(b).

Figure 2-14 illustrates the situation in the time domain. The variation in rotor angle corresponds to a change in the cycle length, as depicted in Figure 2-14. A vector shift relay utilizes this principle and monitors the voltage angle change by measuring the variation in the duration between zero crossings on the voltage waveforms. The change of the present cycle duration as compared to the previous cycle is used to indicate the change of angle in the vector shift relay. If the variation of the angle exceeds a predetermined setting, this relay is initiated. Typical vector shift relays settings are in the range of 6^o-12^o [29]. Similarly, the setting depends on the strength of the system, i.e. a higher setting is suggested on a weaker system to avoid mal-operation during loads switching and vice versa [15]. Typical vector shift settings recommended by ETR 113 are 6^o for mainland UK and 10^o-12^o for Northern Ireland [30].

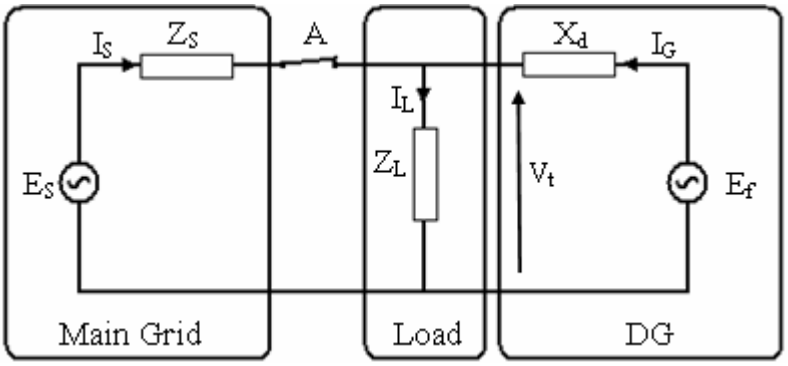

Figure 2-11 Equivalent Circuit of a DG Operating in Parallel with the Main Grid

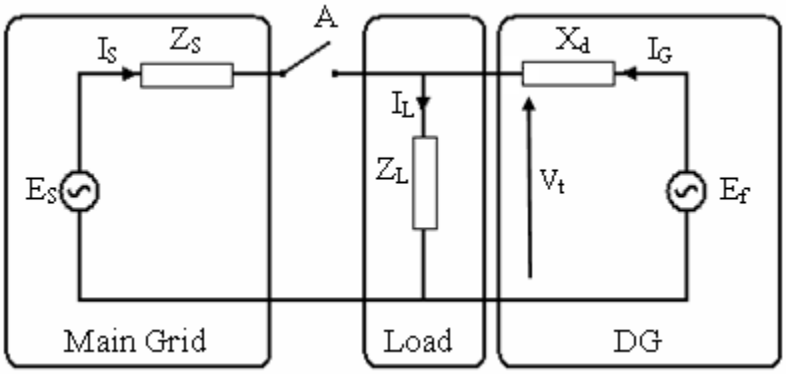

Figure 2-12 Equivalent Circuit of a DG Operating in Islanding Mode

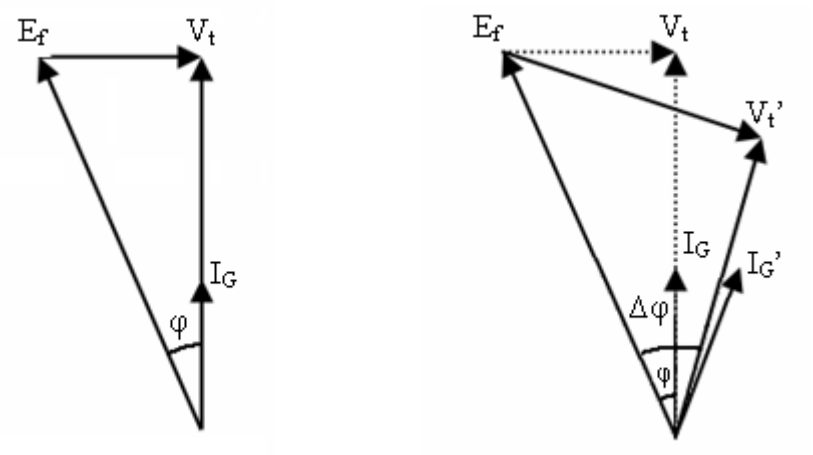

(a) (b)

Figure 2-13 Vector Diagram (a) before islanding (b) after islanding

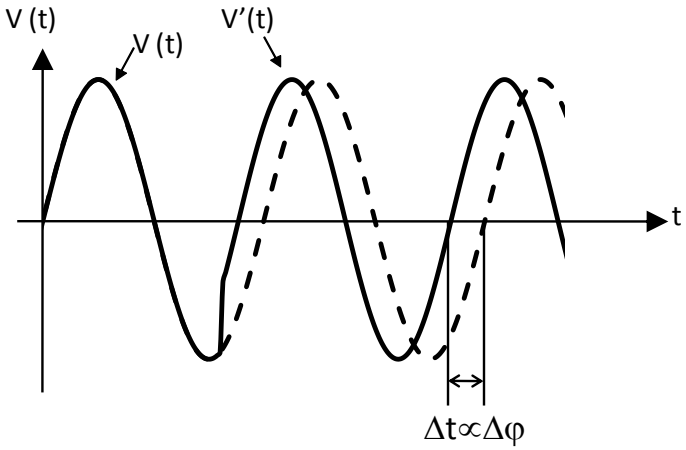

Figure 2-14 Voltage Waveform of DG at the Instant of Islanding

Due to the similarity of this relay with other frequency based relays, which is also based on measuring the cycle duration of the voltage waveform, it is also being categorized as a type of frequency based relay [16, 33]. And hence, like frequency relay, it suffers from non-detection zone when the generation-load mismatch in the formed island is very small.

Besides, it is aware that this relay is susceptible to network fault occurring on adjacent feeder. Other network transients, such as load switching events may also falsely initiate the relay [15]. The mal-operation of this relay has been reported in [32] and [34].

Increasing the threshold setting may help in reducing the false operation, but this will in turn compromise the sensitivity of this relay, making it vulnerable to non-detection zone. Compromise must thus be made between the dependability and sensitivity of the relay.

Equation to predict the performances of the vector shift relay has been developed in [35]. The relay's detection time can be approximated by

$$t = \frac{-(2\omega_o K(\alpha - \pi)) - \sqrt{D}}{2K^2(\alpha - 2\pi)} \tag{2-3}$$

Where

$$K = \omega_o \frac{\Delta P}{2H} \tag{2-4}$$

$$D = (2\omega_o K(\alpha - \pi))^2 - 4K^2(\alpha - 2\pi)(\omega_0^2 \alpha + 2\pi^2 K) \tag{2-5}$$

t is the duration of time

H is the machine inertia constant

α is the relay trip setting in radians

ω_o is the synchronous speed in rad/sec

ΔP is the per-unit power mismatch between generation and load at the instant of islanding

2.5.2.5. **Other Techniques**

i) Change of Power Output [39]

This method monitors the changes in DG's active power output. During normal operation, load changes will be supplied by the mains and not the DG. When islanding occurs, DG has to change its output to meet the load change. When this change exceeds a predetermined setting, a trip signal is initiated. It has a fast LOM detection capability (within 120ms) and demands a minimum of processing resources. However, due to the fact that frequency change is a direct consequence of active power change, this method is very likely to have similar performance as frequency-based relays [16]. In addition, this method is influenced by other disturbances (e.g. from the prime mover) [16] which could change the power output level, resulting in spurious tripping.

ii) Reverse Reactive Power [15, 16]

When running in parallel with the utility supply, a DG operates close to unity power factor and reactive power demand at that site is supplied by cable capacitance and imports from the utility (Figure 2-15(a)). Once islanding occurs, there will be a deficit of reactive power supply and the DG unit must now supply the reactive power

demand (Figure 2-15 (b)). In effect, there will be a reverse direction of reactive power flow at the DG inter-tie. A reverse reactive power relay measures the reactive power flow at each phase of the DG point of supply and will operate, after some time delay, when the reverse flow (i.e. reactive power flows towards the utility) in any phase exceeds the predetermined settings.

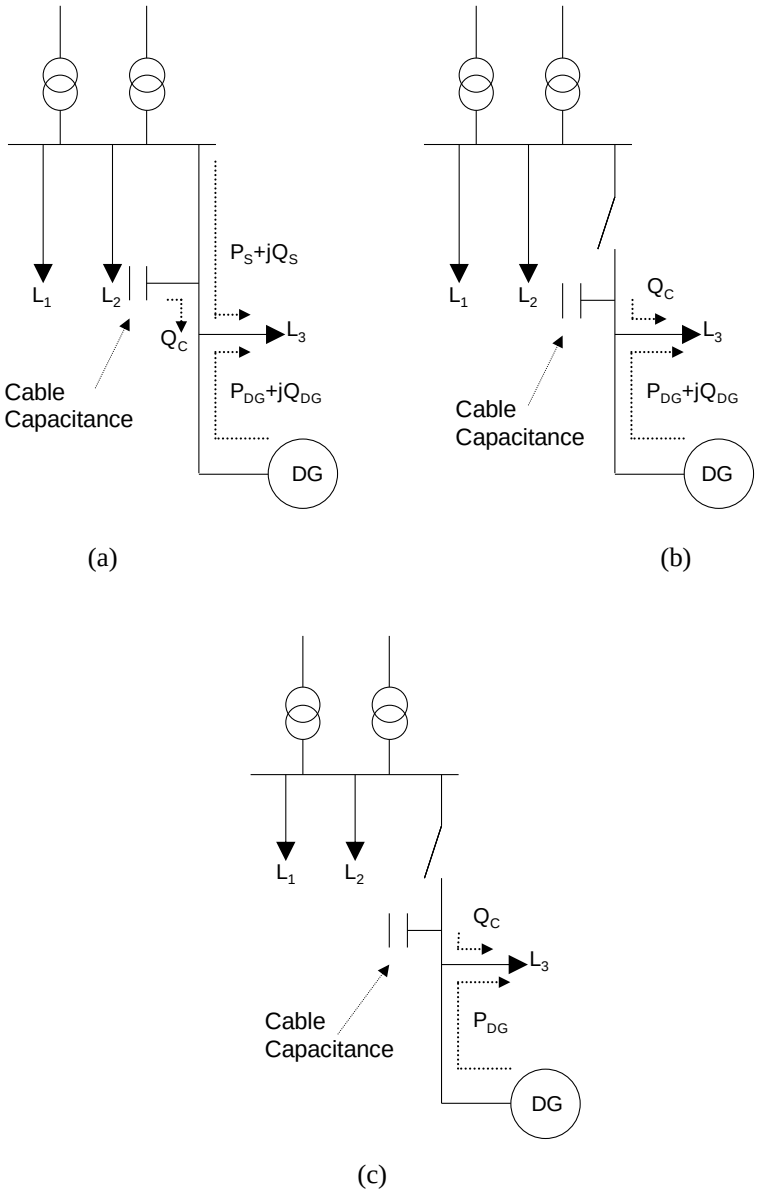

Figure 2-15 Reverse Reactive Power Scheme: (a) Running in Parallel with Grid (b) Islanded Operation (c) Islanded operation with cable capacitance

Reactive power change is a sensitive index and could have better performance than the voltage-based relay, especially in a low penetration application, considering that it takes far more reactive power change to result in a detectable voltage change.

This method is however, not feasible if the load reactive power demand is low and can be sufficiently supplied by the cable capacitance. This problem could arise if feeders have long cable and low load density (Figure 2-15 (c)).

iii) Elliptical Trajectories [31, 40]

This technique was developed based on the fact that whenever a fault occurs on a line, the corresponding voltage and current changes at the sending end, which can be described by an orbital equation, are related to each other by an elliptical trajectory. However, the trajectory's shape changes significantly when islanding occurs, enabling detection of islanding.

iv) Voltage Unbalance and Total Harmonic Distortion Technique (THD) [41, 42]

This hybrid technique operates based on the assumption that load in distribution level is usually unbalanced and different loading condition may give rise to different level of harmonic current. Hence, by monitoring the voltage unbalance at the DG terminal and the THD of the DG current can reliably distinguish loss of mains situation. The studies done in [41] shows that this technique is not affected by the variation of DG loading.

2.5.3 **Active Methods**

Active detection methods inject disturbances directly into the system and detect islanding condition based on the system's responses measured locally [16]. These methods are more reliable in detecting islanding as compared to the passive methods. The main downside of these methods is their interference on the power quality due to the direct interaction. There are also claims that the dependability of these methods

may be compromised with multiple penetration of DG these days [24]. Besides, too many injections of disturbances may very well drive the system into instability [9].

2.5.3.1. **Reactive Error Export Detection (REED) [15, 43]**

This relay interfaces with the DG's automatic voltage regulator (AVR) to control the DG's and generate a specific level of reactive power flow in the inter-tie between the local site and the utility grid. This condition can only be maintained when the grid is connected. Relay operation is initiated when the deviation between the desired reactive power and actual flow being exported persists longer than a specified time period.

A new approach [44] is to vary the internal induced voltage of the synchronous generator by a small percentage from time to time and monitor the changes of the terminal voltage and reactive power flow at the inter-tie between the DG site and utility grid. Islanding is detected when there is a large change in the terminal voltage at the inter-tie while reactive power flow almost remains unchanged [43]. The real and reactive power, P and Q supplied to the network from the DG unit can be calculated by:

$$P = \frac{|E_0||V_t|}{X_T} \sin\delta \tag{2-6}$$

$$Q = \frac{|V_t|}{X_T}\left(|E_0|\cos\delta - |V_t|\right) \tag{2-7}$$

Where

P = Real Power

Q = Reactive Power

E_0 = Field Voltage of DG

V_t = Terminal voltage of DG

δ = Power angle

X_T = Synchronous Reactance

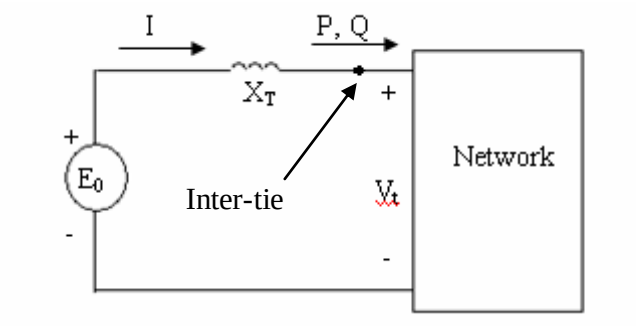

Figure 2-16 Equivalent circuit with DG unit

This scheme is very practical as its implementation needs to change the excitation system of the generator only [16]. Besides, the variation of the induced voltage magnitude is so small that it doesn't interact with the operation of the power system [44].

This relay is very effective in detecting islanding, even when there is no change in the generator's loading. However, the operation time of this relay is very slow, varying from 2-5 seconds, causing it to be considered only as back-up protection to other 'faster' anti-islanding systems. This relay is also not suitable for inverter-based DG system which operates at unity power factor.

2.5.3.2. **System Impedance Monitoring [45]**

When DG is connected in parallel with the utility supply, the system impedance seen at the DG terminal is dominated by the utility and hence is very small compared to the case when it is islanded. This scheme utilizes this fact and measures the changes in system impedance in order to detect islanding.

To measure system impedance, a method superimposing a small high frequency (HF) signal onto the voltage was proposed in [46] and [47]. This method employs a coupling capacitor connected at the DG terminal to inject HF signal into the system, as depicted in Figure 2-17. The system impedance is then computed from the voltage and current responses. When the DG and utility are connected, the impedance

Z_{DG}//Zs is low, therefore the HF-ripple at the coupling point is negligible. The impedance increases markedly to Z_{DG} after islanding, resulting in the derived HF signal to be detectable.

This relay operation is very fast and it is immune to nuisance tripping from network frequency transients. It does not suffer from non-detection zone due to small power mismatch level in the formed island. However, concern arises when there is more than one DG in the formed island. Interference among the disturbances injected by multiple generators may affect the effectiveness of this scheme. Cost is also an issue as this scheme requires a signal generator at each DG site [15].

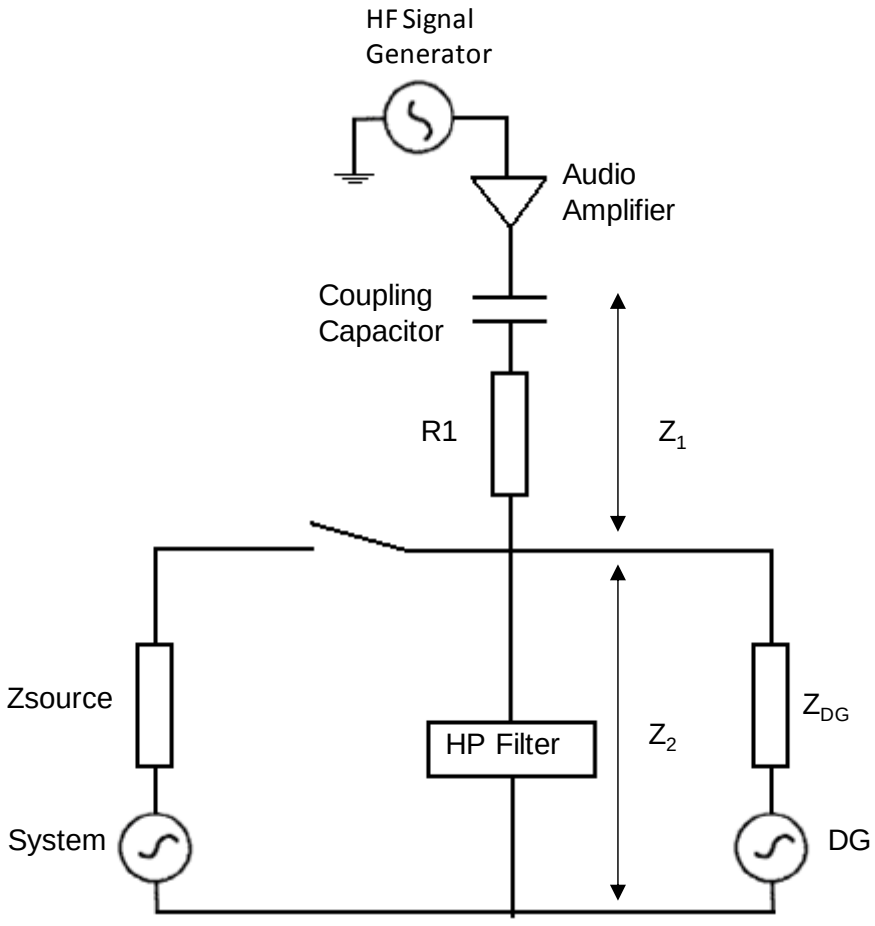

Figure 2-17 System Impedance Monitoring

2.6 Motivation for Islanding

For risk-free operation, it is perhaps easiest to disconnect all DG units connected the network that are separated from the mains to prevent islanding operation. This may be sensible, in meeting with technical and economical constraints, when the share of DG connected in the network is insignificant compared to the system total generation. However, as the installed capacity of DG increases, people start to view this matter in a different perspective [10-12, 36-37]. Although the challenges with respect to islanding operation remain, more and more people came to realisation of the potential behind operating DG during an islanding event.

In the past, the DG contribution to the system was so small that the generation and load mismatch upon islanding was often so significant till the point that an islanded system was inoperable. This is however no longer the case as the DG penetration into the network grows. Upon islanding, DG capacities are comparable to the load demand in the islanded network, and with appropriate controls, are capable of keeping the island frequency and voltage within statutory limits.

This serves as a big motivation to keeping DG online after fault isolation as it is not sensible to disconnect them when they are able to sustain the island and keep the voltage and frequency within permissible limits.

Besides, allowing islanding operation also helps to reduce customer interruption and consequently improves the reliability of the distribution networks. This serves as the second motivation and seems logical against the alternative of blackout after part of the network separation from the grid.

Nevertheless, for islanding operation to be widely accepted and adopted, technical issues mentioned in section 2.3 must first be resolved:

Power quality – The voltage and frequency in the island must be regulated within the permissible statutory limits. With proper control implementation, this issue is not hard to counter.

Personnel safety - Operational procedures can be introduced to prevent maintenance workers and member of public from safety risk when islanding operation is allowed.

Earthing – Unearthed operation during islanding is dangerous and thus prohibited. Several methods are useful in introducing earth to the islanded network, as described in [22, 48, 49].

Out-of-synchronism reclosure – This is perhaps the most critical among the technical challenges associated with islanding operation. One of the possible solutions is to include sync-check relays at the point of common coupling between the islanded network and the grid. This however defined the possible islanded areas. To increase islanding operation flexibility and allowed larger scale of islands to form, sync-check relays would need to be installed at every possible point of common coupling and proper control methods are needed for the synchronisation between the two systems. Obviously, this method involves considerable cost.

An alternative is to hold the islanded network in synchronism with the grid throughout the islanding operation. This novel scheme, in which the author refers to as synchronous islanded operation, provides maximum flexibility for island to form, enabling the operation of islanded network without the risk of out-of-synchronism reclosure.

2.7 Synchronous Island

Prior to reconnecting an island to the grid, it is important to make sure that the three-phase voltage waveforms for both systems met the following requirements: [50]

i) voltage amplitudes are equal
ii) frequencies are the same
iii) phases are equal, i.e no phase difference
iv) phase rotation (sequence) is equal

The fourth requirement is usually checked during installation while the first three requirements must be controlled with the typical tolerances shown in Table 2-1 [18, 30, 51, 52]

Table 2-1 Typical Limit for Synchronisation

	IEEE std 1547-2003 [18]	**ETR 113 [30]**	**Maximum Limit [51]**
	1.5-10.0 MVA	**Typical Relay**	
Phase difference( )	10	20	30
Slip Frequency (Hz)	0.1	0.22	0.4
Voltage difference (p.u.)	0.03	≤ 0.1	0.2

By applying appropriate governor and AVR control, it is not difficult to stay within the synchronisation limits (Table 2-1) and meet the top two requirements. Figure 2-18 shows the voltage, frequency and phase deviation of an islanded network in response to a load disturbance.

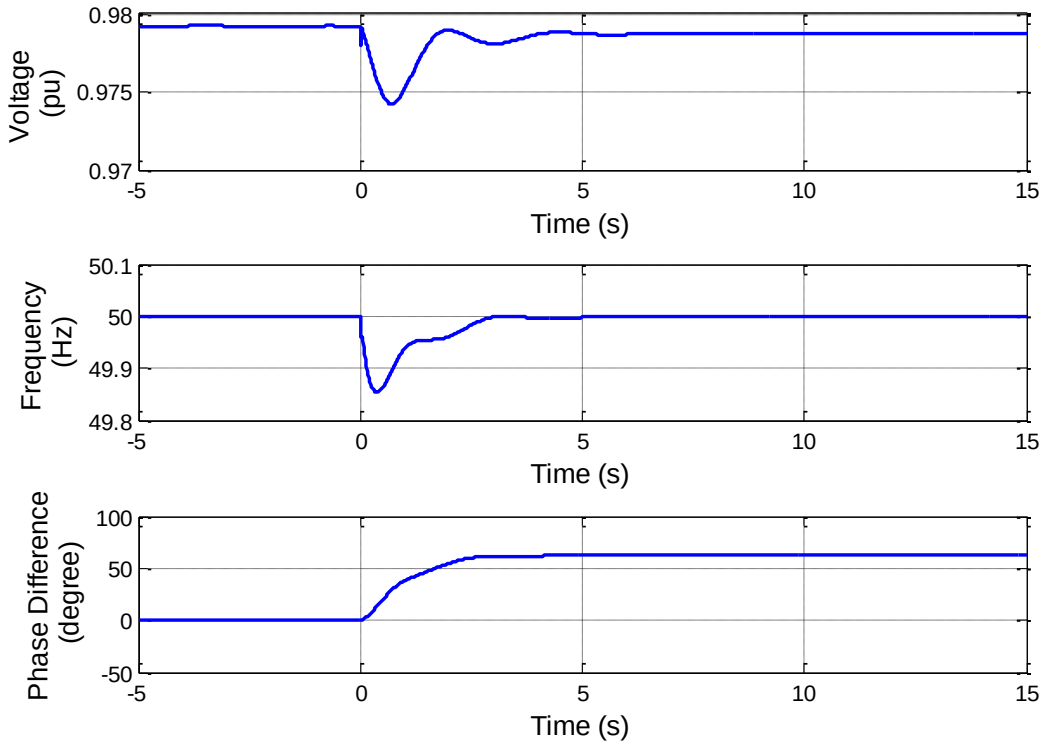

Figure 2-18 Island responses following load disturbance: (a) voltage response (b) frequency response (c) phase deviation

As observed from the figure, even though the frequency and voltage of the island are restored within recommended synchronisation limits, there is a constant phase deviation between the two systems. Clearly, there is a risk of out of phase reclosing when reconnecting the island to the grid.

A novel control algorithm is proposed in [1-3] to deal with this problem. This method proposes a supplementary phase difference control to be added to the DG governor's control, concurrently controlling the frequency and phase of the islanded system. This method requires a reference signal containing frequency and phase to be transmitted from the grid to the DG for computation of control signal. The same load disturbance study that resulted Figure 2-18 is repeated, but with phase difference control added to the generator's governor. Figure 2-19 illustrates the effectiveness of the phase deviation regulation.

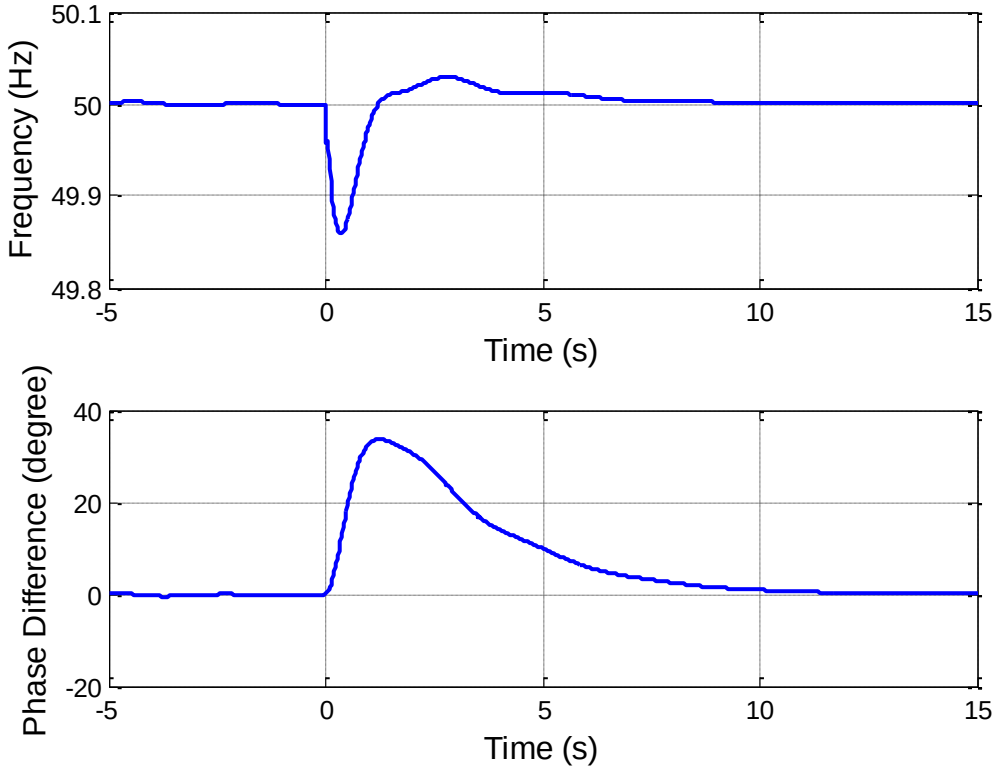

Figure 2-19 Synchronous Island responses following load disturbance: (b) frequency response (c) phase deviation

Robert Best [57] further demonstrated the practicality of this method by performing extensive laboratory experiments on a single diesel generator island network. Satisfactory and correlated results from both simulation and practical experiments ascertain the feasibility of the proposed method in forming stable island without the risk of out-of-synchronism reclosure.

Nevertheless, the investigation had mainly concentrated on the application of this method on a single synchronous generator-based island. With the increasing penetration of DG into the network, it is necessary to investigate how the proposed control performs in a multiple-unit island.

It should also be recognised that not all islanded DG units will have the advantage of the proposed method. It is hence important to establish the effect of those generators has on the proposed phase control. To make matter worse, these generators may be constituted of different type of generation, which is not uncommon at distribution network. In some cases, if not most, they may even have highly variable output.

Robert Best [57] has also shown that contrary to current practices (Table 2-1), phase differences of $\pm 60^{o}$ should be acceptable for synchronisation of DG with a robust construction. As such, this value is taken as benchmark for the work carried out in this thesis.

2.8 Chapter Summary

This chapter has provided a basic introductory to power system islanding operation. The risk associated with islanding operation is discussed in detailed, followed by the current approaches use to deal with islanding. A detail review of the common islanding detection techniques is given. Two major categories of loss of mains detection techniques have been identified, with each having their distinctive benefits and drawbacks.

Currently, in the event of islanding detection, loss of mains protection will send out a signal to trip the DG. However, increasing connection of DG into the network coupled with improved capability of DG in sustaining an island has started to raise question on this practice. Continual operation of DG during islanding is clearly an added benefit offered by DG and disconnecting it unnecessarily during mains failure is clearly limiting this potential. Nevertheless, this move is not completely incomprehensible, judging from the risk related to the islanding operation. Hence, initiatives that can support islanding operation, negating the need to disconnect DG, and at the same time able to prevent the risks associated with this operation is required. One of such schemes that seem promising has been singled out and reviewed.

CHAPTER 3

PROBLEMS WITH EXISTING LOSS OF MAINS (LOM) PROTECTION SCHEMES

3.1 Introduction

To date, the ROCOF relay is the most commonly employed loss of mains detection technique, owing to its simplicity and low cost. It operates based on the assumption that most island formation will not have a balance between generation and load, which will result in measurable changes in the system frequency. Hence, by monitoring the frequency changes, island formation can be detected. However, with the increasing number of distributed generators (DG) connected into the distribution network, this assumption may not be valid for all circumstances. Thus, its application can be a problem when the load and generation are closely matched in the formed island.

In addition, this scheme is also often criticized for its nuisance tripping. It is unable to reliably discriminate between a real islanding event and some system transient events, resulting in unnecessary disconnection of DG. Thus, in this chapter, extensive simulations have been done to investigate the operating performance of ROCOF relay in a bid to understand and identify its weaknesses.

As DG penetration into the distribution network grows, it has become increasingly common to have multiple DG units, and subsequently LOM detection relays, connected to the same feeder. Therefore, simulations are carried out to investigate the

operating performance of ROCOF relay in a multiple DG system. To increase understanding, these studies are organized into two sections.

The first section covers the simulations carried out to investigate the effect of different internal algorithm implemented in ROCOF relay. The second section presents the simulations carried out to assess the effect of multiple DG on the operating performance of ROCOF relays. This includes the effect on the ability of a ROCOF relay to detect an islanding event and to reject a non-islanding event.

3.2 Simulation Model in EMTDC/PSCAD

Figure 3-1 shows a single line diagram of the network used for the studies in the following section. It comprises a 33kV, 50Hz grid with a short circuit level of 1300MVA, represented by a Thevenin equivalent, which feeds a 11kV busbar through two parallel 33/11kV on-load tap changer transformers. The DG, connected to the 11kV feeder at bus 3, is represented by a synchronous machine equipped with exciter. Due to the short simulation time, prime mover and governor control are neglected, i.e. mechanical power is considered constant.

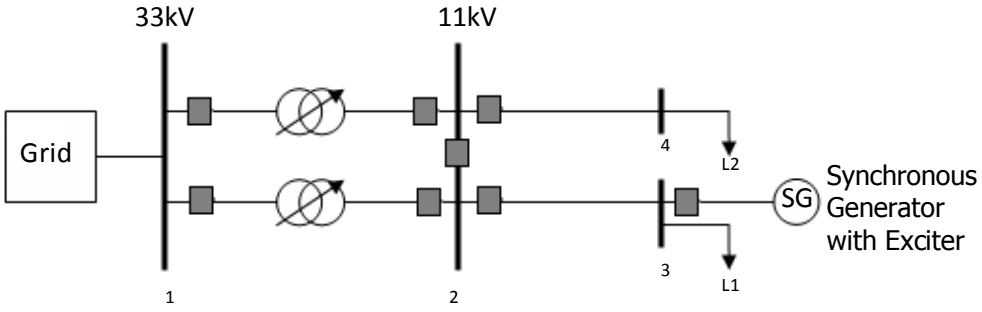

Figure 3-1 Single Line Diagram of Distribution Network Model

3.2.1 ROCOF Relay Model

The model of the ROCOF relay used in the simulation studies was developed in Matlab. Figure 3-2 illustrates the operating principle of the developed model. The system frequency, *f* is determined from the DG terminal voltage waveform using a

zero-crossing technique, which will be discussed in more detail in the following section. The derived system frequency is then used to calculate the effective rate of change of frequency. This is calculated based on a 100ms moving windows, according to equation (3-1).

$$\frac{df}{dt} = \frac{1}{5}\sum_{i=1}^{5}\frac{\Delta f_i}{\Delta t_i} \tag{3-1}$$

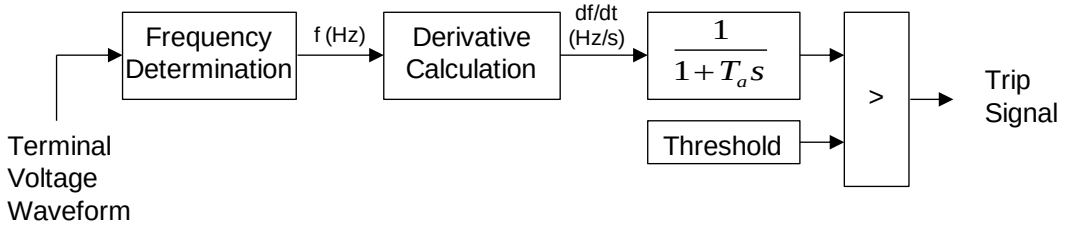

Figure 3-2 Operating Principle of ROCOF Relay

The resulting signal is subsequently filtered by a first order function to eliminate high frequency transients. The time constant, T_a represents both the time constant of the filters and the adopted measurement window. Its outcome is finally compared with the threshold value. If the former value exceeds the latter, a trip signal is initiated. Once a trip decision is made, the simulation considers it as the operating time. It is worth noting that if the relay is not activated within 0.5 seconds, it is considered that this device failed to detect the islanding condition.

3.2.1.1. **Zero-Crossing Technique**

Figure 3-3 illustrates the zero-crossing technique adopted by the ROCOF model to determine the system frequency. The voltage waveform is sampled at a fixed sampling time in which the time intervals between samples are *dt*. The frequency, *f* of each cycle is determined using equation (3-2) by measuring the cycle duration, T of two successive positive zero-crossing points.

$$f = \frac{1}{T} \tag{3-2}$$

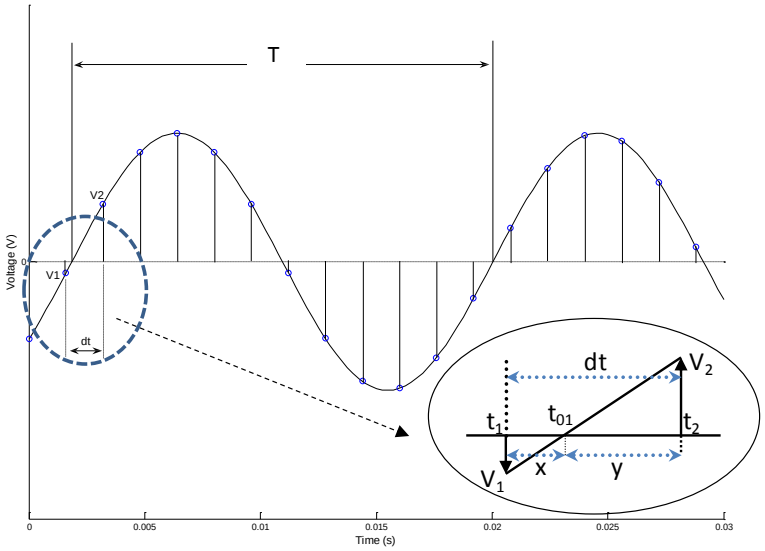

Figure 3-3 Zero-crossing Technique

Zero-crossing points can be calculated using the method shown in the same figure. As the time intervals, *dt* between two samples are assumed to be very small, the voltage between these samples can be approximated as a straight line.

$$x + y = dt \tag{3-3}$$

$$\frac{|V_1|}{|V_1| + V_2} = \frac{x}{x + y} \tag{3-4}$$

Substituting equation (3-3) into equation (3-4)

$$x = \frac{|V_1|}{|V1| + V_2} \times dt \tag{3-5}$$

Thus, the zero-crossing point, t_{01}

$$t_{01} = t_1 + x \tag{3-6}$$

Similarly, the subsequent positive zero-crossing point, t_{02} can be obtained using the above calculations. The cycle duration is then derived by

$$T = t_{02} - t_{01} \tag{3-7}$$

It is important to note that the voltage waveform needs to be pre-processed first before being sent to the ROCOF model for frequency determination. This is to eliminate elements that can interfere with the accurateness of zero-crossing calculation. For this purpose, a Band Pass Filter (BPF) with upper and lower cutoff frequencies of 35Hz and 65Hz respectively is employed within the model.

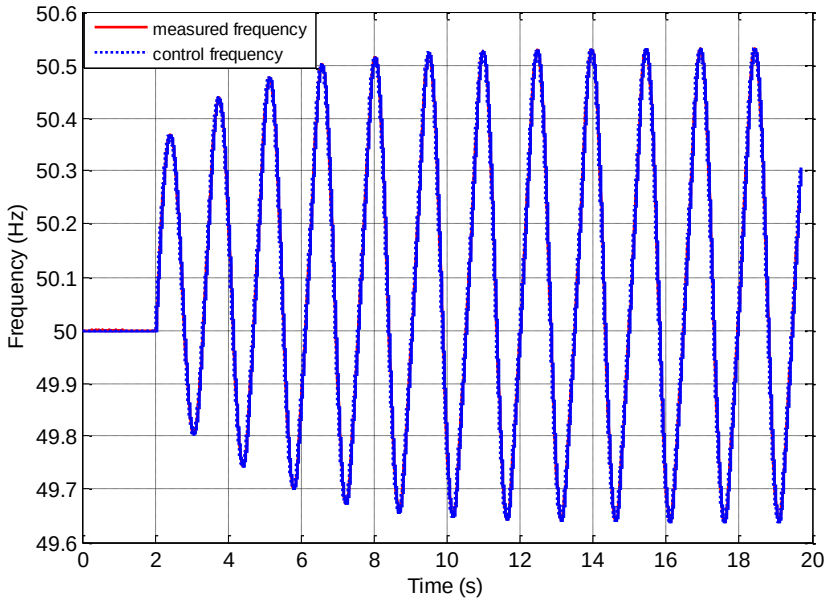

Figure 3-4 Frequency Measurement using Zero-crossing Technique

In order to validate the implemented zero-crossing technique, a simple test is carried out. A sinusoid waveform is generated with time varying frequency as seen in Figure 3-4.

The generated waveform is then input to the relay model and the frequency detected by the relay is plotted in the same figure. It can be seen that both measured frequency and control frequency are closely matched, which verify the employed technique.

3.3 Factors Affecting ROCOF Relays

Immediately after disconnection from the grid, the frequency starts to change dynamically due to the real power imbalance in the formed island. The ROCOF relay

utilizes this principle and measures the rate of change of frequency. Once the rate of change of frequency exceeds the predetermined setting, a trip signal is initiated. As mentioned in the previous chapter, the rate of change of frequency is approximated by

$$\frac{df}{dt} = -\left(\frac{P_L - P_G}{2H \times S_{GN}} \times f_r \right) \tag{3-8}$$

Where P_G = Output of the distributed generator

P_L = Load in the island

S_{GN} = Rated capacity of the distributed generator

H = Inertia constant of generating plant

f_r = Rated frequency

From this equation, it can be seen that the frequency changing rate depends upon the real power imbalance as well as the inertia of the generator, which in turn affect the operating performance of the relay. Further studies are carried out in the following section to examine the impact of these factors on a ROCOF relay.

3.3.1 **Generator Inertia Constant**

The value of the inertia constant has great effect on the dynamic behaviour of the generator. A generator with a small inertia constant responds faster than a generator with a large inertia constant, and thus the frequency variation changes faster.

In order to examine the influence of the inertia constant, H, on the performance of a ROCOF relay, simulations were carried out with three different H values, namely 1s, 2s and 3s. The simulation result shown in Figure 3-5 illustrates the rate of change of frequency with respect to different inertia constants, under the same islanding condition. It is observed that the generator with the smallest inertia constant has the fastest rate of change of frequency, and vice versa. Thus, although seeing the same islanding condition, ROCOF relay performance may differ depending on the DG characteristic.

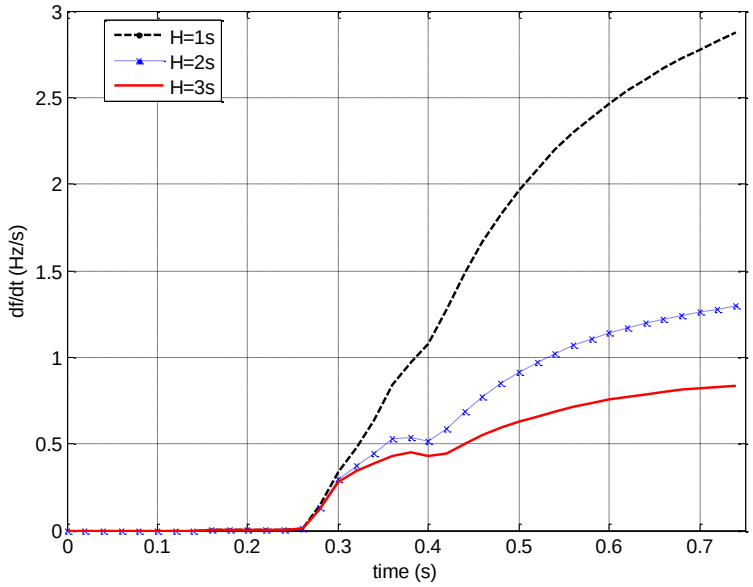

Figure 3-5 Rate of Change of Frequency with Respect to Different Inertia Constant

The impact of the generator inertia constant can be insignificant if the ROCOF relay is set sufficiently sensitive. However, as the setting gets higher, the influence becomes notable, as shown in Figure 3-6. It is observed that a ROCOF relay with a typical "maximum" setting of 1Hz/s failed to detect the islanding condition when the involved generator inertia constant was very large (3.0s).

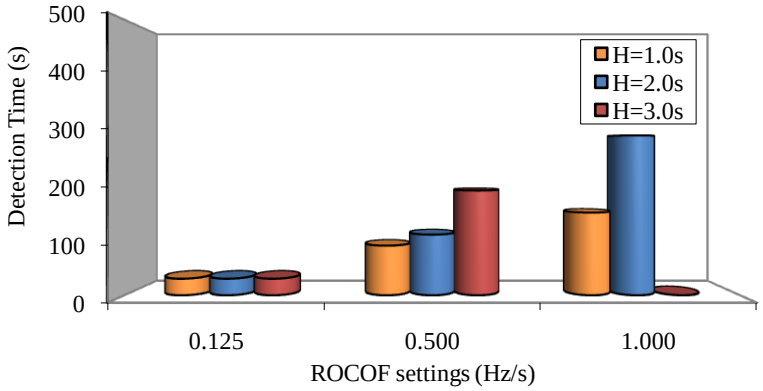

Figure 3-6 Effect of Inertia Constant on ROCOF

3.3.2 **Voltage Dependant Loads**

Figure 3-7 shows the minimum power imbalance required to activate the ROCOF relay with a setting of 1 Hz/s. The threshold setting of 1 Hz/s (least sensitive) is

chosen deliberately in this study to determine the lowest power mismatch that is needed for ROCOF relay activation. It must be noted that this setting is significantly higher than the recommended value (0.125Hz/s in UK and 0.45-0.5Hz/s in Northern Ireland).

It is observed that a higher power imbalance is required to activate the relay when the load is of constant impedance type. This is because when islanding happens, the voltage usually changes, which then modifies the voltage dependant load demand and directly affects the power imbalance in the formed island. The voltage dependency of the load can be represented by

$$P = P_0 \left(\frac{V}{V_0} \right)^a \tag{3-9}$$

Where a=0 represents constant power load
a=1 represent constant current load
a=2 represents constant impedance load

As shown by equation (3-9), the load variation is greatest with a constant impedance load while it is negligible for a constant power load.

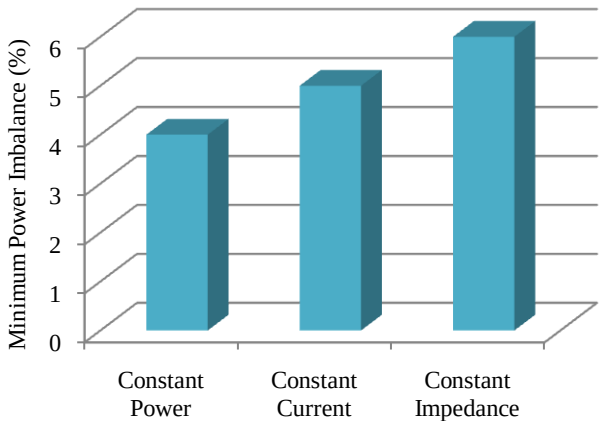

Figure 3-7 Effect of Load Type on ROCOF

The most conservative circumstance happens when there is a deficit of real and reactive power. The load reduces due to the voltage drop and consequently the real power imbalance decreases. As a result, the ROCOF relay becomes less sensitive in detecting the islanding condition.

Conversely, the most optimistic situation occurs when there is a real power surplus and a reactive power deficit. The load will still decrease due to the voltage drop but now the power imbalance increases. Hence, the ROCOF relay becomes more sensitive.

Considering the impact of load type on the ROCOF relay, the load used in the simulation studies for the remainder of this report will be of constant impedance type.

3.3.3 **Load Power Factor**

The load power factor changes the voltage profile and subsequently affects the dynamic behaviour of the voltage dependant load. This indirectly influences the operating performance of the ROCOF relay. The smaller the load power factor, the greater the voltage reduction at the instant of islanding. Depending on whether there is a surplus or deficit of real power, the ROCOF relay may become more or less sensitive.

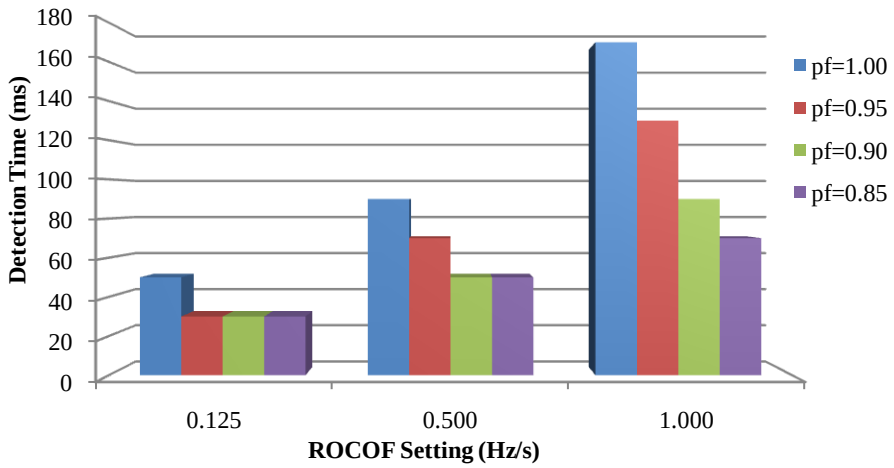

Figure 3-8 Effect of Load Power Factor on ROCOF

With the real power imbalance kept at 0.1pu, the performance of the ROCOF relay at different load power factor was investigated. The results presented in Figure 3-8 clearly show the effect of load power factor on the ROCOF operating performance. The impact is more significant when the relay setting increases.

3.4 Case Studies

Various case studies have been carried out to investigate the performance of the ROCOF relay during real islanding situations and system disturbances. The network model used in the simulation is illustrated in Figure 3-9.

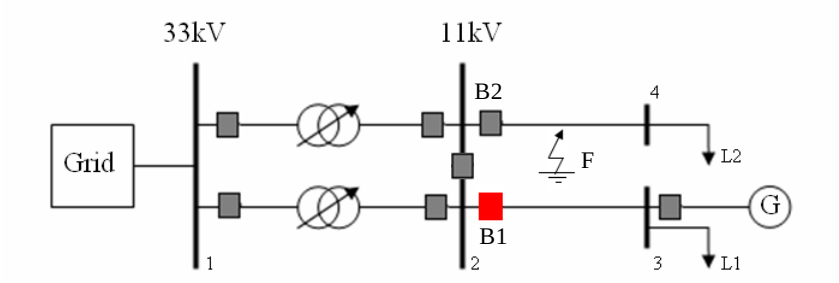

Figure 3-9 Network Diagram Used for Case Studies

3.4.1 Islanding Events

Case studies 1 and 2 were carried out to investigate the ability of ROCOF relay to detect islanding events. As these scenarios are true islanding events, the relays should reliably detect the islanding occurrences and trip the DG.

3.4.1.1. Case Study 1

An islanding condition with about 0.2pu power imbalance was simulated by opening B1 at 0.25 seconds. Immediately after islanding, the voltage decreases as illustrated in Figure 3-10, in which the dotted lines represent the voltage waveform if islanding had not happened. The frequency variation can be clearly observed in Figure 3-11. The ROCOF relay set at 1.0 Hz/s tripped correctly after 90 milliseconds.

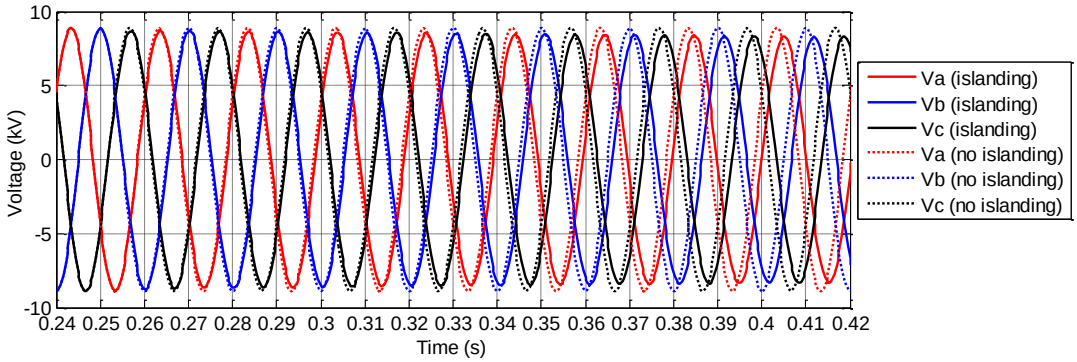

Figure 3-10 Voltage Waveform during islanding

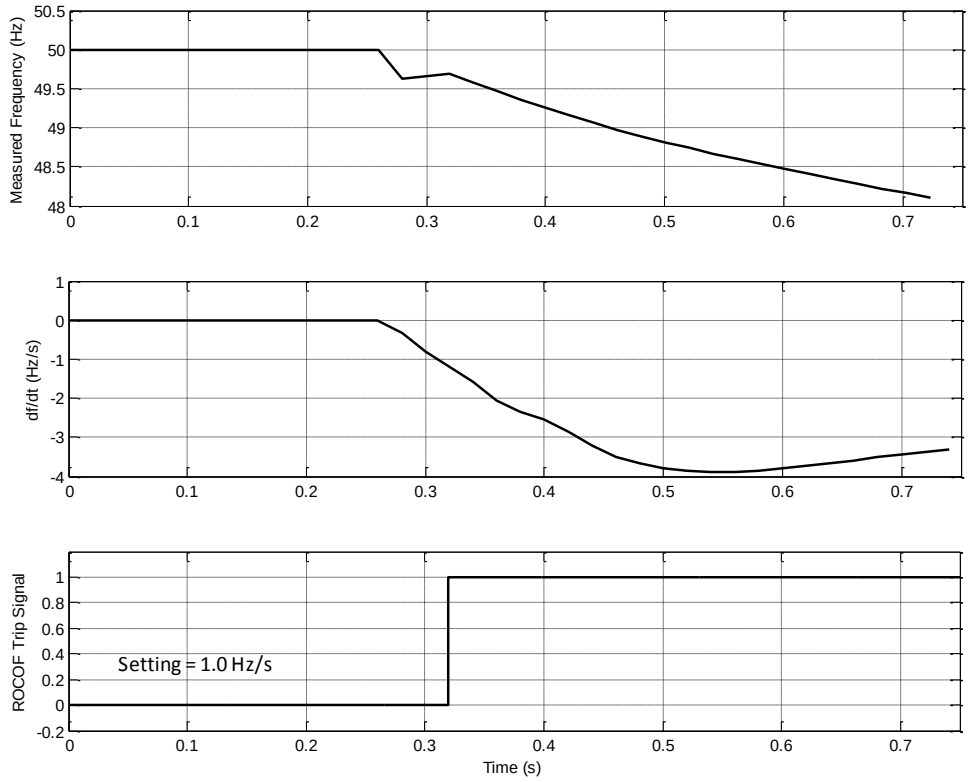

Figure 3-11 Response of ROCOF Relay to Islanding with 0.2p.u. Power Imbalance

The recommended ROCOF relay setting in UK is 0.125Hz/s, whilst in Northern Ireland is 0.45-0.5 Hz/s. The setting of 1.0 Hz/s used in the simulation test is significantly higher than the suggested value. This implies that ROCOF relay has sufficient sensitivity towards islanding events when the power imbalance in the formed island is large.

The duration of measuring window used in the rate of change of frequency calculation is 0.1 seconds. The choice of measuring window has a direct effect on the operation of ROCOF relay. If a shorter measuring window is adopted in this study, a greater rate of change of frequency is anticipated and hence, the more sensitive the relay is. The effect of measuring window duration is investigated in more detail in section 3.7.2.

3.4.1.2. **Case Study 2**

The dependability of the ROCOF relay was examined when the load and generation are closely matched at the instant of grid disconnection. Since the islanding event has occurred, the ROCOF relay was expected to initiate a trip signal. Conversely, as can be seen from Figure 3-12, it can be difficult for the ROCOF relay to detect islanding when the local load and generation output are balanced. From the same figure, it is observed that the frequency deviation after islanding was very small. Even configured at the recommended setting in UK – 0.125Hz/s, the relay still failed to detect the islanding situation.

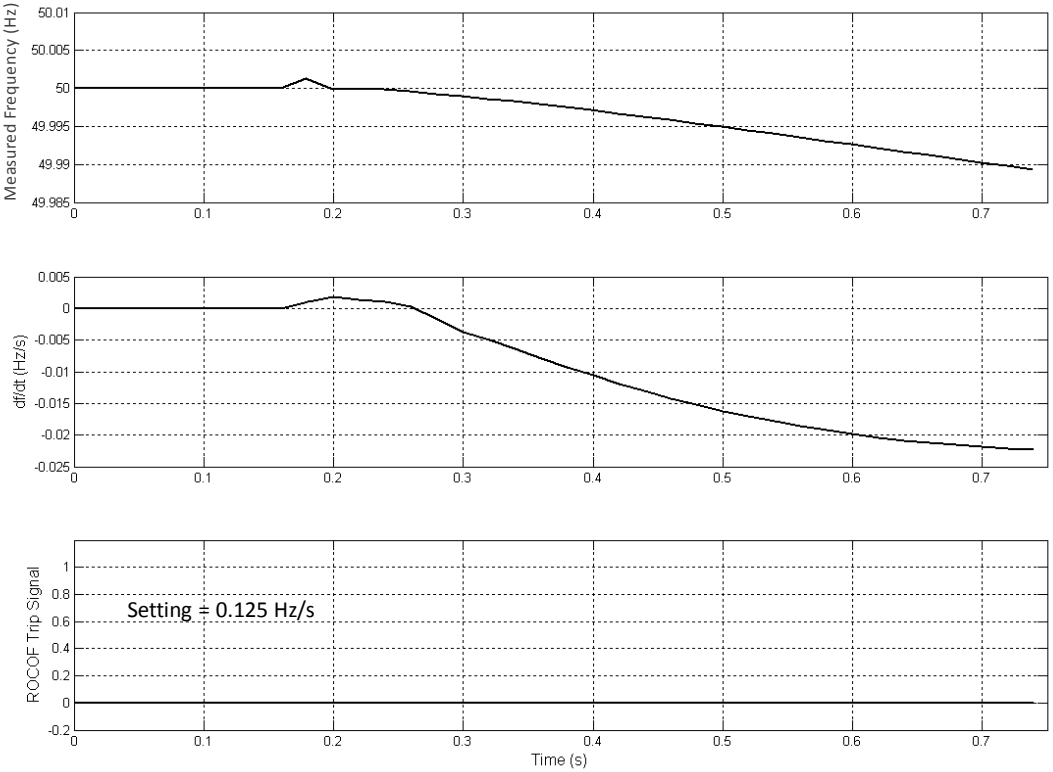

Figure 3-12 Response of ROCOF Relay to Islanding with Balance Load and Generation

3.4.2 **Network Disturbances**

Case studies 3 to 6 were carried out to investigate the stability of ROCOF relay when subjected to network disturbances. As these scenarios are not islanding events, the relays should not trip for any of the events.

3.4.2.1. **Case Study 3**

A scenario was simulated to investigate the effect of switching actions on the ROCOF relay. In this test, one of the parallel 33kV/11kV transformers in Figure 3-9 was switched out. The ROCOF relay set at 0.125Hz/s incorrectly operated. The test was then repeated with 0.2Hz/s and this time the relay remained stable after the switching event.

The false operation of the ROCOF relay is due to the phase shift resulting from the switching incident, which consequently affects the rate of change of the frequency calculation. This poses a problem for ROCOF relays especially those which employ a small measuring window in their derivative calculation.

In addition, it was also found that the higher the DG's loading (L_1), the greater the effect of switching on the ROCOF relay, as illustrated in Figure 3-13. Note: the load per-unit (pu) calculations are based on the DG's MVA rating.

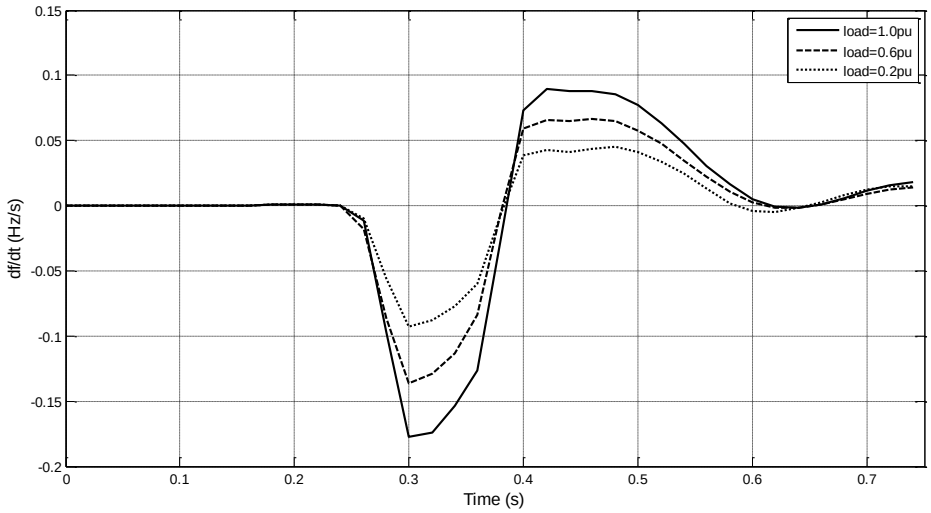

Figure 3-13 Effect of DG's loading on Rate of Change of Frequency

3.4.2.2. **Case Study 4**

This test was simulated to observe the operating performance of the ROCOF relay during network fault conditions. A three-phase fault was applied on the adjacent feeder (feeder 2-4), shown as F in Figure 3-9. The fault is subsequently removed after 0.25 seconds by B2. In this case, the ROCOF relay was not expected to work as there is no islanding event.

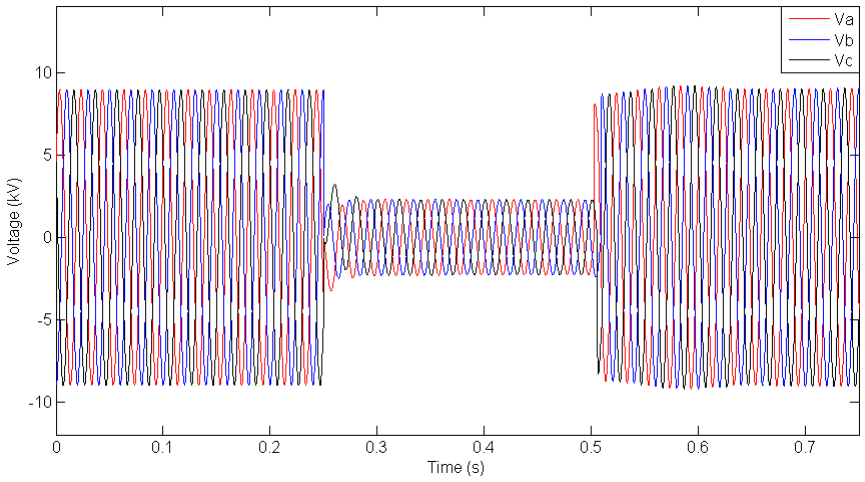

Figure 3-14 Voltage Waveform during Fault at Adjacent Feeder

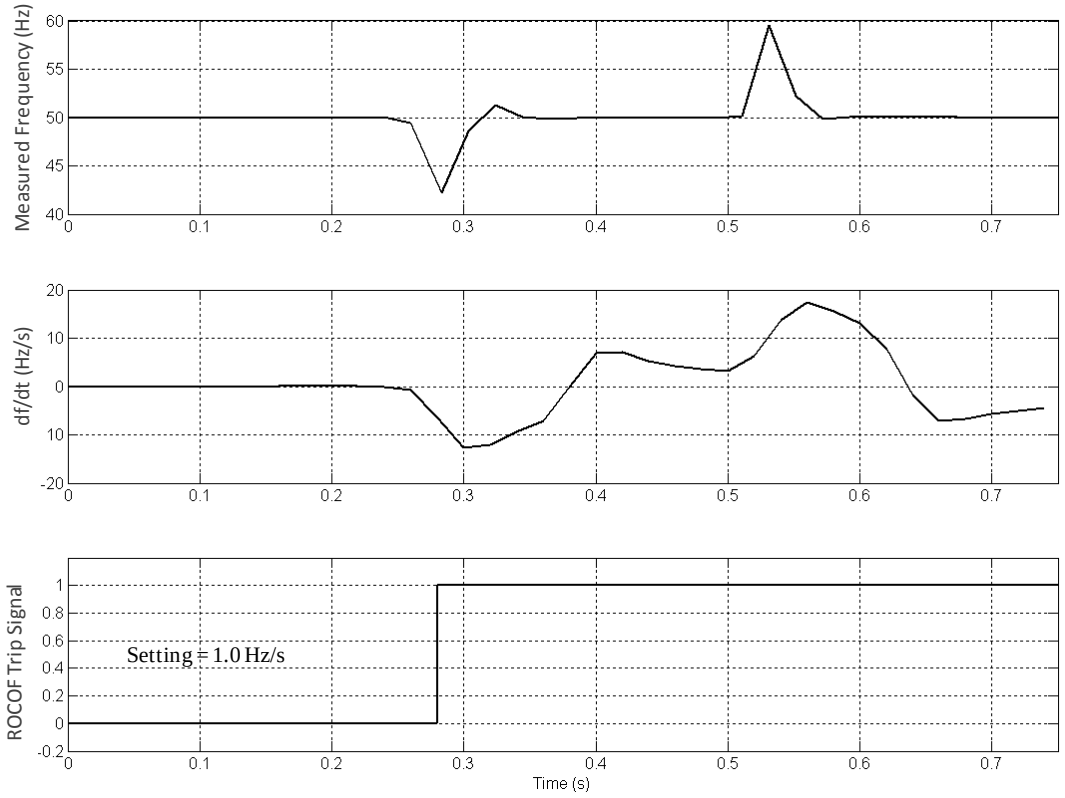

Figure 3-15 Response of ROCOF Relay at Adjacent Fault

The voltage waveform captured at the DG terminal is illustrated in Figure 3-14. The result for this scenario is shown in Figure 3-15. The setting represents the maximum value at which the ROCOF relay still produces spurious tripping. It is seen that ROCOF relay failed to discriminate between a real islanding condition and the adjacent feeder fault even with a setting as high as 1.0Hz/s.

3.4.2.3. **Case Study 5**

In this case, loads are either switched on or off at the DG terminal to investigate the effect of load switching on the ROCOF relay. A total of four different scenarios were simulated:

Case (a): Switching on a 5MW/phase load at the terminal of DG

Case (b): Switching on a 10MW/phase load at the terminal of DG

Case (c): Switching off a 5MW/phase load at the terminal of DG

Case (d): Switching off a 10MW/phase load at the terminal of DG

From Figure 3-16 to Figure 3-19, it can be observed that the larger the amount of load changes, the greater the disturbance seen at the generator terminal. It is noticed that the voltage drop and frequency variation caused by switching on a 10MW/phase load are more significant than switching on a 5MW/phase load. The same situation happened when switching off load, voltage increased due to fewer loads, but the increment is more significant when switching off larger amount of loads.

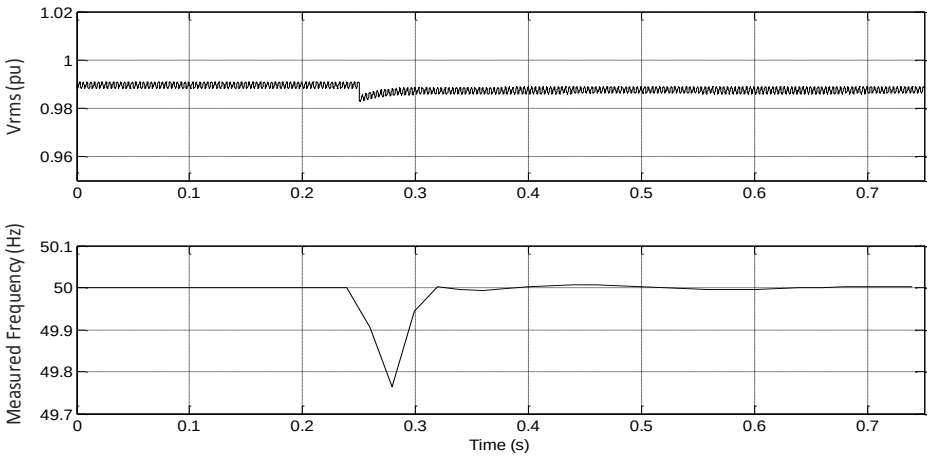

Figure 3-16 Voltage and Frequency of DG in Case (a)

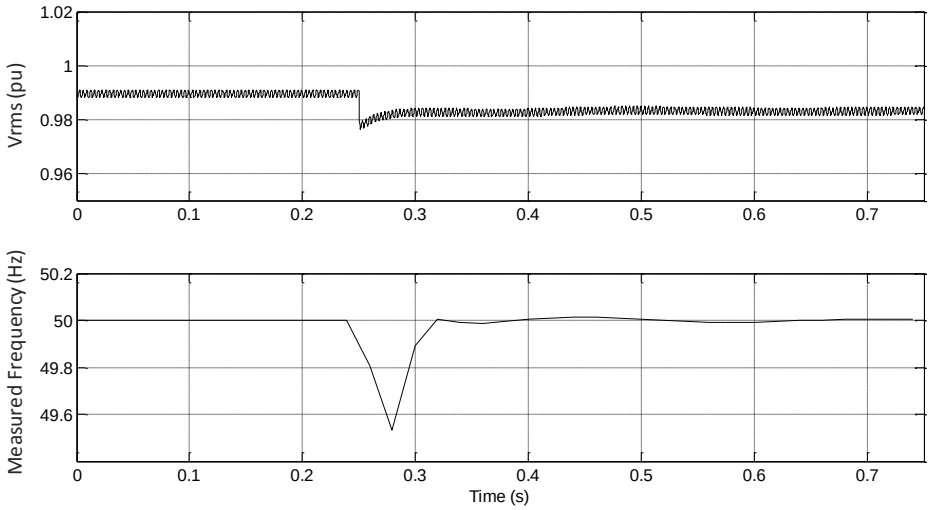

Figure 3-17 Voltage and Frequency of DG in Case (b)

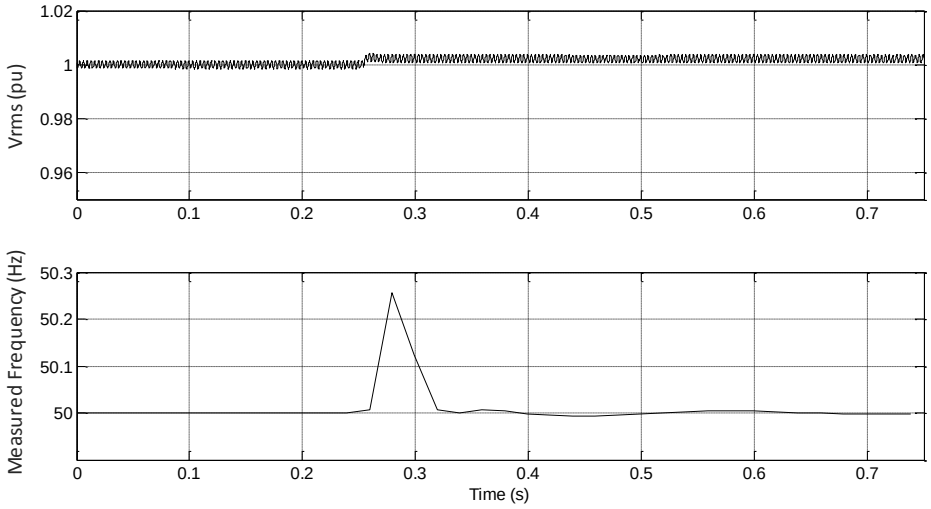

Figure 3-18 Voltage and Frequency of DG in Case (c)

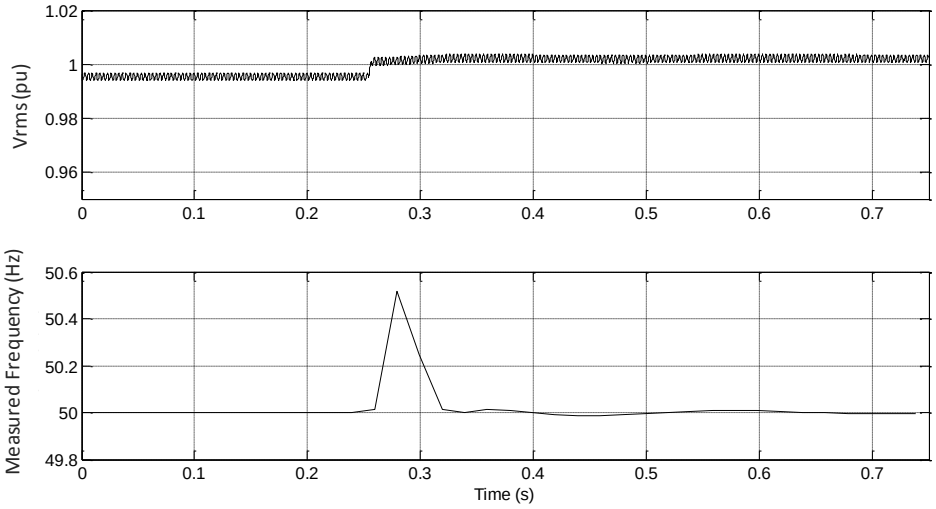

Figure 3-19 Voltage and Frequency of DG in Case (d)

Table 3-1 Minimum ROCOF Trip Setting for Case (a)-(d)

Case	Minimum Trip Setting (Hz/s)
a	0.4
b	0.9
c	0.5
d	0.9

From Table 3-1, it is noticed that the greater the switching event seen by generator, the higher the setting threshold to prevent mal-operation of the ROCOF relay. However, setting the ROCOF relay with these high values may be unrealistic as it may compromise its capability in detecting real islanding events.

3.4.2.4. **Case Study 6**

Sudden loss of major generation infeed may have an adverse effect on a ROCOF relay. The under-frequency transient that occurs during the loss of generation infeed may falsely activate the relay. This may lead to considerable consequences such as widespread tripping of distributed generators. According to an engineering technical report, loss of generation in the UK can occasionally result in a rate of change of frequency of up to 0.16 Hz/s [30]. In order to test the stability of the ROCOF relay during the network disturbance, a test signal with frequency as shown in Figure 3-20 has been generated. The frequency increases with a fixed rate of 0.16 Hz/s for 0.5 seconds and then decreases with the same rate for 0.5 seconds.

ROCOF relay with setting of 0.125 Hz/s falsely responded to the frequency disturbance. The setting was then progressively increased to 0.2Hz/s and the ROCOF relay remained stable at this setting.

As illustrated by the test result, if ROCOF relays set at the UK recommended setting - 0.125 Hz/s, large numbers of distributed generators will be spuriously tripped during network frequency disturbance. This action will only serve to worsen the

situation and further risk the integrity of the network. This is because loads which are previously supplied by DG now need to be supplied by the bulk generation from an already heavily stressed network.

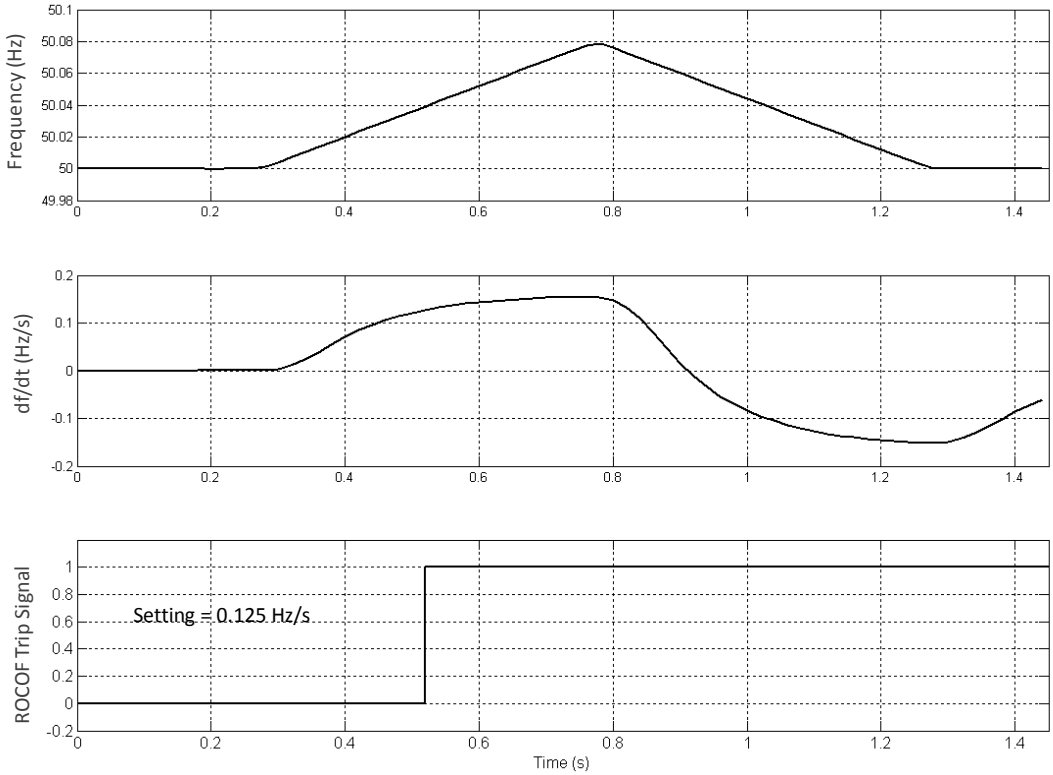

Figure 3-20 Response of ROCOF Relay to System Frequency Excursion

3.5 Summary of Operating Performance of ROCOF Relay

Having illustrated the operating performance of ROCOF relays under different network scenarios, it can be concluded that ROCOF relays are not capable of detecting loss of mains when the load and generation in the formed island is exactly matched (Case Study 2). In addition, this relay is very susceptible to nuisance tripping, and in order to reduce the numbers of spurious trip, a higher threshold value need to be set on the relay. This, however, will compromise relay dependability and may further increase the non-detection zone.

A lot of alternative solutions have been implemented to increase the security of ROCOF relay, at the same time attempting to preserve its dependability. Some of these methods are outlined below:

i) Time Delays

In order to increase the security of the ROCOF relay and reduce the numbers of nuisance tripping, short time delays are employed in some relays. The time delay may vary from 50 milliseconds to 500 milliseconds [15]. This is usually achieved by monitoring the rate of change of frequency over a few successive cycles, to confirm there is a permanent change, before issuing a trip command.

ii) Measuring Windows

Measuring window is defined as the number of power frequency measuring periods over which the rate of change of frequency is calculated [29]. The typical measuring windows adopted in most relays are in the range of 40 milliseconds (2 cycles at 50 Hz) to 2 seconds (100 cycles at 50 Hz) [29]. Increasing the measuring windows of relay helps to improve the relay's discrimination with non-islanding events and reduce false trips.

iii) Under-voltage Interlock

This function will block the ROCOF relay trip signal if the DG terminal voltage drops below a predetermined level, V_{min}. It helps to restrain the actuation of ROCOF relay during non-islanding situation such as generator start-up and short circuits [53]. Typical value for under-voltage pick-up setting is 0.8pu [15].

It is important to note that even with the implementation of the above-mentioned methods, it cannot completely prevent the mal-operation of ROCOF relay towards non-islanding events. A compromise in the setting is still required to provide a balance between security and dependability.

3.6 Multiple Distributed Generators

As DG integration into the distribution network increases, it has become more and more common to have multiple DG units connected to the same feeder. This complicates the operating behaviour of LOM relays and is expected to become an increasing problem.

As discussed in the previous section, and in order to curb spurious tripping, a number of alternatives have been suggested and implemented on a typical ROCOF relay. This factor is thought to be the main reasons which gives rise to the comment in [32] -"commercially available ROCOF relays behave very differently despite seeing the same disturbances". Hence, simulations were done to investigate the impact of these differences on the operating performance of a ROCOF relay.

This is then followed by simulation studies to investigate how multiple generators on the same feeder affect the ability of a ROCOF relay

a) to detect an islanding event
b) to reject a non-islanding event

3.7 Effect of Different Internal Algorithm

Investigations were done when the following design changes were applied to the ROCOF relay:

a) Different frequency measuring algorithms
b) Different measuring window durations
c) Different time delay durations
d) With and without under-voltage interlock

The same relay employed in the previous section was used, except some minor modifications were applied to achieve the necessary effects. Network model used in section 3.4 is employed here.

3.7.1 **Different in Frequency Determination Techniques**

There are generally two main frequency measurement algorithms used in commercially available ROCOF relays. One is based on zero crossing techniques whereas the other is based on a Fourier transformation [22]. The principle of the former technique has already been described in previous section. Meanwhile, the latter technique derives the system frequency by carrying out continuous Fourier transformation on the voltage waveform [22]

Simulations were carried out to investigate the effect of these algorithms on the ROCOF operating performance. In these simulations, the same ROCOF model employed in the previous chapter was used, except that the frequency determination element was substituted with the Fast Fourier Transform (FFT) to represent a Fourier-based relay.

Islanding events were simulated by opening B1 in Figure 3-9. The real power imbalance in the formed island is varied from 0 to 1pu, referred to the DG's rating. For each case, the relay's detection time is determined and the results obtained are summarized as Figure 3-21. For this simulation, ROCOF is set at 1.0 Hz/s. It is observed that ROCOF relay utilizing FFT generally detects islanding faster than zero-crossing based relay. However, the time differences are by most 20ms, which does not pose huge impact on the relay's dependability, considering both of them are able to detect islanding well ahead of the G59 recommended time frame (within 0.5s).

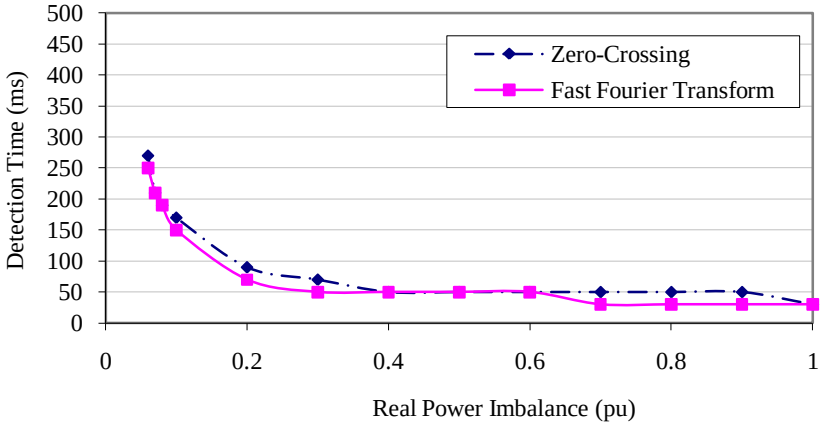

Figure 3-21 Comparison between Curves obtained Using Zero-Crossing Techniques and Fast Fourier Transform Technique

3.7.2 **Different In Duration of Measuring Windows**

The duration of measuring windows used in the rate of change of frequency calculation directly affects the operation of ROCOF relay. To provide a clearer idea of its impact, the following simulation has been carried out. One of the parallel 33kV/11kV transformers in Figure 3-9 was switched out. Three cases were analyzed:

i) ROCOF relay with measuring window 0.04 seconds
ii) ROCOF relay with measuring window 0.1 seconds
iii) ROCOF relay with measuring window 0.2 seconds

The result obtained is presented in Figure 3-22. From that figure, it is observed that the shorter the measuring windows, the greater the rate of change of frequency, and hence the more sensitive the relay is. On the contrary, the longer the measuring periods adopted in the calculation, the less sensitive the relay will be. Yet, the main advantage of this is the relay is now more immune to network disturbances, reducing the number of false tripping.

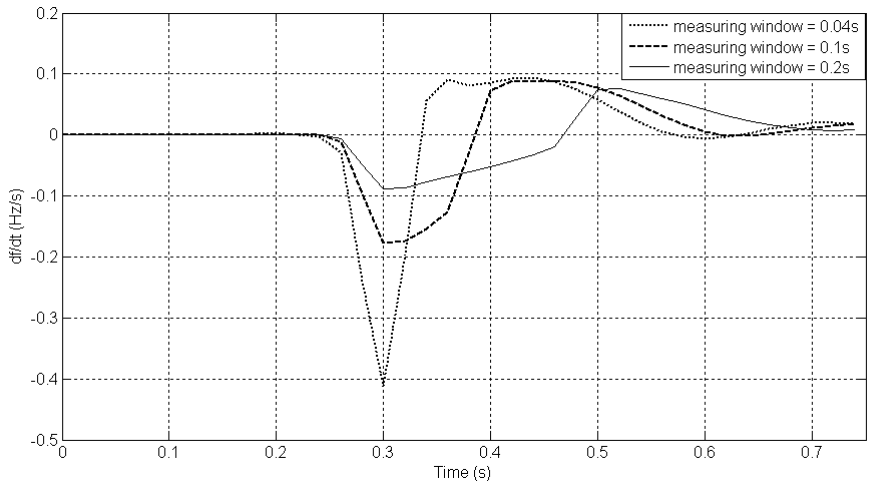

Figure 3-22 Comparison of Rate of Change of Frequency Using Different Measuring Windows Duration

3.7.3 **Different In Duration of Delays**

Employing a time delay can also enhance the security of ROCOF relay and helps to cut down on spurious tripping. Figure 3-23 portrays the effect of time delays on the ROCOF operation. It has to be pointed out that in these tests, disturbances were introduced into the network shown in Figure 3-9 and ROCOF relay was not expected to respond to any of the events. Even if it is activated, the longer time it takes to be activated is considered as more desirable.

From the result, it is observed that the longer the time delays, the more resistant the relay is to network disturbances. Note: The missing bars indicate no trip.

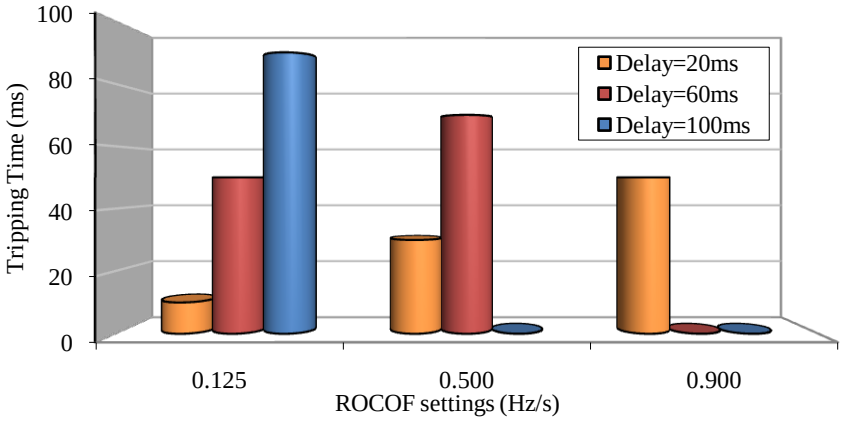

Figure 3-23 Comparison of Tripping Time Using Different Duration of Time Delay

3.7.4 **Under-voltage Interlock Function**

A three phase fault, F which lasted for 0.25 seconds was applied on feeder 2-4 (refer Figure 3-9) to examine the effect of including under-voltage interlock function in the ROCOF algorithm. ROCOF relay was not supposed to trip due to non-islanding event has occurred.

The voltage waveform captured at the DG terminal is illustrated in Figure 3-24, in which the dotted lines represent the voltage waveform if fault had not occurred. An

enlarged version of Figure 3-24 is shown in Figure 3-25, detailing the waveform in the period of 0.242 seconds to 0.52 seconds.

The result for this scenario is shown in Figure 3-26. It is seen that with the under-voltage interlock function, the trip decision was, although not prevented, deferred to a later time.

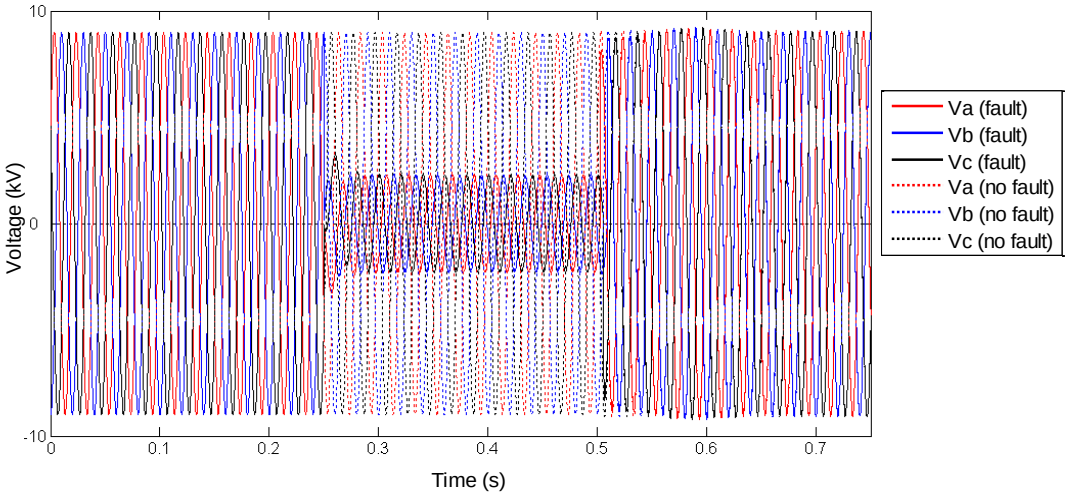

Figure 3-24 Voltage Waveform during fault at Adjacent Feeder

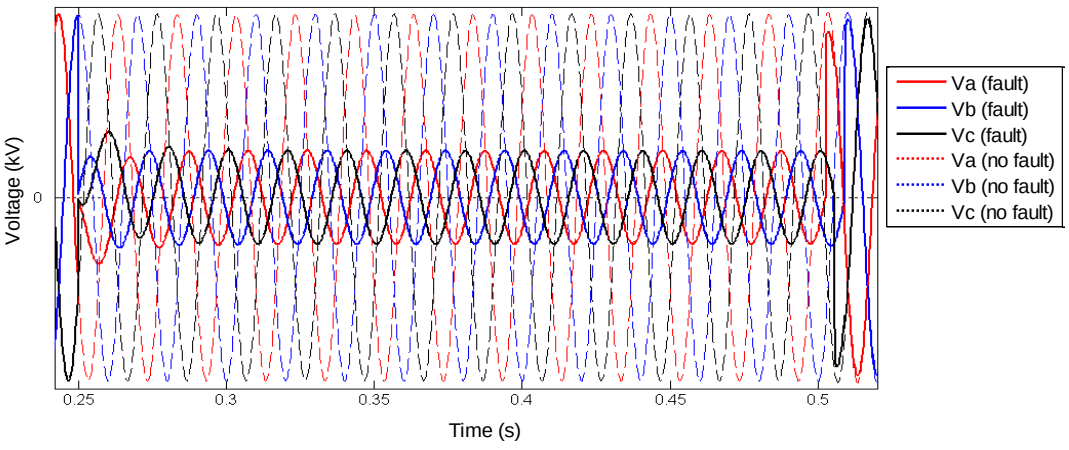

Figure 3-25 Voltage Waveform during Fault at Adjacent Feeder

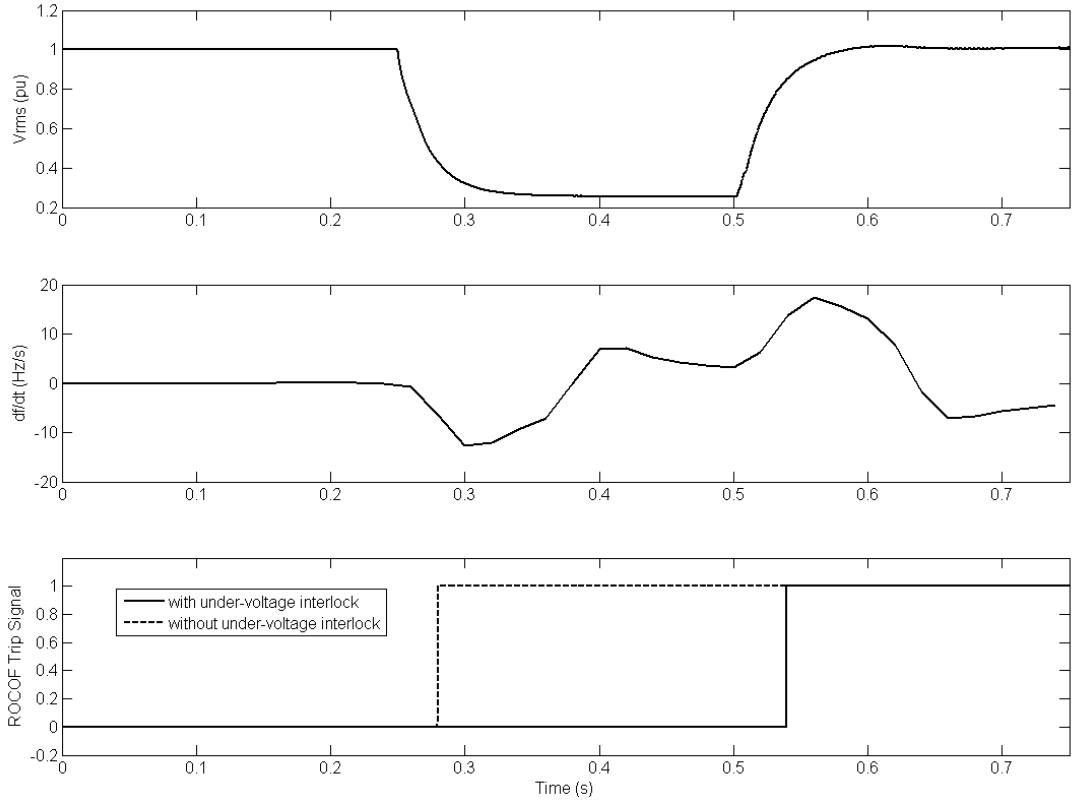

Figure 3-26 Comparison of ROCOF Relay's Response to Adjacent Fault (with and without Under-voltage Interlock Function

3.8 Simulation with Multiple Distributed Generators

The distribution network presented in Figure 3-27 was utilised to analyse cases with multiple distributed generators. This system comprises a 33kV, 50Hz grid with a short circuit level of 1300MVA, which feeds a 11kV busbar through two parallel 33/11kV on-load tap changer transformers. In this system, there are two identical synchronous generators; both with capacity of 4.51 MVA connected at buses 5 and 7. Each generator is equipped with a ROCOF relay and circuit breaker. It should be noted that there was a simulated delay of 50 milliseconds between the instant of ROCOF's trip decision and the instant of circuit breaker opening [55]. The objective of these simulations is to investigate the possibility of interference between various ROCOF relays, in terms of both dependability and security.

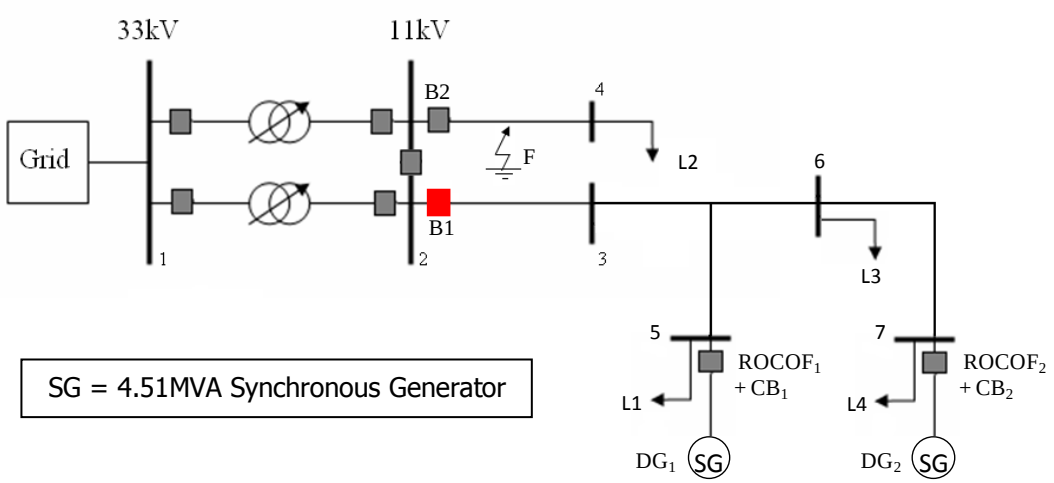

Figure 3-27 Network Diagram of Multiple DG System

3.8.1 **Islanding Event**

An islanding condition with 0.1pu power imbalance was simulated by opening B1 at 0.25 seconds. Three distinct situations are analysed. In each case, the ROCOF2 threshold setting was varied. For the first case, ROCOF2 was set at 1.0Hz/s. Then, for the second case, the setting was reduced to 0.5Hz/s and then further reduced to 0.125Hz/s in the last case. For these three cases, the detection time of ROCOF1 for different settings were obtained. The results were illustrated in Figure 3-28.

It is seen that when ROCOF2 has an equal or higher setting than ROCOF1, there is no influence on ROCOF1 due to the presence of ROCOF2. However, if ROCOF2 has a lower setting than ROCOF1, then the latter will has a more sensitive behaviour due to the presence of ROCOF2. This is because ROCOF2 detects the islanding condition faster than ROCOF1. Subsequently after the successful detection, CB2 opens and thus the power imbalance in the formed island suddenly increased. As a result, ROCOF1 acts earlier than in the case where ROCOF2 had not operated.

The obtained result shows that multiple ROCOF relays will not give rise to an adverse impact to the relay's ability in detecting islanding. The relay with a more sensitive setting will lead other relays to behave more sensitively.

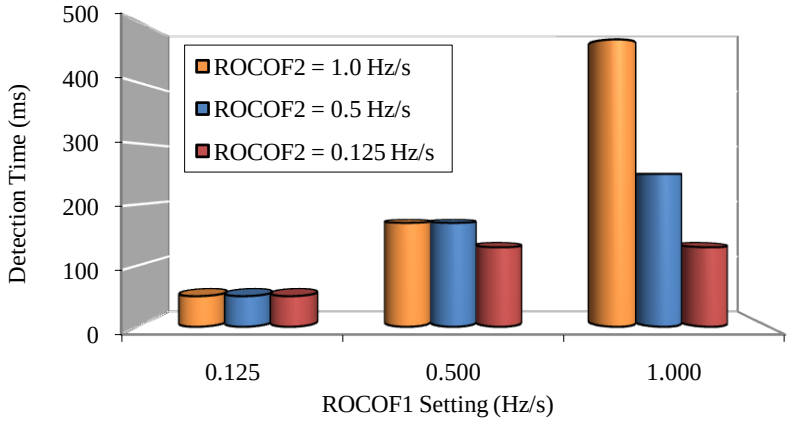

Figure 3-28 Impact of Multiple DG on ROCOF1's Performance

3.8.2 **Network Disturbances**

Having illustrated the effect of multiple ROCOF relays on their ability to detect islanding, it is also important to study how these relays behave during network disturbances. Three types of disturbances have been simulated:

Scenario 1: Line switching

Scenario 2: Load switching

Scenario 3: Adjacent Fault

As these scenarios are not islanding events, none of the relays are expected to trip. Even if they did, the longer they took to trip is considered more desirable.

3.8.2.1. **ROCOF1 and ROCOF2 with Different Settings**

For each disturbance scenario, three situations are analysed:

i) ROCOF2 is set at 1.0Hz/s

ii) ROCOF2 is set at 0.5Hz/s

iii) ROCOF2 is set at 0.125Hz/s

For these three situations, the detection time of ROCOF1 for different settings was obtained.

Scenario 1: Line Switching

One of the parallel 33kV/11kV transformers in Figure 3-27 was switched out. The results obtained are presented in Figure 3-29.

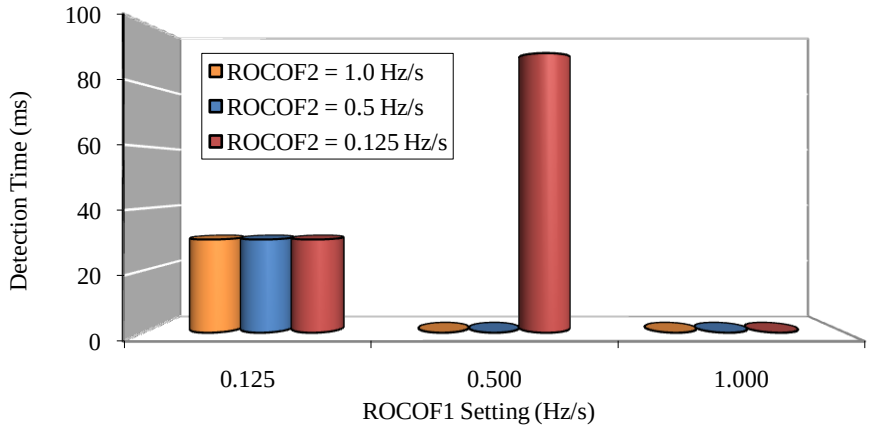

Figure 3-29 Effect of Line Switching on ROCOF1's Stability

It is observed that when ROCOF1 has a high threshold setting (1.0Hz/s), ROCOF1 is not susceptible to the disturbance, irrespective of the setting used in ROCOF2.

However, as the ROCOF1 setting gets lower, the presence of ROCOF2 (with a lower setting than ROCOF1) may affect the stability of ROCOF1 and increase the likelihood of an incorrect trip by ROCOF1. For instance, when ROCOF1 is set at 0.5Hz/s, it did not trip when ROCOF2 had a higher or similar setting. However, when the ROCOF2 setting (0.125Hz/s) is lower than the ROCOF1 setting (0.5Hz/s), ROCOF2 responded to the disturbance and tripped. This aggravated the disturbance seen at the terminal of DG1, causing ROCOF1 to also initiate a trip decision.

The obtained result shows that multiple ROCOF relays may give rise to an adverse impact to the relay's ability in rejecting non-islanding event. The relay with a more sensitive setting will lead other relays to behave more sensitively, which increase the likelihood of widespread false tripping of DG.

Scenario 2: Load Switching

A load, with 5MW/phase, was switched on at the terminal of DG1. The results obtained are depicted in Figure 3-21. From the result, it is observed that for this kind of disturbance, the setting used with ROCOF2 does not affect the stability of ROCOF1.

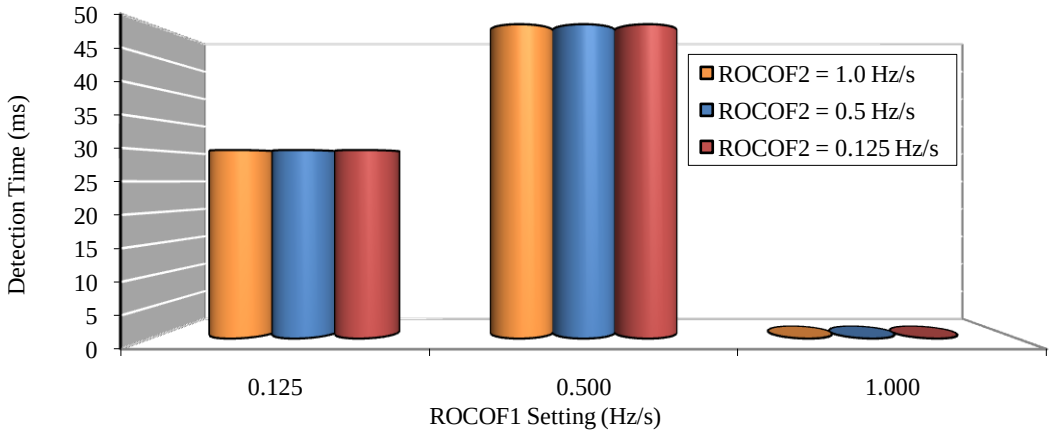

Figure 3-30 Effect of Load Switching on ROCOF1's Stability

Scenario 3: Adjacent Fault

A three-phase fault was applied on the adjacent feeder (feeder 2-4), shown as F in Figure 3-27. The fault is subsequently removed after 0.25 seconds by the responsible circuit breaker. The simulation results are portrayed in Figure 3-31. From the result, it is also observed that the setting applied to ROCOF2 does not affect the stability of ROCOF1.

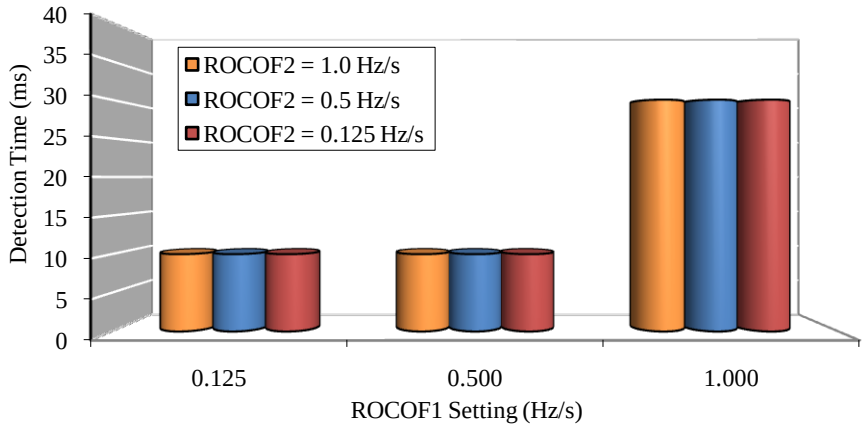

Figure 3-31 Effect of Adjacent Fault on ROCOF1's Stability

3.8.2.2. **ROCOF1 and ROCOF2 with Same Settings**

As discussed in the previous section (section 3.7), ROCOF relay can behave very differently with different internal algorithm. Hence, it is anticipated that even configured with the same setting, relays with different internal algorithm will respond differently to the same disturbance. Hence, the following work has been carried out to investigate how two relays with different algorithms but the same threshold settings perform when subjected to the same network disturbance.

The main factors contributing to the difference in performance were investigated, which includes the following:

a) Duration of measuring window
b) Duration of time delays
c) Under-voltage Interlock function

a) Duration of Measuring Windows

Scenario 1 of Section 3.8.2.1 was repeated for this simulation. Three cases were analysed here:

Case 1: Duration of ROCOF2 measuring windows is less than ROCOF1.
Case 2: Duration of ROCOF2 measuring windows is same as ROCOF1.
Case 3: Duration of ROCOF2 measuring windows is more than ROCOF1.

Table 3-2 Results of ROCOF1's Responses for Cases 1-3

ROCOF settings (Hz/s)	**Case 1**	**Case 2**	**Case 3**
0.125	√	√	√
0.200	√	√	√
0.300	√	X	X
0.400	X	X	X
0.500	X	X	X

√	Trip
X	No Trip

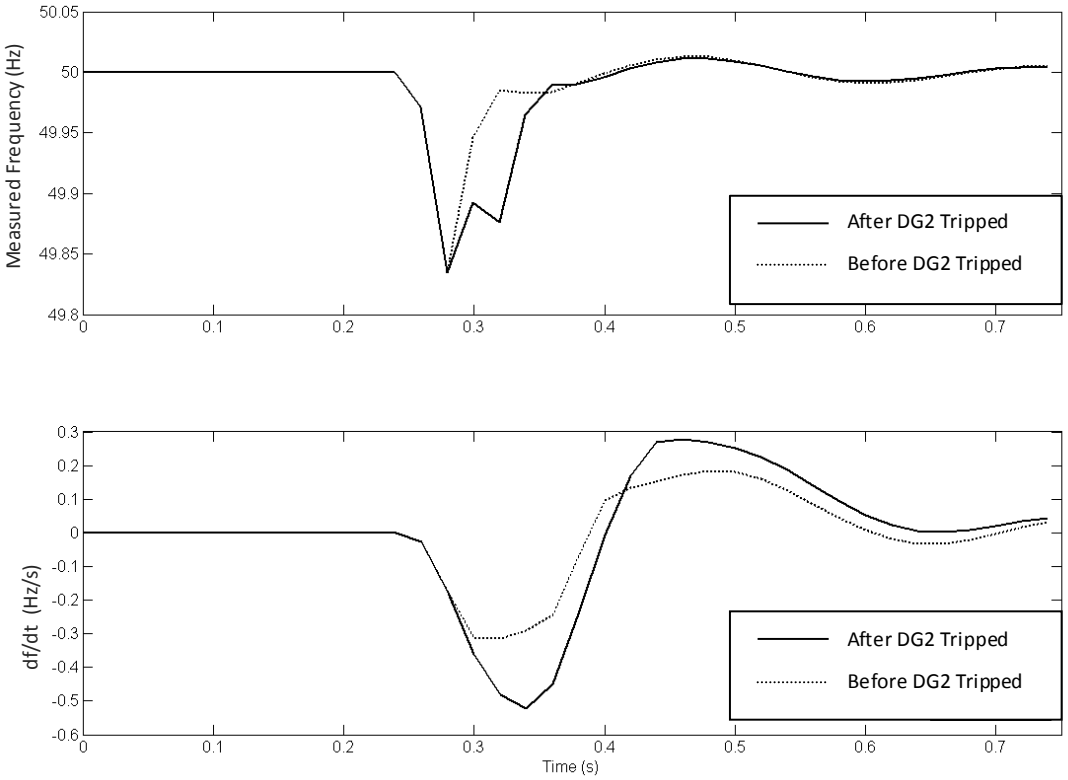

Figure 3-32 Frequency and *df/dt* Sensed by ROCOF1 before and after DG2 Tripped

From the result shown in Table 3-2, it is observed that for settings ≥ 0.3Hz/s, ROCOF2 with same or longer duration of measuring windows did not interfere with the stability of ROCOF1. At ROCOF setting of 0.3Hz/s, ROCOF2 having shorter measuring window than ROCOF1 easily responded to the disturbance and tripped DG2. Consequently, ROCOF1 sees a larger disturbance than expected and tripped DG1 as well. Figure 3-32 shows the frequency and df/dt sensed by ROCOF1 before and after the tripping of DG2 (at setting 0.3 Hz/s).

b) Duration of time delays

Scenario 2 of Section 3.8.2.1 was simulated. The following three cases were analyzed:

Case 1: ROCOF2 with shorter time delay than ROCOF1.

Case 2: ROCOF2 with same time delay than ROCOF1.

Case 3: ROCOF2 with longer time delay than ROCOF1.

The result obtained is summarized as Table 3-3. When ROCOF2 has similar or longer duration of time delays in its internal algorithm, ROCOF1's stability is not affected by its presence. However, interestingly, it is observed that at setting 0.4Hz/s, ROCOF2 with shorter time delay than ROCOF1 has improved the stability of ROCOF1. In this case, ROCOF2 responded to the disturbance and tripped DG2. The frequency and rate of change of frequency before and after DG2 was tripped is shown in Figure 3-33. It is observed that the frequency changing rate has reduced after the tripping of DG2, resulting in ROCOF1 not being activated.

Table 3-3 Results of ROCOF1's Responses for Cases 1-3

ROCOF settings (Hz/s)	**Case 1**	**Case 2**	**Case 3**
0.125	√	√	√
0.200	√	√	√
0.300	√	√	√
0.400	X	√	√
0.500	X	X	X

√	Trip
X	No Trip

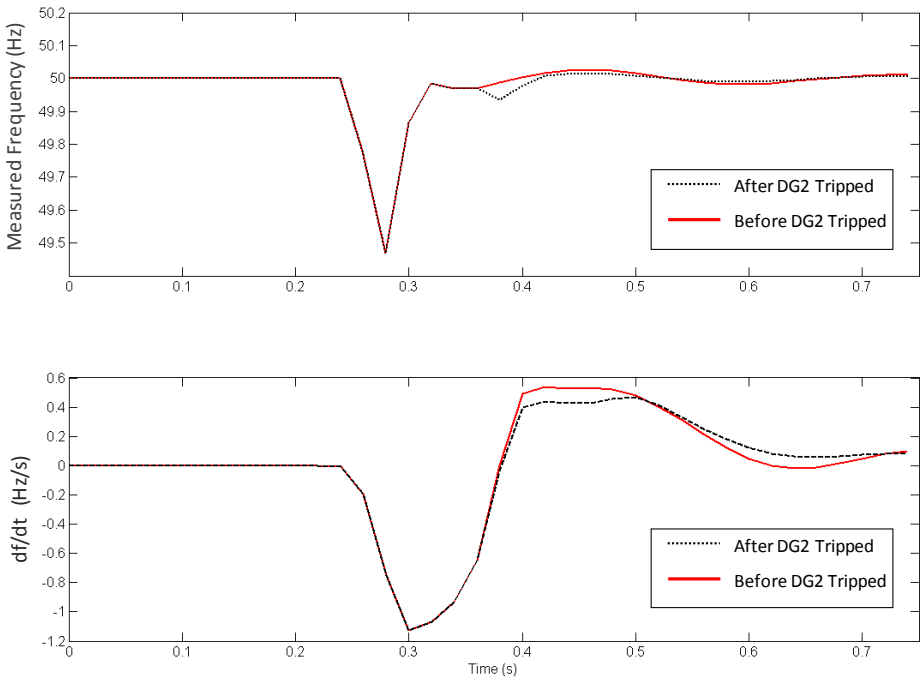

Figure 3-33 Frequency and *df/dt* Sensed by ROCOF1 before and after DG2 Tripped

c) Under-voltage Interlock

Scenario 3 of Section 3.8.2.1 was simulated. The following four cases were analyzed:

Case 1: Both ROCOF1 and ROCOF2 without under voltage interlock function

Case 2: Both ROCOF1 and ROCOF2 with under voltage interlock function

Case 3: ROCOF1 with under voltage interlock function and ROCOF2 without under voltage interlock function

Case 4: ROCOF1 without under voltage interlock function and ROCOF2 with under voltage interlock function

Table 3-4 Results of ROCOF1 Tripping Time for Cases 1-4

ROCOF settings (Hz/s)	**Trip Time* (ms)**			
	Case 1	**Case 2**	**Case 3**	**Case 4**
0.125	10	290	290	10
0.500	10	290	290	10
1.000	30	290	290	30

*Trip time is measured with respect to 250 ms

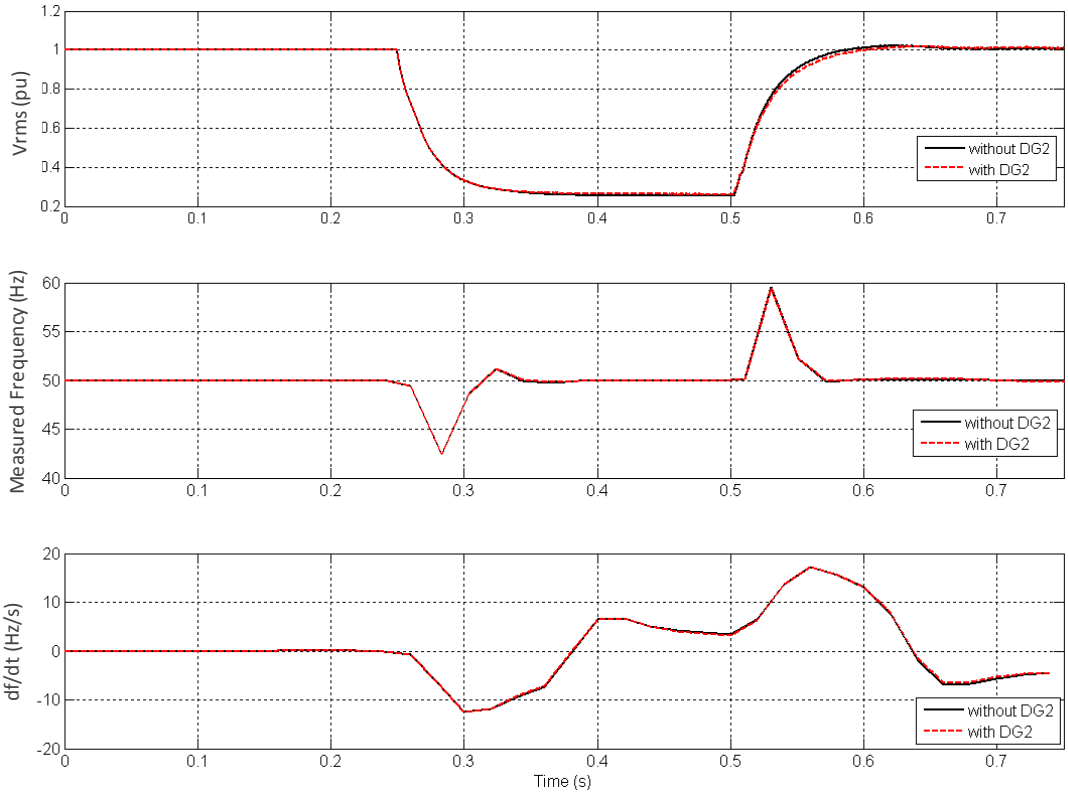

Figure 3-34 ROCOF1's Responses to Adjacent Fault (with or without DG2 tripped)

From the results shown in Table 3-4, it is found that combination of ROCOF relays with and without under-voltage interlock function in the same feeder does not increase or decrease the possibility of nuisance tripping. As shown in Figure 3-34, the parameters used to initiate a trip decision did not change excessively with or without (tripped) DG2.

3.9 Summary of Multiple ROCOF Relays Operation

In term of dependability, multiple ROCOF relays with different setting will not have adverse impact on their abilities to detect islanding. Relays which have lower settings will help the higher setting relay act earlier in its response to islanding.

However, the stabilities of the relays are affected when they operate together. The relay with the lower setting may cause the relay with the higher setting to trip incorrectly. This, however, does not apply to all kind of disturbances. Besides, a relay with a sufficiently high threshold may retain its stability and will not be affected by the other relay's behaviour.

Also, it is observed that ROCOF relays with different internal algorithms can behave very differently when subjected to the same disturbance. When these different (internal algorithm) relays are employed in the same network, even configured to the same threshold setting, the less stable relay may lead the more stable relay to incorrectly trip. Again, this does not apply to all types of disturbances.

CHAPTER 4

MULTIPLE-SET SYNCHRONOUS ISLAND

4.1 Introduction

The connection of distributed generation into the distribution network has seen a rapid growth in recent years. It is expected that in the near future, distributed generation (DG) will become a significant element in the distribution network. However, operating the DG units in a system not designed for them has raised numerous technical challenges. One of the most raised issues is islanding. Islanding refers to a situation where a section of the distribution network continues to be energized by one or several DG units when it is electrically disconnected from the main utility supply.

Current legislation, G59/1 [19] has prohibited the operation of islanding and requires all DG units to be automatically disconnected when islanding occurs. This is due to the complication and safety hazard that islanding poses to the power system. The major issues are maintaining power quality, ensuring personnel safety, preventing unearthed operation and most importantly, avoiding out-of-synchronism reclosing between the island and the grid.

Tripping the DG during a mains failure has obviously limited the benefits offered by DG, particularly when it is capable of supplying the local load within the statutory voltage, frequency and power quality limits. With the expectation of greater use of DG, intentional islanding has created considerable research interest. Different

approaches have been investigated in order to operate DG in island mode.[3, 10-12, 56]

R.J. Best in [57] has proposed a novel scheme which enables islanding without the risk of out-of-synchronism reclosure. Whilst isolated from the grid, this scheme, which he refers to as synchronous islanded operation, holds the island in synchronism with the grid at all times, thus avoiding the risk of out-of-synchronism reclosure. Significant work reported in [1, 2, 57] has shown that this is a feasible solution to the stated problem for single-DG island.

As DG penetration into the distribution network grows, it has become increasingly common to find multiple-DG islands. It is believed that with appropriate adaptation, the afore-mentioned scheme is suitable for multiple-DG island as well.

Hence, this chapter will focus on DG's control in a multiple-DG island, discussing the advantages and disadvantages of different control approaches. Studies will concentrate on synchronous-based generators due to their inherent speed droop characteristics and ability to sustain an island.

4.2 Control for Grid Connected and Island Operation

When running in parallel with the grid, DG units are often required to operate in real and reactive power (PQ) mode, exchanging a predetermined real and reactive power with the grid.

Once disconnected from the main grid, it is obvious that any attempt to continue the use of PQ mode will fail since it is practically impossible to balance the generation and load demand accurately. Besides, the utility is no longer having control over the islanded system, and hence relies upon the DG units to control the frequency and voltage in the formed island within statutory limits. To achieve this, DG units have to be immediately switched to voltage-frequency (v-f) control mode, supplying the load demand in the island whilst regulating the frequency and voltage of the island within

permissible limits. Clearly, there is a need to control switching between the grid-connected and islanding operation mode.

This problem is becoming even more complex when multiple DG units are operating in parallel in an island. At least one of them needs to switch to v-f mode and regulate the voltage and frequency of the islanded network. The DG unit that is responsible for this role can be predefined. However, problems may exist when the predefined DG unit is not in the islanded network or out-of-service.

Switching all of them into v-f mode on the other hand may also create problems, as shown in section 4.3.3, as all of them will try to control the system frequency to their own setting if they are allowed to operate unregulated. Hence, proper coordination between the DG units is obviously required.

4.2.1 Fundamental Governor Control of DG Units Interfaced Through Synchronous Machines

Governor control for DG units interfaced using synchronous generators can essentially be classed into three types [38, 50, 55]:

a) Droop control

A droop control mode is adopted when more than one unit is operating in parallel. The change in power output for a given change in frequency is determined by the governor's droop characteristic, R which can be expressed as [50, 55]

$$R(\%) = \frac{\Delta f}{\Delta P} \times 100 \qquad (4\text{-}1)$$

Where

Δf = per unit change in frequency

ΔP = per unit change in unit output

R can be represented graphically by a negative linear slope, as depicted in Figure 4-1. As shown, when the load increases from P_1 to P_1', the generator slows down from f_o

to *f'*. When more than one generator with drooping characteristics are operating in parallel, this characteristic will help in ensuring stable load division between the generators. For example, referring to Figure 4-1, two generators with droop characteristics of R_1 and R_2 respectively are operating in parallel in the network. A load increment of ΔP_L will cause both generators to slow down. Governors of each generator will increase their power output until they reach a common operating frequency, *f'*. The droop characteristic of each generator will determine the amount of load picked up by each unit.

$$\Delta P_1 = P_1{}' - P_1 = \frac{\Delta f}{R_1} \tag{4-2}$$

$$\Delta P_2 = P_2{}' - P_2 = \frac{\Delta f}{R_2} \tag{4-3}$$

Therefore,

$$\frac{\Delta P_1}{\Delta P_2} = \frac{R_2}{R_1} \tag{4-4}$$

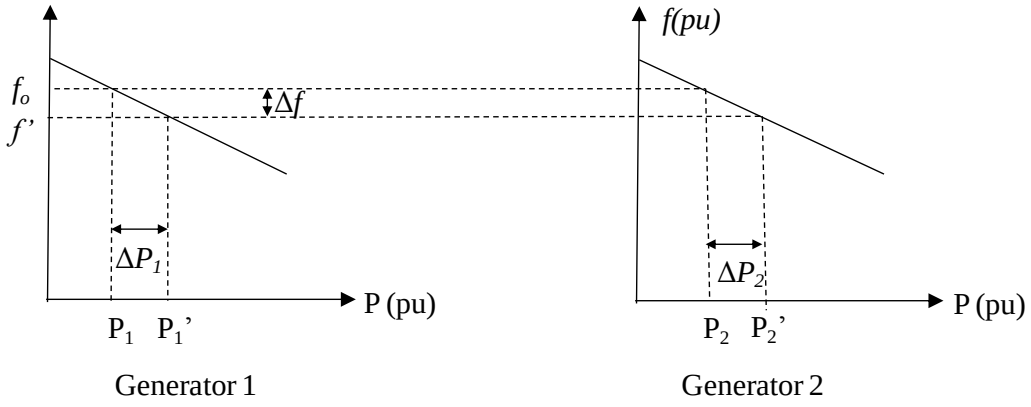

Figure 4-1 Speed-droop Characteristic and Load Sharing between Parallel Units

b) Fixed power control

When running in parallel with the grid, DG units are not required to participate in frequency or voltage regulation. Hence, a fixed power control mode is usually adopted, dispatching a fixed amount of active and reactive power to the system. This can be done by adjusting the speed droop setpoint, f_0 (refer Figure 4-2) of the governor. As the grid frequency fluctuations are usually very small (essentially

constant) throughout the time, the choice of f_0 determines the DG power output. When two or more generators are operating in parallel and are not grid connected, the load sharing between the units are determine by their droop characteristics. However, this can be varied by changing the droop setpoint, which effectively move the speed-droop characteristic up and down.

As mentioned before, when operating in parallel with the grid, the adjustment of speed-droop setpoint changes the output power of the generator. Depending on the size of the generator in relative to the network it is connected, the effect it has on system frequency is negligible. However, it is worth to note that when the generator is feeding an isolated load, the changes of speed-droop setpoint will change the generator's speed.

In practice, the adjustment of the setpoint is done by operating the speed-changer motor.

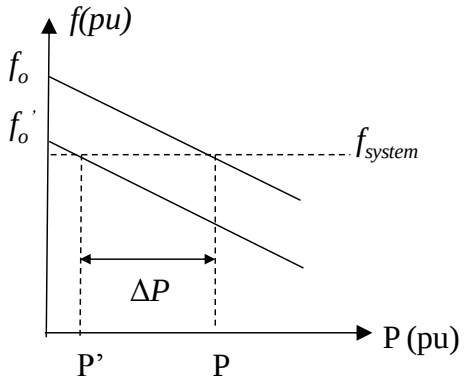

Figure 4-2 Speed-changer Settings

c) Isochronous mode control (Fixed speed control)

Isochronous mode control is often used when a generator is supplying an isolated load, i.e. in an island. This enable the generation to match the load demands while keeping the frequency at a predetermined constant value.

4.3 Case Studies

As discussed in the previous section, there are essentially three types of governor operating controls. If there are more than one generator operating in an island network, at least one of them must be operating in the isochronous mode. The rest can be operated using any of the control mode. Therefore, simulations will be carried out in this section to investigate each of the combination.

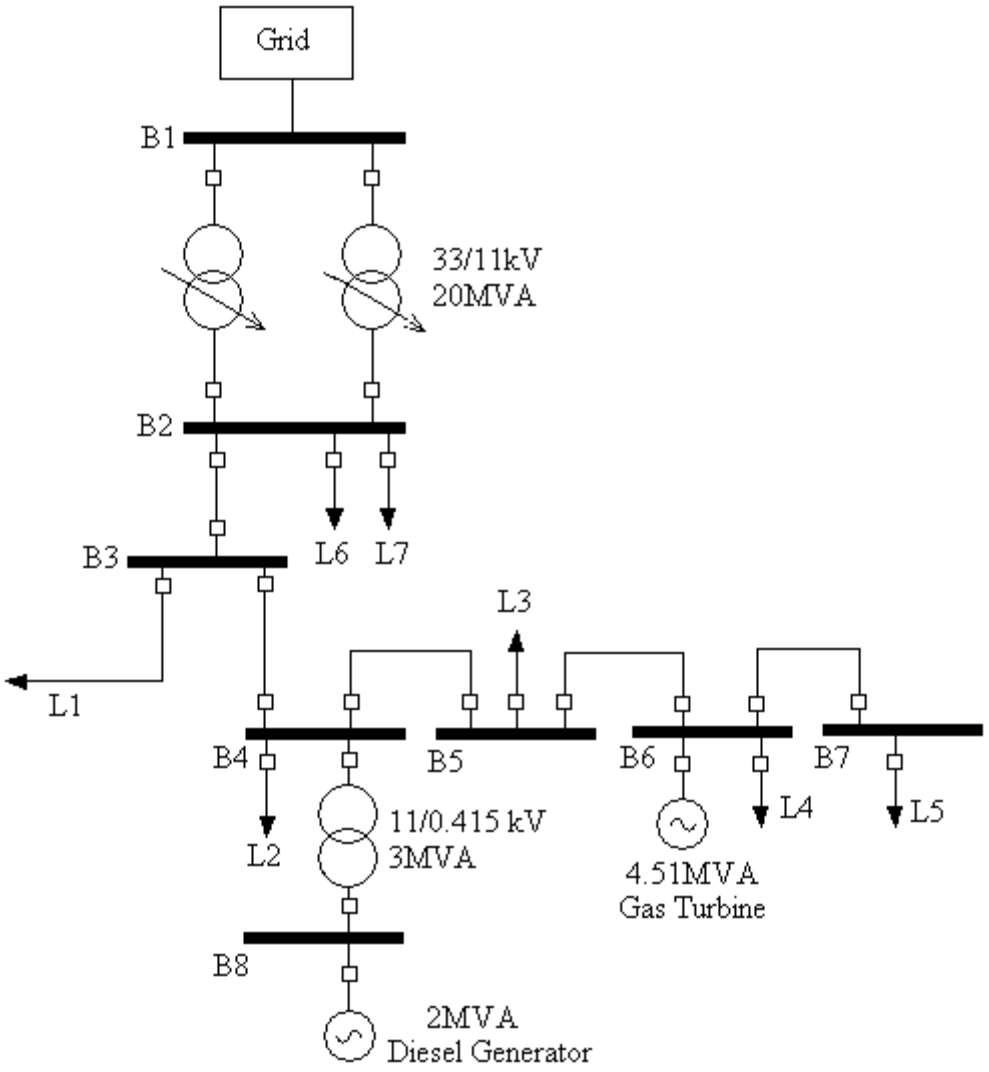

Figure 4-3 Single Line Diagram of Distribution Network Model

A typical section of UK distribution network, adapted from [58], is used as the simulation model in this section. The distribution network model, as depicted in

Figure 4-3, comprises a 33 kV, 50 Hz grid which feeds an 11 kV busbar through two parallel 33/11 kV transformers. A detailed description of the network along with its parameters is provided in Appendix A.

In the simulation, a 4.51 MVA gas turbine (DG1) and a 2 MVA diesel generator (DG2) are connected to busbar 6 and busbar 8 respectively. Both of them are modelled using 5^{th} order DQ representations of a synchronous machine, each equipped with an exciter and governor. The excitation system used is the AC5A model from IEEE Std. 421.5-2005 [59]. Reactive power is shared between them using a quadrature current droop compensation method [50]. The loads are distributed along the feeder and are modelled as constant impedance static loads.

Prior to islanding, both DG units operate in fixed power control mode (DG1 – 0.5 pu and DG2 – 0.8 pu; based on their respective generator rating). Islanding is simulated by opening the line between busbar 2 and busbar 3 at t = 0.5s. In this study, it is assumed that both DG units have the capability of detecting islanding. As soon as they detect the occurrence of island event, their governor control mode is switched. Three different governor control combinations considered are:

i) DG1 in isochronous mode while DG2 in droop control mode
ii) DG1 in isochronous mode while DG2 remains in fixed power control mode
iii) Both DG units in isochronous mode

4.3.1 **Case Study 1: DG1 in isochronous mode while DG2 in droop control mode**

Immediately after islanding, DG2 changed its governor control to droop mode (5%) by resetting its governor frequency setpoint. It can be observed from Figure 4-4(a) that DG1 (isochronously-governed unit) supplied the entire load demands within its machine rating in order to keep the frequency constant.

In order to study the frequency response of both generators during the load transient, load increment is carried out at t=25s and t=41.5s. As DG1 has now reached its

machine rating and is incapable of supplying the total load, frequency starts to drop, deviating from the nominal value. As the units slow down, the drooping characteristic of DG2 acts to increase its output.

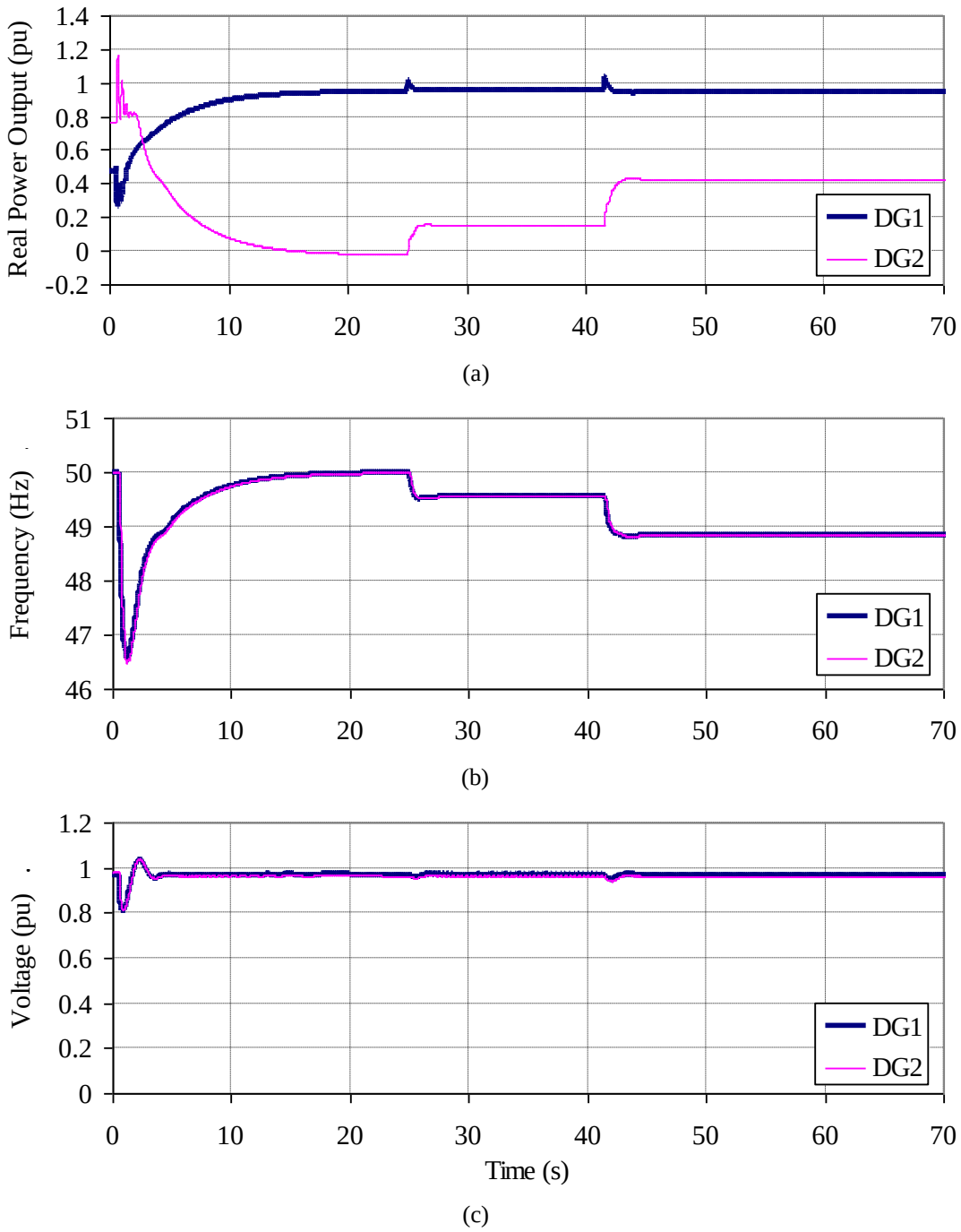

Figure 4-4 Response of DG1 and DG2 for case 1: (a) Real Power Outputs (b) Frequency (c) Voltage

Clearly, it is seen that in this case study, droop-mode unit, i.e. DG2 may not get to deliver any real power if the load demand stays within the isochronous unit's rating. Even when it gets to deliver, it is at the expense of frequency drops. Note that the new operating frequency is proportional to the generator's droop characteristic as well as the load frequency's characteristic [60].

A change in frequency may be undesirable for frequency-sensitive loads, i.e motors [5] and without proper coordination; underfrequency relay may be activated to trip loads from the islanded system in some cases. [5]

Transfer of load from the isochronous unit to the other unit may be favourable so as to shed load from the former unit. This can be done by altering the speed changer setting of the droop governor.

Obviously, the main disadvantage of this scheme is its inability to regulate the island's frequency close to nominal value, unless a signal command is constantly being sent to the droop-mode generator to vary its droop speed setting. Clearly, this option requires communication availability.

4.3.2 **Case Study 2: DG1 in Isochronous mode while DG2 remains in fixed power control mode**

Again, islanding is simulated at t=0.5s. A 240kW with 0.9 power factor load was switched in at t=25s followed by a switching out of 150kW with 0.95 power factor load at t=41.5s. As depicted in Figure 4-5, all load changes are absorbed by DG1 while DG2 provides constant real power output (0.8 pu).

In this case study, it is observed that this scheme is able to control the island's frequency at the nominal value. Nonetheless, this scheme also suffers the main drawback as the previous scheme. Once the isochronously-governed generator hits its output limit, the frequency will drift from the desired nominal value.

Configuration for case 1 and case 2 works on the basis that the generator responsible for the frequency-governing is predetermined. As this generator is responsible for absorbing all the load changes, fast response governor and huge capacity machine are among the factors looked in determining the isochronous mode generator.

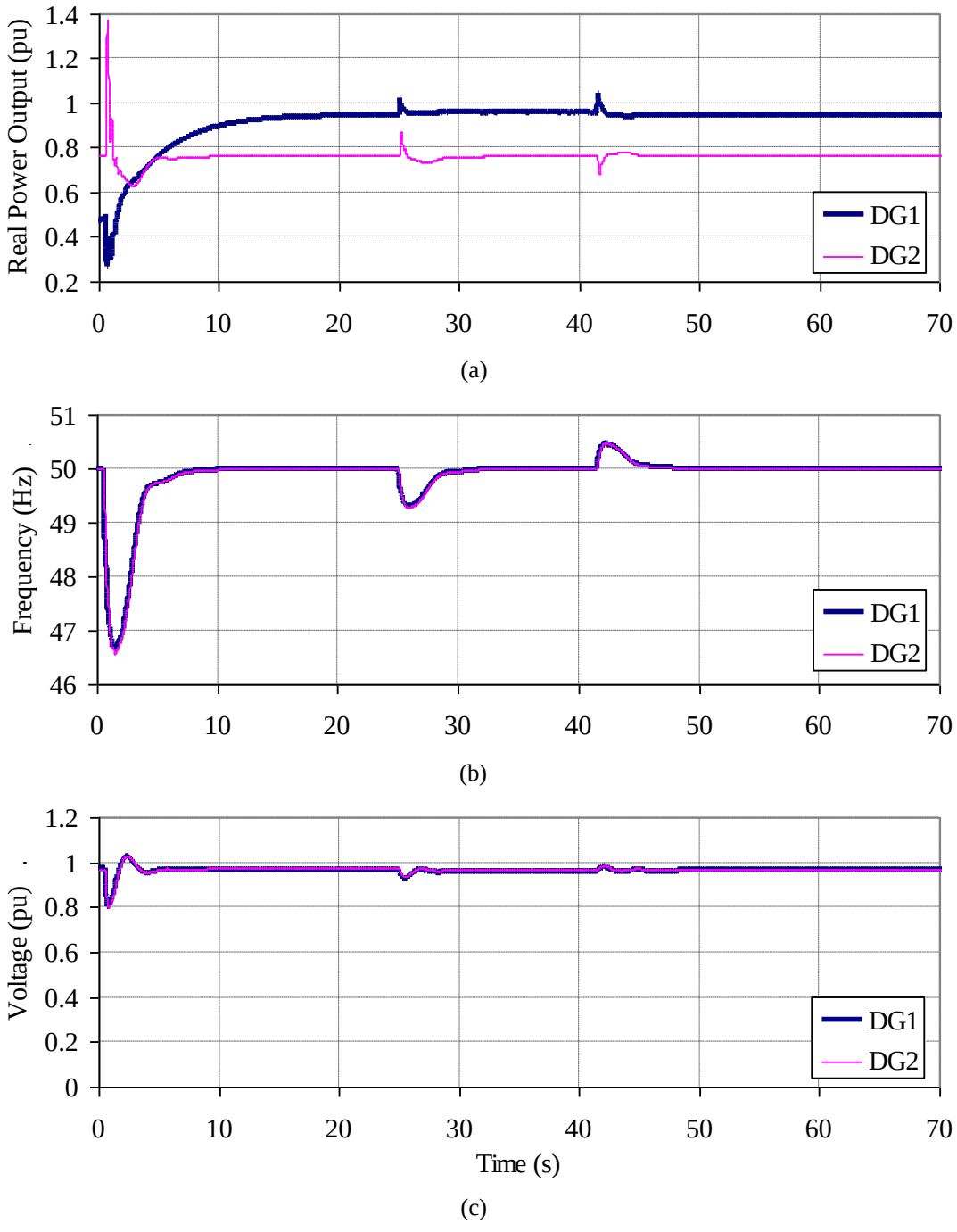

Figure 4-5 Response of DG1 and DG2 for case 2: (a) Real Power Outputs (b) Frequency (c) Voltage

If the generator responsible for the isochronous control trips, in this case DG1, the island system may need to be shut down unless there is a signal command given to the other generator to take up the task/responsibility.

As the connection of distributed generator increases, the size of island may vary. To make the matter worst, more than one island may be formed. The generator responsible for the isochronous-mode may be predetermined, but it has to be ensured that this particular generator is within the island and it is online at the time islanding occurs. As such, the communication requirement may be inevitable.

4.3.3 **Case Study 3: Both units in isochronous mode**

It is reported in the literature that no more than one isochronous unit is to be connected to the same system [50, 55, 59]. This is because it is impossible to set multiple machines at exactly the same speed when paralleling. The machine which runs faster may absorb all the loads while the slightly slower machine will shed all its loads [50], as shown in Figure 4-6.

It is also observed that both generators experienced a continuously increasing power oscillation. Eventually, the frequency will become unstable as observed in Figure 4-7 and as a result the system needs to be shut down. The rate at which this situation may happen is related to the steady state measurements errors, the difference in the gains and time constants for the governor of each generator [57].

However, communication may be employed to increase the stability of this scheme. Information exchange between generators can help in preventing measurement errors and thus eliminating the conflict between their governor controls (Figure 4-6).

The same study as case study 2 has been carried out, but with both DG with isochronous mode governor. In order to prevent the real power deviation as seen in Figure 4-6, communication has been employed to facilitate the load sharing between the generators.

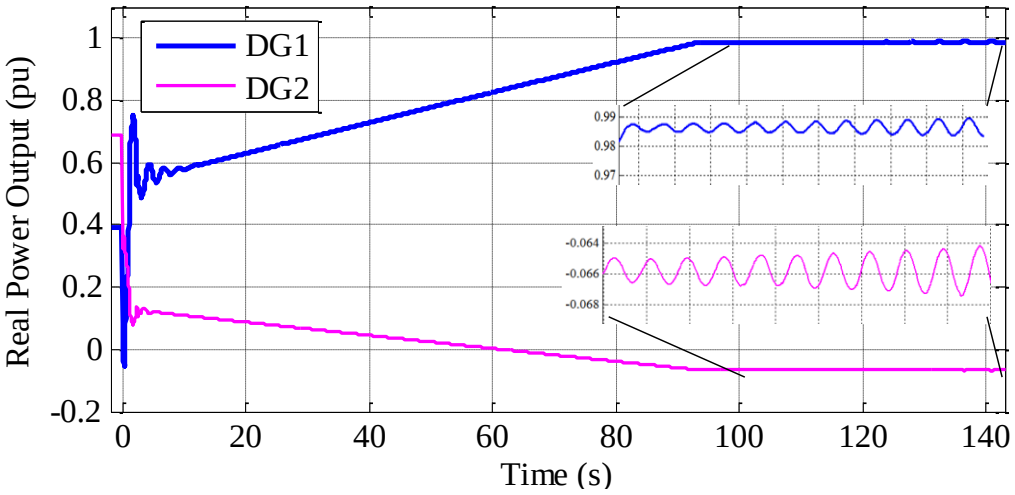

Figure 4-6 Real Power Outputs of DG1 and DG2 (both generators running in isochronous mode)

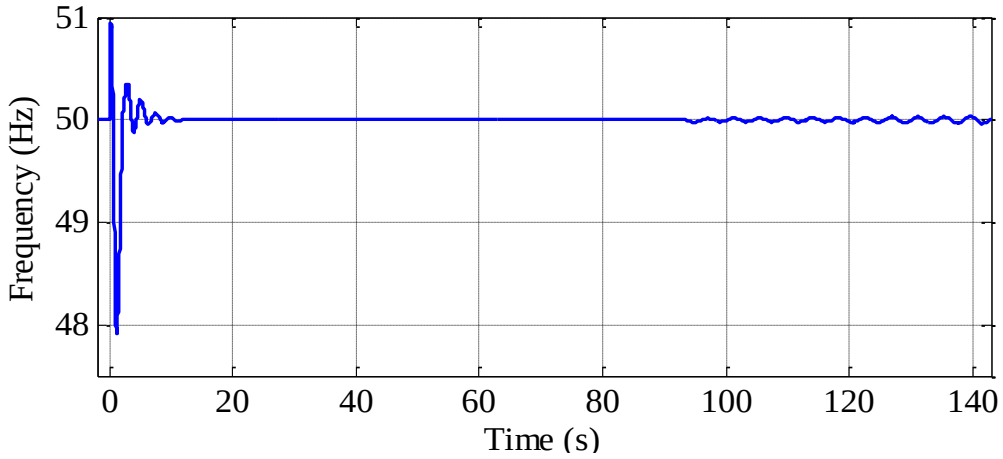

Figure 4-7 Frequency profile of case 3

It is depicted in Figure 4-8 that the frequency response with all units operating in isochronous mode (with communication) is better than the previous case. The frequency deviation during system transient has clearly reduced. Besides, with this scheme, there isn't a need to appoint any generator responsible for the speed-control. All the generators will switch to isochronous mode once they detect the occurrence of islanding. Even when one of them trips, there is always a backup generator regulating the island frequency. In addition, this method has enabled equal sharing of loads between generators, as shown in Figure 4-9.

It is worth to note that for all three cases, voltages are restored within statutory limits, as depicted in Figure 4-4(c), Figure 4-5(c) and Figure 4-10.

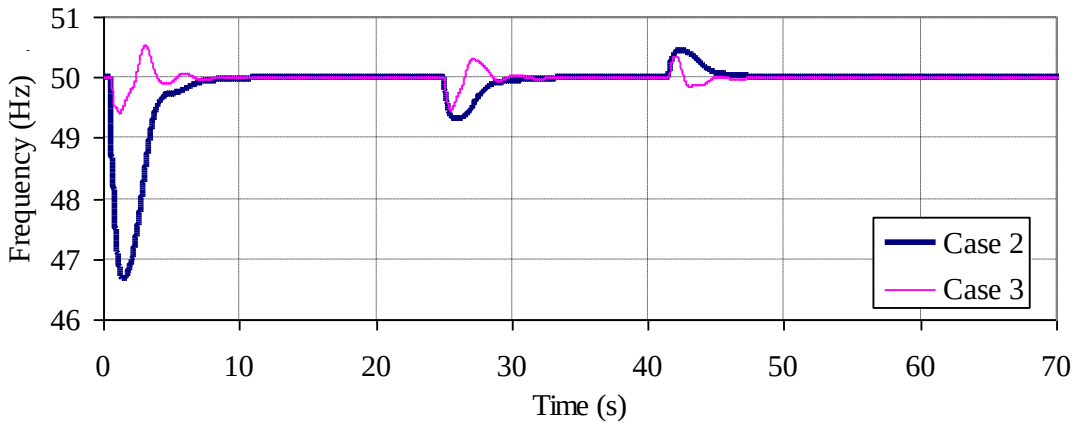

Figure 4-8 Comparison of Frequency Response between Case 2 and Case 3

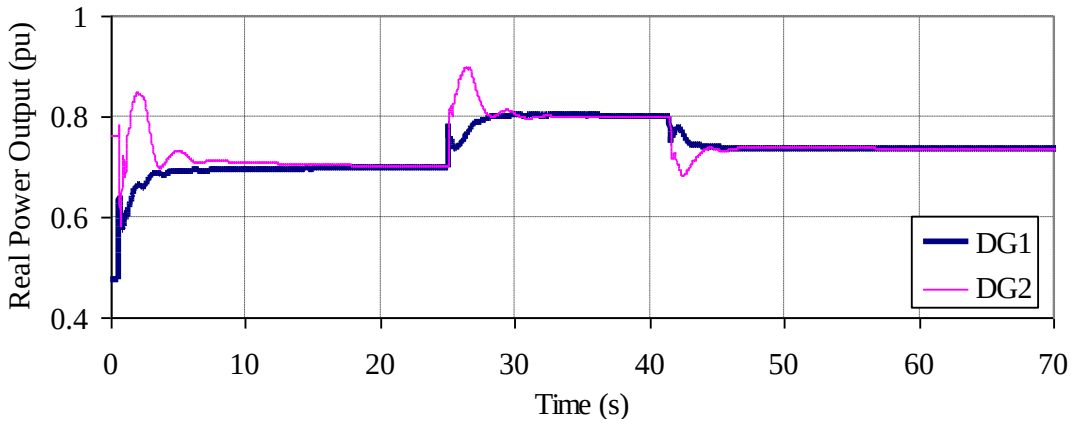

Figure 4-9 Real Power Sharing between DG1 and DG2 for Case 3

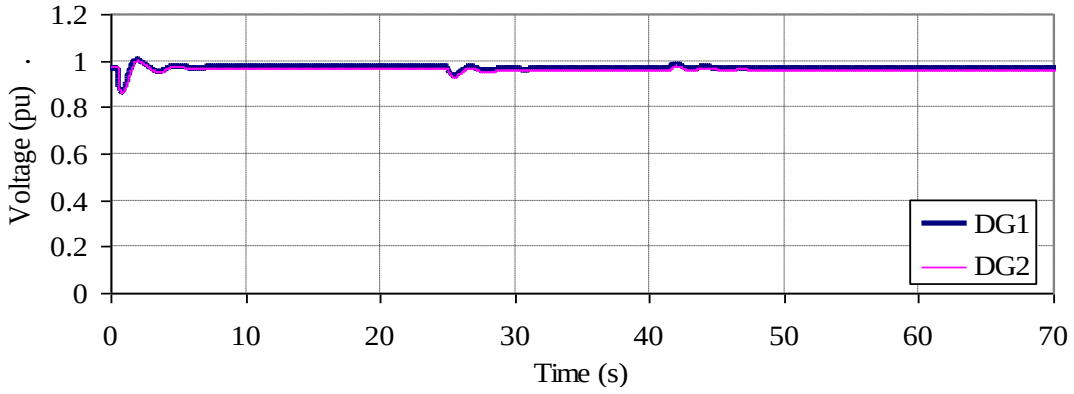

Figure 4-10 Voltage Response of DG1 and DG2 for case 3

4.4 Concept of Multiple-Set Synchronous Island Operation

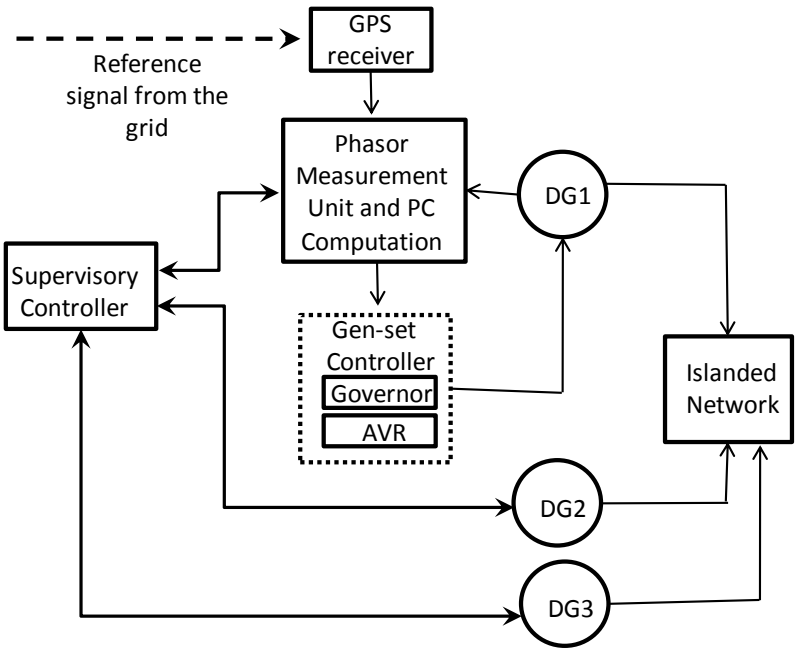

Figure 4-11 Concept of Multiple-set Synchronous Islanded Operation

The concept of multiple-set synchronous islanded operation is illustrated in Figure 4-11. Islanding may occur due to pre-planned outages or following a fault in the network. Clearly, the latter case imposes greater challenges than the former scenario. In any case, loss of mains protection is required to detect the occurrence of islanding and switch the control mode of generators. As discussed in previous chapter, there are numerous ways proposed to detect islanding. It must however be emphasized here to consider the interaction effect between loss of mains detection devices in a multiple unit system, as illustrated in section 3.8. For synchronous islanded operation, detection of island can be done using angular difference method since the main grid's reference and islanded generators' phasor measurements will be available [57, 59].

Following islanding, this scheme requires a reference signal (voltage phasor) to be transmitted from the utility's substation to the controller of the islanded DG units. This measurement is then compared with the voltage phasor measured locally from the DG units. The resulting phase angular difference is used in the phase controller to regulate the island's phase to match the mains.

GPS synchronised phasor measurements is proposed for this application in order to reduce the time error between the two measurements [57]. Rapid updates and short transmission delay, i.e. <100ms are preferable for the operation of synchronous islanded operation. However, a longer delay of up to 300ms is allowed with a more advanced predictive method [57].

The island must have sufficient dynamic regulating capability in order to tolerate changes in power flow as a result of the loss of mains. Not all DG units in the island will have the capability for synchronous island control, but they may contribute to the voltage and frequency function. It would be beneficial if these DG units could ride through the island initiation transient should a synchronous island be formed. This could be achieved by desensitising the settings of the loss of mains protection. This is however suitable only if the automatic reclosure times have been lengthened in the knowledge that synchronous islanding may occur, or else there may be a risk of out-of synchronism reclosure.

The island may also be importing power from the grid prior to the islanding incidence, and may not be able to provide for all the loads trapped in the island. It is hence essential to shed non-essential load (which can be pre-defined) following islanding to maintain the island stability and allow for secure operation of the critical load.

In a multiple-set synchronous island, supervisory control is necessary to coordinate the generators within the island and avoid conflict between the generators control, as discussed in the previous section. It will provide a communication link between those generators, exchanging important information such as connection status and load sharing setpoint. Supervisory control can be either centralised or distributed at several locations.

4.5 Island Operating Algorithm

The operating algorithm of synchronous islanded operation is presented by flow chart in Figure 4-12. During normal operation, DG units operate in parallel with the mains. Usually, they are required to operate in PQ mode when grid-connected, supplying a pre-defined active and reactive power to the network.

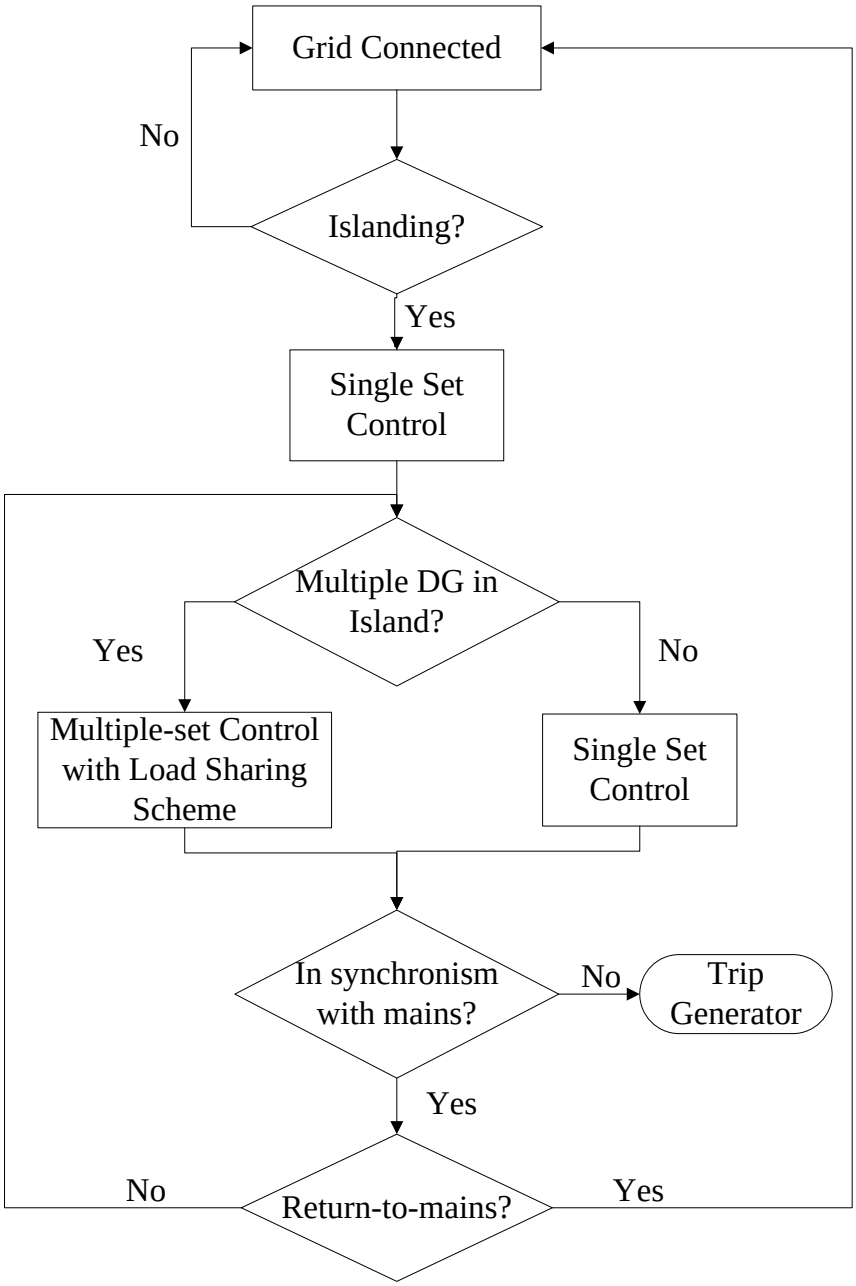

Figure 4-12 Flow Chart of the operating strategy of synchronous islanded operation

It is proposed that each generator is equipped with the capability to detect the occurrence of islanding for rapid change of operation. Fortunately this is achievable as this requirement conforms to the current practice where loss-of-mains detection forms part of the typical protection scheme for DG [19]. On the detection of islanding, each DG assumes itself in a single DG island and changes their operation mode to support the island, regulating the frequency and voltage in the island, while trying to control the island's phase to be synchronised to the mains.

Subsequently, information is exchanged with the supervisory controller and DG units are updated with the status of the island. If there are more than one generator with phase control capability in the island, DG units will change their control accordingly, along with load sharing initiation.

Any load disturbance happening in the island is likely to cause frequency transient and ultimately phase deviation. Thus, the island is also constantly checked to be in phase with the mains. Any disturbance causing phase difference beyond the acceptable limits will lead to tripping of generators. This is essential to prevent out-of-synchronism reclosure and represents the limit for synchronous island operation.

The island is also continuously checked to determine if it has been re-connected with the mains. This is essential to switch back the generator to its pre-islanding setting and avoid the consequence of unstable operation. As the island is held in synchronism with the mains, it is envisaged that only a minimal transient will be observed. This is desirable from the view point of power system operation, but creates an additional challenge to the determination of the state of operation. Fortunately, return-to-mains determination is not as crucial as other operation. Hence it can be performed with a longer time frame, i.e several seconds. In [61], a method based on phase difference variance is proposed to detect return-to-mains. Other methods include knowledge of circuit breaker status, loss-of-mains detection technique not based on frequency or phase deviation etc.[61]

4.6 Proposed Governor Control

Once islanding occurs, at least one generator has to switch from real power control mode to isochronous mode in order to regulate the frequency in the island. This can be achieved by using proportional integral (PI) type governors for the merit of simplicity.

However, even though the frequency of the island is restored to exactly the same as the grid, there is a constant phase deviation between the two, as depicted in Figure 4-13. Hence, there is always a risk of out of phase reclosing when reconnecting the island to the grid.

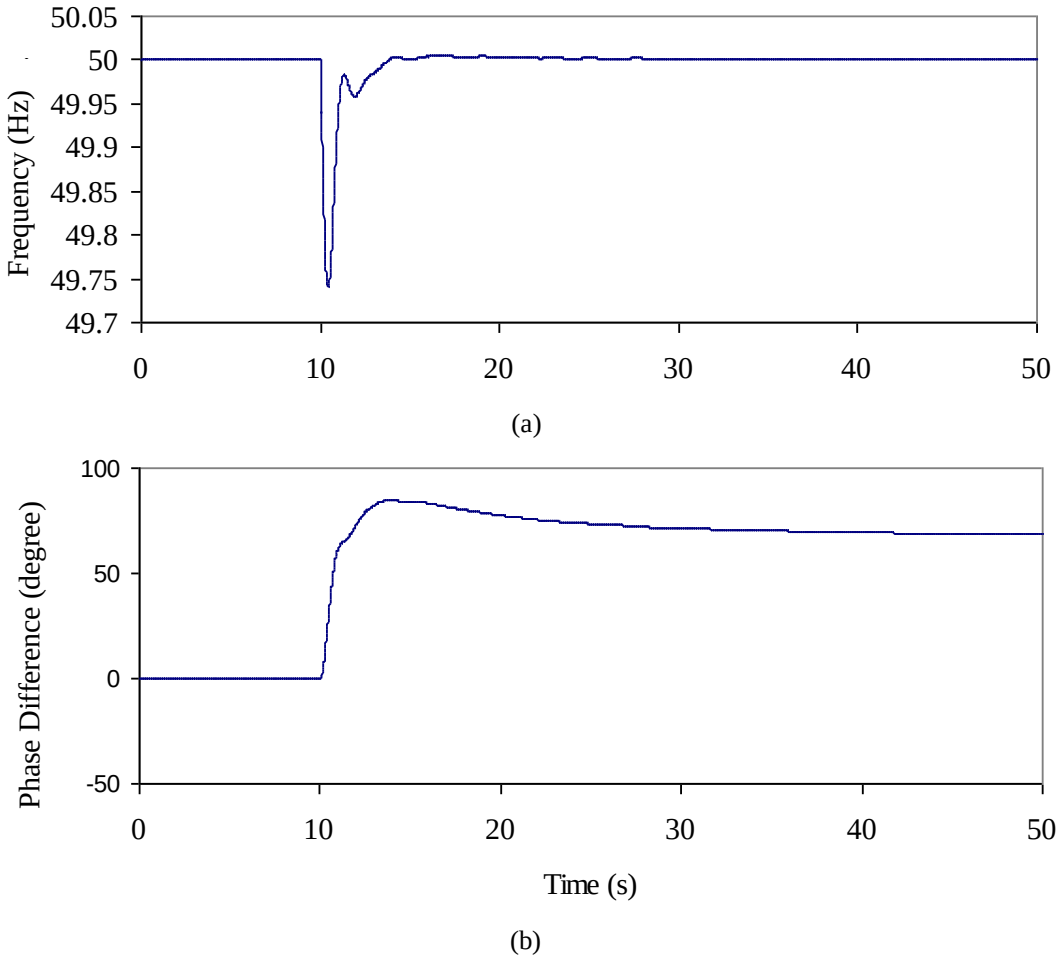

Figure 4-13 Frequency Response and Phase Deviation after Islanding

In order to eliminate the phase difference, a phase difference control signal is added to the frequency error at the input of the PI controller. The PI controller can also be substituted with a PID controller. In a later part of this thesis, the improvement of the governor control due to the use of the latter controller, as compared to the former controller, is proved by the better results obtained.

Besides, in order to prevent the situation depicted in Figure 4-6 and Figure 4-7, a load sharing scheme is developed by passing the real power sharing error through the integral of the PI controller. Communication between generators is necessary in determining the amount of load shared and this is facilitated by the supervisory controller.

The governor control model with phase difference control and load sharing scheme is given in Figure 4-14.

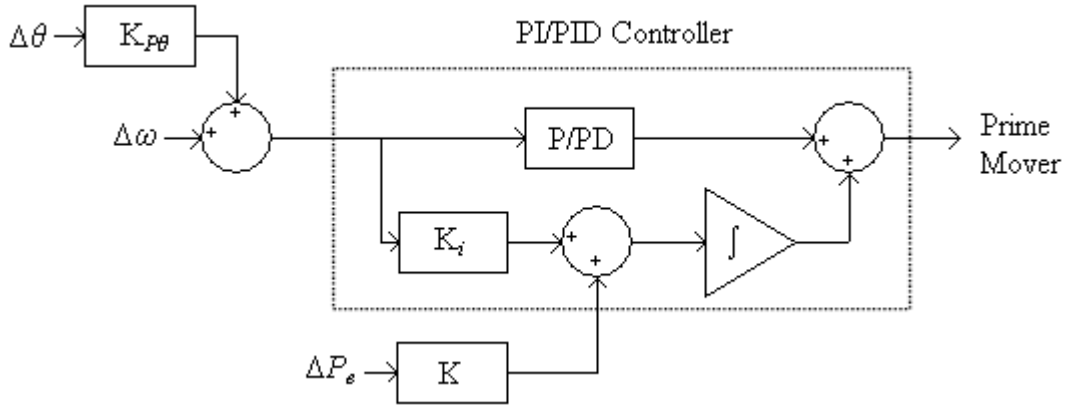

Figure 4-14 Governor Control Model

4.7 Case Studies

4.7.1 Island Formation

Islanding is simulated by tripping the line between busbar 2 and busbar 3 in Figure 4-3 at t=0.5s. It is assumed that both DG units have the capability of detecting islanding. Once islanding is detected, they switch their governor control from constant power control mode to isochronous mode (PI controller). Two scenarios have been simulated:

i) Islanding without phase difference control
ii) Islanding with phase difference control

Figure 4-15 shows the comparison of frequency and phase deviation when there is phase difference control and without phase difference control. It is observed that with the usage of phase difference control, the phase difference between the island and the grid is adjusted to zero. Thus, the island is held in synchronism with the grid and the risk of out-of-phase reclosure is eliminated.

Figure 4-16 shows the sharing of load between DG1 and DG2 for the second scenario. The scheme performed slowly and it takes around 30 seconds for the generators to equally share the load. This is essential in order to prevent steady state phase difference error. It is worth noting that there is a large difference between the output powers of both generators before islanding. In practice, it is not usual to run a generator at such a low power output due to efficiency reason, but it is simulated in such a way to portray the effectiveness of load sharing control.

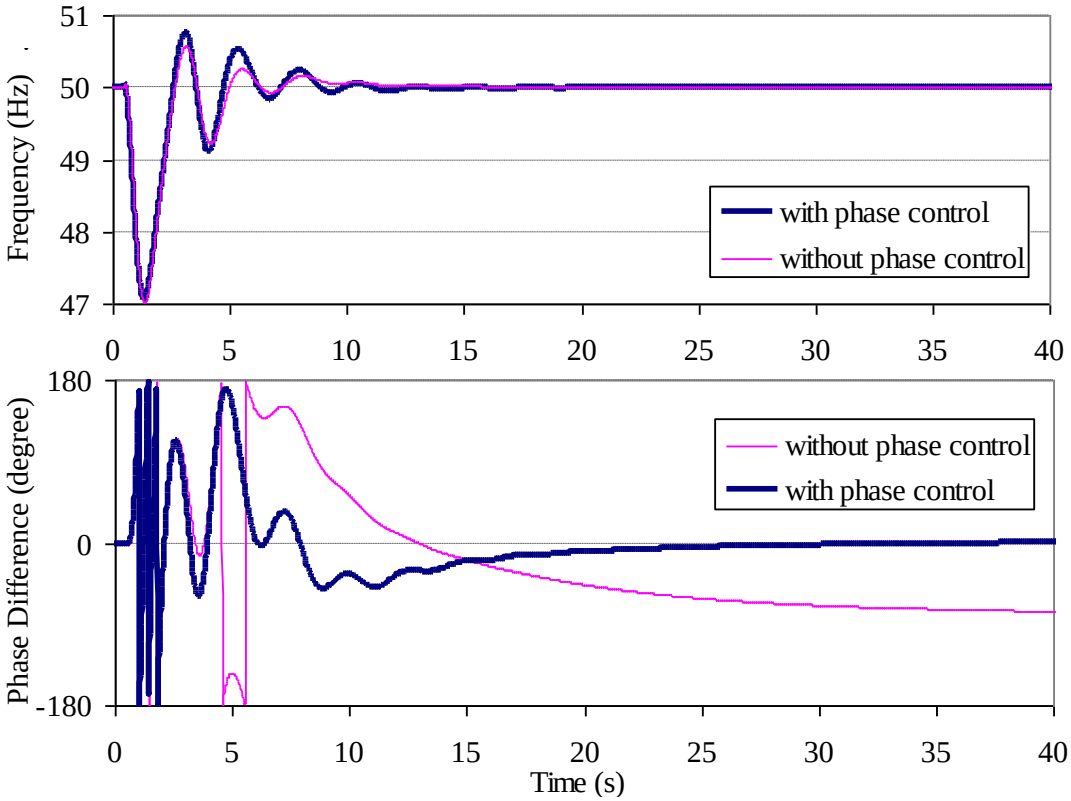

Figure 4-15 Comparison of Frequency and Phase Deviation With and Without Phase Difference Control

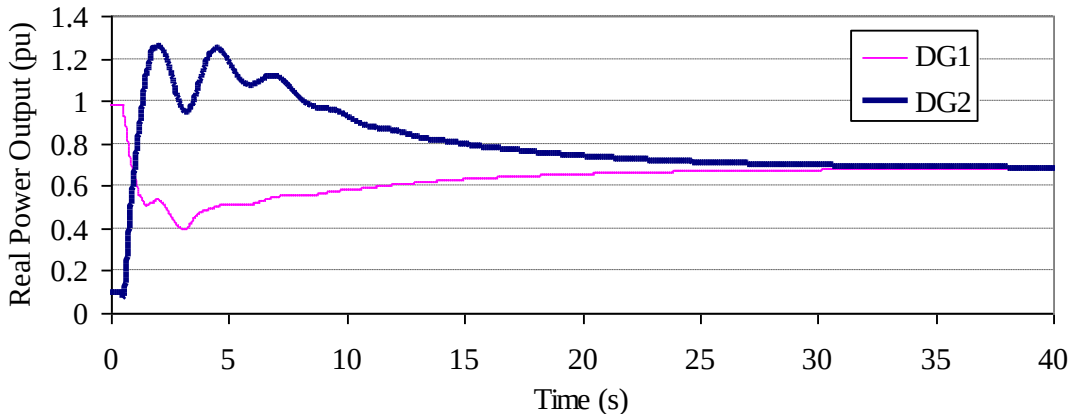

Figure 4-16 Load Sharing between DG1 and DG2

4.7.2 **Governor Control Combination**

A load disturbance is simulated at t=0s by adding a 495kW load to the island. Three different governor control combination has been simulated as followed:

Case 1) DG1 in isochronous mode while DG2 in droop control mode

Case 2) DG1 in isochronous mode while DG2 remains in fixed power control mode

Case 3) Both DG units in isochronous mode

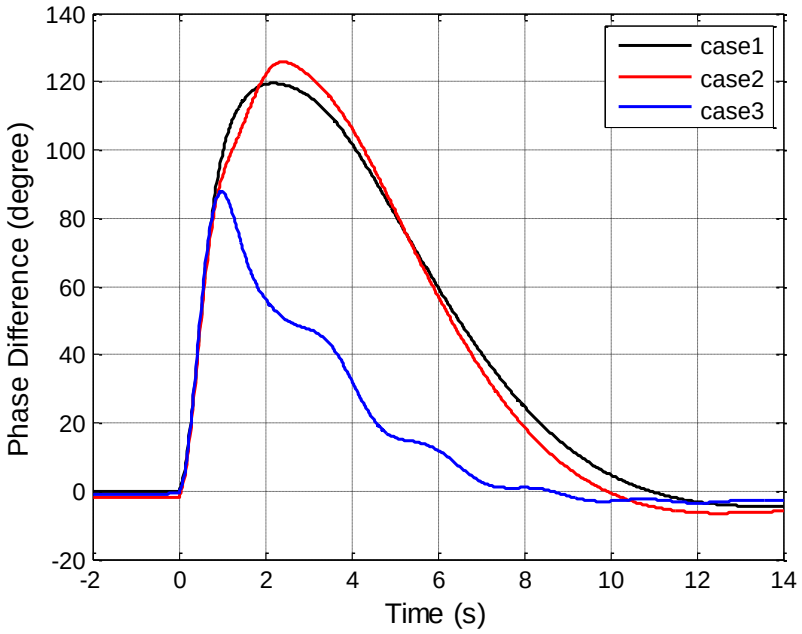

Figure 4-17 Comparison of phase control for all cases

From Figure 4-17, it is seen that case 3, which is the multi-isochronous control mode is the best in controlling the phase deviation following a load disturbance among all combination. It is however worth to note that in this example, phase difference for all three cases has exceeded the limits for synchronous islanded operation, which is $\pm 60^0$.

4.7.3 **Load Disturbance**

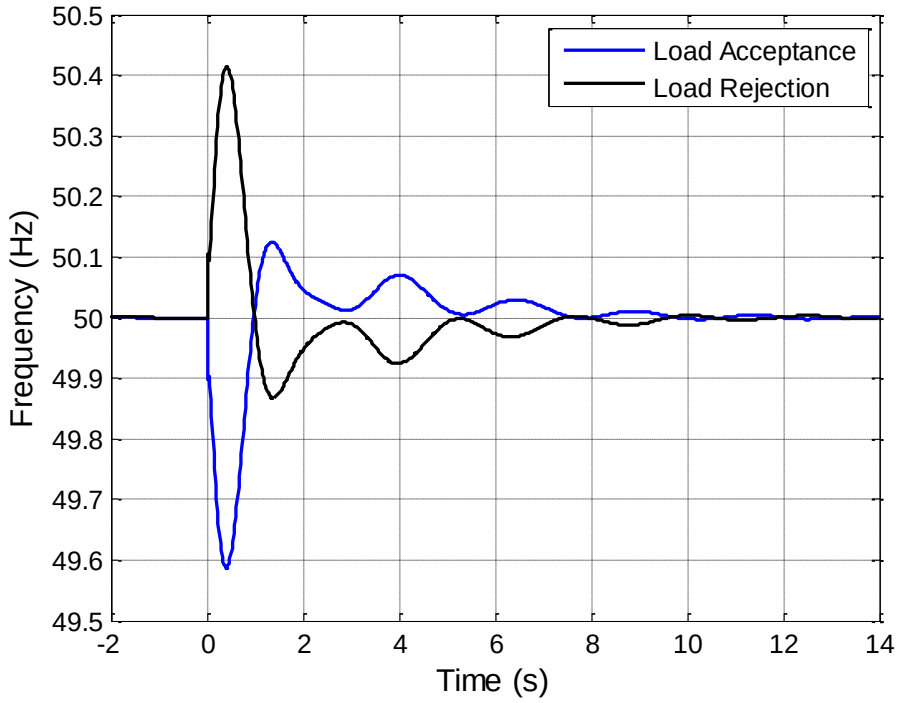

Figure 4-18 Frequency profile for load acceptance and rejection

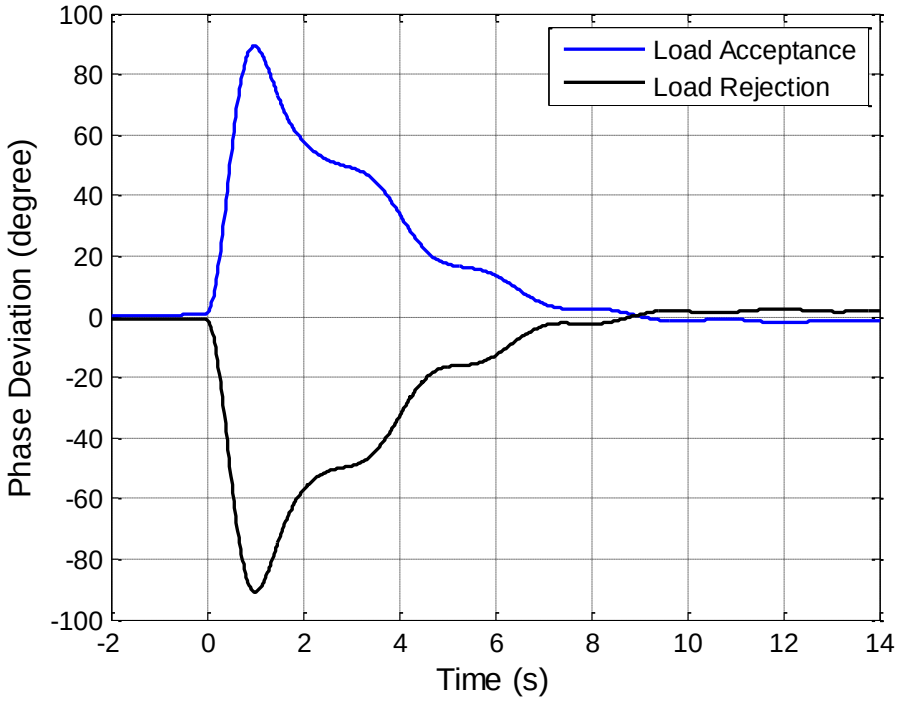

Figure 4-19 Phase Deviation for load acceptance and rejection

Figure 4-18 and Figure 4-19 show the frequency and phase deviation for load acceptance and rejection of 495 kW static load simulated at t=0s respectively. Interestingly, it is observed that the same amount of load will subject the island to the same voltage phase deviation, regardless of load acceptance or rejection. This is for both DG operating in isochronous mode.

4.8 Chapter Summary

This chapter has highlighted the advantages and disadvantages of different governor control scheme in a multiple-set synchronous island. It is proposed that multi-isochronous governor control is used in order to cater for the possibility of loss of generation unit. It is also shown that this scheme is able to control the phase deviation to the predefined value more rapidly compare to the other two combinations.

This chapter also described the concept of multiple-set synchronous islanded operation, along with the explanation of possible difficulties in implementation. A detailed operating algorithm is also presented for further clarification. It is worth to highlight that in future, if islanding is allowed, one may find a greater size of island with more than two DG units in the island. At that stage, during islanding operation, island may split/merge into smaller/bigger island. Hence, a suitable algorithm to detect the splitting or merging of island is then required. The algorithm must also be able to differentiate between merging of island and return-to mains operation.

CHAPTER 5

SYNCHRONOUS ISLAND WITH SIGNIFICANT CONTRIBUTION FROM INTERMITTENT SOURCE

5.1 Introduction

The control and operation of multiple-set synchronous island has been thoroughly discussed in the previous chapter. Hitherto, the island considered comprises only distributed generation (DG) units interfaced through controllable synchronous generators. This however, may not illustrate a realistic scenario. With the integration of renewable resources into the network, it is envisaged that an island might contain a diversity of DG units. Thus, for maximum flexibility, power system islands must be capable of operating with a different mix of generation.

One of the prominent features shared by many renewable resources (except hydro and bio-gas type scheme) is intermittency. A topic worthy of investigation is the impact of this variation on the ability of power system island to stay within statutory frequency and voltage limits. This is even more crucial in the case of synchronous islanded operation; whereby tight frequency regulation is required to ensure the island remains within the synchronization limits.

Hence, the focus of this chapter is to investigate the performance of synchronous island control in the presence of significant renewable power sources within the island. Since wind energy is deemed as the most promising renewable resources in UK, it has been chosen to reflect the variable power sources in the simulation. Two

types of wind turbine technologies, namely fixed speed induction generator (FSIG) based wind turbines and doubly fed induction generator (DFIG) based wind turbines have been developed in PSCAD/EMTDC to aid the investigation. Each of them will be tested in turn to illustrate the advantages of DFIG as compared to FSIG for synchronous islanded operation. The maximum load disturbances that can occur while remaining within an acceptable phase difference are also explored for each case in this chapter.

5.2 Background of Wind Energy

Wind energy is becoming increasingly competitive with other power generation alternatives and has emerged as one of the main and most promising sustainable energy resources. According to [62], the installed capacity of wind power in the world has reached 159 GW by the end of 2009. UK has contributed approximately 2.5% (over 4 GW) to this figure, ranking within the top ten countries that have the most installed wind power capacity [62]. Overall, the installed capacity has increased by 28.1% in year 2009 compared to the previous year, and this figure is set to rise in the future [62].

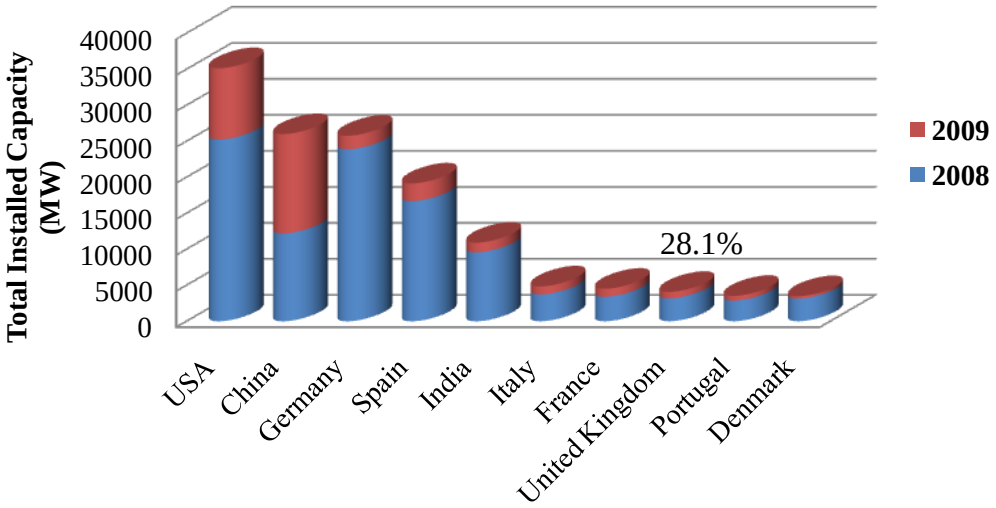

Figure 5-1 Total Installed Wind Power Capacity in Top Ten Countries of the World

One of the key challenges in wind energy is that the electricity production depends solely on wind availability rather than customer's demand. A power system with wind energy penetration can be described using equation (5-1) [63]

$$P_G + P_W = P_D + P_L \tag{5-1}$$

Where P_G = additional required power balance

P_w= wind power production

P_D = load power consumption

P_L= network losses

From equation (5-1), it can be seen that any changes in wind production (or load demand) must be subsequently balanced by other generation sources in the power system, typically by allocating more spinning reserves. When wind power production decreases, the system sees as though there is an increment in the load demand and vice versa. This intermittent nature creates substantial challenges to power system balancing and subsequently increases the requirements as well as cost for power system operation. This impact is especially profound in a weak network (i.e. island) with substantial wind penetration.

5.2.1 **Wind Energy Properties**

The mechanical power that can be extracted by a wind turbine from the wind is given by

$$P_m = \frac{1}{2}\rho A U^3 C_p(\lambda, \beta) \tag{5-2}$$

where ρ is the air density, A is the area swept by the wind turbine blades, U is the wind speed, C_p is the power coefficient, λ is the tip speed ratio and β is the pitch angle of the blades. Tip speed ratio is the ratio between the velocity of the rotor tip and wind speed and is defined by

$$\lambda = \frac{\omega_r R}{U} \tag{5-3}$$

where ω_r is the aerodynamic rotor speed and R is the radius of the rotor.

From equation (5-2), it is seen that power coefficient, C_p depends on both the wind turbine's aerodynamic characteristic and operating conditions [64]. Figure 5-2 depicts the power coefficient, C_p as a function of tip speed ratio, λ with different values of pitch angle, β. It can be observed that the peak value of C_p is significantly reduced by increasing the pitch angle. This characteristic (blade-pitch control) is thus

used to extend the range of wind speeds at which the generator can be operated at rated power. When the turbine's power generation is lower than the rated power, it is designed to extract as much power from the wind as possible. Once the rated power is reached, the blades are pitched to decrease the power coefficient and thus maintain the generated power at rated value.

According to Betz law, C_p has a maximum value of 0.59 [65]. In practical however, due to economic and physical limitation reasons, achievable Cp values are in the range of 0.4 to 0.5 [66].

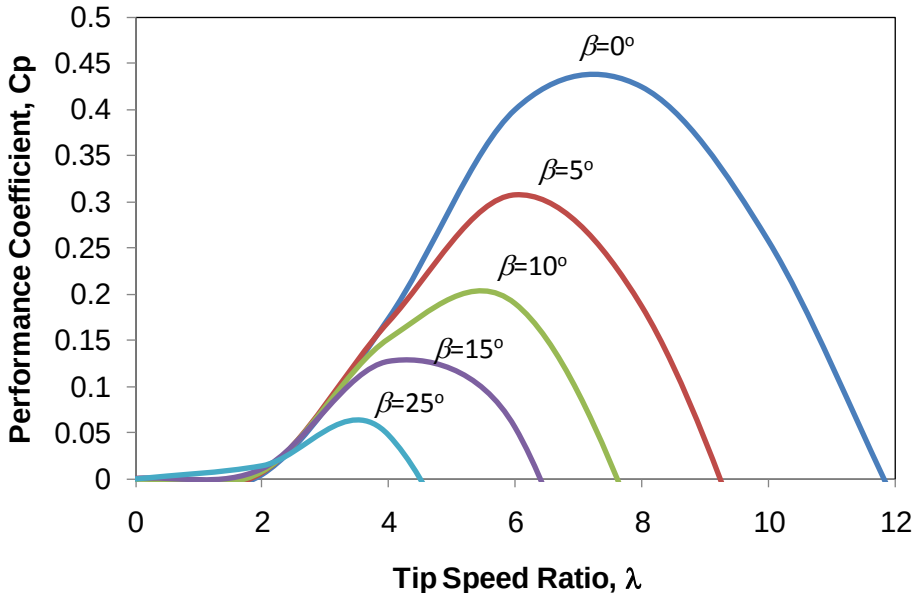

Figure 5-2 Cp-λ curve

With the knowledge of the power characteristic, it is possible to change the rotor speed in accordance with the wind speed to ensure Cp and subsequently the wind power generation is maximised. This is the concept behind the operation of a variable speed wind turbines.

5.2.2 **Overview of Wind Turbine Concepts**

Wind turbine technologies have improved significantly over the years. Typically, wind turbines are interfaced to the grid through either fixed speed or variable speed generators. These generators can be either synchronous or asynchronous, though the latter are more commonly used.

5.2.2.1. **Fixed Speed Systems**

Also known as "Danish Concept", induction generator (usually squirrel cage) of fixed speed wind turbine is directly coupled to the grid as illustrated in Figure 5-3. Thus, regardless of the wind speed, the turbine's rotor speed is fixed (within speed range of about 1%) and is determined by the frequency of the supply grid, gear ratio and generator design [63].

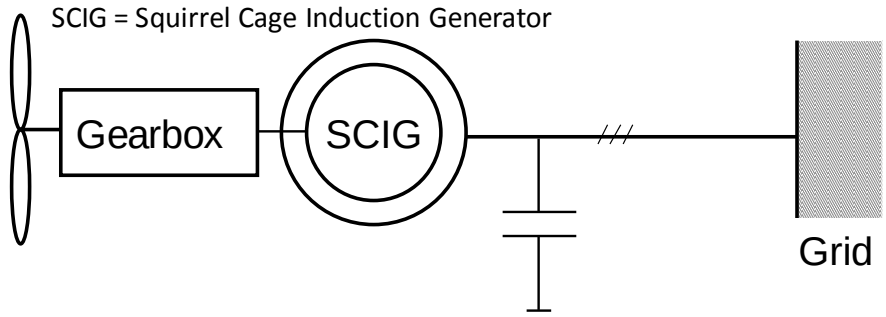

Figure 5-3 Fixed Speed Induction Generator.

Fixed speed wind turbines are favoured for their simple and robust construction with very low investment and maintenance cost [63, 67]. However, the fixed rotational speed has several drawbacks [63, 67, 68] :

- The turbines are often not operating at the optimal operating point for different wind speed and thus are not extracting the maximum power from the wind
- The generator's output power cannot be regulated quickly (dependant on pitch control time constant [64]) as the only way to influence it is by changing the blade's pitch angle.
- Wind turbulence will result in output's power fluctuation that not only cause mechanical stresses that reduce the turbine's lifetime but also affects the power quality.
- Additional capacitor bank is required to compensate its uncontrollable reactive power consumption.
- Excessive noise due to lack of excitation control.

In order to increase power production, the fixed speed wind turbine system is often equipped with two generators, one for medium and strong wind condition and the other for weak wind condition (with lower rating and lower rotational speed). Another alternative is to use only one generator with two switchable winding sets to suit different wind velocities (typically 4-6 poles for high wind speeds and 8 poles for low wind speeds). [63, 67]

5.2.2.2. **Variable Speed Systems**

For the past decades, the variable speed wind turbine systems have become the dominant type among the installed wind turbines [67]. This is mainly due to the advantages offered by it over the fixed speed system:

- Variable speed wind turbines configurations provide the ability to change the turbine's rotational speed in accordance with the wind speed. This allows the system to operate constantly at its optimum tip speed ratio, thus achieving maximum efficiency over a wide range of wind speeds. Depending on the turbine aerodynamics and wind regime, variable speed system on average increases the annual energy production up to 10% in comparison to fixed speed system [69].
- Mechanical stresses on turbines are reduced because variations in the wind are absorbed by the changes in the generator speed.
- The power outputs fluctuations are reduced as the instantaneous condition present in the wind are buffered by its mechanical systems, thus improving the power quality.
- Implementation of a simpler blade pitch mechanism is possible with the longer time constant in variable speed system.
- Noise emission during weak wind conditions is reduced due to the wind turbines' lower rotational speed.

Despite the above-mentioned advantages, variable speed systems also suffered from several drawbacks. The most apparent disadvantage of this configuration is the use of more components (power electronics) and the additional cost associated with them.

The overall controls are also more complex and losses in the power electronics are not negligible.

Figure 5-4(a)-(c) depict some of the typical variable speed wind turbines configurations. The advantages and disadvantages of each configuration will be briefly discussed here:

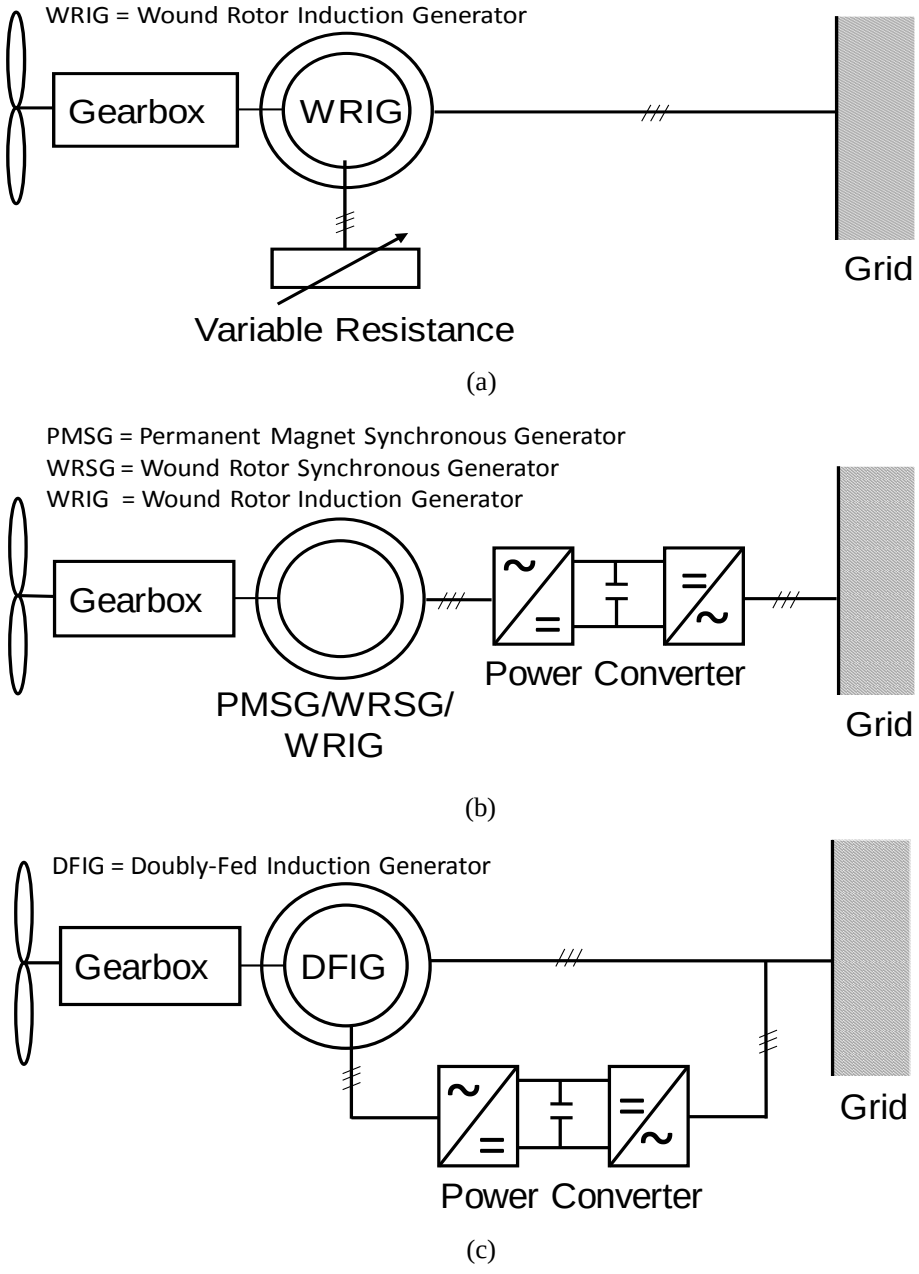

Figure 5-4 Variable Speed Wind Turbines Configurations (a) Limited Variable Speed, (b) Full Variable Speed, (c) Doubly-Fed Induction Generator

a) Limited Variable Speed [68]

Similar to fixed speed system, the generator in this configuration is directly coupled to the grid. However, it uses a wound rotor induction generator as contrary to the squirrel cage induction generator used in fixed speed system. It has a variable external rotor resistance, which can be changed to control the slip. By varying the rotor resistance and thus the slip, the total output power can be controlled. The size of the variable rotor resistance determines the dynamic speed range, which typically ranges from 0 to 10% above synchronous speed. The main drawback of this scheme is that energy is dissipated in the external rotor resistance unnecessarily. It is also not possible to drive the rotor speed below synchronous speed or control the reactive power consumption.

b) Full Variable Speed System [69]

The generator in this configuration is interfaced to the grid via a back-to-back voltage source converter, as shown in Figure 5-4(b). This scheme provides the liberty of using either permanent magnet synchronous generator, wound rotor synchronous generator or wound rotor induction generator as its generator. Depending on the choice of generator, the gearbox may or may not exist.

This configuration is favoured for its well developed and robust control. It is also possible to control the power factor over a wide speed range. Nonetheless, this scheme requires the power electronic converter to be sized at the rated system power, which renders it expensive and economically unattractive.

c) Doubly Fed Induction Generator (DFIG)

In this configuration, the stator of the wound rotor induction generator is connected directly to the grid whilst the rotor is connected to the grid via a back to back voltage source converter. The rotor side converter is used to provide speed control, and thus the stator's active power, together with terminal voltage and/or power factor control. On the other hand, the grid side converter is employed to maintain a constant DC-bus voltage between the converters. This unique configuration enables the generator to operate at super-synchronous (above synchronous speed) and sub-synchronous

(below synchronous speed) speed, and thus optimises the extraction of wind energy. Depending on the generating mode, active power may be transferred from the rotor through the converter into the grid or vice versa (Figure 5-5). The total power delivered to the grid is a sum of the power delivered by the stator and that to or from the rotor [68]:

$$P_s = v_{ds} \times i_{ds} + v_{qs} \times i_{qs} \quad (5\text{-}4)$$

$$P_r = v_{dr} \times i_{dr} + v_{qr} \times i_{qr} \quad (5\text{-}5)$$

$$P_g = P_s - P_r \quad (5\text{-}6)$$

Where P_s is the stator power, P_r is the power to the rotor and P_g is the total power generated and delivered to the grid.

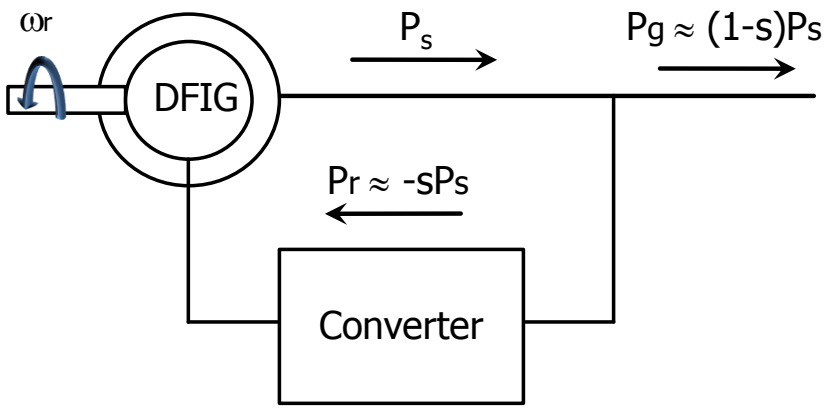

Figure 5-5 Power Flow in DFIG

The speed range of DFIG is typically between 70% to 130% of rated speed (±0.3 slip). As the converters only need to handle the slip power of the rotor, its size can be reduced to typically 25%-30% of the total system power [70]. The reduced converter size makes this scheme cost-effective. Besides, rapid and decoupled control over active and reactive power offers better performance concerning system stability during disturbances [71]. The main downside of this scheme is the use of slip rings which requires regular maintenance. Although DFIG converters need only to be rated at a fraction of its steady state rating, they may fail to cope with faults and transient as their dynamic rating can be considerably higher [72]. For that, a crowbar is typically employed to limit the fault currents and protect the converters.

5.3 Scope of Simulation

A set of simulation will be performed to determine the ability of fully controllable synchronous machine interfaced generators to maintain synchronous islanded operation in the presence of distributed generation with variable power output, i.e. a wind farm. To simplify matters, certain assumptions are placed on these case studies:

- All distributed generators in the simulation model except wind farm are equipped with synchronous islanded operation capabilities, i.e. phase difference control and real power load sharing during islanding.
- A reliable communications link with supervisory control are readily available to facilitate island control function
- Immediately after islanding, all distributed generators, except wind farms, change their governor control mode to support synchronous islanded operation.
- The size of the island is limited by the modelled network and island fragmentation is not considered throughout the simulation time.

Two types of wind farm technologies have been modelled for case studies in this chapter:

- fixed speed induction generator (FSIG) based wind farm
- doubly fed induction generator (DFIG) based wind farm

The rationales behind the choice of wind farm modelled in the simulation are:

- FSIG based wind farm is deemed as the classic and simplest concept in wind turbine technology. It has no control over its output and fluctuations in the wind velocities are reflected in its power output to the grid. This poses a huge challenge especially in a weak grid, i.e. islanded network. It is even more a concern when operation of a synchronous islanded network is desired, whereby a tight frequency control is required to remain within synchronization limit. Hence, these studies represent the worst case scenario for synchronous islanded operation with intermittent power sources.
- DFIG based wind farm represents a more advanced technology and can be commonly found in medium and large size wind farms. It has a greater

control over its power output and is included in the simulation to investigate how this technology benefits synchronous islanded operation.

5.4 Simulation Model

5.4.1 Network Model

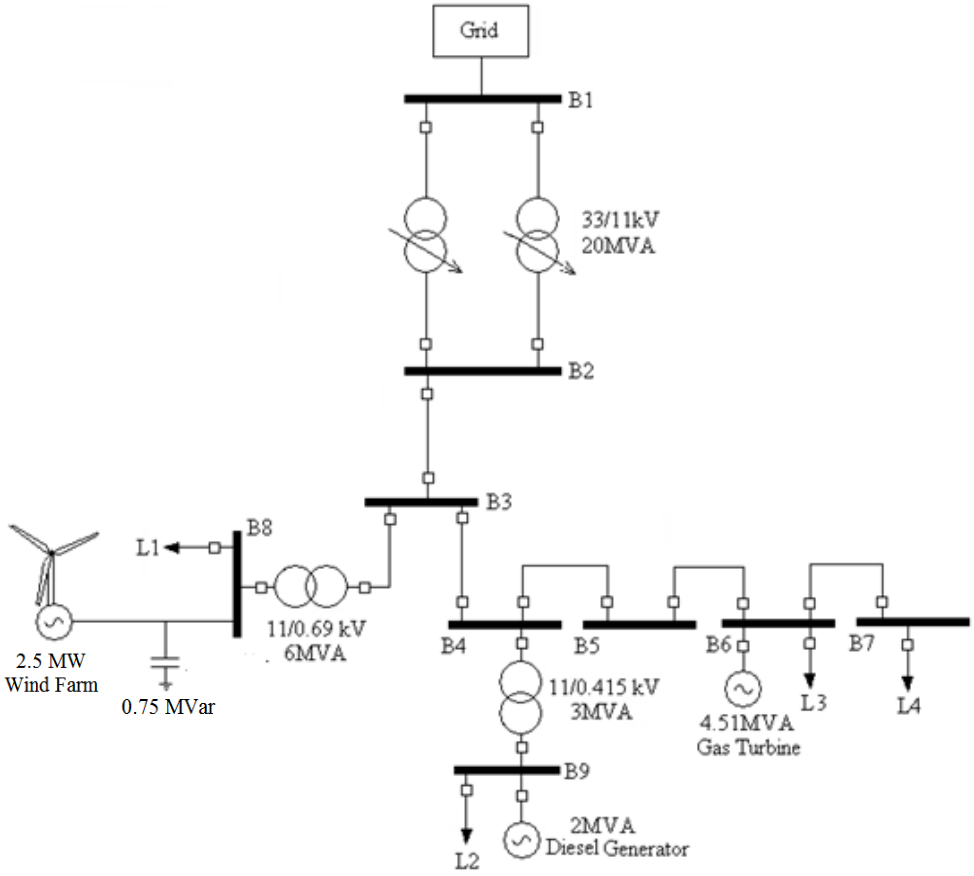

Figure 5-6 Single Line Diagram of Distribution Network Model

A typical section of UK distribution network shown in Figure 5-6 is developed in PSCAD/EMTDC simulation package. Adapted from [58], the distribution network comprises a 33 kV, 50 Hz grid which feeds an 11 kV busbar through two parallel 33/11 kV transformers. A detailed description of the network along with its parameters is provided in Appendix A.

With the increasing penetration of DG into the power network, it is normal to find a diversity of DG units connected to the same network location. This scenario is reflected in the simulation by considering three different types of power source, namely a gas turbine, a diesel engine and a wind farm. They are connected at different locations along the feeder.

In the simulation, a 4.51 MVA gas turbine and a 2 MVA diesel generator are connected to busbar 6 and busbar 9 respectively. Both of them are modelled using 5th order DQ representations of a synchronous machine, each equipped with an exciter and governor. They are capable of island control functions, such as real power load sharing and multiple set phase difference control. These functions are facilitated by a communications link with supervisory control. The excitation system used is the AC5A model from IEEE Std. 421.5-2005 [59]. Reactive power is shared between them using a quadrature current droop compensation method.

A 2.5 MW wind farm is connected to the network through a 11/0.69 kV transformer. The wind farm is modelled either as a FSIG or DFIG model. The real power output is derived from actual measurements taken from Elliot's Hill wind farm with 5 MW capacities in Northern Ireland, thus giving the simulated wind farm a realistic power variation. The data used in the simulation ranges from 34% to 60% of the rated power output and thus contains the section where the largest wind power output variation tends to occur.

The loads, totalling 4.5 MW, are distributed along the feeder and are modelled as constant impedance static loads. The loads distributions are detailed in Appendix A.

5.4.2 **FSIG Wind Farm Model**

The FSIG wind farm is represented by a set of five coherent squirrel cage induction generators each rated at 500 kW. The parameters used are detailed in Appendix A. Additional reactive power support is provided by a fixed capacitor of 0.75 MVAr connected at the wind farm's terminal [73]. A basic aerodynamic representation is incorporated using static aerodynamic efficiency curves presented in Appendix B.

5.4.3 **DFIG Wind Farm Model**

The DFIG based wind farm is represented by a single wind turbine. It is modelled using a standard wound rotor induction generator with its stator windings connected directly to the grid while its rotor windings are fed through back-to-back voltage source converters, linked via a DC-bus. By controlling those converters, DFIG characteristic can be tuned to capture maximum power available in the wind and to generate output power with less fluctuation [74, 75].

The control scheme employed in the simulation is shown in Figure 5-7 and the DFIG parameters are given in Appendix A.

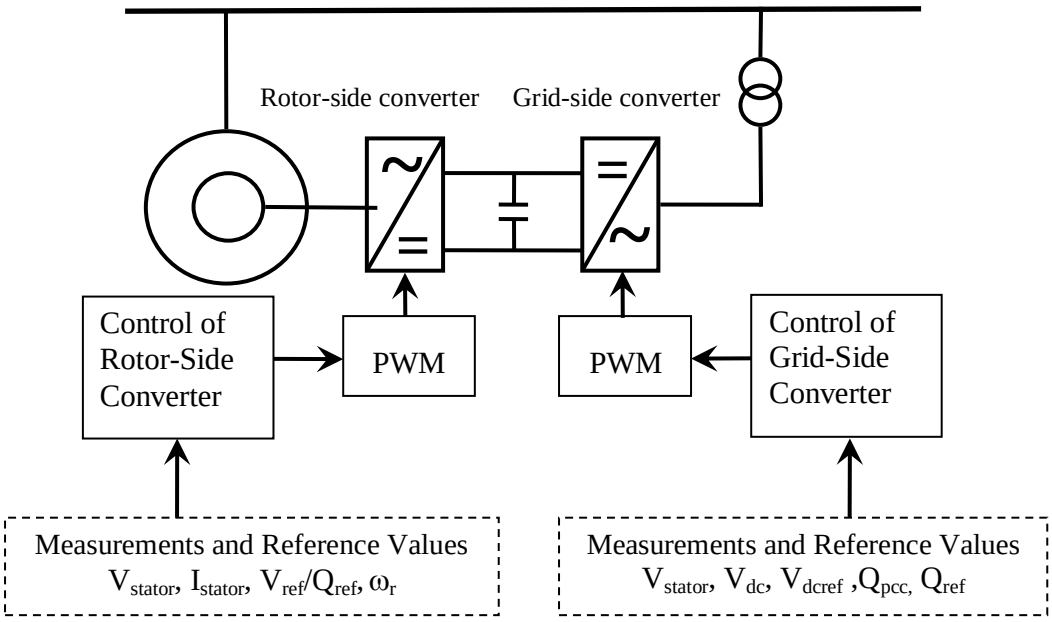

Figure 5-7 DFIG Control Scheme

5.4.3.1. **Control of Rotor Side Converter**

The rotor side converter (RSC) controller operates using stator-flux oriented control [76-79], with the synchronous reference frame attached to the stator-flux linkage, Ψ_s vector position. The detailed concept of this method and relevant equations are

presented in Appendix B. With this, the relationship between the rotor current components and the stator active and reactive powers are reproduced here [80]

$$P_s = -\frac{3}{2}\frac{\sqrt{2}V_s L_m}{L_s} i_{qr}^e \tag{5-7}$$

$$Q_s = \frac{3}{2}\frac{\sqrt{2}V_s}{L_s}\Psi_s^e - \frac{3}{2}\frac{\sqrt{2}V_s L_m}{L_s} i_{dr}^e \tag{5-8}$$

It is clearly seen that there is a linear relationship between the stator active power and q-component of the rotor current while the stator reactive power is a function of d-component of the rotor current. Thus, an independent control of electrical torque and rotor excitation current is possible.

RSC controller regulates the stator active power, P_s and reactive power, Q_s by controlling the I_q and I_d respectively. Figure 5-8 and Figure 5-9 show the control schemes implemented in the simulation. The P_{ref} is obtained from a look-up table representing the maximum power tracking (MPT) algorithm (see Appendix B) [64, 81]. The Q_{ref} can be obtained either from voltage or power factor controller [81]. Otherwise stated, unity power factor is chosen in the studies throughout the thesis.

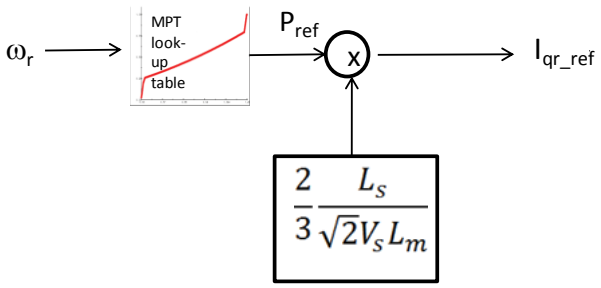

Figure 5-8 Active Power Controller of RSC

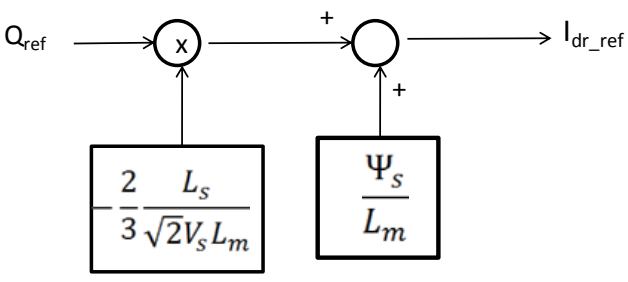

Figure 5-9 Reactive Power Controller of RSC

5.4.3.2. **Control of Grid Side Converter**

Grid side converter (GSC) is employed to maintain a constant DC-link bus voltage, regardless of the rotor power flow direction. It operates using vector control, with the synchronous reference frame fixed to the stator voltage vector position [64, 77]. By this, a decoupled control of active and reactive power flowing between the grid and GSC is possible. Detailed explanation and formula derivation of this technique is given in Appendix B.

Figure 5-10 and Figure 5-11 show the control schemes implemented in the simulation.

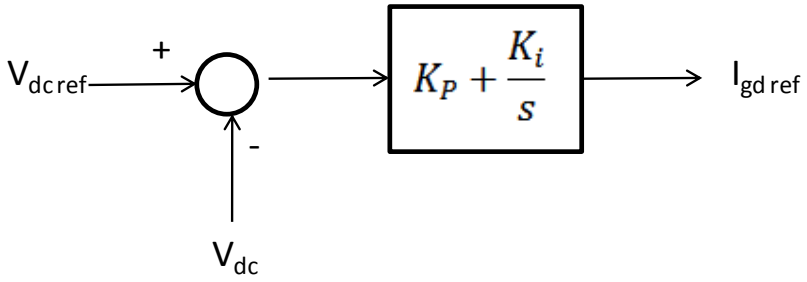

Figure 5-10 DC-link Controller of GSC

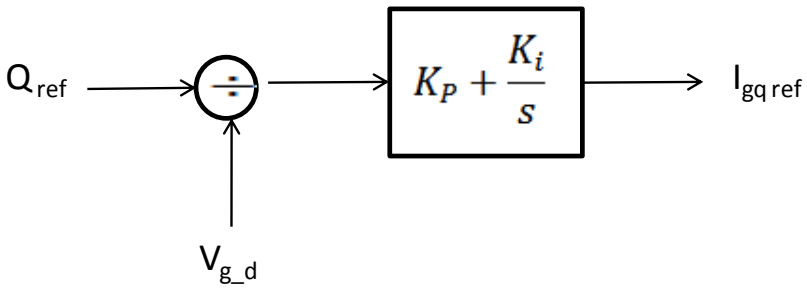

Figure 5-11 Q Controller of GSC

5.4.3.3. **Model Validation**

In order to verify the developed model, an artificial linear wind series is generated from 6.5 m/s to 12.5 m/s, covering the interested region of DFIG as shown in Figure 5-12(a).

From Figure 5-12(b), it is seen that the rotor speed increases accordingly with the increasing wind speed. It is also observed from Figure 5-12(c) that the RSC controllers are working exactly as designed, capturing the maximum power from the wind between the simulated wind speeds. The merits of decoupled control between active and reactive power can be clearly seen in Figure 5-12(d). Despite the increment of i_q due to the increasing wind speed, i_d is undisturbed and is controlled to a constant value. It is observed that i_d is not zero throughout the simulation as it is providing the magnetizing current to the rotor.

In practice, blade pitch controller needs to be activated when wind speed is higher than 12.5 m/s to reduce the C_p and to keep the wind farm power output at rated value. However, as the focus of the simulation is on the fluctuation region of the wind farm power output, blade pitch controller is not considered in the simulation model ($\beta=0^o$). Hence, this model is valid up to wind speed of 12.5 m/s.

Figure 5-12(f) shows the DFIG stator active power, rotor active power and its total active power output. It is observed that below synchronous speed, rotor operates in sub-synchronous mode and absorbs active power from the grid whilst above synchronous speed, rotor operates in super-synchronous mode and supplies active power to the grid. It is seen that at rated condition, the rotor power constitutes ~20% of the total power output and therefore should not be neglected. The DFIG is operated at unity power factor as depicted by Figure 5-12(e).

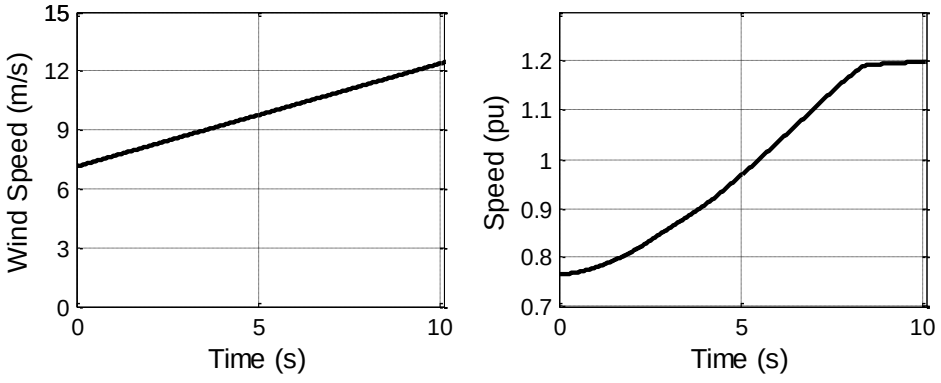

(a) (b)

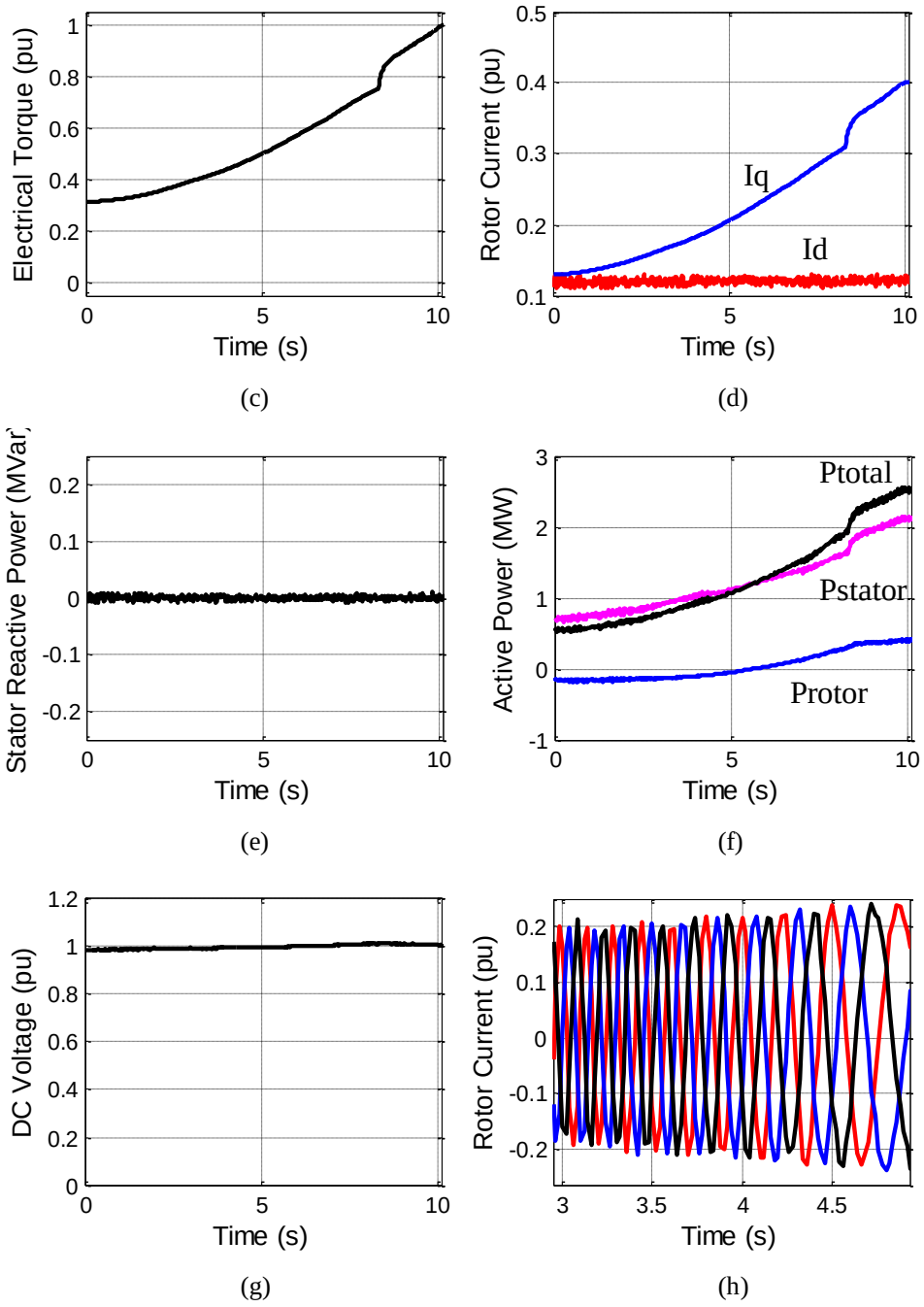

Figure 5-12 Validation of DFIG model : (a) artificial wind speed (b)rotor speed (c) electrical torque (d) rotor current (e) stator reactive power (f) active power (g) DC-link voltage (h) rotor 3-phase current

The GSC is operating correctly as well, keeping the DC-link voltage constant (1 p.u.) throughout the simulation (Figure 5-12(f)). Figure 5-12(g) shows the three phases of rotor current. The characteristic of variable speed is clearly seen here.

Figure 5-13 shows the rotor current changes when the rotor speed passed synchronous speed.

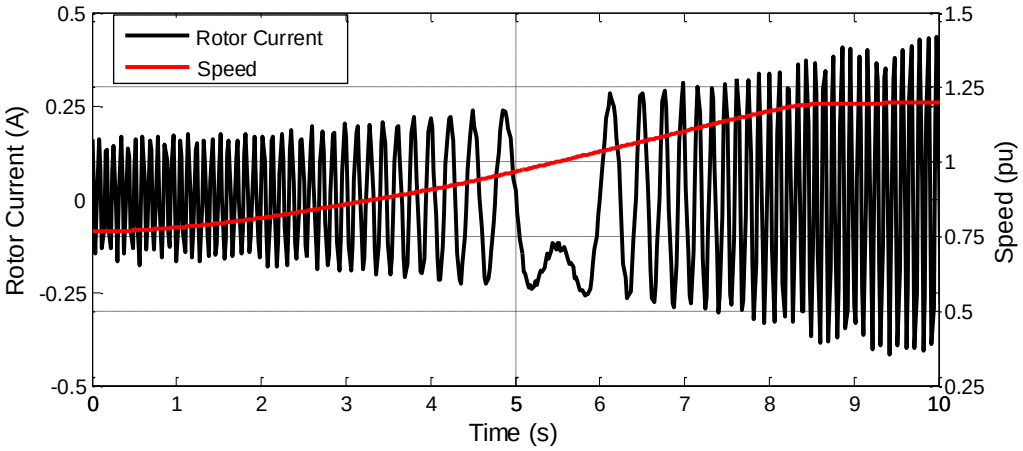

Figure 5-13 Speeds and currents for dynamic operation across synchronous speed

5.5 Simulation, Results and Discussion

The capability of the phase controller to maintain synchronism with the grid in the presence of intermittent power sources is investigated in the following case studies.

5.5.1 Case Study 1: Governor's Control Mode

This case study is done to observe how different combinations of governor control mode performed in an islanded network with intermittent power sources. As discussed in Section 4.3, there are various combinations of governor control strategy in a multiple-DG synchronous islanded network. Hence, it is sensible to first choose the best governor control combination before any further case studies are carried out. Since the main purpose of this case study is to select the best governor control combination, only FSIG wind farm is tested in this scenario.

Islanding is initiated at t=0 seconds by the removal of line connecting busbars 2 and 3 of Figure 5-6. Immediately after islanding, both synchronous generators switched their governor control mode to support synchronous islanded operation.

Four different governor control combinations have been simulated, with parameters given in Appendix A:

i. the gas turbine in PI control while the diesel generator is in droop mode
ii. gas turbine in PID control while the diesel generator is in droop mode
iii. both synchronous generators with PI control
iv. both synchronous generators with PID control

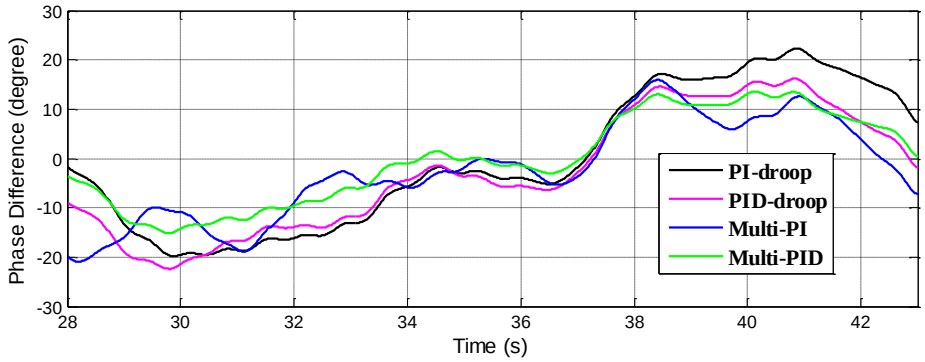

Figure 5-14 Phase difference during steady-state with 2.5 MW capacity wind farm, different controllers

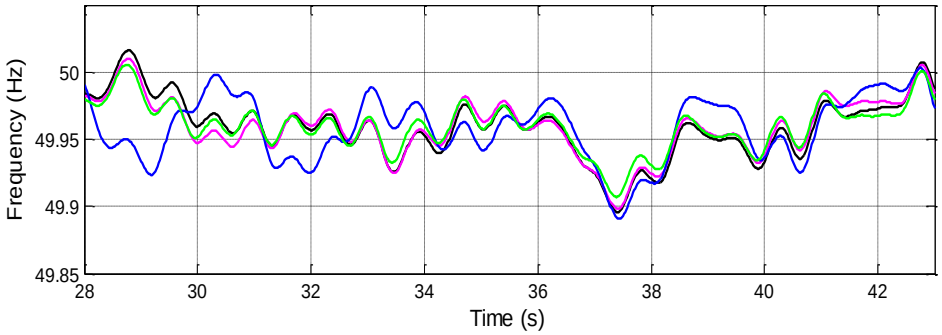

Figure 5-15 Frequency during steady-state with 2.5 MW capacity wind farm, different controllers

It can be seen in Figure 5-14 and Table 5-1 that in all cases, the controllers are capable of maintaining the phase difference $\pm 60°$ despite the power output fluctuation from the wind farm. Figure 5-15 shows how tight the frequency is regulated throughout the islanding operation.

It is noticed that there is a frequency drop between t=36s to t=37.5s. On closer inspection, this frequency drop is found to be caused by the reduction in the wind farm power output (refer figure 5-16). This in turn causes an increment in the phase deviation, since the phase deviation is determined by the integration of frequency change over a time period (equation (5-9)).

$$\Delta\theta = 2\pi \int (f_{island} - f_o) \times dt \qquad (5\text{-}9)$$

where f_{island} is the islanded system frequency and f_o is the reference frequency (grid frequency)

Table 5-1 Maximum Phase Difference during Steady State with 5 MW Capacity Wind Farm

Controller Combination	**Maximum Phase Difference (^{o})**
PI-droop	27
PID-droop	23
Multi-PI	20
Multi-PID	17

It can be seen from Table 5-1 that the multi-PI and multi-PID control schemes can control the phase difference to a lower value, hence better than the control schemes where only one DG provides PI or PID control. However it is worth to note that multi-master control is only possible if a suitable communications structure and supervisory controller are in place, as already discussed in section 4.3.3.

In conclusion, the multi-PID controller (case iv) demonstrated the best phase difference control and consequently, this combination will be used in the rest of the case studies, unless otherwise specified.

5.5.2 **Case Study 2: Wind Turbine Technology**

The same islanding procedure as case 1 was carried out in this study. Three cases have been simulated, with case 3 used for comparison purposes:

a) Island with FSIG wind farm
b) Island with DFIG wind farm
c) Island with no wind farm

Figure 5-16 shows the active power output produced by FSIG wind farm and DFIG wind farm compared to the actual wind farm's power output measurements. It is observed that the output from both types of wind farms matched the reference value closely, with the latter showing a less fluctuated output.

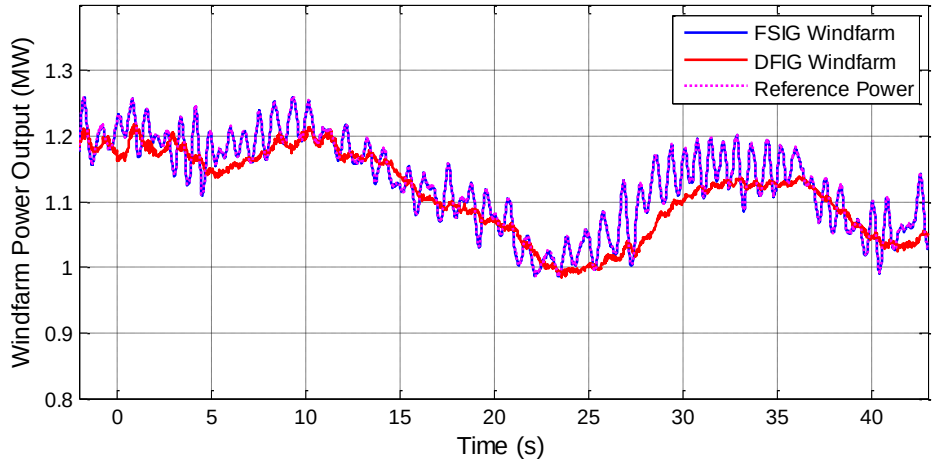

Figure 5-16 Comparison of Power Output between Wind farms and Reference Power

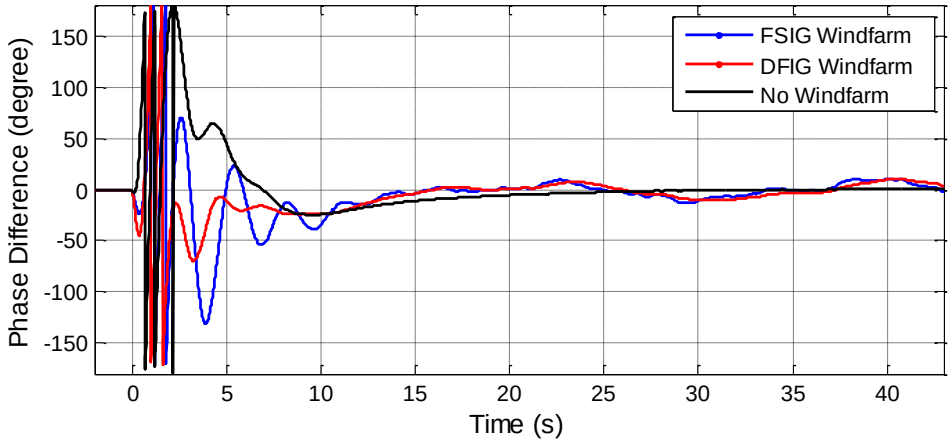

Figure 5-17 Voltage Phase Difference throughout Islanding

Voltage phase deviation for all three cases throughout the islanding operation is presented in Figure 5-17. It is seen that phase difference for all cases is reduced to within $\pm 60°$ by t=5 seconds, indicating that the operation time of automatic re-closing relays should be increased to at least 5 seconds in order to avoid out-of-synchronism re-closure.

From the same figure, it is also observed that phase difference is eventually controlled to zero degree for case 3, i.e. without wind farm in the island. This is however not the case for the wind farm connected cases. Varying power output from the wind farm has caused the phase difference to fluctuate. Island with DFIG wind farm connected shows better phase difference control compared to island with FSIG wind farm. This is believed to be attributable to the reduced power output fluctuations of the DFIG wind farm.

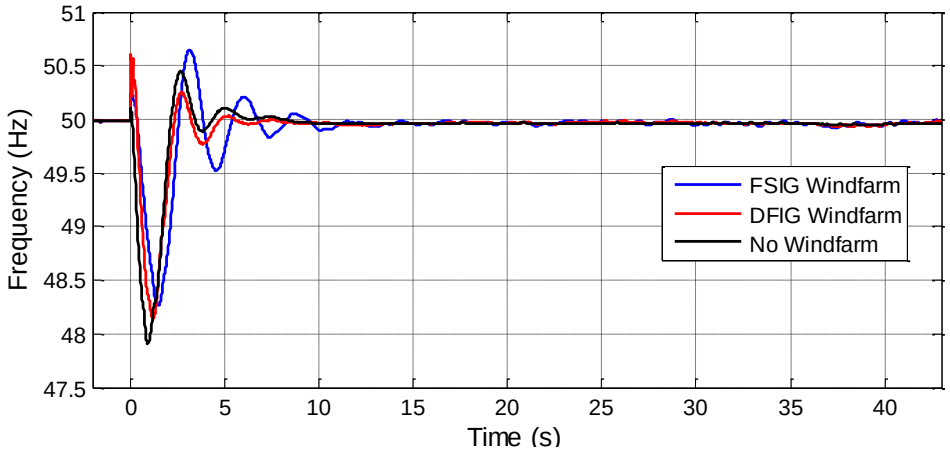

Figure 5-18 Frequency profile throughout islanding for all cases

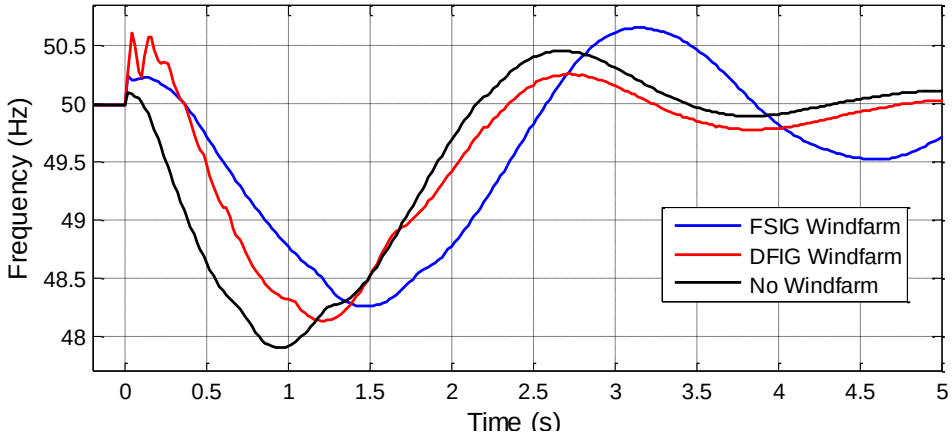

Figure 5-19 Freq close-up from t= –0.2 to t=5s for all cases

Figure 5-18 shows the frequency profile throughout the simulation and Figure 5-19 illustrates the close-up of Figure 5-18 from t= –0.2 to t=5 seconds. Immediately after islanding, frequency in all three cases increases due to excess of active power generation. This can be equated to load rejection event. As shown in the figure, cases with wind farm connected show higher frequency increment. This can be explained by using equation (5-1). From the synchronous generators point of view, wind farm power outputs are akin to "negative load". Although there ought to be changes in load (voltage dependent load) and power losses immediately after islanding, these changes are similar in all three cases since the voltage drops are almost the same in all cases (as shown in Figure 5-20). With the wind farms connected, the total generation excess immediately after islanding is more than the case without wind farm connected (see Figure 5-21), and consequently results in higher frequency increments.

Another interesting observation from Figure 5-19 is that the rate of change of frequency (ROCOF) for case 2 and case 3 are similar. This is down to the fact that DFIG is low inertia [71, 80]. The way DFIG is controlled decouples its mechanical and electrical system, causing it to be immune from the changes of frequency in the system. This judgement is confirmed by looking at the DFIG power output (Figure 5-21). It follows the reference signal throughout the simulation time, unaffected by the island transition. FSIG on the other hand increased the overall system inertia, results in a reduced ROCOF. Also, the provision of inertial response by FSIG reduced the frequency drop, resulting it to have a higher minimum frequency point compared to case 2.

Load sharing is achieved in all three cases, as shown in Figure 5-21. Load is shared equally between the synchronous generators in approximately 30 seconds after islanding. The effect of load sharing function can be clearly seen in the phase difference error of case 3, between t=5 and t=30 seconds (Figure 5-17), due to the ramping of output power. This however is not so obvious in case 1 and case 2 due to the continually fluctuating phase difference.

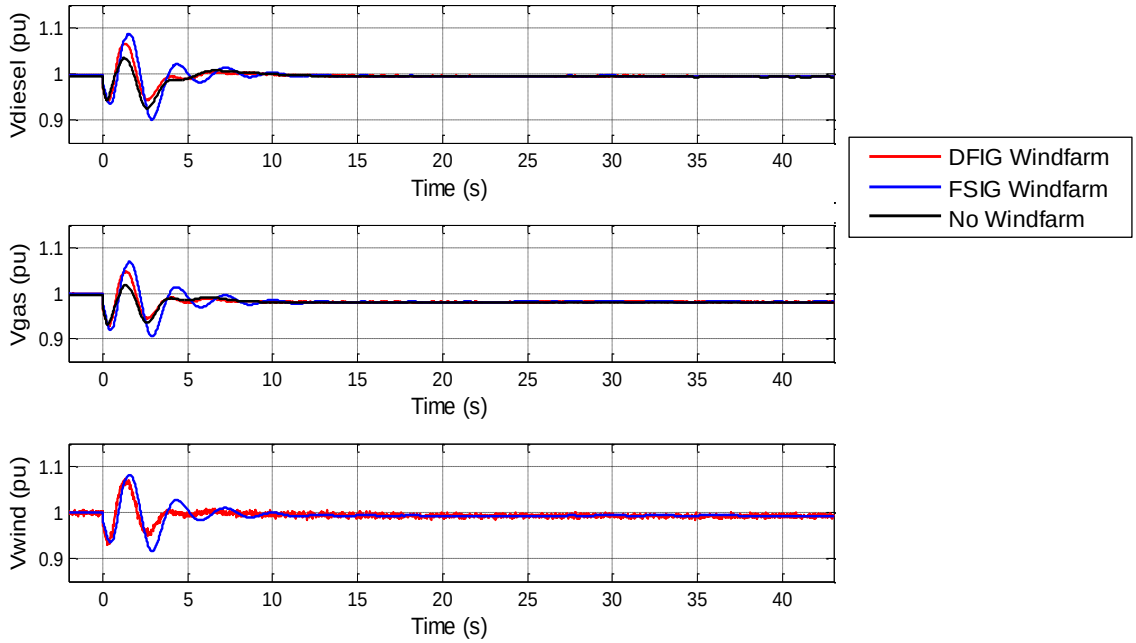

Figure 5-20 Voltage profile throughout islanding for all cases

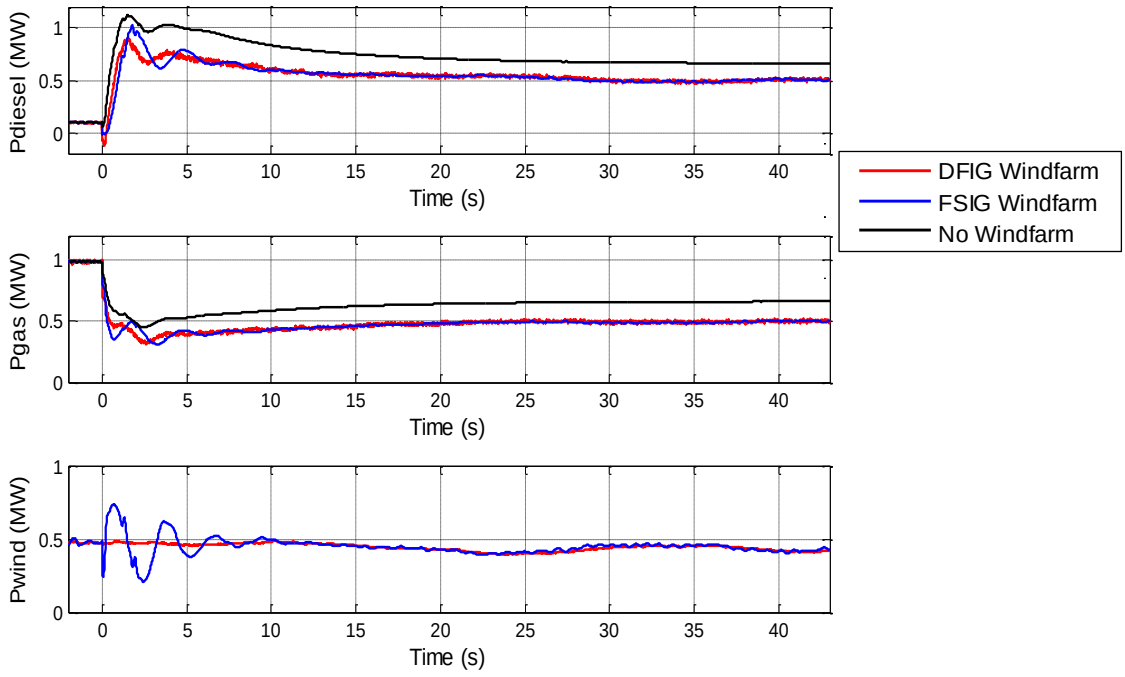

Figure 5-21 Power Output throughout islanding for all cases

5.5.3 **Case Study 3: Load Disturbance**

The results in the previous case studies shows that synchronous islanded operation is feasible in a multiple-set distribution system island with significant penetration of wind energy, i.e. ~32% of total generation capacity in the island. However, the island will be subjected to continuously changing loads and the effect of these load disturbances on the control scheme must be assessed, in particular to determine the maximum load disturbance that can occur. It is worth to note that both load rejection and load acceptance will add to the phase deviation. It is essential that the phase difference does not go beyond the $\pm 60°$ limit. As shown in previous chapter, both load rejection and load acceptance have equal effect on the phase deviation. Hence, only the load acceptance will be performed here and similar conclusion can be drawn from the load rejection simulation.

Case study 2 was repeated in this study. For case of islanding without the wind farm connected, the load acceptance occurs at t = 35 seconds. However, when the wind farm power output varies normally, the phase difference in the island is never in a true steady-state, as shown in Figure 5-14, and so the load is applied in 0.5% resolution at several different times, as indicated below and in Figure 5-22.

Case 1) Phase difference peak
Case 2) Phase difference trough
Case 3) Frequency peak
Case 4) Frequency trough
Case 5) Time when frequency and phase variation are low

The results in Table 5-2 lists the maximum load acceptance possible for each test while not exceeding $\pm 60°$ phase difference. They are presented in percentage terms of the controllable generation in the island, i.e. of 5.208 MW.

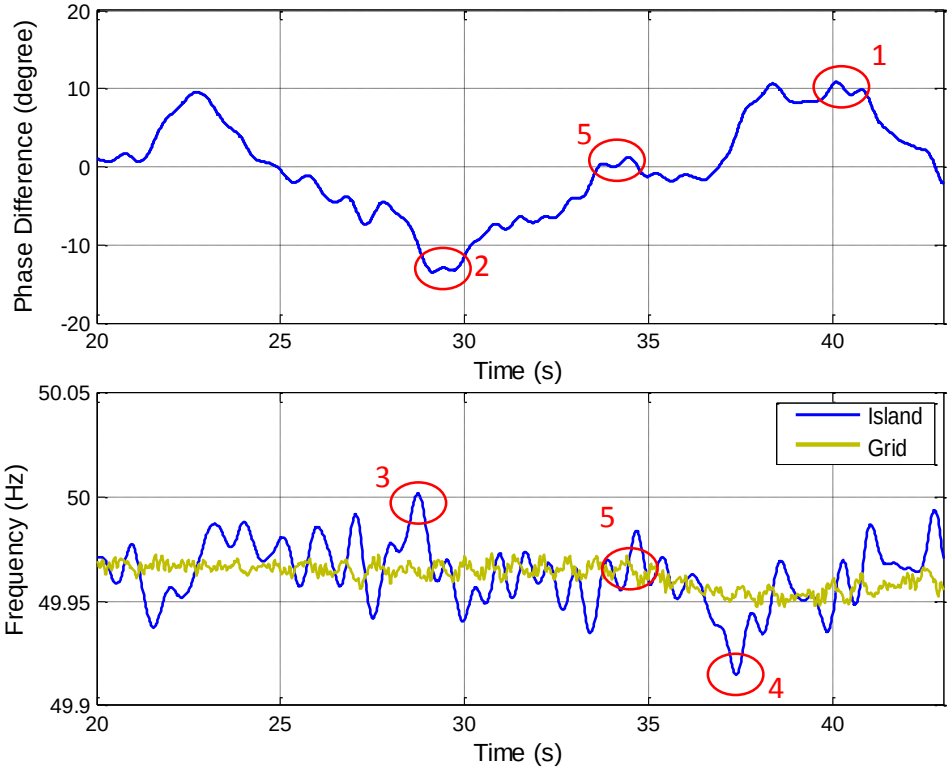

Figure 5-22 Times of load application for cases 1-5, relative to phase difference and frequency

Table 5-2 Maximum Load Acceptance for Cases where Both Synchronous Generators Operate in Isochronous Frequency and Phase Control

CASE		MAXIMUM LOAD ACCEPTANCE (%)	
		PID	PID + real power input
No Wind		9.0	17.5
FSIG	1	6.5	13.5
	2	8.0	14.5
	3	8.5	14.5
	4	6.0	12.5
	5	7.5	14.0
DFIG	1	8.5	16.0
	2	9.0	17.0
	3	9.0	16.0
	4	8.0	15.5
	5	8.5	16.5

It is seen that the effect of wind variation is to reduce the amount of load acceptable in the island while not going beyond the synchronization limits. For instance, in case 1, the maximum load acceptance of 9% in the no wind farm case with multi-PID control reduces to 6.5 % and 8.5% for the FSIG and DFIG case respectively.

From the results, it is also observed that case 4 represents the worst time to apply load. In this case, the island frequency is already lower than the reference frequency. During the load acceptance, the island frequency is further depressed. As the value of phase deviation is determined by the integration of frequency change over a time period (equation (5-9)), the additional frequency change further increases the phase difference. As a consequence, it hits the synchronisation limit faster than other cases.

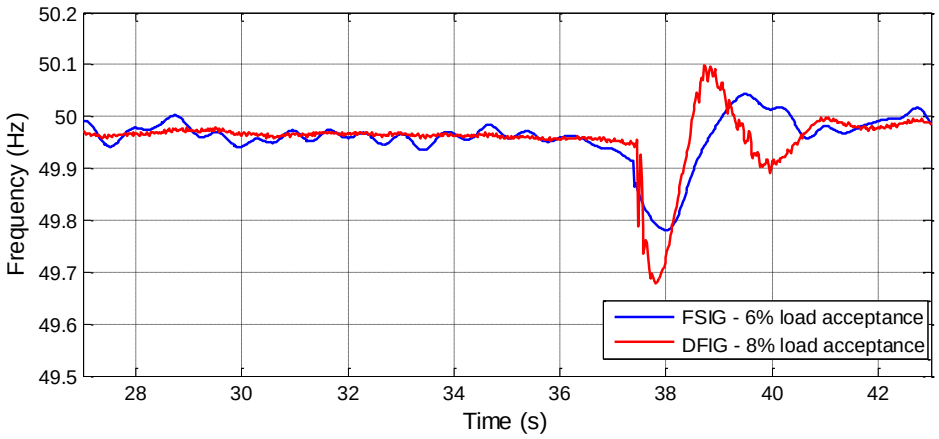

Figure 5-23 Frequency Variation due to load acceptance for FSIG and DFIG

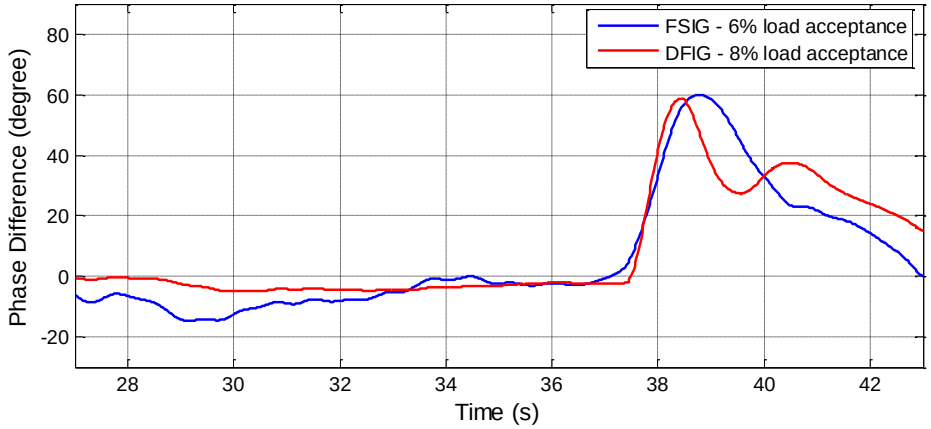

Figure 5-24 Phase Deviation due to load acceptance for FSIG and DFIG

The simulation is also tested using a governor that includes a supplementary power input on both synchronous generators [82]. This type of governor is reported to have a better speed regulatory capability and hence is more superior than the typical speed-only input governor [82]. The results for all cases are presented in Table 5-2. A marked improvement is seen in both type of wind farms cases for all scenarios, with the least being 12.5% and 15.5% (case 4) for FSIG and DFIG respectively.

From Table 5-2, Figure 5-23 and Figure 5-24, it is also observed that the replacement of FSIG wind farm with DFIG wind farm has increased the maximum allowable load acceptance. This is due to the reduction in inertia allowing faster return to zero frequency error. However, control performance does not quite reach the level of the no-wind case.

5.6 Chapter Summary

Renewable resources with varying power output have always posed a challenge to the operation of power network. The big question is how these resources behave in a much stricter environment, in this case, synchronous islanded operation? How will they affect the operation, and to which extent?

These are the main subjects investigated in this chapter. Wind energy has been chosen to reflect the intermittent power sources, and is believed apt to represent UK scenarios. Two types of wind turbine technology have been modelled in PSCAD/EMTDC for this purpose.

This chapter progresses from developing two types of wind turbine technology in PSCAD/EMTDC, namely FSIG and DFIG wind turbines. The developed models were then subject to numerous simulations to verify their performance.

The results presented in this chapter show that synchronous islanded operation in a multiple-DG island with substantial penetration of wind energy (2.5MW installed

wind capacity versus 5.208 MW of controllable DG) is feasible. Synchronous island control shows satisfactory performance when subjected to the intermittent power sources.

By comparing results between the control schemes, 'multi-master' control combination performs better than the 'master-slave' scheme. It is however worth to note that both schemes are capable of operating islanded synchronous operation.

From the results presented in this chapter, the issues surrounding continuously fluctuating power sources on the phase control is evident. However, improvement of phase control can be achieved by using a more advanced type of governor, as presented in case study 3.

The replacement of FSIG wind generation with DFIG technology also improves the phase control of the island. Load acceptance for all cases using the latter technology is higher than when using the former technology. It is also found that the worst time to increase load is during frequency trough.

The reduced inertia of the latter technology has increased the maximum allowable load disturbance in the island without exceeding the phase difference limit of $\pm 60^{o}$. It must be noted however that this feature also caused a larger frequency deviation and may lead to undesirable consequences in some cases, i.e. reduced stability.

CHAPTER 6

INTEGRATION OF ENERGY STORAGE

6.1 Introduction

The results presented in the previous chapter suggested that operation of synchronous island in the presence of intermittent power sources is feasible. Having said that, it is seen that a more advanced technology, be it wind turbine technology or governor combination selection plays a significant role in reducing the phase difference between the grid and the temporary island.

Nevertheless, the adverse effect wind intermittency has on the operation of synchronous island, in particular the limitation on the amount of load disturbance that can happen during the islanding operation should not be overlooked. Since controlling the wind availability is out of the question, ways to reduce the wind farm power output variation may be an alternative that is worth exploring.

Another interesting observation from previous case studies is that the inertial response provided by a wind farm (FSIG) helps to improve the frequency response. It would be beneficial if this feature can be incorporated into a DFIG machine to aid synchronous islanded operation during the disturbance, along with improved frequency profile.

Hence, building on these considerations, this chapter investigates the prospect of using energy storage to reduce the intermittent nature of the wind farm, and ultimately support the operation of the synchronous island. This chapter will concentrate on the application of a DFIG wind farm, owing to the better performance and controllability it demonstrated against FSIG.

A novel control algorithm that incorporates the merits of steady output and provision of inertial response is then presented. Case studies are executed to examine the capability of the proposed method in supporting the synchronous islanded operation.

6.2 Energy Storage in Power System

Energy storage has found its way in various applications in power system (i.e. microgrid, renewable generation, electric vehicle, etc.). Essentially, the main attractiveness of energy storage lies in its capability to store energy when the generation is in excess and to provide it at a later stage when there is a deficit in generation. This key feature not only helps to reduce energy curtailment (from intermittent power sources) but also enhance the value of the electricity by time-shifting delivery to the network [83].

i) Microgrid

Energy storage is one of the main components forming a microgrid. In microgrid, most generation units (microsources) are connected to the system using power electronic converters and thus have very small inertia [84-86]. Consequently, substantial power transient pose a huge challenge to the operation of microgrid. Energy storage is thus essential and plays significant roles in maintaining stability during such transients.

Batteries are mostly employed as the main storage method, although there are also systems using flywheels and supercapacitors in conjunction with batteries [87, 88]. Energy storage could be either centralised or distributed across the microgrid. However, the latter option is more economical during storage expansion.

ii) Renewable Generation

As the penetration of renewable energy sources onto the grid reaches a higher level, there has been increasing demand for them to provide a more reliable power output, just like conventional generators. Therefore, the inherent intermittent nature of most renewable energy sources (i.e. solar power, wind) must be overcome using supplementary measures. Energy storage is one of the available options, balancing the variation in the generators' output between high and low availability of wind and sun.

iii) Electric Vehicle

Electric vehicles (EV) have created the potential of providing a pool of mobile energy storage to support the operation of power systems. W.R. Lachs et al proposed a strategy which exploits the energy stored in EV to even out the demand for electricity during daily peak periods and only charges the storage during off-peak periods, when there is an excess in generating capacity.[89]

In this concept, EV serve as a large pool of distributed spinning reserves and thus has the potential of reducing the need for new power plants. Furthermore, it is seen as one of the options to address the issues relating to renewable power sources penetration. It could possibly be utilized to store excess energy during windy/sunny periods and providing it back to the grid during peak periods, hence effectively buffering the intermittency of these renewable sources (i.e. solar power and wind power).

The fact that EV are mobile is an added advantage. They can essentially be placed close to the consumers. These are ideal as they are the source of demand variations, and thus the effect of their changing needs throughout the day to the grid can be effectively countered.

The application of EV in the power system is often seen as part of the smartgrid initiatives. It increases the engagement of consumer in the operational control of energy usage and ultimately establishes a distributed demand management.

6.2.1 **Energy Storage Application in Wind Power System[90]**

Modern wind power system, predominantly variable speed systems are equipped with power electronic converters. Their readily available dc bus and excellent controllability render them technically attractive to incorporate energy storage devices such as flywheels, battery, supercapacitors and etc. This factor, along with others, has encouraged the idea of complementing wind power systems with energy storage, and has been considered in various published papers.

In [91-93], Chad Abbey et al proposes the use of energy storage to smooth out the short term variation of DFIG power output. The simulation results show that with the inclusion of energy storage, a pre-specified amount of power can be delivered to the grid despite wind power fluctuations. The advantage of energy storage inclusion to the DFIG is even more apparent when they demonstrated the effectiveness of this topology in enhancing the low-voltage ride through (LVRT) capability [93].

Integration of storage has also encouraged the idea of operating wind power system during islanding event. Due to the intermittent nature of wind generation, it is generally hard to keep the island within operational limits during this undesirable circumstance. However, with the inclusion of energy storage, and with proper controls algorithm, [94] and [95] has demonstrated the capability of DFIG (with storage) in maintaining a stable island. In particular, Amirnaser Yazdani has proposed in [94] a superior, unified control strategy that can operate in grid-connected mode and islanded mode without the need of switching between different controllers.

Incorporation of energy storage to the wind power system is not limited to the converter's dc bus only. Energy storage can also be added as an auxiliary system with the purpose of smoothing out the output variation, as demonstrated in [96] and [97]. Experimental results are presented extensively in [96], illustrating the effectiveness of the proposed strategy. It must be noted that auxiliary schemes are relatively more expensive than incorporating energy storage in the converter's dc bus, although it has more liberty in terms of storage capacity.

Without doubt, integration of energy storage helps in improving the power output profile of intermittent power sources. Depending on the scale of the storage, it may also increase the level of penetration of intermittent power sources to the network without the need for grid reinforcement [83]. This however comes at a greater cost and may not necessarily be economically justifiable.

6.2.2 **Energy Storage Technologies**

Depending on the type of applications, there are a wide variety of energy storage technologies available on offer. The required capacity of the storage depends largely on the time scale it is needed to smooth out the power variation. Naturally, smoothing long-term power variation requires energy storage in larger capacity, which is obviously more costly and inevitably adds to the cost of the wind farm. It is reported in [98] and [99] that the power system is more susceptible to the variation in wind speed in the range of 0.01Hz to 1Hz (medium frequency). In order to smooth out the fluctuation in this frequency range, and taking into consideration the economic cost, short term energy storage is considered sufficient. The most commonly implemented short term energy storage technologies are as listed in Table 6-1:

Table 6-1 Comparison of Short Term Energy Storage Properties [54, 90]

Parameter	**Lead Acid Batteries**	**Supercapacitors**	**Flywheels**
Energy Density* (p.u.)	1	0.1	0.125
Power Density^{+} (p.u)	1	20	3
Response Time (ms)	100	0.1	10
Discharge Time Range (min)	0.25-480	0.002-1	0.03-3
Recharge Time Range	Minutes - Hours	Seconds - Minutes	Seconds - Minutes
Roundtrip Efficiency (%)	80	90-97	92-97
Typical Life Cycle (cycles)	2000	100,000	10,000
Maintenance	Moderate	Low	High

*Energy density is the amount of energy available from an energy source

$^{+}$Power density is the rate of which energy can be taken from an energy source

From the table, it is seen that supercapacitors are the most promising devices, offering greater advantages over the other two alternatives. Due to their higher power density and ability to charge and discharge rapidly, they are suited for short term power exchange with the wind farm. In addition, they present good efficiency, have long life cycle and require low maintenance. It is hence considered the best selection and applied in the work presented in this chapter.

6.3 Supercapacitor

Supercapacitors are made up of two electrodes immersed in an electrolyte, with an ion-permeable separator in between the electrodes, as shown in Figure 6-1 [118]. A supercapacitor can be regarded as two conventional capacitors connected in series, where each electrode-electrolyte interface represents a capacitor [119]. However, unlike conventional capacitors, where their electrodes are separated by a dielectric material (i.e. ceramic, polymer films or aluminium oxide) [120], supercapacitors do not have dielectric material between their electrodes. Instead, supercapacitors use two electrodes that are made of special materials, which can be activated carbons, metal oxide or conducting polymers. [121]

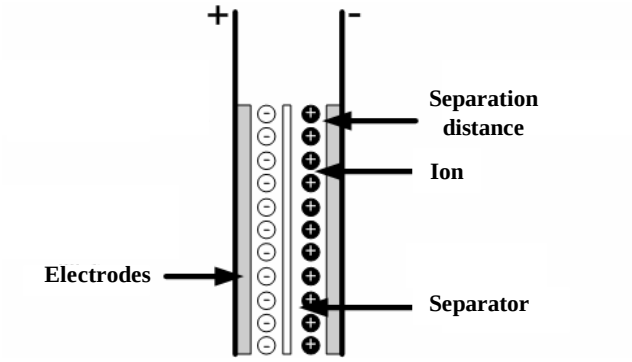

Figure 6-1 Supercapacitor

Among these three materials, the activated carbon electrodes are the most common and the cheapest to manufacture. When an electrical charge is applied to these electrodes, an electrical double layer is generated.[122] The generated layer acts like a dielectric between the electrodes, providing an effective separation of charge with an extremely small physical separation distance (in the range of nanometers).[119]

The carbon-based electrodes also create a large equivalent surface area, yielding several thousands of m^2/g [120]. The large surface area coupled with the small separation distance of supercapacitor enabled a high capacitance value to be achieved, as can be seen from equation (6-1). This in turn increases the energy storable in a supercapacitor compared to a conventional capacitor, using equation (6-2).

$$C = \frac{\varepsilon A}{d} \tag{6-1}$$

where C is the capacitance of the supercapacitor, ε is the dielectric constant of the electrical double layer region, A is the surface-area of the electrodes and d is the distance between the electrodes.

$$E = \frac{1}{2} CV^2 \tag{6-2}$$

where E is the stored energy in the supercapacitor, C is the capacitance of the supercapacitor and V is the terminal voltage of the supercapacitor.

As seen from equation (6-2), the supercapacitor voltage is also an essential determinant of stored energy. The operating voltage of supercapacitors is usually dependent on their electrolytes, which may be aqueous or organic [121]. The aqueous electrolytes (e.g. acids and alkalis) have the advantage of low internal resistance but with a restricted operating voltage range of around 1V [119]. On contrary, the organic electrolytes (e.g. propylene carbonate, acetonitrile) offer a higher cell operating voltage (2.5 V) but with a relatively higher internal resistance [119]. In order to achieve higher operating voltage, supercapacitors are usually connected in series [123].

The most remarkable advantage supercapacitors have over batteries is the number of charge/discharge cycles (life cycle) [124]. Unlike batteries, which have a limited life cycle with a degrading performance, there is very little deterioration induced during these cycles. Therefore, supercapacitors have virtually an unlimited number of life cycles. Also, their performance does not degrade with time.

Supercapacitors also have a rapid charging (in seconds) and discharging (in milliseconds) time [123]. This characteristic is very beneficial in applications where an instant boost of power is required in a very short period, i.e. load levelling. Their low internal resistance results in extremely low heating levels and subsequently high cycle efficiency.

Supercapacitors have a very long lifespan and are extremely safe for storage. Besides, they do not release any hazardous substance, which makes them environmentally friendly.

Supercapacitors, however, have a considerably higher self-discharge rate compared to the batteries [121]. This made them unsuitable for long-term energy storage. They also have lower energy density, which typically store one-fifth to one-tenth of the energy of an equivalent weight battery [121]. This feature makes them heavier and bulkier than an equivalent size battery.

6.3.1 **Simulation Model of Supercapacitor**

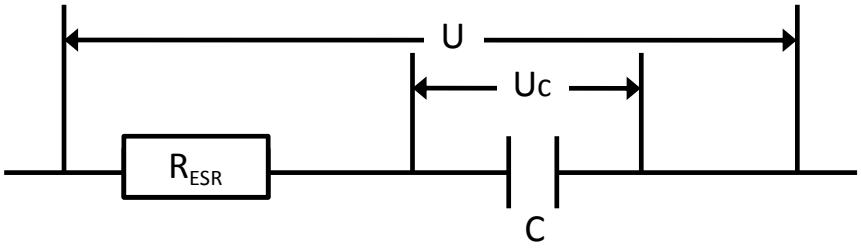

Figure 6-2 Simplified Equivalent Circuit of Supercapacitors

Figure 6-2 shows the model of supercapacitor used in the simulation [100, 101]. The supercapacitor is assumed ideal and consists of an equivalent series resistance, R_{ESR} connected in series with an ideal capacitor. The resistor limits the current flowing into the supercapacitor and is responsible for the electrical losses [102]. There are various other representation of supercapacitor found in literature [93, 103, 104]. However, the studies carried out in this chapter focus on the energy exchange rather

than efficiency and switching transients [93]. Hence this simplified model is considered fit for purpose. The parameters used are provided in the Appendix C.

6.3.2 **Sizing of Supercapacitor Bank (SB)**

The properties of supercapacitor can be defined by

$$i_c = C\frac{dU_c}{dt} \tag{6-3}$$

$$E = \frac{1}{2}C{U_c}^2 \tag{6-4}$$

where i_c is the current flowing through supercapacitor, U_c is the voltage across supercapacitor, C is its capacitance and E is the stored energy. As shown by equation (6-4), the stored energy is dependent on the voltage across it. In order to avoid any electrochemical reactions in the component and consequently limiting its life span, the voltage across the supercapacitor has to be limited to a maximum value U_{max} [101, 105]. The stored energy is hence at its maximum, E_{max} during this condition. To use up the entire amount of stored energy during discharging, U_c theoretically have to be decreased to 0V (minimum value). This however is not possible as the current provided by the supercapacitor will then be infinite (equation (6-3)) and will cause efficiency problems on the power converter [105]. Due to this reason, the minimum voltage when discharging has to be limited to U_{min}. In other words, not all the stored energy could be used. It is thus essential to define the voltage discharge ratio, d where d is the ratio between the minimum allowed voltage, U_{min} that defines the end of discharging and the maximum reachable voltage, U_{max} where the component is fully charged.

$$d(\%) = \frac{U_{min}}{U_{max}} \times 100 \tag{6-5}$$

The total accessible energy from a supercapacitor is hence

$$E_{sc} = \frac{1}{2}C{U_{max}}^2 - \frac{1}{2}C{U_{min}}^2 \tag{6-6}$$

Substituting equation (6-5) into equation (6-6) gives

$$E_{sc} = \frac{1}{2} C {U_{max}}^2 \left(1 - \left(\frac{d}{100}\right)^2\right) \quad (6\text{-}7)$$

From equation (6-7), it is observed that depending on the value of d, the accessible energy from a supercapacitor is only part of the maximum stored energy, as given by equation (6-8) and Figure 6-3.

$$E_{sc} = E_{max} \left(1 - \left(\frac{d}{100}\right)^2\right) \quad (6\text{-}8)$$

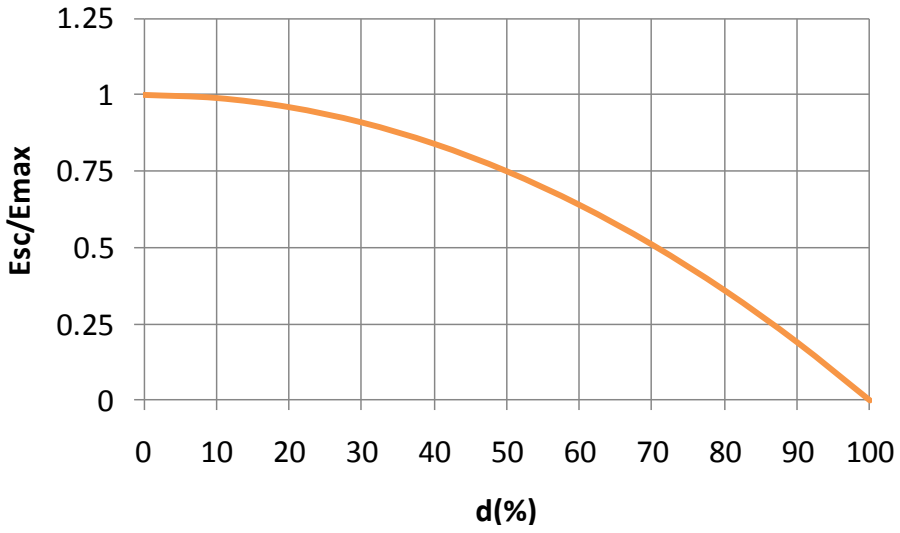

Figure 6-3 Usable energy as a function of discharge ratio

An interesting observation from Figure 6-3 is that by varying the voltage across the capacitor, U_c from maximum to half of its value (d=50%), the obtainable energy from the supercapacitor is 75% of the total stored energy. Due to efficiency reason, the discharge ratio is always kept higher than 50% in most applications [105].

By choosing a discharge ratio, the number of supercapacitors, N required for the supercapacitor bank (SB) is then defined by

$$N = \frac{E_{store}}{E_{sc}} \quad (6\text{-}9)$$

Where E_{store} is the amount of energy required to be stored in the supercapacitor. In this case, the author has designed the supercapacitor in such a way that it is able to supply 20% of DFIG's rated power over a period of 10 minutes:

$$E_{store} = 0.2P_{rated} \times t \quad (6\text{-}10)$$

6.4 Operating Principle of DFIG with Supercapacitor Bank (SB)

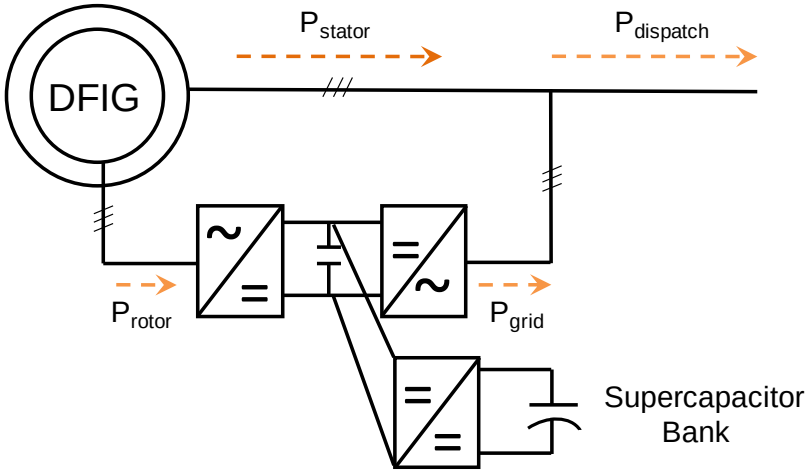

Figure 6-4 DFIG with integrated supercapacitor bank

The SB is interfaced to the DC-link using a bi-directional DC/DC converter, as depicted in Figure 6-4. The advantage of this arrangement is that minimal modification on control is required compared to the conventional DFIG. The rotor side converter (RSC) retains its control strategy and continues to extract maximum energy available from the wind.

6.4.1 Control of Grid Side Converter

The grid side converter (GSC) serves as a sink or source of real power. Contrary to its function stated in section 4.4.3.2, under normal conditions, GSC's real power control is used to regulate the transfer of real power between the grid and the SB, and hence dispatching a pre-specified amount of real power to the grid (Figure 6-5). The control still operates using the vector control technique (refer section 4.4.3.2 and Appendix B). Thus, the benefit of decoupled control of active and reactive power via

i_{gd} and i_{gq} retains. GSC's reactive power control keeps its function and is used to maintain the wind farm terminal voltage or regulates the reactive power exchange between the grid and GSC.

However, if the SB is disconnected from the DC-link (or fails), GSC must revert to its conventional algorithm and regulates the DC-link, operating in a typical DFIG mode (see section 4.4.3).

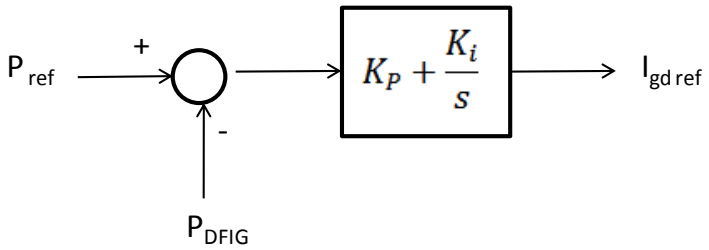

Figure 6-5 Control of GSC

6.4.2 **Control of DC/DC Converter**

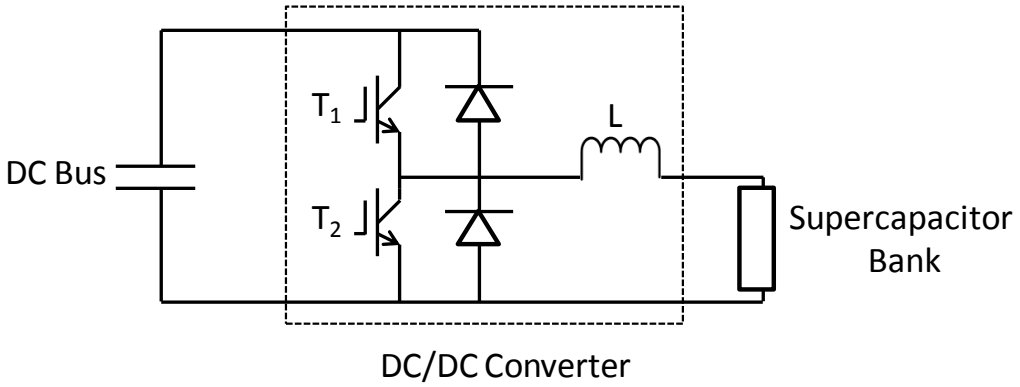

Figure 6-6 Supercapacitor bank interfaced to dc-link using dc/dc converter

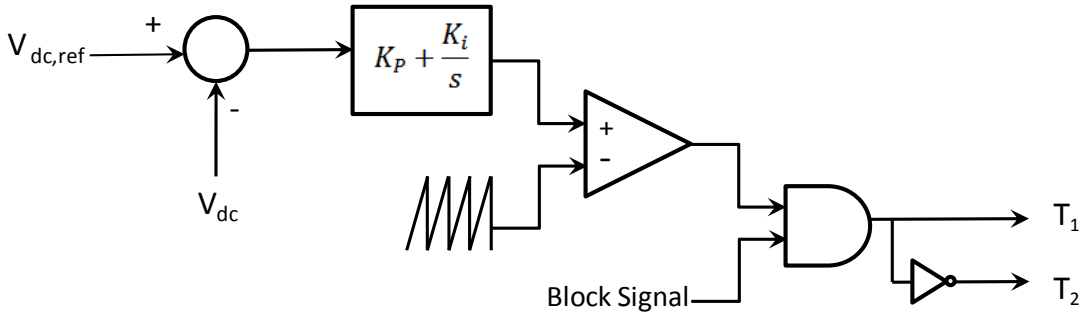

Figure 6-7 Control of DC/DC converter

Figure 6-6 shows the detailed arrangement of the integration of SB to the DC-link using DC/DC converter. Under normal conditions, the control of DC/DC converter (Figure 6-7) is aimed at regulating the DC-link voltage to its reference value. Control of DC-link voltage is accomplished by balancing the input power from the DC bus with the output power delivered to the SB. If these powers do not match, for instance, the output power of the converter is more than the input power, energy will be released from the capacitor and consequently, the DC-link voltage will fall. Conversely, if the output power is less than the input power, energy will be stored in the capacitor, causing the DC-link voltage to increase. Hence, by regulating the dc bus voltage, energy is exchanged indirectly between the SB and the DC link.

There are two operating modes associated with a bidirectional DC/DC converter, namely step down and step up mode, as depicted by Figure 6-8.[106] The former mode transfers energy from the DC link to the SB (charging) while the latter transfers energy out of SB to the DC link (discharging). Depending on the operating conditions, power is transferred to and from the bidirectional converter and hence, the SB is charged and discharged respectively.

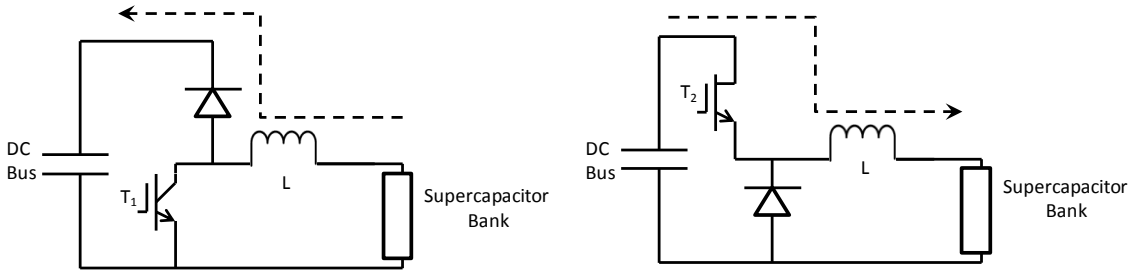

(a) (b)

Figure 6-8 Bidirectional DC/DC converter operating modes: (a) step-up mode (b) step down mode

Table 6-2 Charging and Discharging of SB in Correspond to Operating Conditions

		Pgrid (P_g)	
		$P_g > 0$ ($P_{dispatch} > P_{stator}$)	$P_g < 0$ ($P_{dispatch} < P_{stator}$)
Protor (P_r)	$P_r > 0$ ($w_r > 1$ p.u.)	$\|P_r\| > \|P_g\| \rightarrow P_{sb} > 0$	$P_{sb} > 0$
		$\|P_r\| < \|P_g\| \rightarrow P_{sb} < 0$	
	$P_r < 0$ ($w_r < 1$ p.u.)	$P_{sb} < 0$	$\|P_r\| > \|P_g\| \rightarrow P_{sb} < 0$
			$\|P_r\| < \|P_g\| \rightarrow P_{sb} > 0$

Table 6-2 lists all the possible operating conditions and the subsequent charging ($P_{sb} > 0$) and discharging ($P_{sb} < 0$) of SB. It should be noted that the SB voltage varies depending on the amount of energy stored, increases when charged and decreases when discharged.

6.5 Limitation of Storage

Thus far, the controls for DFIG with SB system have been presented for normal operating condition, where the SB voltage remains within its specified limits, i.e.

$$V_{SB,min} \leq V_{SB} \leq V_{SB,max} \tag{6-11}$$

However, this may not always be the case. As observed from Table 6-2 the charging and discharging of SB is not straightforward and depends on several operating conditions. There will be time when the SB reaches its maximum storage capacity ($V_{SB} = V_{SB,\,max}$) or become fully discharged ($V_{SB} = V_{SB,\,min}$). Under these adverse circumstances, a block signal must be sent to the DC/DC converter Figure 6-7, in effect disconnecting the SB from the system to prevent any further charging and discharging actions. The GSC's control must also be changed. It must now take over the DC/DC converter's role and regulates the DC-link voltage, just like in a typical DFIG system.

It is possible to revert back to the normal control algorithms when conditions become favourable. To do so, either one of these conditions must be satisfied:

$$P_s < P_{dispatch} \quad and \quad V_{SB} = V_{SB,max} \tag{6-12}$$

$$P_s > P_{dispatch} \quad and \quad V_{SB} = V_{SB,min} \tag{6-13}$$

When the stator power, P_s is less than predetermined reference power, $P_{dispatch}$, it implies that energy can be supplied to the system. Thus, if V_{SB} is at its maximum and ready to be discharged, the DC/DC control should be reactivated. Similarly, if P_s is greater than $P_{dispatch}$, it suggests that energy can be stored. Thus, if V_{SB} is at its minimum and ready to be charged, the DC/DC control should be reactivated.

Hence, by monitoring these two signals, switching between normal and contingency condition is possible. In order to prevent continuous switching between these two conditions, a small hysteresis band of 5% is arbitrarily chosen, as shown below:

$$P_s \leq 0.95\, P_{dispatch} \quad and \quad V_{SB} = V_{SB,max} \tag{6-14}$$

$$P_s \geq 1.05\, P_{dispatch} \quad and \quad V_{SB} = V_{SB,min} \tag{6-15}$$

6.6 Management of Storage

The DFIG with SB system is controlled in such a way that it is able to supply a predetermined amount of power to the network, in effect smoothing out the power output fluctuations inherent by the wind farm.

However, as the energy source is dependent on the weather and is likely to vary over time, it is extremely difficult to set an optimum reference power value. As a result, there may be a large mismatch between the predetermined reference power and the generator's power output. Consequently, the SB may not be efficiently used (rapidly discharged or charge unnecessarily) and may need to be disconnected from the system, as discussed in the previous section.

Hence, by allowing the reference power set point to vary over time, the timescale over which SB can be employed is prolonged, thus maximizing the benefits of SB connection. Although this condition occurs in the expense of power variation, the overall effect is improved over typical DFIG output.

In this thesis, a better management of SB is achieved by determining the pre-specified reference value using Exponential Moving Average (EMA) of P_{stator} [97, 107]. The average value of P_{stator} can be determined using

$$\overline{P_{s_n}} = P_{s_n} \times k + \overline{P_{s_{n-1}}} \times (1 - k) \tag{6-16}$$

$$k = \frac{2}{n+1} \tag{6-17}$$

Where $\overline{P_{s_n}}$ is the average value of P_{stator}, n is the number of data.

This technique is admittedly simple and is chosen only to demonstrate the concept of storage management. There is other better yet more complex method available, for example in [93], fuzzy logic-based method is proposed to set the reference power value and hence optimize the benefits of storage. This more advanced method is able to take into account of more factors such as wind power production prediction, energy storage device status and ac voltage measurements.

6.7 Case Studies

The following case studies have been performed in order to illustrate the operation of the DFIG with SB. Otherwise stated, these studies were done using the same network model and data used in the previous chapter, with the same actual wind profile applied to the DFIG system. Islanding is initiated at t=0s by the opening of line connecting busbars 2 and 3 of Figure 5-6.

6.7.1 Normal Operation

Simulation studies were carried out to demonstrate the operation of DFIG with SB system during normal conditions. Figure 6-9 and Figure 6-10 present the results for these studies:

6.7.1.1. DFIG output fixed at 1.0 MW

Figure 6-9(a) shows the DFIG stator active power, P_{stator} and the total active power dispatched to the grid, $P_{dispatch}$. It can be seen from the figure that with the integration of SB, the short term fluctuations in output power are successfully smoothed out, with the $P_{dispatch}$ regulated to the predetermined reference value, 1 MW.

The excess power from the difference between P_{stator} and $P_{dispatch}$, P_{grid} is delivered to the SB via the GSC, as depicted in Figure 6-9(b) (represented by the negative convention).

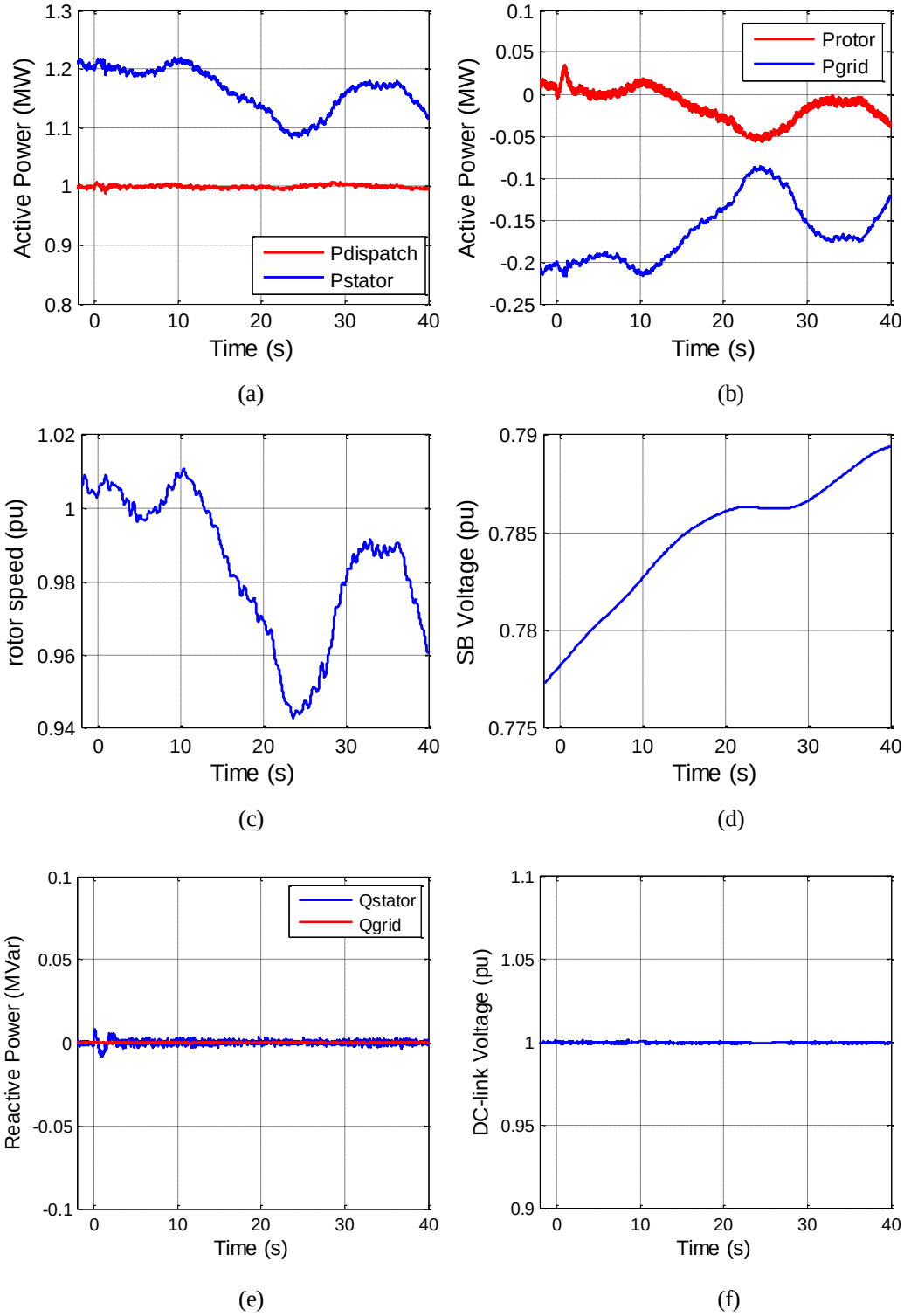

Figure 6-9 Operation of DFIG with SB system under normal operation with reference set point of 1.0MW: (a) dispatch active power (Pdispatch) and stator active power (Pstator); (b) rotor active power (Protor) and active power delivered to/from DC-link (Pgrid); (c) rotor speed; (d) SB voltage; (e) stator reactive power (Qstator) and reactive power delivered to/from DC-link, (Qgrid); (f) DC-link voltage

RSC's controller continues to extract maximum energy available from the wind. From Figure 6-9(b) and Figure 6-9(c), it is observed that when the rotor speed is less than 1 p.u. (synchronous speed), active power, P_{rotor} is absorbed by the generator (sub-synchronous operation), hence the negative convention. When rotor runs above 1 p.u., active power is delivered to the SB (super-synchronous operation).

From Figure 6-9(b), it is seen that P_{grid} is negative throughout the simulation time whilst P_{rotor} is positive for t<13s and negative for the remaining simulation time. Referring to Table 6-2, for t<13s, when $P_g<0$ and $P_r>0$, P_{sb} is positive, which means energy can be stored into SB. For t>13s, with $P_g<0$, $P_r<0$, and $|P_r| < |P_g|$, P_{sb} is again positive. Thus, for the entire simulation time, power is stored into the SB. This is in conformity with the result depicted by Figure 6-9(d), where the SB voltage increases due to the charging. Note that SB voltage is normalised with respect to its maximum voltage, $U_{max.}$

Figure 6-9(e) shows the reactive power flows in the stator and GSC. It can be observed that they are kept constant throughout the simulation, despite the variation in wind and real power exchange that happened in the RSC and GSC respectively. These results clearly illustrate the decoupled control capability between the active and reactive power of both RSC and GSC.

The DC/DC converter's controller is operating as designed as well, maintaining the DC-link voltage constant throughout the simulation (Figure 6-9(f)).

6.7.1.2. **DFIG output fixed at 1.3 MW**

In this simulation, the DFIG system is set to dispatch 1.3 MW power output. It can be clearly observed from Figure 6-10(a) that there is a mismatch between the P_{stator} and $P_{dispatch}$. This power difference is subsequently balanced by the power delivered from SB, P_{grid}.

The same wind profile as case (i) is applied in this case, hence the same rotor speed and P_{rotor} seen in the results.

From Figure 6-10(b), it is seen that P_{grid} is positive throughout the simulation time whilst P_{rotor} is positive for t<13s and negative for the remaining simulation time. Again, referring to Table 6-2, for t<13s, when $P_g>0$, $P_r>0$, and $|P_r| < |P_g|$, P_{sb} is negative, which indicates SB is discharged and energy is supplied to system. For t>13s, with $P_g >0$, $P_r <0$, P_{sb} is again negative. Thus, for the entire simulation time, real power is taken from SB and provided to the system. This is shown by the result presented in Figure 6-10(d), where the SB voltage decreases due to the discharging. Similarly, the reactive power is controlled independently from the active power by both RSC and GSC, as shown in Figure 6-10(e).

The DC/DC controller is performing satisfactorily by keeping the DC-link voltage constant throughout this simulation. Judging from these two cases, it can be concluded that the DC/DC converter controller is performing correctly, capable in stepping up and down in order to maintain the DC-link voltage at desired value.

Figure 6-11 shows the island's voltage phase deviation from the grid's for the entire simulation time. For comparison purpose, the results for typical DFIG, FSIG and no wind farm are also included. It can be clearly seen from Figure 6-11 and Table 6-3 that the phase difference for DFIG with SB system is the best controlled among the three cases with wind farm connected, with a maximum phase difference of 3^o during steady state. It must be noted that with the inclusion of SB, the DFIG output power is greatly smoothed out. However, as opposed to no wind farm case, there is still minor fluctuation presents, which contributed to the small phase variation during steady state.

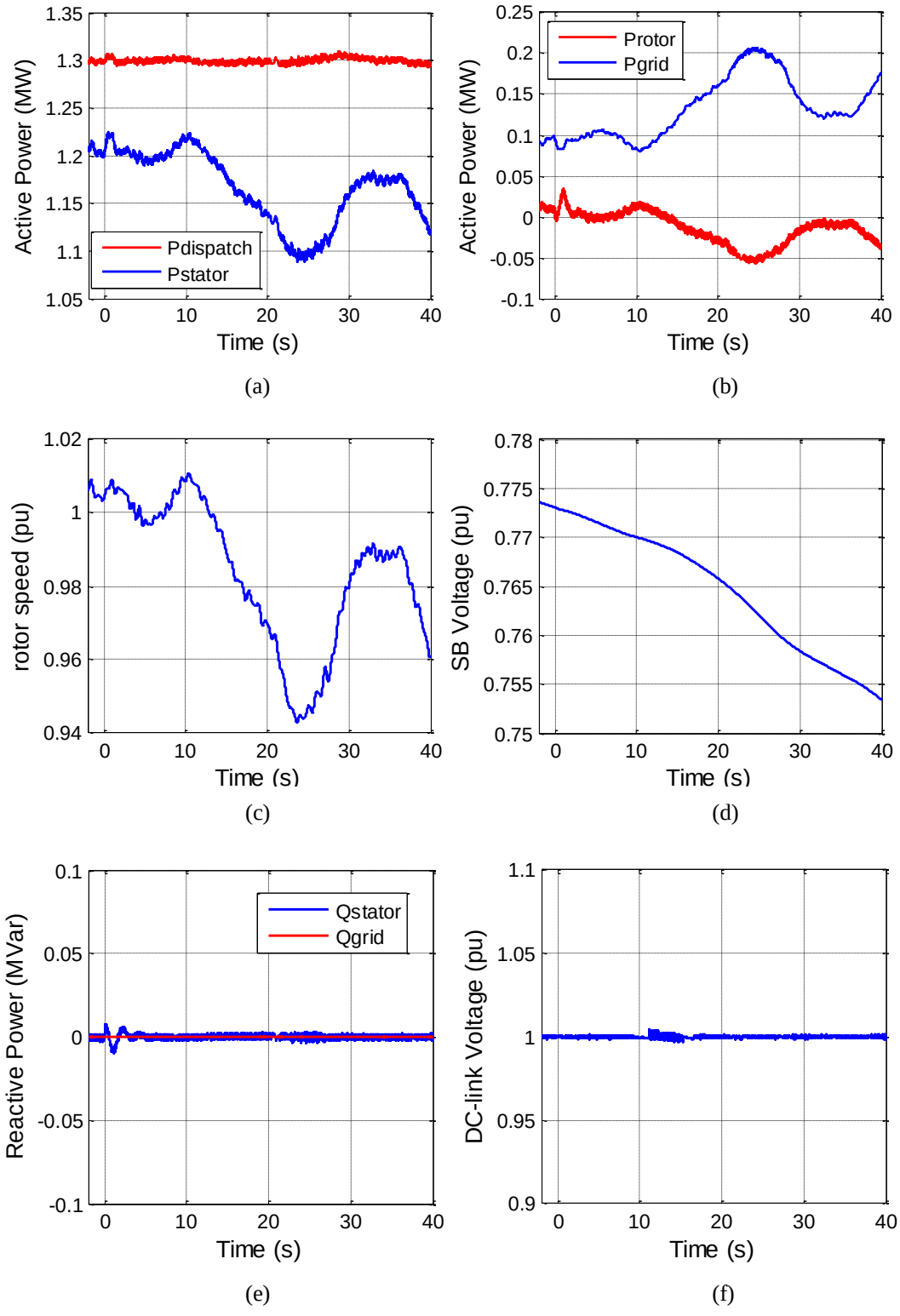

Figure 6-10 Operation of DFIG with SB system under normal operation with reference set point of 1.3MW: (a) dispatch active power (Pdispatch) and stator active power (Pstator) ;(b) rotor active power (Protor) and active power delivered to/from DC-link (Pgrid); (c) rotor speed; (d) SB voltage; (e) stator reactive power (Qstator) and reactive power delivered to/from DC-link (Qgrid); (f) DC-link voltage

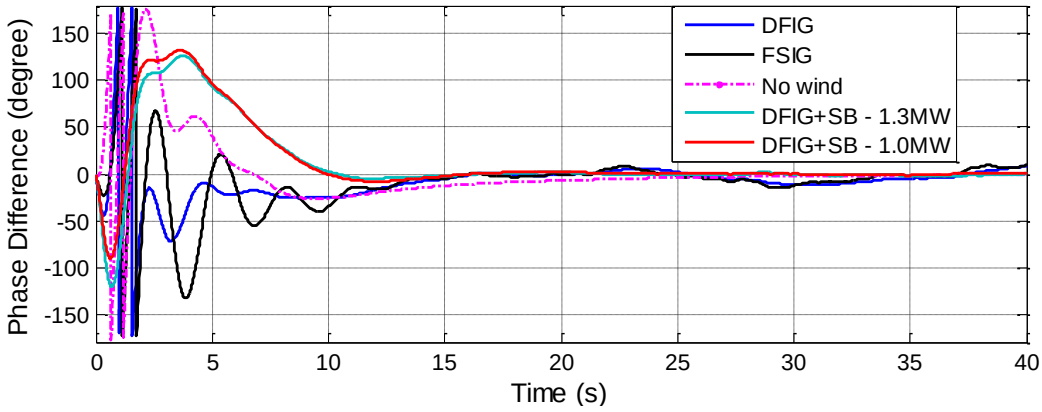

Figure 6-11 Voltage phase difference throughout islanding for different cases

Table 6-3 Maximum Phase Deviation for Different Cases

Case	**Maximum Phase Difference (^{o})**
DFIG + SB	3
Typical DFIG	12
FSIG	15
No Wind	0

6.7.2 **Storage Limitation**

In this simulation, the response of DFIG with SB system when approaching storage limits is tested. To reduce simulation time, the size of the SB applied in this simulation is reduced to 10% of its original rating. This measure ensures that the limits are reached within the simulation time, enabling the analysis on the control's transition during these conditions to be done.

Figure 6-12(a) shows the DFIG stator active power, P_{stator} and the total active power dispatched to the grid, $P_{dispatch}$. The reference power set-point is also included in the plot.It can be seen that at point 'a', the $P_{dispatch}$ is no longer regulated to the reference set-point. This is explained by Figure 6-12(b), where the SB upper limit is reached, prompting the disconnection of SB from the system. The disconnection of SB can be

confirmed by the constant SB voltage, which indicates that no charging or discharging action is taking place.

Subsequently, the wind farm operates like a typical DFIG, where the $P_{dispatch}$ is the summation of P_{stator} and P_{rotor}. This is in agreement with the results shown in Figure 6-12(a) and Figure 6-12(c). Following the disconnection of SB, the role of DC-link voltage regulation is transferred to the GSC. This regulation indirectly facilitates the power transfer between the RSC and GSC, and can be clearly observed from Figure 6-14(c), between point 'a' and 'b', where P_{rotor}=P_{grid}.

At point b, the reference set-point is increased to higher than P_{stator}. This satisfies one of the conditions to reconnect the SB, which is reproduced here:

$$P_s \leq 0.95\, P_{dispatch} \quad and \quad V_{SB} = V_{SB,max} \qquad (6\text{-}18)$$

This SB reconnection is confirmed by the result where the $P_{dispatch}$ is once again regulated to the reference value, from point 'b' to 'c'. With the reconnection of SB, the regulation of DC-link voltage is taken over by DC/DC converter. Hence, between these points, it is seen that $P_{grid} \neq P_{rotor}$. At this instant, P_{grid} serves as the balancing power to supply the power mismatch between $P_{dispatch}$ and P_{stator}. It is observed that between point 'b' and 'c', P_{grid} is far greater than P_{rotor}, hence by referring to Table 6-2, P_{sb} is negative, which indicates that SB is discharged and power is supplied to the system. The provision of power from the SB leads to the drop in SB voltage.

At point 'c', it is again observed that the $P_{dispatch}$ is not equal to the set-point. This is due the disconnection of SB and is confirmed by Figure 6-12(b), in which the lower limit of SB is reached. The disconnection can be clearly observed from the constant SB voltage. The output power, $P_{dispatch}$ is seen to be lower than the stator power. This is because power is absorbed by the rotor due to sub-synchronous mode (w_{rotor} <1 p.u.) operation. This is in line with the results shown in Figure 6-14(c) and Figure 6-13.

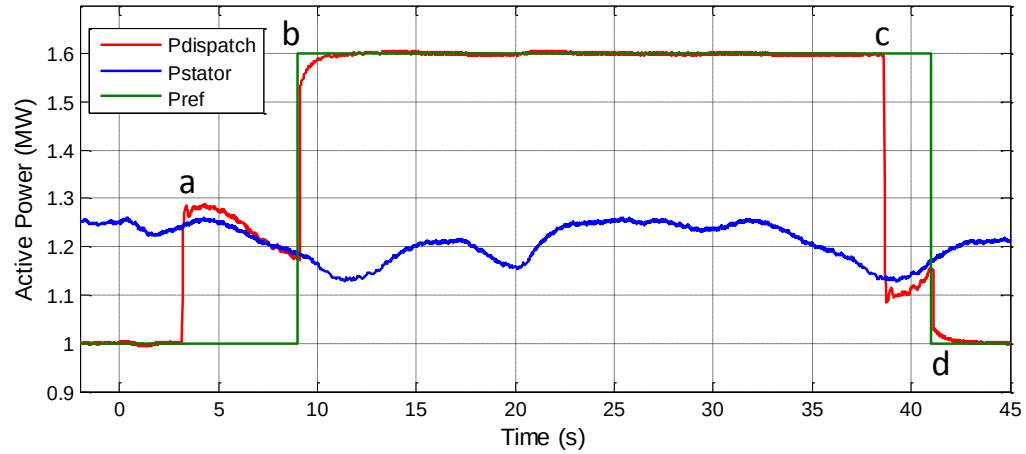

(a)

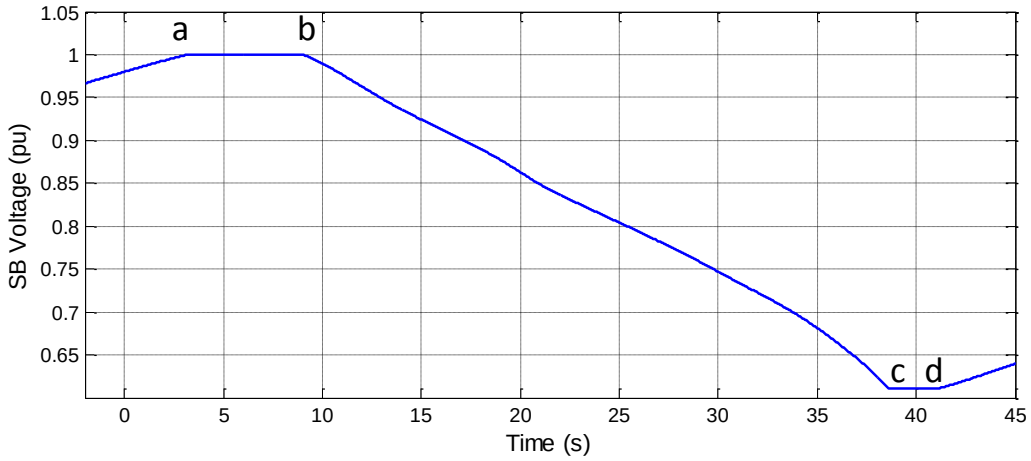

(b)

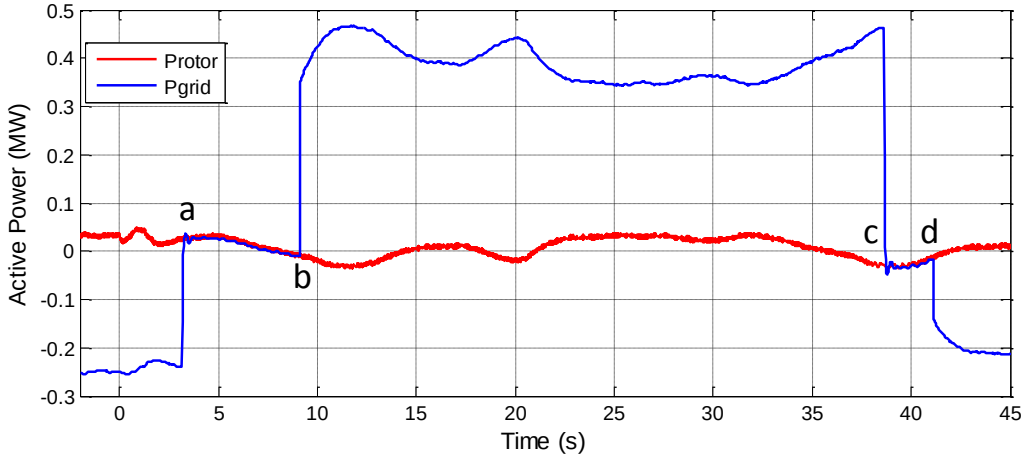

(c)

Figure 6-12 Operation of DFIG with SB system under limited storage capacity: (a) dispatch active power ($P_{dispatch}$), stator active power (P_{stator}) and reference power (P_{ref});(b) SB voltage; (c) rotor active power (P_{rotor}) and active power delivered to/from DC-link (P_{grid})

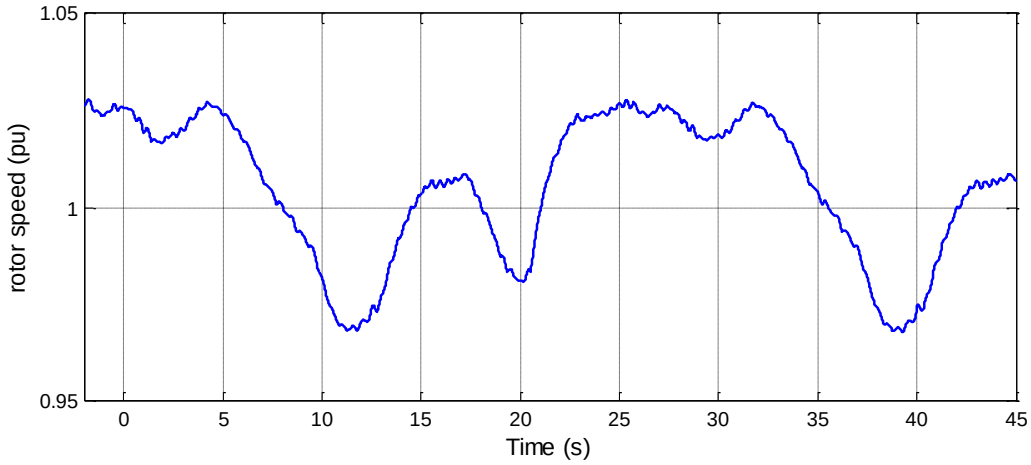

Figure 6-13 DFIG rotor speed

At point 'd', the reference set-point is reduced to lower than Pstator. This satisfies the other condition to reactivate the SB, which is reproduced here:

$$P_s \geq 1.05\, P_{dispatch} \quad and \quad V_{SB} = V_{SB,min} \qquad (6\text{-}19)$$

The reactivation of SB is verified by the steady DFIG output. Referring to Table 6-2, after point 'd', excess power is stored in SB, hence the increment in SB voltage due to the charging.

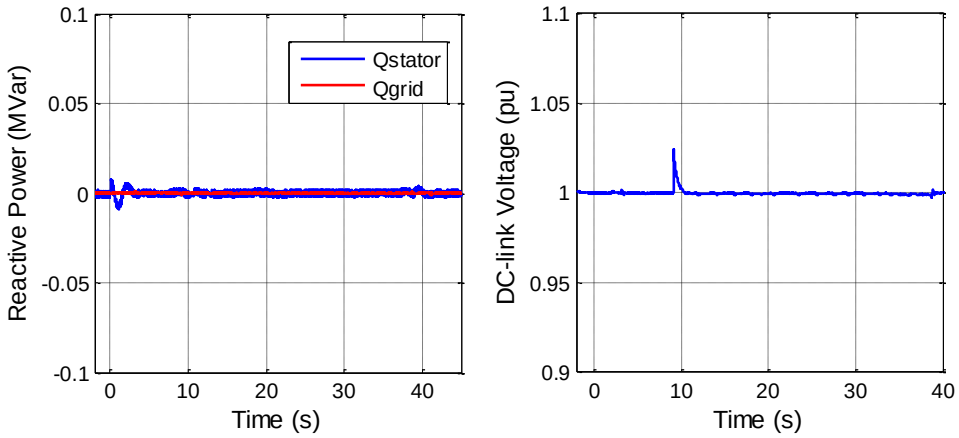

(a) (b)

Figure 6-14 Operation of DFIG with SB system under limited storage capacity: (a) stator reactive power (Q_{stator}) and reactive power delivered to/from DC-link (Q_{grid}); (b) DC-link voltage

Figure 6-14(a) shows the reactive power flows in the stator and via the GSC. It can be observed that they are kept constant throughout the simulation, despite the transition between normal and contingency mode. These results also illustrate the decoupled control capability between the active and reactive power of both RSC and GSC.

Although the regulation of DC-link voltage is transferred between the controller of DC/DC converter and GSC in this example, it is observed from Figure 6-14(b) that the voltage is kept constant throughout the simulation.

6.7.3 **Management of Storage**

It has been demonstrated in the previous section that DFIG with SB system is capable of switching between normal operating condition and contingency condition, enabling the continued operation of the wind farm, and hence keeping it connected to the network even without storage system, operating like a conventional DFIG. However, depending on the frequency of these occurrences, the benefit of storage integration will not be maximized. This is even more undesirable for synchronous island operation, for every control transition will incur transients in the island, as depicted in Figure 6-15.

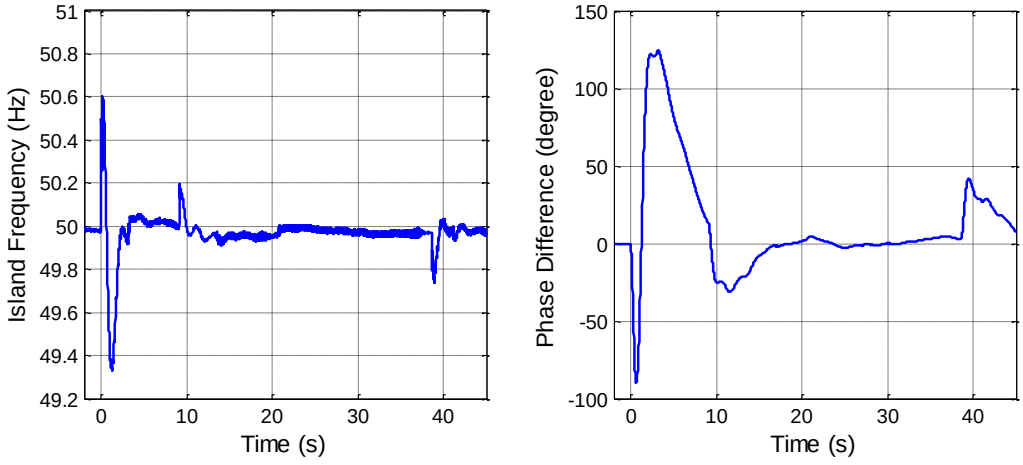

Figure 6-15 Transient during control transition: (a) frequency (b) phase deviation

Moreover, it is generally hard to set a reference output value. Step changing the reference value from time to time is possible, but again is detrimental to the implementation of synchronous island, as it will cause unnecessary transients in the island.

Hence, this case study is carried out to investigate the effect of allowing the reference power set point to vary. The same setting as case study 1 was used, but with the set point calculated using equations (6-16) and (6-17).

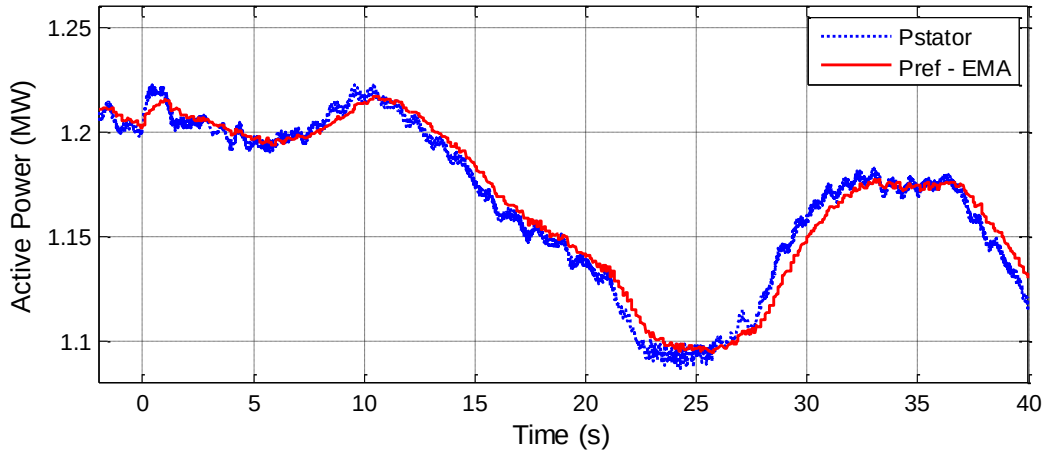

Figure 6-16 Comparison between P_{stator} and calculated $P_{reference}$ using EMA

Figure 6-16 shows the calculated reference power set point compared to the stator real power. For comparison purpose, two other cases have been simulated, as follow:

i) Varying reference set point calculated using Exponential Moving Average, EMA

ii) Constant reference set point of 1.2MW

iii) Constant reference set point of 1.15MW

Figure 6-17 presents the results from these case studies. Figure 6-17(a) depicts the total output power, $P_{dispatch}$ dispatched from the wind farm. Figure 6-17(b) shows the balancing power, P_{grid} delivered to/from the DC-bus via the GSC. It is worth to note that P_{rotor} for all cases are the same, for the same wind data are applied to the DFIG.

Figure 6-17(c) shows the SB voltage for all cases. Comparing cases of constant reference set-point, it can be observed that a small difference in set-point value, i.e. 0.05 MW can make a considerable difference to the SB voltage. From this example, it can be seen that moving the constant reference set-point downwards (<1.15MW) will inevitably move the SB voltage curve higher, causing it to reach the upper limit quicker. On the other hand, setting the constant reference set-point upwards (>1.2MW) will shift the SB voltage curve lower, and subsequently reaching its lower limit faster. By allowing the set-point to vary over time, it is seen that SB voltage variation is less extreme. Clearly, this will prevent it from approaching its limits as soon as compared to setting a constant reference set-point, and thus effectively extend the time scale over which the SB can be applied.

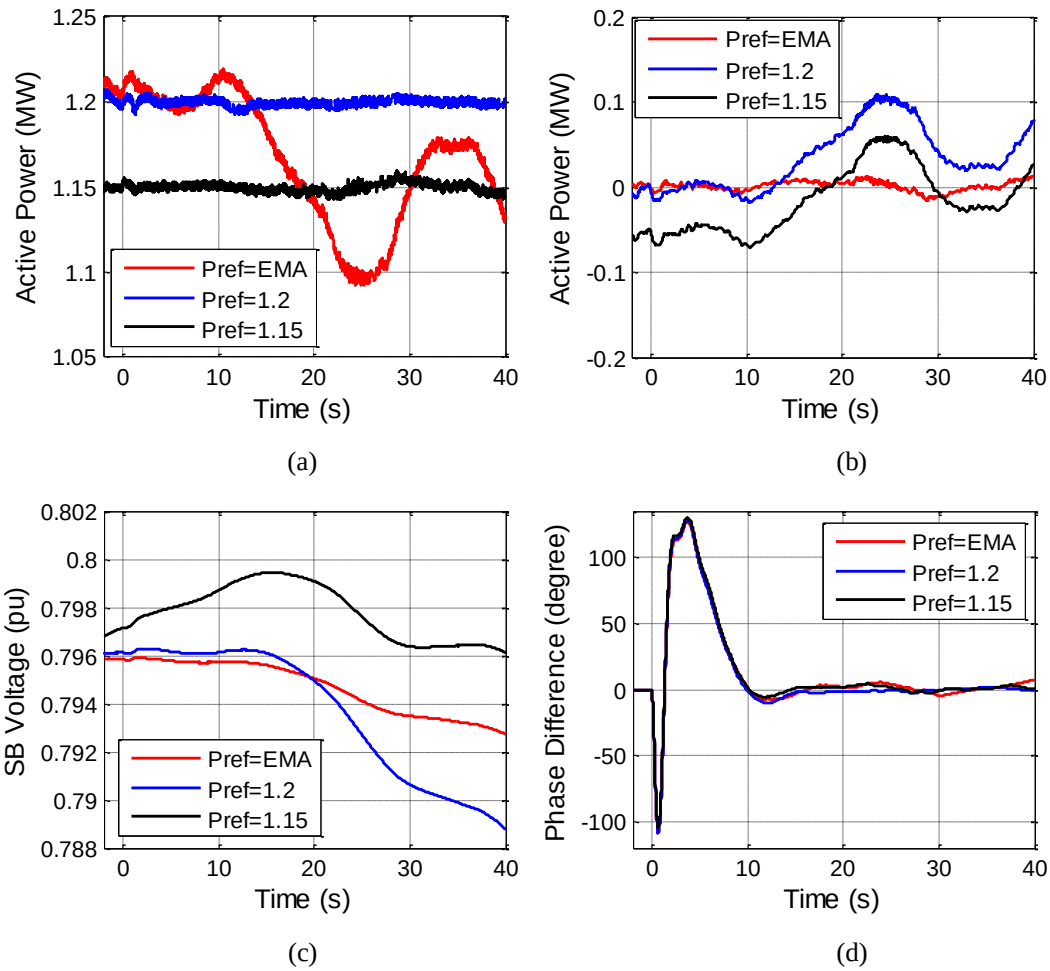

Figure 6-17 Comparison of DFIG with SB operation using different reference set point: (a) dispatch active power ($P_{dispatch}$); (b) active power delivered to/from DC-link (P_{grid}); (c) SB voltage; (d) phase difference

However, this comes at the expense of a slightly less firm DFIG power output. As a result, the voltage phase difference between the island and the grid during steady state increased, as can be clearly observed in Figure 6-17(d) and Table 6-4. Nonetheless, the increment is so small compared to the benefits of applying a varying reference set-point.

Table 6-4 Maximum Phase Deviation for Case (i)-(iii)

Case	**Maximum Phase Difference (^{o})**
i	7
ii	4
iii	3.5

Figure 6-18 shows the power output for DFIG with SB compared to the typical DFIG. The power reference set-point for the former type is calculated using EMA. As observed, for the same wind data, the power output fluctuations have greatly reduced with the integration of SB into the wind farm system.

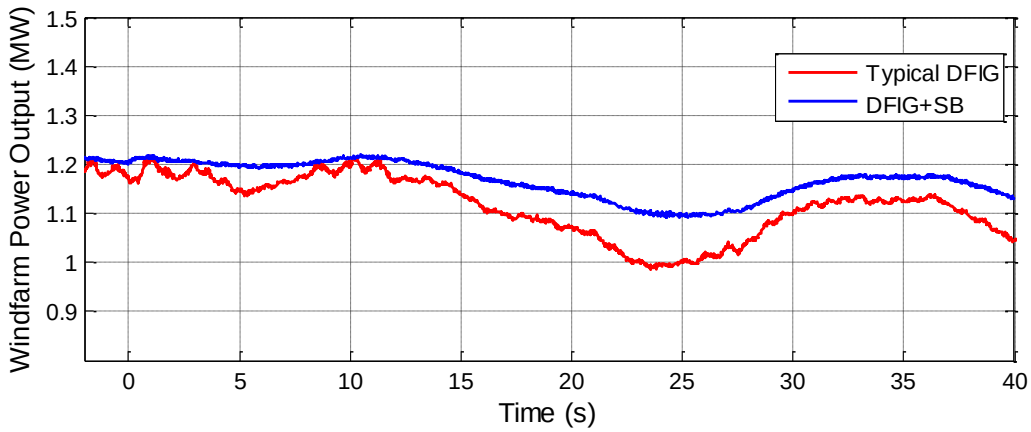

Figure 6-18 Comparison of real power output for typical DFIG and DFIG with SB

6.7.4 **Maximum Load Acceptance**

The maximum load disturbance that can happen in the synchronous island without the phase difference going beyond $\pm 60^{\circ}$ limit is investigated in this case study. The

reference set-point is set using the EMA method. Similar to section 5.5.3, load is applied in 0.5% resolution at several different times, as shown below:

Case 1) Phase difference peak

Case 2) Phase difference trough

Case 3) Frequency peak

Case 4) Frequency trough

Case 5) Time of low frequency and phase variation

The results in Table 6-5 lists the maximum load acceptance possible for each test while not exceeding $\pm 60°$ phase difference. They are presented in percentage terms of the controllable generation in the island, i.e. of 5.208 MW.

From the results, it is observed that there is a minor improvement in the maximum load applicable in the island for some cases using DFIG with SB compared to typical DFIG. However, the control performance still does not quite reach the level of the no-wind case.

Table 6-5 Comparison of Maximum Load Acceptance for Cases (1)-(5)

CASE	MAXIMUM LOAD ACCEPTANCE (%)		
	DFIG + SB	Typical DFIG	No Wind
1	16.0	16.0	17.5
2	17.0	17.0	
3	17.0	16.0	
4	16.0	15.5	
5	16.5	16.5	

6.8 Effect of DFIG Connection to Island's Frequency

An interesting result was observed in section 5.5.2, in which immediately after islanding, the ROCOF of case study with DFIG wind farm connected is similar to the case study in which no wind farm was connected. Following this observation, a series of simulations have been carried out to investigate the influence of DFIG connection to the island's frequency response.

Three case studies have been considered, with case 1 as the base case. Note:- the network model depicted in Figure 5.6 is used in these case studies. A load increment of 174 kW is simulated at t=0s in all cases:

1) The simulated island consists of a 2.5MW DFIG wind farm and 6.5MVA synchronous generators supplying a total load amounting 4.5MW, with the output from wind farm equal 1MW.
2) Same as case 1 but the number of DFIG wind farm connected in the island is increased to 2 (5MW wind farm in total), with each wind farm supplying 1MW load.
3) Same as case 2 but with reduction in synchronous generators rating in proportion with the increase in DFIG rating, such that the total generation in the island remains the same.

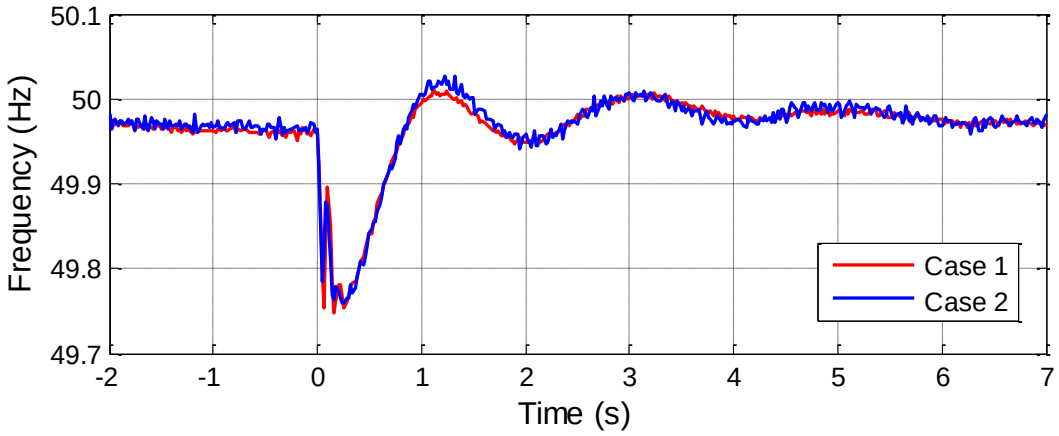

Figure 6-19 Comparison of frequency response for case 1 and case 2

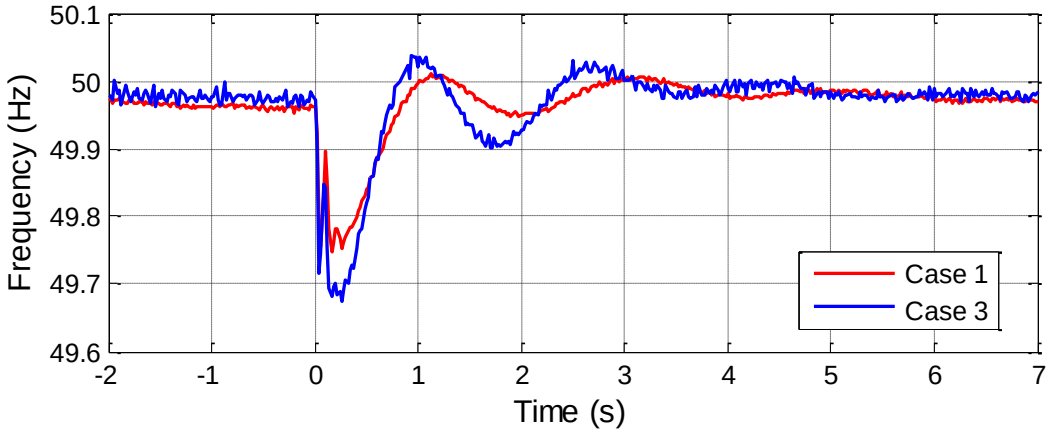

Figure 6-20 Comparison of frequency response for case 1 and case 3

The results from these case studies are presented in Figure 6-19 and Figure 6-20. From Figure 6-19, it is observed that increasing the number of DFIG wind farms connected in the island has almost no effect on the frequency deviation following load disturbance, if the rating of synchronous generators in the island does not change. However, if the synchronous generators are replaced with DFIG (represented by the reduced synchronous generators rating), the ROCOF increased immediately after the load disturbance, as depicted by Figure 6-20. In addition, it leads to a lower minimum frequency point compared to the base case.

These results can be further explained by using equation of motion (6-20)

$$J\omega_m \frac{d}{dt}\omega_m = P_{gen} - P_{load} \qquad (6\text{-}20)$$

With J = Total System Inertia

ω_m = Mechanical rotation speed of generator

P_{gen} = Total power supplied by all generators in the system

P_{load} = Total load in the system

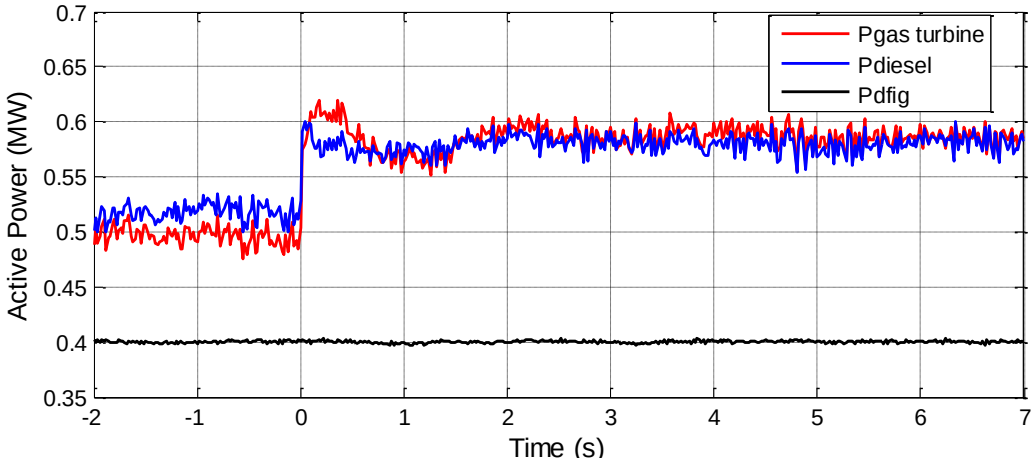

Figure 6-21 Inertia response of synchronous generators

The imbalance between generation and load will result in a change in the rotational speed of generators, and consequently a change in the system's frequency. The rate at which the generators decelerate/accelerate is determined by the total inertia of the

system. The lower the system inertia, the more the rotor speed of the generators will change during a power imbalance. This change in rotational speed converts the generators' kinetic energy to electrical energy, hence giving rise to a power surge, as depicted in Figure 6-21. This response is called inertial response and is an inherent characteristic of synchronous generators.

However, this is not the case for DFIG wind turbine. The control of DFIG decouples the mechanical from the electrical system and thus any deviation in system frequency will not be "seen" by the wind turbine's rotor. In other words, DFIG's rotor speed is independent from the system's frequency and therefore it does not contribute to the system inertia. Hence, connection of DFIG does not affect system frequency regulation. This is confirmed by the results depicted in Figure 6-19 and Figure 6-21.

However, this only applies when the rating of synchronous generators in the system stays the same. When the rating of synchronous generators in the system is reduced (replaced by DFIG), the total system inertia decreased. As a result, any variation in load or generation will lead to a larger frequency deviation and in some cases, may compromise system stability. This explains the results presented in Figure 6-20.

This situation is undesirable especially in a small power system such as an island. With the increasing penetration of DFIG (and the like, i.e. variable speed wind turbines) into the system, there is a high chance for an island with a large proportion of DFIG wind farm as opposed to synchronous generators to form. This can be a challenge especially to the implementation of synchronous islanded operation.

Figure 6-22 compares the island's voltage phase deviation between case 1 and case 3 following the load disturbance. The reduced island inertia has resulted in a larger frequency deviation, and consequently bigger phase difference between the island and the grid. This situation will limit the magnitude of the load disturbance that can happen in the island without going beyond the relaxed synchronisation limits.

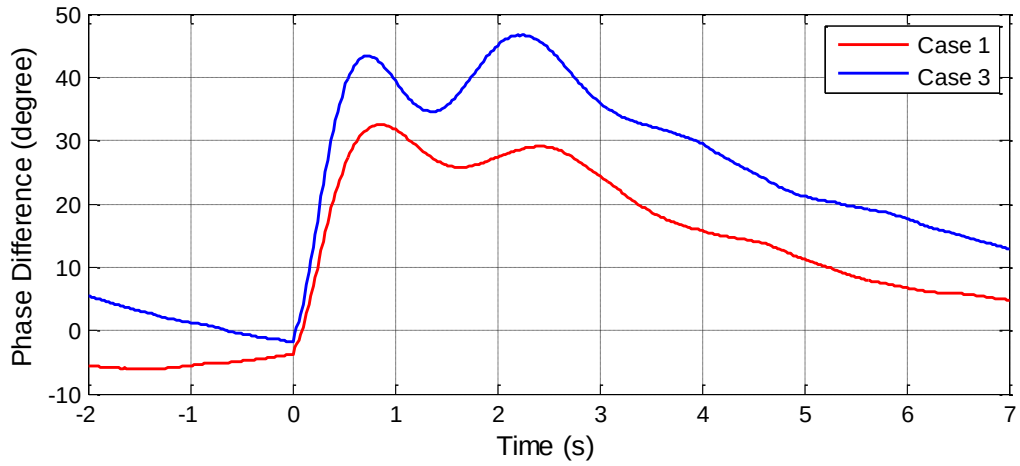

Figure 6-22 Comparison of Phase Difference between case 1 and case 3

Other researchers have also noticed the challenge associated with the increased penetration of DFIG and realized the importance for DFIG to contribute to the inertia of the system [71, 108-112]. It has been demonstrated that DFIG can mimic the inertial response by adding a supplementary control in the power/speed control loop, as described in [71, 108, 109, 112]. These methods exploit the kinetic energy stored in the wind turbine and introduce a change to the DFIG output power during system disturbances, hence improving the frequency regulation. The output can be designed to change either based on the rate of change of system frequency, as proposed in [71, 108], or proportional to the grid frequency deviation, as suggested in [109] or according to the load increment, as advocated in [112].

6.9 Proposed Supplementary Control for Inertial Response

As discussed above, the unavailability of inertia provision by DFIG proves to be a setback in implementation of synchronous islanded operation. This is especially the case when the percentage of DFIG wind farm trapped in the island is comparable to the synchronous generators. A supplementary control is thus proposed to enable DFIG to emulate the inertial response.

Previous works generally proposed provision of inertia by regulating the electrical torque. Hence, the supplementary control is usually added to the power/speed loop in the rotor side converter (RSC). This is applicable for a typical DFIG. However, if a storage system is added to the DFIG system, as discussed in section 6.3.2, any changes at rotor side converter output will be buffered by the storage, resulting in no changes to the output power.

Hence, in order to benefit from the firm output, as well as enabling the DFIG to contribute to the inertial response, an auxiliary control depicted in Figure 6-23 is proposed. This control is added in cascaded to the real power control loop of the grid side converter (GSC). The choice of K_a and T_a determines the magnitude and shape of the response, which is discussed in section 6.7.2.

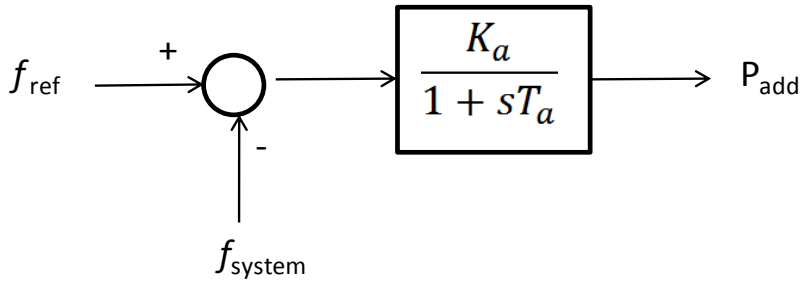

Figure 6-23 Proposed supplementary control for inertial response

6.10 Case Studies

The following case studies have been performed in order to illustrate the operation of the proposed control loop. Otherwise stated, the network model shown in Figure 5.6 is used in all case studies.

6.10.1 Performance of Proposed Inertial Control

This case study is carried out to illustrate the performance of the proposed inertial control. The results obtained are also compared against the case of DFIG with SB to highlight the benefits of the proposed control, in particular to the implementation of synchronous island. Cases simulated are as follow:

1) The simulated island consists of 2.5MW typical DFIG (with SB) wind farm and 6.5MVA synchronous generators supplying a total load of 4.5MW. The output from wind farm is 1.125 MW.
2) Same as case (i) but with proposed inertial control added to the GSC's controller of the DFIG with SB system

Both cases are operating as synchronous island throughout the simulation. At t=0s, an additional load amounting to 434 kW was added to the network in all cases. For ease of observation, the grid frequency is set to constant 50Hz.

During the load disturbance, the system with inertial control increases its power output (Figure 6-24(a)) and consequently helps to reduce the frequency deviation. This improves the frequency response significantly, as depicted in Figure 6-24(b), the minimum frequency point is increased by 0.1Hz.

The provision of power during this disturbance can also be observed from Figure 6-24(c) and Figure 6-24(d). Without the supplementary control, the load imbalance is supplied entirely by the synchronous generators in the island. However, when supplementary inertial control is added, DFIG contributes towards the load mismatch and provides part of the additional load. This translates to a lower power output from both diesel and gas turbine generators.

The improved frequency profile in turn reduces the phase deviation during the load acceptance, as shown in Figure 6-24(e). This is in favour to the implementation of synchronous islanded operation, in which the phase deviation between the grid and island has to be maintained within relaxed synchronous limits of $\pm 60°$ throughout the islanding operation. Note that in this case study, the phase deviations for both cases have exceeded the synchronisation limits. However, for the same load disturbance, it is seen that addition of supplementary inertial control can reduce the phase deviation significantly.

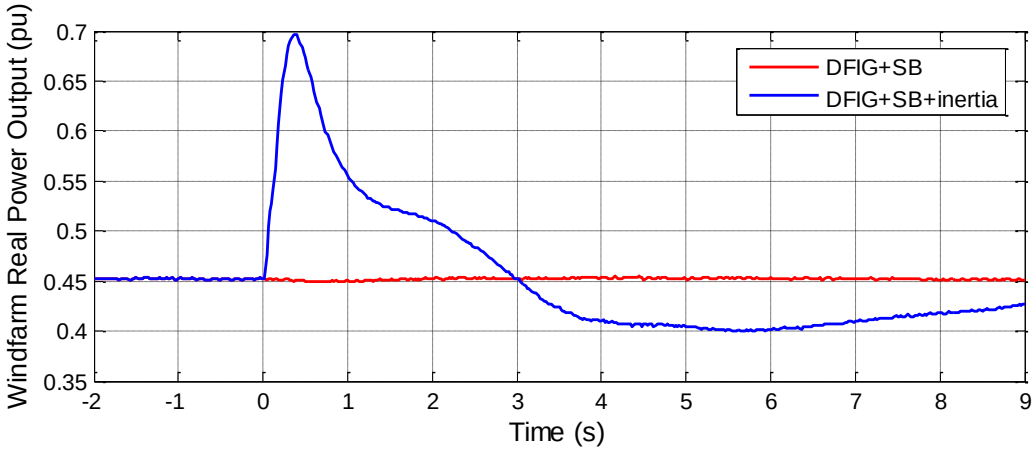
Windfarm Real Power Output (pu)
0.7
0.65
0.6
0.55
0.5
0.45
0.4
0.35
-2
-1
0
1
2
3
4
5
6
7
8
9
Time (s)
DFIG+SB
DFIG+SB+inertia

(a)

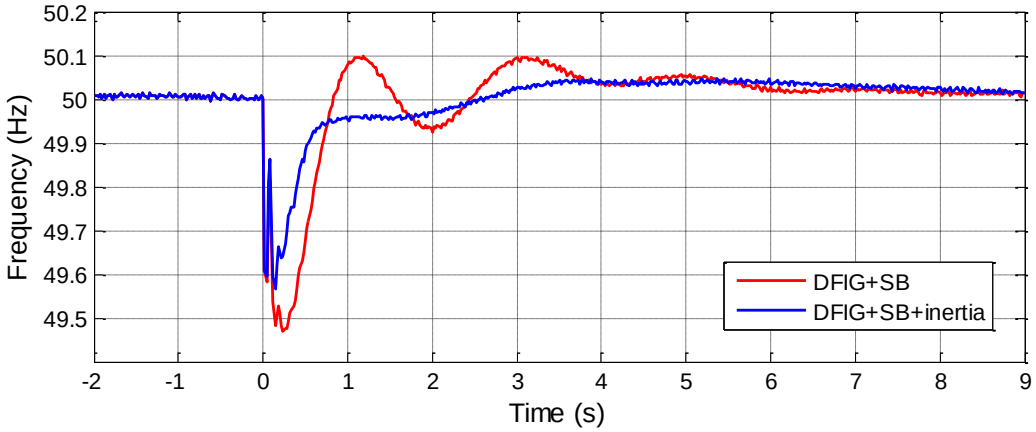
Frequency (Hz)
50.2
50.1
50
49.9
49.8
49.7
49.6
49.5
-2
-1
0
1
2
3
4
5
6
7
8
9
Time (s)
DFIG+SB
DFIG+SB+inertia

(b)

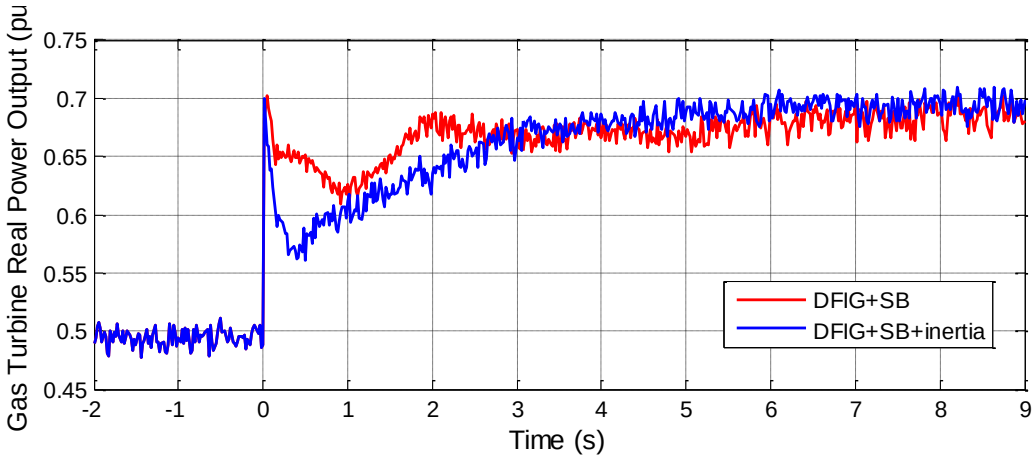
Gas Turbine Real Power Output (pu
0.75
0.7
0.65
0.6
0.55
0.5
0.45
-2
-1
0
1
2
3
4
5
6
7
8
9
Time (s)
DFIG+SB
DFIG+SB+inertia

(c)

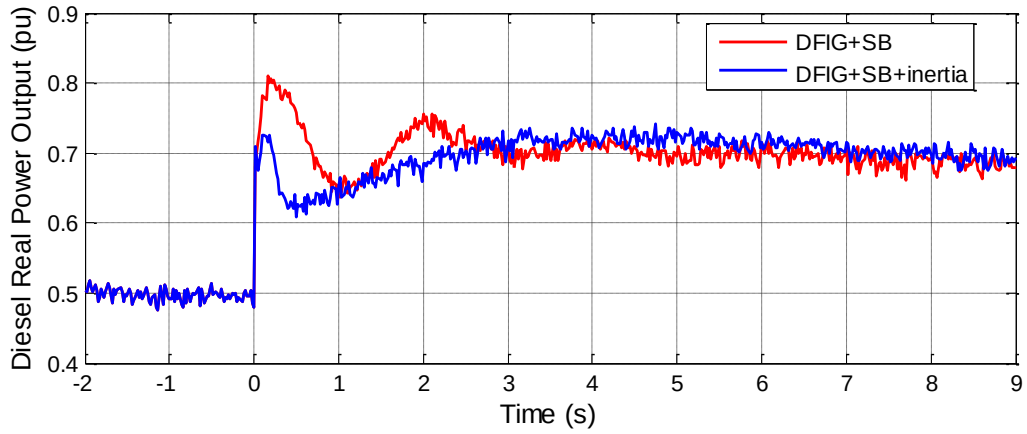

(d)

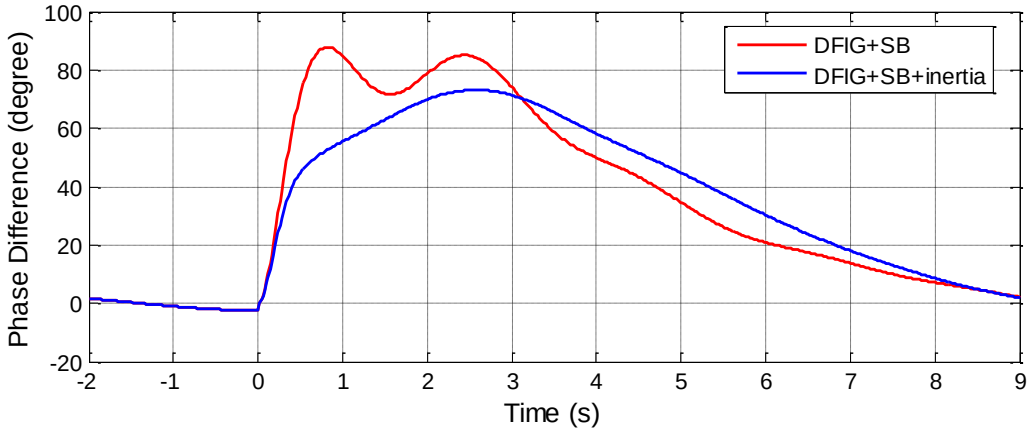

(e)

Figure 6-24 Comparison of island response during a load acceptance with different DFIG wind farm type connected: (a) frequency ;(b) wind farm real power output; (c) gas turbine generator real power output; (d) diesel generator real power output; (e) voltage phase difference

6.10.2 **Influence of Parameters**

This case study is carried out to investigate the influence of parameter K_a and T_a of the proposed control (Figure 6-23) has on the inertial response. The same setting used in section 6.7.1 case (ii) is applied in this simulation. A load increment of 434 kW is simulated at t=0s.

6.10.2.1. **Influence of Proportional Gain, Ka**

In this simulation, the proportional gain of proposed controller is varied from 35, 65 and 95 whilst keeping the time constant, T_a at 0.2 second. The frequency responses,

wind farm real power outputs and phase deviations due to the load disturbance with respect to these gains are illustrated in Figure 6-25, Figure 6-26 and Figure 6-27 respectively.

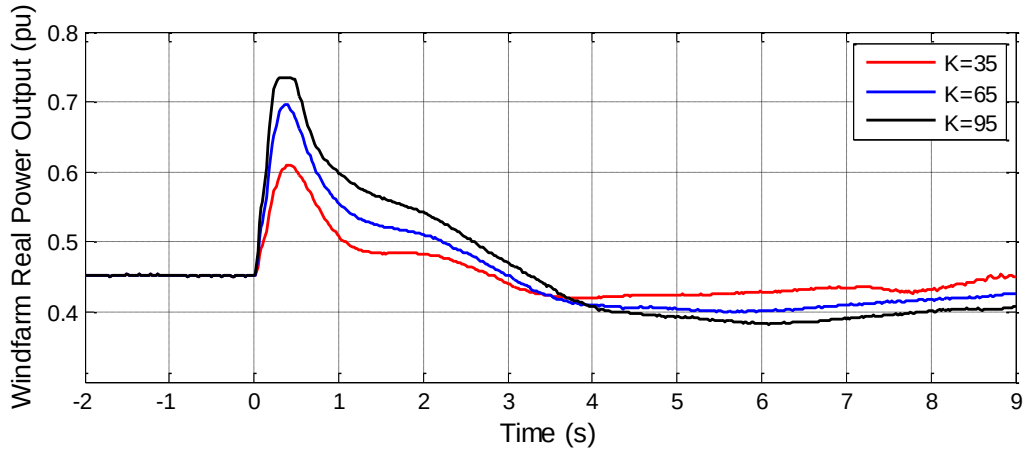

Figure 6-25 Wind farm real power output with respect to different gain

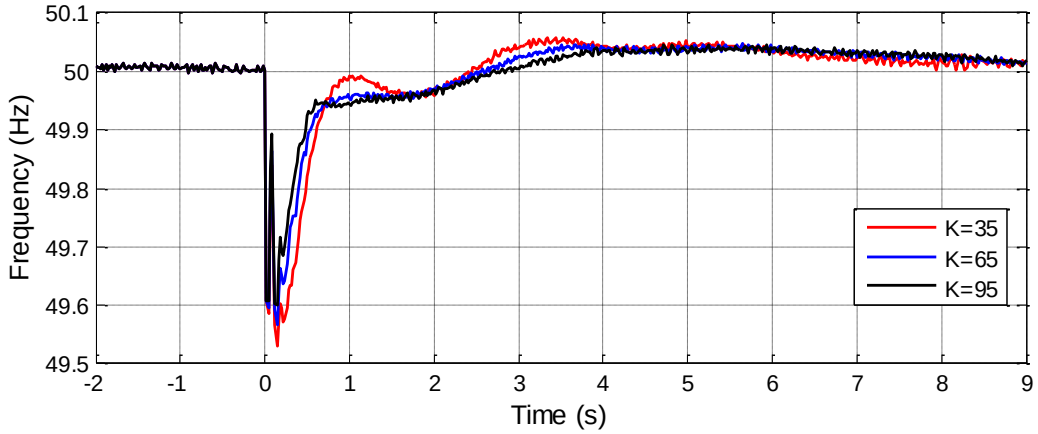

Figure 6-26 Frequency profile with respect to different gain

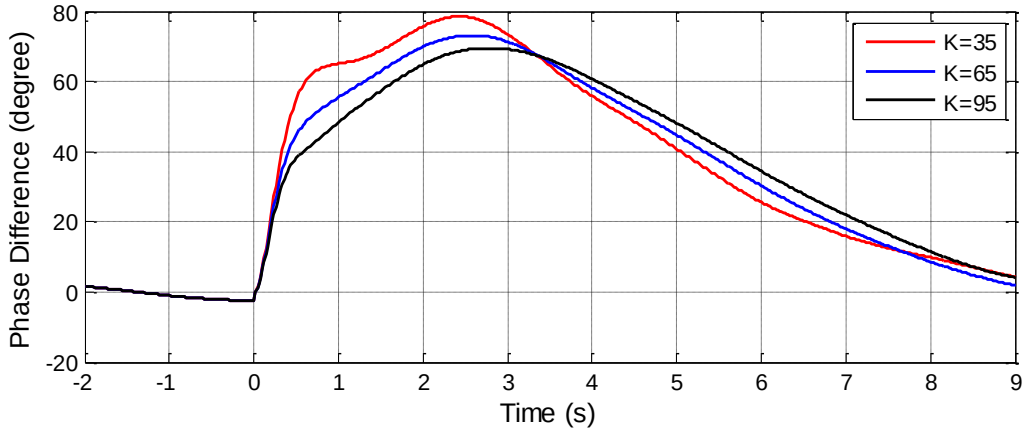

Figure 6-27 Phase difference with respect to different gain

As observed from Figure 6-26 and Figure 6-27, a higher gain results in higher real power output from the wind farm, which in turn helps to reduce the frequency deviation following the disturbance. Note that for case K= 95, the power output has a flat top. This is due to the limitation of GSC converter rating, which represents the maximum amount of real power deliverable to support the system during disturbance. Any further increase in the gain will not help in increasing the output power.

The reduction in frequency reduction as the gain increases also translates to a reduction in phase deviation, which is beneficial in terms of synchronous island implementation. It can be seen from Figure 6-27 that the phase deviation curve is shifted downwards as the gain increases. It is worth to note though that while a high gain is effective in rescuing frequency drop and subsequently reducing phase deviation; it may on the other hand amplify noise and risk instability.

6.10.2.2. **Influence of Time Constant, T_a**

The previous simulation case is repeated with respect to different time constants (T_a=0.01s, T_a =0.2s and T_a =0.4s) for the controller whilst keeping its gain constant at 65.

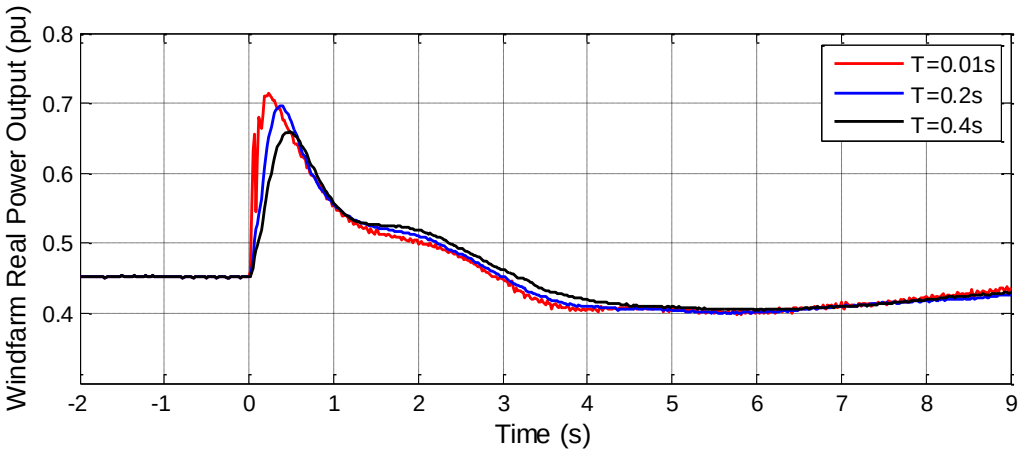

Figure 6-28 Wind farm real power output with respect to different time constant

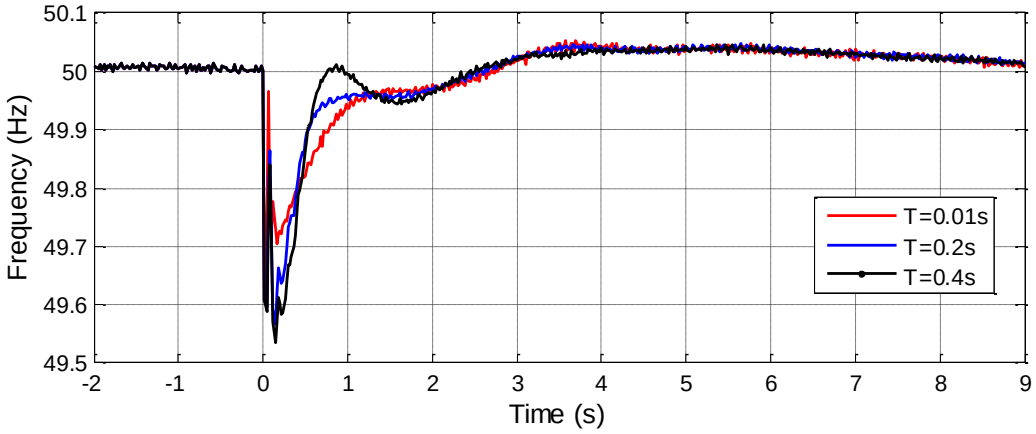

Figure 6-29 Frequency profile with respect to time constant

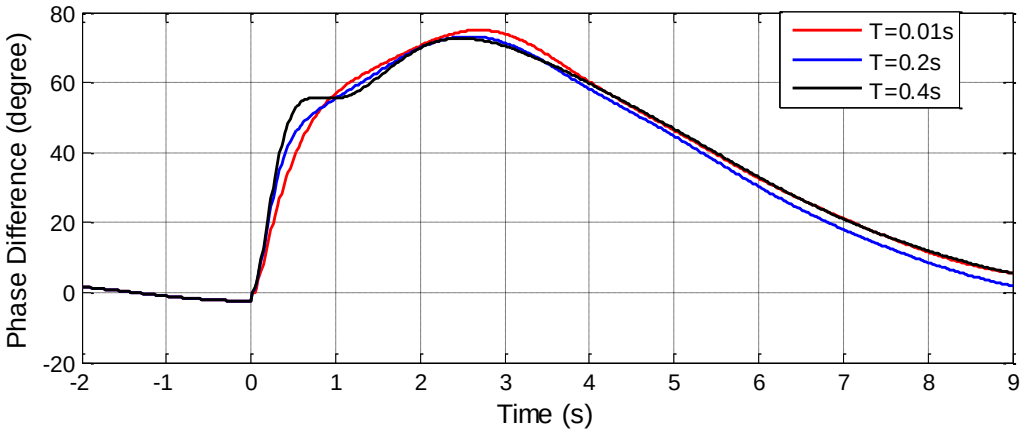

Figure 6-30 Phase difference with respect to time constant

Figure 6-29 illustrates the influence of time constant, T_a on the DFIG inertial response to a load disturbance. It is observed that the increment in T_a introduce a delay and attenuation to the DFIG output power. This in turn increases the island's frequency deviation due to the same load disturbance in the island. Although smaller time constant reduces the frequency deviation remarkably, it has little effect on improving the phase control response. The magnitudes of phase deviation following the same disturbance for these three cases are similar, as depicted in Figure 6-30.

6.10.3 **Maximum Load Acceptance**

In synchronous islanded scheme, it is essential that the voltage phase deviation between the island and grid is controlled within $\pm 60°$ synchronisation limits. Once

these limits are exceeded, a synchronous island should not be continued and should be shut down.

It has been shown in previous case studies that although synchronous islanded operation with significant wind farm connection is feasible, their connection somehow limits the disturbances that can happen in the islanded system while not going beyond the synchronization limits. Even though island phase control performance can be improved by the use of more advance wind farm technology and governor type, the results still do not quite reach the level of no-wind island.

In this case study, the effect of replacing typical DFIG with an enhanced DFIG type which incorporates SB and proposed inertial response control on synchronous islanded control scheme is investigated. This is evaluated in terms of the maximum load acceptance that can occur in the island without the phase deviation exceeding $\pm 60°$. The same actual wind profile used in previous chapter is applied to the DFIG system.

Islanding is initiated at t=0 seconds by the removal of line connecting busbars 2 and 3 of Figure 5-6. Immediately after islanding, both synchronous generators switched their governor control mode to support synchronous islanded operation. The load is applied in 0.5% resolution at several different times, as shown below:

Case 1) Phase difference peak
Case 2) Phase difference trough
Case 3) Frequency peak
Case 4) Frequency trough
Case 5) Time of low frequency and phase variation

The results in Table 6-6 lists the maximum load acceptance possible for each test while not exceeding $\pm 60°$ phase difference. They are presented in percentage terms of the controllable generation in the island, i.e. of 5.208 MW. Results for cases of typical DFIG and no wind farm are also included for comparison purpose.

Table 6-6 Comparison of Maximum Load Acceptance for Cases (1)-(5)

CASE	MAXIMUM LOAD ACCEPTANCE (%)		
	DFIG + SB + inertia control	Typical DFIG	No Wind
1	23.5	16.0	17.5
2	24.5	17.0	
3	24.0	16.0	
4	23.0	15.5	
5	24.5	16.5	

By replacing the typical DFIG with enhanced type DFIG, a remarkable improvement is observed in all cases in the amount of load applicable in the island while remaining within synchronisation limits. For instance, in case 5, the maximum load acceptance of 16.5% in the typical DFIG case increases to 24.5% for the enhanced type DFIG case.

Case 4 remains the worst time to apply load. However, it has improved from 15.5% to 23% for typical DFIG case and enhanced type DFIG case respectively.

This replacement also showed a significant improvement of at least 5.5% when compared to no wind farm case. Contrary to previous findings, these results suggest that wind farm connection is no longer a limiting factor and can be employed to support synchronous islanded operation.

6.10.4 **Size of Wind Farm**

This case study serves as an extension from the previous case study and is carried out to investigate how the proportion of wind farm related sources in the island affect the maximum load applicable in the island without going beyond $\pm 60°$ limits.

The same setting as section 6.7.3 is used in this case study. Four types of wind farm technology haven been tested in turn namely, FSIG, typical DFIG, DFIG with SB

and DFIG with SB and inertial control. For each case, the wind farm rating was increased from 2.5MW to 5MW, whilst the rating of synchronous generators remains (5.208 MW). Only the worst case scenario is tested, which is load acceptance during frequency trough (case 4).

Figure 6-31 shows the maximum load applicable during a frequency trough for different types of wind farm technology with respect to their rating, i.e. 2.5MW and 5MW respectively. It is observed that all cases, except one, showed a reduction in maximum load acceptable with the increase of wind farm size. This is undesirable, especially in implementation of synchronous islanded operation, as the number, type and size of generation trapped in the island is always uncertain. If a large proportion of these types of wind farm versus controllable generator are trapped in the island, partial disconnection of wind farm, or wind curtailment may be necessary; or else may render synchronous island inoperable and results in the shut down of the entire island.

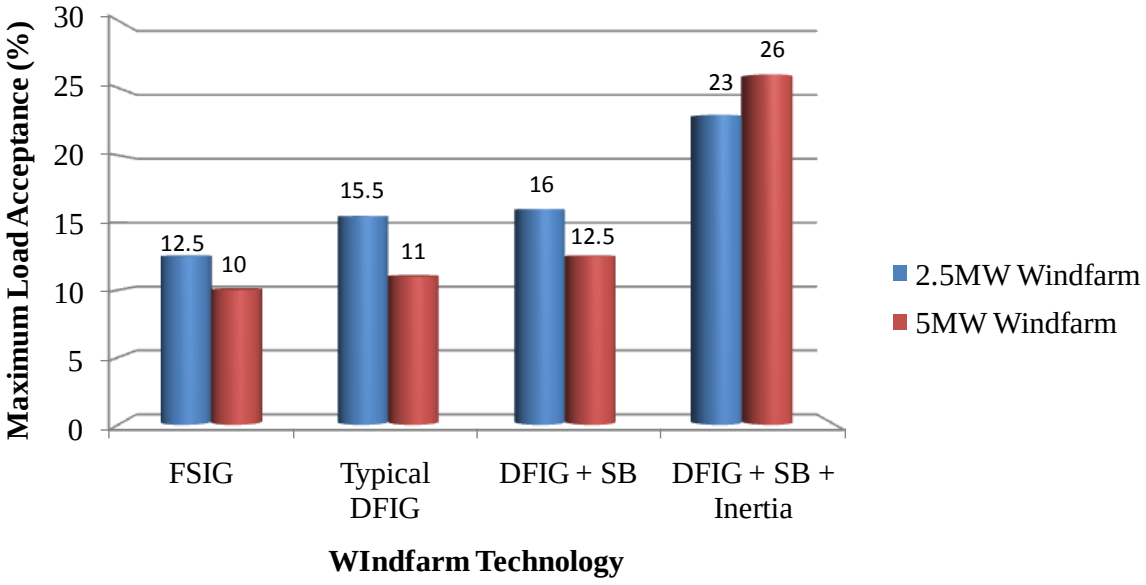

Figure 6-31 Maximum load acceptance during frequency trough for different types of wind farm technology with respect to their rating

The inclusion of storage into DFIG shows only marginal improvement in the maximum acceptable load for case with 2.5MW wind farm compare to typical DFIG

case. However, it is interesting to observe that as the wind farm size increases, the margin of improvement also increases. As the wind generation increases, its intermittency shortcoming will amplify. This result suggests that steadier output is definitely beneficial to the implementation of synchronous island.

On the other hand, the proposed DFIG type, which incorporates storage and inertial control shows an improvement in maximum load acceptable despite the increased rating. Evidently, the proposed DFIG type is beneficial to the implementation of synchronous islanded operation.

6.11 Chapter Summary

Increased penetration of wind energy into the power system has made the latter more vulnerable and dependent on the wind energy production. This effect is even more obvious in a weak system such as island and has been shown in the previous chapter that wind intermittency is disadvantageous towards the implementation of the proposed synchronous islanded operation. In particular, it limits the magnitude of load disturbance that can happen in the island.

Hence, this chapter has suggested method to reduce the wind output variation by complementing the wind farm with energy storage. It has been demonstrated on DFIG that storage inclusion can effectively smooth out the wind farm output fluctuation. Realistic limitation of storage has also been included in the simulation model and control transition between normal and contingency conditions are suggested in order to keep the wind farm connected even when storage is disconnected or failed. The effects of these controls' transitions on island phase control are discussed.

The results presented in this chapter show that phase control of the synchronous island is improved with the integration of storage into DFIG. Load acceptance for

most cases, although marginal, show improvement over the case using typical DFIG. This result is more obvious when the share of wind farm in the island increases.

The benefit of storage inclusion to the DFIG is further enhanced with the addition of a supplementary inertial control. It has been demonstrated that with the addition of the auxiliary control, wind farm connection no longer pose as a limiting factor and can be employed to support synchronous islanded operation. Furthermore, the proposed controller helps to improve the island's frequency response during transient. The benefit of the proposed system becomes more apparent as the wind farm proportion in the island grows.

It is worth to note that the proposed system advantages are not only limited to the application of synchronous islanded operation but are beneficial during grid-connected operation.

CHAPTER 7

CONCLUSIONS AND FUTURE WORKS

7.1 Conclusions

This thesis is developed based on the motivation that islanding operation will become an essential part of a future distribution network. It is beneficial, or rather crucial to maintain the continuity of power supply to the islanded network, against the alternative of a blackout. Nevertheless, it has been recognised that before the islanding concept can be fully deployed, thorough studies need to be undertaken and numerous challenges associated with islanding operation need to be resolved.

A thorough review of the islanding condition was presented, this includes the background necessary to understand the challenges concerning its operation and the current practices and regulations necessary for its operation.

Extensive simulation studies were undertaken to investigate the performance of the most widely used LOM detection technique, i.e ROCOF. Factors affecting the relay's ability in detecting islanding condition were identified. The possible interactions among LOM detection techniques were also assessed.

With increasing penetration of distributed generation into the network, it is envisaged that, in the event of an up-stream fault, or the pre-planned switching-out of parts of the utility network, a multiple-DG island is more likely to form. A suitable governor control scheme that permits the operation of a multiple-set synchronous island was

proposed. Although other governor control schemes are also feasible in operating an island synchronous with the grid, it was proposed to employ multi-isochronous governor control for its rapid response. An additional advantage of this scheme is that it provides redundancy in the event of loss of generation unit during islanding operation. The proposed control scheme also facilitates load sharing between generation units in the island. It is worth noting that the proposed scheme requires exchange of information between controllable generating units in the island, hence raising the requirements for a supervisory controller.

An islanding operating algorithm was also described in detail; this provides a full representation of the proposed concept when applied to a multiple DG environment.

Synchronous islanded operation under the presence of significant varying power sources was also investigated. Two types of wind turbine technologies were developed to represent intermittent power sources in the simulation studies. Using simulation results the effectiveness and feasibility of the proposed scheme was confirmed even under the effect of varying power sources. Issues related to continuously fluctuating power sources on the island's phase control are evident. Nevertheless, improvement of the phase control can be achieved by using a more advanced type of governor.

It was also demonstrated that more advanced wind farm technology is beneficial for the deployment of synchronous islanded operation.

Factors that influenced phase control were identified. A novel control scheme that incorporates energy storage and supplementary control for the DFIG wind farm were also proposed. Simulation results showed the effectiveness of the proposed method in aiding synchronous islanded operation. It must be noted that this scheme is not limited to the application of synchronous island. It could potentially aid the network response even during grid-connected situation.

7.2 Unique Contributions

The contributions of the thesis are summarised as below:
(Note: Paper numbers given in parentheses show that the related findings are published in proceedings of international conferences. A full list of the publications is given in Appendix D.)

This thesis performed an intensive study on the most widely employed LOM detection technique [D6]. The possible interaction between these relays, when they are applied on the same feeder are investigated and discussed in terms of both dependability and security [D1].

A feasible control method that allows the operation of multiple DG in island mode without the risk of out of synchronism reclosure was also proposed. This control scheme also provides load sharing facilities among generators in the islanded network [D2, D4]. The robustness of the proposed control method was tested under the presence of significant intermittent power sources in the island. Real wind measurements were used in the simulation to reflect a realistic varying pattern. Factors influencing the proposed control were identified [D3].

A novel scheme, which includes integration of energy storage and implementation of supplementary control to the DFIG wind farm was proposed. This technique requires minimal alteration to the conventional DFIG control method and retains its ability to capture the maximum power available in the wind. It demonstrated a massive improvement to the load acceptance limits compared to both the conventional DFIG and no wind farm connected scenarios. This is a major advancement as load disturbance limits provide an indication of the magnitude of the disturbance that can happen in the island without the phase going beyond acceptable synchronisation limits. Without the proposed scheme, synchronous islanded operation may not be suitable for islands with a large proportion of varying power sources and in particular those that are expected to experience significant load disturbances. The benefit of the proposed scheme becomes more apparent as the wind farm contribution to the island grows.

An added advantage of the proposed scheme is that it helps in improving the island's frequency response during disturbances. This benefit also applies during grid connected operation. It must be noted that this scheme does not require any control switching of the DFIG between grid-connected and islanded operation.

7.3 Future Works

An experimental facility would be beneficial in demonstrating the actual feasibility of applying the proposed control for multiple DG synchronous islanded operation. It is also important to further develop the supervisory control system proposed in the thesis. Issues regarding the communication requirements and security have to be addressed. More valuable features could be incorporated into the supervisory controller to fully utilise the available facilities. This includes, but is not limited to, economic dispatch and load shedding scheme.

The synchronous islanded operation is planned in such a way that it operates in separation from the mains to maintain supply continuity whilst the cause of the interruption on the main grid is being resolved. The island will be reconnected to the grid as soon as the interruption is cleared. Suitable methods are required in detecting the return-of-mains in order for proper switching between controls during these transitions.

As the concept of synchronous islanded operation being more widely applied, the complexity of the islanded network will undoubtedly increase accordingly. For maximum flexibility, the topology of island should be reconfigurable even during islanded operation. A smaller island should be allowed to merge into a bigger island and vice versa. At that stage, techniques to identify the merging/splitting of island will be required. Proper discrimination between the merging of an island and the return-of-mains may face challenges but is necessary.

The synchronous islanded operation concept could be developed for other type of distributed generation. Different control approach may be needed for different types of generation but the concept remains. Additional investigation may also be

accomplished at simulation level by investigating the impact of different load type to the synchronous islanded operation. The concept can also be modelled to an actual UK distribution network model and parameters.

Further modification can be done on the developed simulation model of DFIG with energy storage system in order for it to actively participate in aiding synchronous islanded operation. For instance, signals, such as active power or reactive power required by the islanded system could be sent from the supervisory control to the DFIG to enable the active involvement of the wind farm in supporting synchronous islanding operation. The control of power electronics can also be further enhanced to include more features such as damping, synchronisation, etc.

Protection coordination in the island needs to be resolved before islanding can be deployed. A change in protection relay setting is inevitable to cope with the changing fault current between grid-connected and islanded operation. In addition, the protection must be capable of coping with bi-directional flow of fault currents.

REFERENCES

[1] R. Best, D. J. Morrow, D. Laverty, and P. Crossley, "Universal application of synchronous islanded operation," in *CIRED Seminar: SmartGrids for Distribution*, Frankfurt, Germany, 2008.

[2] R. J. Best, D. J. Morrow, D. J. McGowan, and P. A. Crossley, "Synchronous Islanded Operation of a Diesel Generator," *IEEE Transactions on Power Systems* , vol. 22, pp. 2170, 2007.

[3] X. Ding, P. A. Crossley, and D. J. Morrow, "Future distribution networks with distributed generators capable of operating in islanded mode," in *39th International Universities Power Engineering Conference*, 2004.

[4] "The UK Low Carbon Transition Plan: National Strategy for Climate and Energy," The Stationery Office, 2009.

[5] IEEE Std 242-2001, *IEEE Recommended Practice for Protection and Coordination of Industrial and Commercial Power Systems*.

[6] J. C. Gomez and M. M. Morcos, "Distributed generation: Exploitation of islanding operation advantages," in *IEEE/PES Transmission and Distribution Conference and Exposition*, Latin America, , 2008.

[7] P. Fuangfoo, T. Meenual, L. Wei-Jen, and C.-i. Chow, "PEA Guidelines for Impact Study and Operation of DG for Islanding Operation," *IEEE Transactions on Industry Applications*, vol. 44, pp. 1348, 2008.

[8] L. Seca and J. A. P. Lopes, "Intentional islanding for reliability improvement in distribution networks with high DG penetration," in *International Conference on Future Power Systems*, 2005.

[9] R. A. Walling and N. W. Miller, "Distributed generation islanding-implications on power system dynamic performance," in *IEEE PES Summer Meeting*, 2002.

[10] G. Fang and M. R. Iravani, "A Control Strategy for a Distributed Generation Unit in Grid-Connected and Autonomous Modes of Operation," *IEEE Transactions on Power Delivery*, vol. 23, pp. 850, 2008.

[11] M. M. Al-Mulla and N. C. Seeley, "Distributed generation control in islanded industrial facilities: A case study in power management systems," in *PCIC Europe 2010 Conference Record*, 2010.

[12] P. Mahat, Z. Chen, and B. Bak-Jensen, "Control strategies for gas turbine generators for grid connected and islanding operations," in *IEEE PES Transmission and Distribution Conference and Exposition*, 2010.

[13] M. A. Anuar, U. Dorji, and T. Hiyama, "Principle Areas for Islanding Operation Based on Distribution Factor Matrix," in *15th International Conference on Intelligent System Applications to Power Systems*, 2009.

[14] Y. M. Atwa, E. F. El-Saadany, and A. C. Guise, "Supply Adequacy Assessment of Distribution System Including Wind-Based DG During Different Modes of Operation," *IEEE Transactions on Power Systems*,vol. 25, pp. 78.

[15] X. Ding, "Synchronised Phasor Measurement and Islanding Operation of Distributed Generation," Ph.D thesis, Faculty of Engineering and Power System, Queen's University, Belsfast, June 2006.

[16] W. X. Konrad M., Sylvain M, "An Assessment of Distributed Generation Islanding Detection Methods and Issues for Canada," July 2004.

[17] IEEE Std C37.104-2002, *IEEE Guide for Automatic Reclosing of Line Circuit Breakers for Ac Distribution and Transmission Lines*

[18] IEEE Std 1547-2003, *IEEE Standard for Interconnecting Distributed Resources with Electric Power Systems*

[19] Engineering Recommendation G59/1, *Recommendations for the connection of embedded generating plant to the regional electricity companies*

[20] N. Strath, "Islanding Detection in Power Systems," thesis, Department of Industrial Electrical Engineering and Automation, Lund University, Lund, 2005.

[21] S. K. Salman and D. J. King, "Monitoring changes in system variables due to islanding condition and those due to disturbances at the utilities' network," in *IEEE Transmission and Distribution Conference*, 1999.

[22] Econnect Ltd, "Assessment of islanded operation of distribution networks and measures for protection," ETSU K/EL/00235/REP, 2001.

[23] C. G. Bright, "COROCOF: comparison of rate of change of frequency protection. A solution to the detection of loss of mains," in *IEE Seventh International Conference on Developments in Power System Protection*, 2001.

[24] Z. Ye, R. Walling, N. Miller, P. Du, K. Nelson, "Facility Microgrids," NREL/SR-560-38019, 2005.

[25] D. M. Laverty, D. J. Morrow, T. Littler, and P. A. Crossley, "Loss-of-Mains Detection by Internet Based Rocof," in *IET 9th International Conference on Developments in Power System Protection*, 2008.

[26] D. M. Laverty, D. J. Morrow, R. J. Best, and P. A. Crossley, "Differential ROCOF relay for Loss-of-Mains protection of Renewable Generation using phasor measurement over Internet Protocol," in *CIGRE/IEEE PES Joint Symposium Integration of Wide-Scale Renewable Resources Into the Power Delivery System*, 2009.

[27] X. Ding and P. A. Crossley, "Islanding detection for distributed generation," in *IEEE Power Tech,Russia*, 2005.

[28] A. Ishibashi, M. Imai, K. Omata, S. Sato, T. Takagi, Y. Nakachi, and S. Ogawa, "New type of islanding detection system for distributed generation based on voltage angle difference between utility network and distributed generation site," in *Eighth IEE International Conference on Developments in Power System Protection*, 2004.

[29] R. A. Jenkins N., P. Crossley, D. Kirschen, G. Strbac, *Embedded Generation*. London: The Institution of Electrical Engineers, 2000.

[30] Engineering Technical Report (ETR) 113, *Notes of Guidance for the Protcetion of Embedded Generating Plant Up to 5MW for Operation In Parallel With Public Suppliers' Distribution System*

[31] M. Geidl, "Protection of Power Systems with Distributed Generation: State of the Art," Swiss Federal Institute of Technology (ETH), Zurich, 2005.

[32] A. Beddoes, P. Thomas, and M. Gosden, "Loss of mains protection relay performances when subjected to network disturbances / events," in *CIRED*

18th International Conference and Exhibition on Electricity Distribution, 2005.

[33] F. Noor, R. Arumugam, and M. Y. Vaziri, "Unintentional islanding and comparison of prevention techniques," in *Proceedings 37th Annual North American*, 2005.

[34] W. Freitas and X. Wilsun, "False operation of vector surge relays," *IEEE Transactions on Power Delivery*, vol. 19, pp. 436, 2004.

[35] W. Freitas, H. Zhenyu, and X. Wilsun, "A practical method for assessing the effectiveness of vector surge relays for distributed generation applications," *IEEE Transactions on Power Delivery*, vol. 20, pp. 57, 2005.

[36] S. Sishuba and M. A. Redfern, " Adaptive control system for continuity of supply using dispersed generators," in *Proceedings of the IEE Generation, Transmission and distribution*, 2005.

[37] M. A. Redfern, W.T. Shang and R. O'Gorman, "Auto-reclose for remote breakers in networks containing distributed generators," in *IET 10th International Conference on Developments in Power System Protection*, Manchester, 2010.

[38] W.T. Shang and M. A. Redfern, "Control schemes for distributed generators connected to distribution networks," in *Proceedings of the 44th International Universities Power Engineering Conference*, Glasgow, 2009.

[39] M. A. Redfern, J. Barrett, and O. Usta, "A new microprocessor based islanding protection algorithm for dispersed storage and generation units," *IEEE Transactions on Power Delivery*, vol. 10, pp. 1249, 1995.

[40] S. K. Salman, "Detection of embedded generator islanding condition using elliptical trajectory technique," in *Sixth International Conference on Developments in Power System Protection*, 1997.

[41] J. Sung-Il and K. Kwang-Ho, "An islanding detection method for distributed generations using voltage unbalance and total harmonic distortion of current," *IEEE Transactions on Power Delivery*, vol. 19, pp. 745, 2004.

[42] V. V. Menon, "A New Islanding Detection Technique for Distributed Generation," MSc thesis, Electrical Engineering Faculty, Montana State University, Montana, 2006.

[43] Y. Jun, C. Liuchen, and C. Diduch, "Recent developments in islanding detection for distributed power generation," in *Large Engineering systems Conference on Power Engineering*, 2004.

[44] J. E. Kim and J. S. Hwang, "Islanding detection method of distributed generation units connected to power distribution system," in *International Conference on Power System Technology*, 2000.

[45] P. D. Hopewell, N. Jenkins, and A. D. Cross, "Loss-of-mains detection for small generators," in *IEE Proceedings Electric Power Applications*, vol. 143, pp. 225, 1996.

[46] P. O'Kane and B. Fox, "Loss of mains detection for embedded generation by system impedance monitoring," in *Sixth International Conference on Developments in Power System Protection*, 1997.

[47] P. J. O'Kane, B. Fox, and D. J. Morrow, "Impact of embedded generation on emergency reserve," in *IEE Proceedings Generation, Transmission and Distribution*, vol. 146, pp. 159, 1999.

[48] M. A. Redfern, D. Brown, and M. G. Bartlett, "Detecting loss of earth for embedded generation," in *Seventh International Conference on Developments in Power System Protection*, 2001.

[49] H. Mohamad and P. A. Crossley, "Islanded operation of UK radial distribution: Earthing strategy," in *Proceedings of the 44th International Universities Power Engineering Conference ,* 2009.

[50] M. L.L.J, *Diesel Generator Handbook*. UK: Elsevier Butterworth-Heinemann, 1992.

[51] W. M. Strang, C. J. Mozina, B. Beckwith, T. R. Beckwith, S. Chhak, E. C. Fennell, E. W. Kalkstein, K. C. Kozminski, A. C. Pierce, P. W. Powell, D. W. Smaha, J. T. Uchiyama, S. M. Usman, and W. P. Waudby, "Generator synchronizing industry survey results," *IEEE Transactions on Power Delivery*, vol. 11, pp. 174, 1996.

[52] R.J Best, D. J. Morrow, "Interim Report: Work package 3.3.3. and 3.3.5," 2008.

[53] C. M. Affonso, W. Freitas, W. Xu, and L. C. P. da Silva, "Performance of ROCOF relays for embedded generation applications," *IEE Proceedings Generation, Transmission and Distribution*, vol. 152, pp. 109, 2005.

[54] EPRI PEAC Corporation and Sandia National Laboratory, "Energy storage technologies for distributed energy resources and other electric power systems," 2003(available at http://www.netl.doe.gov/technologies/coalpower/ fuelcells/ seca/tutorial/TutorialI_files/TutorialI.pdf, accessed September 2010)

[55] P. Kundur, *Power System Stability and Control*. New York: McGraw-Hill Inc, 1996.

[56] S. Barsali, M. Ceraolo, P. Pelacchi, and D. Poli, "Control techniques of Dispersed Generators to improve the continuity of electricity supply," in *IEEE Power Engineering Society Winter Meeting*, 2002.

[57] R.J Best, "Synchronous Islanded Operation of Isolated Power System Areas," Ph.D thesis, Faculty of Engineering and Power System, Queen's University, Belfast, 2008.

[58] I. M. Chilvers, "11kV Cable Protection to Permit Increase in Distributed Generation," Ph.D thesis, Faculty of Engineering and Physical Sciences, University of Manchester, Manchester, 2005.

[59] IEEE Std 421.5-2005, *IEEE Recommended Practice for Excitation System Models for Power System Stability Studies*

[60] W. B. F. Wood A.J., *Power Generation Operation and Control*. UK: John Wiley & Sons Inc, 1996.

[61] R. J. Best, D. J. Morrow, C.F.Ten, D. M. Laverty, and P. A. Crossley, "Management of a multiple-set synchronous island," in *IEEE Power & Energy Society General Meeting*, 2009.

[62] World Wind Energy Association, "World Wind Energy Report," 2010 (available at http://www.wwindea.org/home/images/stories/worldwindenergy report 2009_s.pdf, accessed September 2010).

[63] T. Ackermann, *Wind Power in Power Systems*. UK: John Wiley & Sons Ltd, 2005.

[64] P. H. Marques J, Grundling H, Pinheiro J, Hey H, "A Survey on Variable Speed Wind Turbine System," in *Proceedings of Brazilian Conference of Electronic of Power*, 2003.

[65] D. S. Tony Burton, Nick Jenkins, Ervin Bossanyi, *Wind Energy Handbook*, UK: John Wiley & Sons Ltd, 2001.

[66] M. Aktarujjaman, M. A. Kashem, M. Negnevitsky, and G. Ledwich, "Control Stabilisation of an Islanded System with DFIG Wind Turbine," in *IEEE International Power and Energy Conference*, 2006.

[67] S. Soter and R. Wegener, "Development of Induction Machines in Wind Power Technology," in *IEEE International Electric Machines & Drives Conference*, 2007.

[68] A. Petersson, "Analysis, Modeling and Control of Doubly Fed Induction Generators for Wind Turbines," thesis, Department of Electric Power Engineering, Chalmers University of Technology, Goteborg, 2003.

[69] P.W. Carlin, A. S. Laxson and E.B. Muljadi, "The History and State of the Art of Variable Speed Wind Turbine Technology," NREL/TP-500-28607, 2001.

[70] Z. Dawei and X. Lie, "Direct Power Control of DFIG With Constant Switching Frequency and Improved Transient Performance," *IEEE Transactions on Energy Conversion* , vol. 22, pp. 110, 2007.

[71] M. Kayikci and J. V. Milanovic, "Dynamic Contribution of DFIG-Based Wind Plants to System Frequency Disturbances," *IEEE Transactions on Power Systems*, vol. 24, pp. 859, 2009.

[72] S. Chondrogiannis and M. Barnes, "Specification of rotor side voltage source inverter of a doubly-fed induction generator for achieving ride-through capability," in *Proceedings of the IET Renewable Power Generation,* , vol. 2, pp. 139, 2008.

[73] L. Holdsworth, X. G. Wu, J. B. Ekanayake, and N. Jenkins, "Comparison of fixed speed and doubly-fed induction wind turbines during power system disturbances," in *Proceedings of the IEE Generation, Transmission and Distribution*, vol. 150, pp. 343, 2003.

[74] L. Shuhui and T. A. Haskew, "Analysis of Decoupled d-q Vector Control in DFIG Back-to-Back PWM Converter," in *IEEE PES General Meeting*, 2007.

[75] J. S. W L Kling, "Wind Turbines as Power Plants," in *Proceedings of the IEEE/Cigre Workshop on Wind Power and the Impacts on Power Systems*, Oslo, Norway, 2002.

[76] B. Hopfensperger, D. J. Atkinson, and R. A. Lakin, "Stator-flux-oriented control of a doubly-fed induction machine with and without position encoder," in *Proceedings of the IEE Electric Power Applications*, vol. 147, pp. 241, 2000.

[77] R. Pena, J. C. Clare, and G. M. Asher, "Doubly fed induction generator using back-to-back PWM converters and its application to variable-speed wind-energy generation," *in Proceedings of the IEE Electric Power Applications*, vol. 143, pp. 231, 1996.

[78] J. B. Ekanayake, L. Holdsworth, W. XueGuang, and N. Jenkins, "Dynamic modeling of doubly fed induction generator wind turbines," *IEEE Transactions on Power System* , vol. 18, pp. 803, 2003.

[79] J. G. Slootweg, H. Polinder, and W. L. Kling, "Dynamic modelling of a wind turbine with doubly fed induction generator," in *IEEE PES Summer Meeting*, 2001.

[80] J.T.G Pierik, J. Morren, "Validation of Dynamic Models of Wind Farms (Erao-3)," ECN-E-07-006, 2007.

[81] M. Kayikci and J. V. Milanovic, "Assessing Transient Response of DFIG-Based Wind Plants: The Influence of Model Simplifications and Parameters," *IEEE Transactions on Power System* , vol. 23, pp. 545, 2008.

[82] D. J. McGowan, D. J. Morrow, and B. Fox, "Integrated governor control for a diesel-generating set," *IEEE Transactions on Energy Conversion*, vol. 21, pp. 476, 2006.

[83] J. P. Barton and D. G. Infield, "Energy storage and its use with intermittent renewable energy," *IEEE Transactions on Energy Conversion*, vol. 19, pp. 441, 2004.

[84] R. H. Lasseter, "MicroGrids," in *IEEE PES Winter Meeting*, 2002.

[85] J. A. P. Lopes, C. L. Moreira, and A. G. Madureira, "Defining control strategies for MicroGrids islanded operation," *IEEE Transactions on Power Systems*, vol. 21, pp. 916, 2006.

[86] Y. Zoka, H. Sasaki, N. Yorino, K. Kawahara, and C. C. Liu, "An interaction problem of distributed generators installed in a MicroGrid," in *Proceedings of the IEEE International Conference on Electric Utility Deregulation, Restructuring and Power Technologies*, , 2004.

[87] Y. Kojima, M. Koshio, S. Nakamura, H. Maejima, Y. Fujioka, and T. Goda, "A Demonstration Project in Hachinohe: Microgrid with Private Distribution Line," in *IEEE International Conference on System of Systems Engineering*, 2007.

[88] B. Kroposki, R. Lasseter, T. Ise, S. Morozumi, S. Papatlianassiou, and N. Hatziargyriou, "Making microgrids work," *IEEE Power and Energy Magazine*, vol. 6, pp. 40, 2008.

[89] W. R. Lachs and H. Tabatabaei-Yazdi, "Energy storage in power systems," in *Proceedings of the IEEE International Conference on Power Electronics and Drive System* , 1999.

[90] B. K. Bose, M. H. Kim, and M. D. Kankam, "Power and energy storage devices for next generation hybrid electric vehicle," in *Proceedings of the 31st Intersociety Energy Conversion Engineering Conference*, 1996.

[91] C. Abbey and G. Joos, "Integration of energy storage with a doubly-fed induction machine for wind power applications," in *IEEE 35th Annual Power Electronics Specialists Conference*, 2004.

[92] C. Abbey and G. Joos, "A doubly-fed induction machine and energy storage system for wind power generation," in *Canadian Conference on Electrical and Computer Engineering*, 2004.

[93] C. Abbey and G. Joos, "Supercapacitor Energy Storage for Wind Energy Applications," *IEEE Transactions on Industry Applications*, vol. 43, pp. 769, 2007.

[94] A. Yazdani, "Islanded Operation of A Doubly-Fed Induction Generator (DFIG) Wind-Power System with Integrated Energy Storage," in *IEEE Electrical Power Conference*, Canada, 2007.

[95] C. Abbey and G. Joos, "Short-term energy storage for wind energy applications," in *Conference Record of the Industry Applications Conference*, 2005.

[96] R. Cardenas, R. Pena, G. Asher, and J. Clare, "Power smoothing in wind generation systems using a sensorless vector controlled induction Machine driving a flywheel," *IEEE Transactions on Energy Conversion, ,* vol. 19, pp. 206, 2004.

[97] S. M. Muyeen, M. H. Ali, R. Takahashi, T. Murata, and J. Tamura, "Wind Generator Output Power Smoothing and Terminal Voltage Regulation by Using STATCOM/ESS," in *IEEE Power Tech*, Lausanne, 2007.

[98] L. Wei, G. Joos, and C. Abbey, "Wind Power Impact on System Frequency Deviation and an ESS based Power Filtering Algorithm Solution," in *IEEE Power Systems Conference and Exposition*, 2006.

[99] L. Changling, H. Banakar, S. Baike, and O. Boon-Teck, "Strategies to Smooth Wind Power Fluctuations of Wind Turbine Generator," *IEEE Transactions on Energy Conversion* , vol. 22, pp. 341, 2007.

[100] P. J. Binduhewa, A. C. Renfrew, and M. Barnes, "Ultracapacitor energy storage for MicroGrid micro-generation," in *4th IET Conference on Power Electronics, Machines and Drives*, 2008.

[101] R. L. Spyker and R. M. Nelms, "Optimization of double-layer capacitor arrays," *IEEE Transactions on Industry Applications*, vol. 36, pp. 194, 2000.

[102] R. G. Adrian Schneuwly, "Properties and Applications of Supercapacitors From the State-of-the-art to Future Trends," in *Proceeding of the International Conference on Power Electronics, Intelligent Motion and Power Quality*, 2000.

[103] R. L. Spyker and R. M. Nelms, "Classical equivalent circuit parameters for a double-layer capacitor," *IEEE Transactions on Aerospace and Electronic Systems*, vol. 36, pp. 829, 2000.

[104] Y. Y. Yao, D. L. Zhang, and D. G. Xu, "A Study of Supercapacitor Parameters and Characteristics," in *International Conference on Power System Technology*, 2006.

[105] A. R. Phillippe Barrade, "The Use of Supercapacitors for Energy Storage in Traction Systems," in *IEEE Vehicular Power and Propulsion Symposium*, Paris, France, 2004.

[106] T. M. U. Ned Mohan, William P Robbins, *Power Electronic Converters, Applications and Design*, UK: John Wiley & Sons Ltd, 1996.

[107] T. Yamazaki, R. Takahashi, T. Murata, J. Tamura, K. Masahiro, Y. Matsumura, A. Kuwayama, and T. Matsumoto, "Smoothing control of wind generator output fluctuations by new pitch controller," in *18th International Conference on Electrical Machines*, 2008.

[108] D. Gautam, L. Goel, R. Ayyanar, V. Vittal, and T. Harbour, "Control Strategy to Mitigate the Impact of Reduced Inertia Due to Doubly Fed Induction Generators on Large Power Systems," *IEEE Transactions on Power Systems*, vol. PP, pp. 1.

[109] I. Moore and J. Ekanayake, "Frequency response from wind turbines," in *Proceedings of the 44th International Universities Power Engineering Conference*, 2009.

[110] M. Akbari and S. M. Madani, "Participation of DFIG based wind turbines in improving short term frequency regulation," in *18th Iranian Conference on Electrical Engineering, 2010.*

[111] B. Khaki, M. H. Asgari, R. Sirjani, and A. Mozdawar, "Contribution of DFIG wind turbines to system frequency control," in *International Conference on Sustainable Power Generation and Supply*, 2009.

[112] G. Ramtharan, J. B. Ekanayake, and N. Jenkins, "Frequency support from doubly fed induction generator wind turbines," in *Proceedings of the IET Renewable Power Generation*, vol. 1, pp. 3, 2007.

[113] T. Thiringer, "Frequency scanning for power system property determination applied to a wind power grid," *IEEE Transactions on Power Systems*, vol. 21, pp. 702, 2006.

[114] A. G. Gonzalez Rodriguez, M. Burgos Paydn, and C. Izquierdo Mitchell, "PSCAD based simulation of the connection of a wind generator to the network," in *IEEE Power Tech Proceedings*, Porto, 2001.

[115] S. Pay and Y. Baghzouz, "Effectiveness of battery-supercapacitor combination in electric vehicles," in *IEEE Power Tech Conference Proceedings*, Bologna, 2003.

[116] IEEE Std C37.118-2005, *IEEE Standard for Synchrophasors for Power Systems*.

[117] K. Narendra, T. Weekes, "Phasor Measurement Unit (PMU) Communication Experience in a Utility Environment", in *Cigre Canada Conference on Power System*, 2008.

[118] A.G. Pandolfo, A.F. Hollenkamp, "Carbon Properties and Their Role in Supercapacitors", *Journal of Power Sources*, vol. 157, pp. 11-27, 2006.

[119] L.M.P Fanjul, "Some New Applications of Supercapacitors in Power Electronic Systems," MSc. Thesis, Department of Electrical Engineering, Texas A&M University, August 2003.

[120] Illinois Capacitor Inc, "Supercapacitor" (available at http://www.illinoiscapacitor.com/pdf/Papers/supercapacitors.pdf)

[121] I. Buchmann, *Batteries in a Portable World: A Handbook on Rechargeable Batteries for Non-Engineers*, Cadex Electronics Inc, 2001.

[122] M. jayalakshmi, K. Balasubramanian, "Simple Capacitors to Supercapacitors – An Overview", *International Journal of Electrochemical Science*, vol. 3, pp. 1196-1217, 2008.

[123] K. Sahay, B. Dwivedi, "Supercapacitors Energy Storage System for Power Quality Improvement: An Overview", *Journal Electrical System*, vol. 5, pp.1-8, 2009.

[124] J. Chmiola, Y. Gogotsi, "Supercapacitors as Advanced Energy Storage Devices", *Nanotechnology Law & Business*, vol. 4, pp. 577-584, 2007.

APPENDIX A: Distribution Network Model Data

The distribution network model used for simulation studies in chapter 4 to chapter 6 is described in this Appendix.

A.1 Utility Grid

The utility grid was represented by its thevenin equivalent impedance at the 33kV voltage level. It was modelled based on fault level data obtained from [58], which is 440MVA.

A.2 Distributed Generators

There are three types of distributed energy resources modelled in the simulation, namely a gas turbine, a diesel engine and a wind farm. The former two are modelled using synchronous generators while the latter is represented by induction machine (both squirrel cage and wound rotor).

A.2.1 Synchronous Generator Parameters

The parameters for the synchronous generators, their exciters and governors are given in Table A.1, A.2 and A.3 respectively. The exciters were represented by IEEE AC5A model [30, 59].

Component Description		Unit	Gas Turbine	Diesel
Power Rating		MVA	4.51	2
Rated Voltage		kV	11.0	0.415
Inertia constant	H	MWs/MVA	1.05	1.48
Stator Resistance	R_a	pu	0.01	0.01
Direct axis sub transient reactance	$X_{d"}$	pu	0.17	0.15
Direct axis transient reactance	$X_{d'}$	pu	0.25	0.22
Direct axis synchronous reactance	X_d	pu	2.95	2.65
Quadrature axis subtransient reactance	$X_{q"}$	pu	0.31	0.25
Quadrature axis synchronous reactance	X_q	pu	1.35	2
Direct axis sub transient time constant	$T_{do"}$	s	0.055	0.03
Direct axis transient time constant	$T_{do'}$	s	5.5	3.5

Quadrature axis subtransient time constant	$T_{qo"}$	s	0.27	0.2
Potier Reactance	X_p	pu	0.153	0.135
Air Gap Factor	S_F		1.0	1.0

Table A.1: Synchronous generators parameters

Component Description			**Gas Turbine**	**Diesel**
Prime Mover	Time Constant (s)		0.4	0.2
	Upper limit (pu)		1.5	1.5
	Lower limit (pu)		-0.1	-0.1
	Droop (pu)	R	0.05	0.05
PI	Proportional gain	K_p	9	15
	Integral time constant	K_i	6	20
PID	Proportional gain	K_p	11	18
	Integral time constant	K_i	9	24
	Derivative time constant	K_d	2.2	2.4
	Phase controller gain		0.005	0.005
	Load share gain		0.1	0.1

Table A.2: Governors parameters

Component Description		**Unit**	**Gas Turbine**	**Diesel**
Regulator input filter time constant	T_r	s	0.01	0.01
Regulator gain	K_a	pu	400	500
Regulator time constant	T_a	s	0.02	0.01
Maximum regulator output	V_{Rmax}	pu	7.3	13
Minimum regulator output	V_{Rmin}	pu	-7.3	-13
Exciter time constant	T_E	s	0.55	0.35
Exciter constant	K_E	pu	1	1
Exciter saturation function @ 100%	$S_E[E_{FD1}]$	pu	1.076	1.89
Exciter saturation function @ 75%	$S_E[E_{FD2}]$	pu	0.956	1.1
Feedback gain	K_f	pu	0.03	0.03
Feedback time constant	T_f	s	1	1

Table A.3: Exciters parameters

A.2.2 Induction Generator Parameter [70, 113]

Two types of wind turbine technologies, namely fixed speed induction generator (FSIG) based wind turbines and doubly fed induction generator (DFIG) based wind

turbines have been developed. The former technology was modelled using squirrel cage induction generator while the latter were developed using wound rotor induction generator. The parameters for the FSIG and DFIG are provided in Table A.4 and Table A.5 respectively.

Note: The pre-defined squirrel cage induction generator model in PSCAD is represented as a double cage machine to take into account the deep bar effect of the rotor cage. In order for it not to take part in the simulation, high value has been applied for the second cage [114].

Component Description	**Unit**	**Value**
Nominal voltage	kV	690
Rated output	kW	500
Nominal power factor		0.9
Stator Resistance	pu	0.0067685
First Cage Resistance	pu	0.0063
Second Cage Resistance	pu	10
Stator Leakage Reactance	pu	0.08212
Mutual unsaturated Reactance	pu	0.09642
Rotor Mutual Reactance	pu	3.6296
Second Cage Reactance	pu	10
Pole pair		2
Inertia	kgm^2	130

Table A.4: Squirrel cage induction generator model

Component Description	**Unit**	**Value**
Rated Stator Power	MW	2.09
Rated Stator Voltage	kV	0.69
Stator/rotor turns ratio		0.3
Stator Resistance	pu	0.0108
Rotor Resistance (referred to stator)	pu	0.0121
Magnetizing Reactance	pu	3.362
Stator Leakage Reactance	pu	0.102
Rotor Leakage Reactance (referred to stator)	pu	0.11
Lumped Inertia Constant	s	0.8

Table A.5: Wound rotor induction generator model

A.3 Line data [58]

The following parameters are used for the 33 kV overhead lines and 11 kV underground cables.

A.3.1 33 kV Overhead Line

The 5 km, 33 kV overhead line is based on Aluminium Core Steel Reinforced (ACSR), with a cross sectional area of 150 mm^2. The phase impedance data is:

$$Z_{OH} = 0.1089 + j0.33759\ \Omega/km$$

A.3.2 11 kV Underground

The 11 kV line consists of a number of 2 km underground cables, which were stipulated as 3-core, 185 mm^2 aluminium conductors [58]. The impedance data is:

$$Z_{UG} = 0.165 + j0.094\ \Omega/km$$

A.4 Transformer and Load Parameters

The transformer parameters for the network are given in table A.6.

Voltage Ratio (kV)	R(pu)	X(pu)	Base (MVA)
33/11	0.005	0.06	20
11/0.69	0.01	0.05	6
11/0.415	0.01	0.05	3

Table A.6: Transformer data

The loads in Fig. 2 and Fig 13 are modelled according to table A.7 and table A.8 respectively.

Load	**Static Load**	
	Real Power, P (MW)	**Reactive Power, Q (MVar)**
1	0.72	0.34872
2	1.50	0.72660
3	0.45	0.14700
4	2.70	1.30770
5	0.03	0.00990
6	3.00	1.31480
7	3.00	1.31480

Table A.7: Load data for Figure 4-3

Load	**Static Load**	
	Real Power, P (MW)	**Reactive Power, Q (MVar)**
1	0.30	0.0
2	0.15	0.0
3	0.35	0.0
4	3.70	0.6

Table A.8: Load data for Figure 5-6

APPENDIX B: Control of DFIG

B.1 Control of DFIG [76-78]

This appendix describes the derivation of equation for the control of doubly fed induction generator (DFIG).

B.1.1 Control of Rotor Side Converter (RSC)

List of Symbols	
T_e	Electromagnectic torque
$\bar{\Psi}_s$	Stator flux linkage space vector
$\bar{\Psi}_r$	Rotor flux linkage space vector
V_s	Stator rms phase voltage
$\bar{v}_s$	Stator voltage space vector
$\bar{v}_r$	Rotor voltage space vector
$\bar{\imath}_s$	Stator current space vector
$\bar{\imath}_r$	Rotor current space vector
R_s	Stator resistance
R_r	Rotor resistance
L_m	Mutual inductance
L_s	Stator self inductance
L_r	Rotor self inductance
ω_e	Angular frequency of the excitation reference frame
ω_s	Angular frequency of stator quantities
ω_r	Angular frequency of rotor quantities
μ	Stator flux angle
ρ_A	Machine pole-pair number
P_s	Stator active power
Q_s	Stator reactive power

*Superscripts: e = excitation reference frame for orientation
g = general reference frame
s = stator reference frame

The electromagnetic torque of the doubly fed induction generator (DFIG) can be expressed in a general reference frame, 'g' by

$$T_e = -\frac{3}{2}\rho_A \frac{L_m}{L_s}\left(\bar{\Psi}_s^g \times \bar{\imath}_r^g\right) \quad \text{(B-1)}$$

$$T_e = -\frac{3}{2}\rho_A \frac{L_m}{L_s}\left(\Psi_{ds}^g i_{qr}^g - \Psi_{qs}^g i_{dr}^g\right) \quad \text{(B-2)}$$

Equation (B-2) can then be simplify to equation (B-3) by selecting a reference frame which is attached to the stator flux linkage Ψ_s,

$$T_e = -\frac{3}{2}\rho_A \frac{L_m}{L_s}\left(\Psi_s^e i_{qr}^e\right) \quad \text{(B-3)}$$

Since

$$\Psi_{qs}^e = 0 \; and \; \Psi_{ds}^e = \left|\bar{\Psi}_s^g\right| = \Psi_s^e \quad \text{(B-4)}$$

The reference frame that is attached to the stator flux can be referred as the excitation reference frame, "e". From equation (B-3), it is seen that the torque of the DFIG can be regulated by the q-component of the rotor current in the e-frame, where the stator flux is held constant.

The dynamic machine equations presented in the e-frame are

$$\bar{v}_s^e = R_s \bar{\imath}_s^e + \frac{d\bar{\Psi}_s^e}{dt} + j\omega_e \bar{\Psi}_s^e \quad \text{(B-5)}$$

$$\bar{v}_r^e = R_r \bar{\imath}_r^e + \frac{d\bar{\Psi}_r^e}{dt} + j(\omega_e - \omega_r)\bar{\Psi}_r^e \quad \text{(B-6)}$$

$$\bar{\Psi}_s^e = L_s \bar{\imath}_s^e + L_m \bar{\imath}_r^e \quad \text{(B-7)}$$

$$\bar{\Psi}_r^e = L_r \bar{\imath}_r^e + L_m \bar{\imath}_s^e \quad \text{(B-8)}$$

where ω_e and ω_r is the angular frequency of the e-frame and the rotor respectively.

The relationship between the stator-current components and the rotor-current components can be obtained from equation (B-7) and equation (B-4). Expressing them in *d*- and *q*- components yield

$$i_{ds}^e = \frac{1}{L_s}\Psi_s^e - \frac{L_m}{L_s} i_{dr}^e \quad \text{(B-9)}$$

$$i_{qs}^e = -\frac{L_m}{L_s} i_{qr}^e \quad \text{(B-10)}$$

The stator flux equation in the stator reference frame, "s" expressed in d- and q-components respectively are

$$\Psi_{ds}^{s} = L_s i_{ds}^{s} + L_m i_{dr}^{s} \quad \text{(B-11)}$$

$$\Psi_{qs}^{s} = L_s i_{qs}^{s} + L_m i_{qr}^{s} \quad \text{(B-12)}$$

The stator flux angle, μ can then be determined using equation (B-13)

$$\mu = tan^{-1} \frac{\Psi_{qs}^{s}}{\Psi_{ds}^{s}} \quad \text{(B-13)}$$

Another approach to obtain μ is by using

$$\bar{v}_s^s = R_s \bar{i}_s^s + \frac{d\bar{\Psi}_s^s}{dt} \quad \text{(B-14)}$$

This equation can be simplified by neglecting stator resistance, which is applicable for larger machine where the ($R_s << \omega_s L_s$), yielding

$$\bar{v}_s^s \approx \frac{d\bar{\Psi}_s^s}{dt} \quad \text{(B-15)}$$

From (B-15), it is seen that during steady state, a reference frame that is attached to the stator flux (e-frame) will have the same angular frequency as the stator voltage. The magnitude of the stator flux can be expressed in the e-frame by substituting $\bar{\Psi}_s^s = |\bar{\Psi}_s^s| e^{j\mu}$ in equation (B-15), and applying rules of differentiation

$$\Psi_s^e \approx \frac{\sqrt{2}V_s}{\omega_s} \quad \text{(B-16)}$$

where v_1 is the rms stator phase voltage. Expressing stator voltage in *d*- and *q*-components in the e-frame yields

$$v_{ds}^e = 0 \qquad v_{qs}^e = \omega_s \Psi_s^e = \sqrt{2}V_s \quad \text{(B-17)}$$

Given that stator active and reactive power expressed in general frame are

$$P_s = \frac{3}{2}\left(v_{ds}^g i_{ds}^g + v_{qs}^g i_{qs}^g\right) \quad \text{(B-18)}$$

$$Q_s = \frac{3}{2}\left(v_{qs}^g i_{ds}^g + v_{ds}^g i_{qs}^g\right) \quad \text{(B-19)}$$

Substituting equation (B-18) and (B-19) with equation (B-11), (B-12) and (B-17), stator active and reactive power can then be expressed in the e-frame as

$$P_s = -\frac{3}{2}\frac{\sqrt{2}V_s L_m}{L_s} i_{qr}^e \tag{B-20}$$

$$Q_s = \frac{3}{2}\frac{\sqrt{2}V_s}{L_s}\Psi_s^e - \frac{3}{2}\frac{\sqrt{2}V_s L_m}{L_s} i_{dr}^e \tag{B-21}$$

From equation (B-20) and (B-21), it is clearly observed that the stator active and reactive powers are a function of the *q*- and *d*-component of the rotor current respectively. Thus, the independent control of the stator active and reactive power can be achieved by regulating i_{qr} and i_{dr} respectively.

B.1.2 Control of Grid Side Converter (GSC)

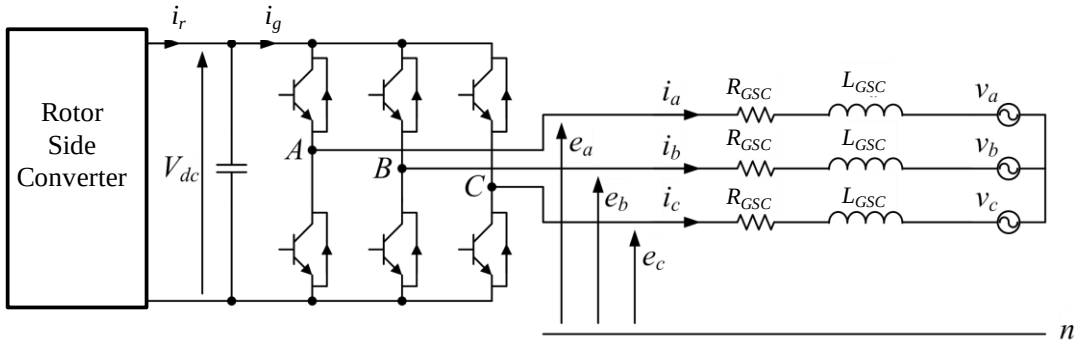

Figure B-2 Grid side converter

Figure B-2 illustrates the arrangement of the GSC. The voltage balance across the inductor is

$$\begin{bmatrix} e_a \\ e_b \\ e_c \end{bmatrix} - \begin{bmatrix} v_a \\ v_b \\ v_c \end{bmatrix} = R_{GSC}\begin{bmatrix} i_a \\ i_b \\ i_c \end{bmatrix} + L_{GSC}\frac{d}{dt}\begin{bmatrix} i_a \\ i_b \\ i_c \end{bmatrix} \tag{B-22}$$

where R_{GSC} and L_{GSC} are the line resistance and inductance respectively. Transforming equation (B-22) into *dq* reference frame rotating at grid angular frequency,ω yields

$$e_d - v_d = R_{GSC} i_d + L_{GSC}\frac{di_d}{dt} - \omega L i_q \tag{B-23}$$

$$e_q - v_q = R_{GSC} i_q + L_{GSC}\frac{di_q}{dt} + \omega L i_d \tag{B-24}$$

In the *dq* reference frame, the grid voltage is given by

$$v_{dq} = v_d + jv_q \tag{B-25}$$

And the current flowing into the grid is

$$i_{dq} = i_d + ji_q \tag{B-26}$$

Assuming that v_d, v_q, i_d and i_q are per unit values, complex power, S can be express by

$$S = v_{dq} i_{dq}^{*} = p + jq \tag{B-27}$$

$$S = (v_d + jv_q)(i_d - ji_q) \tag{B-28}$$

$$S = (v_d i_d + v_q i_q) + j(v_q i_q - v_d i_q) \tag{B-29}$$

By aligning the stator voltage vector with the *d-axis* of the reference frame, the imaginary component of v_{dq} can be eliminated, i.e. v_q=0. Thus, the per unit active power and reactive power flowing between the grid and GSC are given by $p=v_d i_d$ and $q=-v_d i_q$, which can be controlled independently by regulating i_d and i_q respectively.

Assuming that losses of converter and resistance and harmonics due to switching are negligible,

$$V_{dc} i_g = \frac{3}{2} v_d i_d \tag{B-30}$$

$$v_d = \frac{m_{GSC}}{2\sqrt{2}} V_{dc} \tag{B-31}$$

$$i_g = \frac{3}{4\sqrt{2}} m_{GSC} i_d \tag{B-32}$$

$$C \frac{dV_{dc}}{dt} = i_r - i_g \tag{B-33}$$

Equation (B-30) depicts the relation between DC-link voltage,V_{dc} and the *d*-axis current, i_d. Combining equation (B-30) and equation (B-33) yields

$$C \frac{dV_{dc}}{dt} = i_r - \frac{3 v_d i_d}{2 V_{dc}} \tag{B-34}$$

From equation (B-34), the DC-link voltage can be controlled by controlling i_d. The power factor can be regulated using i_q but is set to unity throughout this thesis.

B.2 Aerodynamic Representation

A basic aerodynamic representation is incorporated in the simulation using static aerodynamic efficiency curves as given by

$$C_p(\lambda,\beta) = 0.24\left(\frac{116}{\lambda_i} - 0.4\beta - 5\right)e^{\frac{-12.5}{\lambda_i}} \quad \text{(B-35)}$$

$$\lambda_i = \left[\frac{1}{\lambda+0.08\beta} - \frac{0.035}{\beta^3+1}\right]^{-1} \quad \text{(B-36)}$$

where β is pitch angle and λ is the tip speed ratio

B.3 Maximum Power Tracking

The back-to-back voltage source converter decouples the induction generator from the grid, enabling operation within a wide speed range, thus optimises the extraction of wind energy. Equation (B-37) depicts the mechanical power that can be extracted by a wind turbine from the wind

$$P_m = \frac{1}{2}\rho A U^3 C_p(\lambda,\beta) \quad \text{(B-37)}$$

Utilising the equation (B-35) – (B-37), the mechanical power is computed at various wind speeds and rotor speeds. The results are plotted as a function of rotor speed, hence yielding the maximum power tracking (MPT) characteristic, as depicted in Figure B-3.

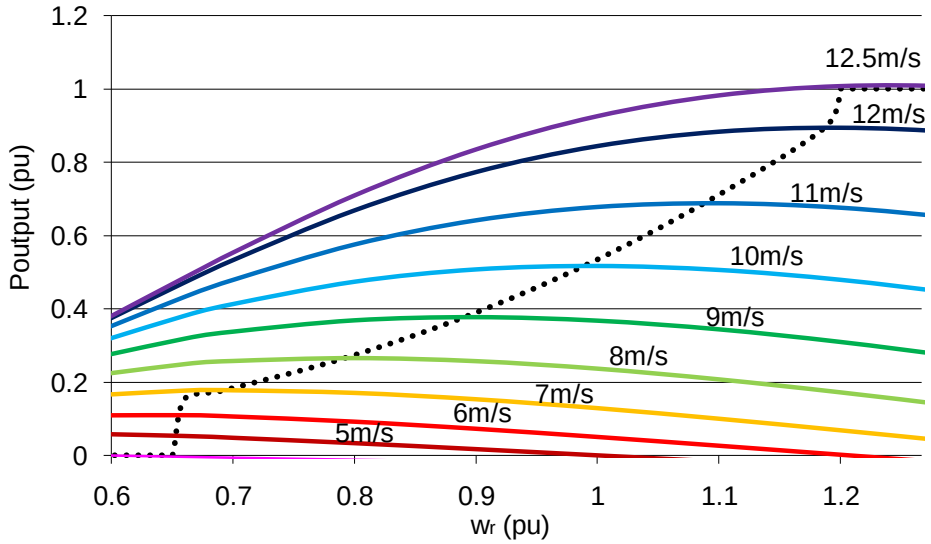

Figure B-3 MPT Characteristic (dotted lines)

APPENDIX C: Supercapacitor Model Data

Table C.1 provides the parameters for the supercapacitor modelled in Chapter 6.

Component Description	Unit	Value
Cell Capacitance	F	2500
Cell Series Resistance	mΩ	1
Cell Rated Voltage	V	2.5
Discharge ratio	%	55

Table C.1 Supercapacitor cell data [115]

APPENDIX D: List of Publications

[D1] C.F. Ten, P.A. Crossley, "Evaluation of ROCOF relay performances in network with distributed generation", in *IET 9th International Conference on Developments in Power Systems Protection*, Glasgow, United Kingdom, 2008.

[D2] C.F. Ten, P.A. Crossley, "Control of multiple distributed generators for intentional islanding", in *CIRED Seminar: Smart Grids for Distribution*, Frankfurt, Germany, 2008.

[D3] R.J. Best, C.F. Ten, D.J. Morrow, P.A. Crossley, "Synchronous island control with significant contribution from wind power generation", in *CIGRE/IEEE PES Joint Symposium*, Calgary, Canada, 2009.

[D4] R.J. Best, D.J. Morrow, C.F. Ten, D.M. Laverty, P.A. Crossley, "Management of a multiple set synchronous island", in *IEEE PES General Meeting*, Calgary, Canada, 2009.

[D5] S.P. Chowdhury, S. Chowdhury, C.F. Ten, P.A.Crossley, "Operation and control of DG based power island in smart grid environment", in *CIRED Seminar: Smart Grids for Distribution*, Frankfurt, Germany, 2008.

[D6] S.P. Chowdhury, S. Chowdhury, C.F. Ten, P.A.Crossley, " Islanding protection of distribution systems with distributed generators – a comprehensive survey report", in *IEEE PES General Meeting*, Pittsburgh, 2008.

[D7] S.P. Chowdhury, S. Chowdhury, P.A.Crossley, C.F. Ten, "UK scenario of islanded operation of active distribution networks – a survey", in *IEEE PES General Meeting*, Pittsburgh, 2008.